Conference Proceedings

7th HBP Student Conference on Interdisciplinary Brain Research

Madrid, Spain

Human Brain Project
Education Programme

7th HBP Student Conference on Interdisciplinary Brain Research, Madrid, Spain

ISBN
9782832512234

DOI
10.3389/978-2-8325-1223-4

Citation
Cano-Astorga, N., Covelo, J., Diaz, S., Fusseis, J., Gran, M., Kathrein, J., Lupascu, C.A., Ochang, P., Özden, T., Pedersen, J.E., Plaza, S., Santarpia, G., Vogel, F., Yegenoglu, A. Eds. (2023)

Human Brain Project Education Programme

January 18–20, 2023, Madrid, Spain

Table of contents

Neuroinformatics

Theoretical neuroscience

Welcome to the 7th HBP Student Conference on Interdisciplinary Brain Research

Human Brain Project
Education Programme

We are excited to present the proceedings of the 7th Human Brain Project Student Conference on Interdisciplinary Brain Research, an open forum for the exchange of knowledge within and across the various research fields addressed by the Human Brain Project (HBP). The conference was organized by young researchers for young researchers, and took place from 18th–20th January 2023 at the Rey Juan Carlos University in Madrid, Spain.

Reflecting the multidisciplinarity of the HBP, the abstracts from young researchers of this year's edition cover a wide range of topics: from brain atlases, brain simulation, ethics and society, brain organisation, medical informatics and clinical neurosciences to neuroinformatics, neuromorphic computing, neurorobotics, systems and cognitive neuroscience, and theoretical neuroscience.

LIST OF ORGANISERS

CONFERENCE PROGRAMME COMMITTEE

Nicolás Cano-Astorga
Joana Covelo
Sandra Diaz
Carmen Alina Lupascu
Paschal Ochang
Taylan Özden
Jens Egholm Pedersen
Sergio Plaza
Giuliano Santarpia
Alper Yegenoglu

CONFERENCE ORGANISERS

HBP Education Programme

PROCEEDINGS EDITORS

Sandra Diaz
Johanna Fusseis
Manuel Gran
Judith Kathrein
Paschal Ochang
Franziska Vogel

Preface

We are excited to present the proceedings of the 7th Human Brain Project Student Conference on Interdisciplinary Brain Research, an open forum for exchange of knowledge within and across the various research fields addressed by the Human Brain Project (HBP). After holding previous editions virtually due to COVID-19, the conference finally took place on-site at the Rey Juan Carlos University, Madrid, Spain, from the 18th to 20th January 2023. We are very grateful to the local hosts for providing an excellent environment for this event to take place in, as well as for the active involvement of local academic and governmental authorities like the rector of the Rey Juan Carlos University and the Major of the city of Aranjuez.

The 7th edition proved once more that the HBP Student Conference offers invaluable opportunities for extensive scientific discussions among fellow early career researchers and faculty. Through a variety of lectures, workshops, discussion sessions and social events, participants could learn about recent developments and tools in brain research, as well as interact with world-leading researchers and experts. Attendees were exposed to the data-driven and multidisciplinary brain research approach of the HBP and had the opportunity to use the EBRAINS platform. At the heart of the conference were the invaluable contributions of all young researchers in the form of talks and posters, whose corresponding abstracts are presented in this book. The accepted abstracts cover a wide range of topics (brain atlases, brain simulation, ethics and society, brain organisation, medical informatics and clinical neurosciences, neuroinformatics, neuromorphic computing, neurorobotics, systems and cognitive neuroscience, and theoretical neuroscience), introducing new and relevant problems, concepts and ideas, with the potential to inspire collaboration across research disciplines.

We would like to thank all authors for submitting their work to the 7th HBP Student Conference and all participants for making the conference a unique event for the future

of brain research. We hope this selected set of abstracts can be of inspiration for new discussions, interactions, and research opportunities for the whole scientific community.

Sandra Diaz & Paschal Ochang
Programme Committee Chairs of the 7th HBP Student Conference on Interdisciplinary Brain Research

This project has received funding from the European Union's Horizon 2020 Framework Programme for Research and Innovation under the Specific Grant Agreement No. 945539 (Human Brain Project SGA3).

Brain atlases

Mechanisms of cerebral processing of complex acoustic signals

Author
katharina Griebel – Department of Neurology, Jena University Hospital, Jena, Germany; Biomagnetic Center, Jena University Hospital, Jena, Germany
Christian Dobel – Department of Otorhinolaryngology, Jena University Hospital, Jena, Germany
Hanna Köhler – Department of Neurology, Jena University Hospital, Jena, Germany; Biomagnetic Center, Jena University Hospital, Jena, Germany; Department of Clinical Psychology, Friedrich Schiller University Jena, Jena, Germany
Franziska Wagner – Department of Neurology, Jena University Hospital, Jena, Germany; Biomagnetic Center, Jena University Hospital, Jena, Germany
Martin Walter – Department of Psychiatry and Psychotherapy, Jena University Hospital, Jena, Germany
Carsten Klingner – Department of Neurology, Jena University Hospital, Jena, Germany; Biomagnetic Center, Jena University Hospital, Jena, Germany

Citation
Griebel, K., Dobel, C., Köhler, H., Wagner, F., Walter, M., Klingner, C. Mechanisms of cerebral processing of complex acoustic signals.

Introduction/Motivation

The concrete cerebral processing of natural sounds has not yet been conclusively clarified. One major cause lies in the complexity of the received signal. The neural processing of complex sounds like spoken language

or music begins in the ear, passes through several subcortical areas, and continues in the cortex to give us a greater sense of the auditory world [1-3].

The auditory cortex's specific contribution is not fully discovered. Although several characteristics of neurons in the auditory cortex resemble those of the subcortical neurons, they show a more complex selectivity for sound characteristics, which can be of great significance for analysing complex natural sounds [4]. Here, the auditory cortex is not only understood as a location of complex sound selectivity but also as an integral component of the network of brain regions, which are responsible for the prediction and the decision-making in auditory perception as well as learning [5-6]. In addition to frequency, location, and superordinate context of the auditory signal, the mere signal complexity should play a significant role in processing auditive information.

In information theory complexity is understood as the information content of data. This can be applied to the analysis of an auditory signal itself, but not to the concept of music, because otherwise white noise, for example, would be more complex than Mozart's symphonies. Various factors such as timbre, rhythm or volume can play a role here, not least the occurrence of Gestalt effects.

The use of musical stimuli is not only an important aspect of basic research to understand the brain but is increasingly being used in patient care. So far, general musical stimuli have been best studied in dementia and strokes, but there are also various treatment studies where they are used, e.g., Parkinson's disease, epilepsy and multiple sclerosis [7, 8]. Complexity is an insufficiently explored part of music that could be of great benefit in understanding the associated effects of music on the body.

Therefore, this study aims to analyse the processing of sounds with different signal complexity operationalised by the number of instruments in a piece of music. The number of instruments and thus their timbre is the only parameter that changes, while other factors such as rhythm or tone remain the same over time. Gestalt effects can also occur here, as they cannot

be prevented, but it is necessary to try to make the latent construct of complexity usable.

We hypothesise that the processing of auditory stimuli of varying complexity is characterised by a different flow of information between cerebral areas that can be distinguished by the analysis of functional connectivity. Here, we assume that more complex acoustic signals induce stronger and more homogeneous network connectivity of auditory areas compared to simpler acoustic signals and that network structures, which correlate with the signal's complexity, can be differentiated from network structures that show on-off behaviour.

Methods

30 right-handed subjects between the age of 18 to 30 years without neurological or psychiatric disorders and loss of hearing in their medical record were included in the study. Standardised questionnaires were utilised to obtain further information about the sample and to detect possible exclusion criteria. Beck's Depression Inventory 2 (BDI2) [9], Epworth Sleepiness Scale (ESS) [10], an adaption of the Edinburgh Handedness Inventory (Handedness Score), Goldsmith's Musical Sophistication Index (GMSI) [11, 12] and a self-developed questionnaire for sociodemographic data (Biomag Questionnaire Standard 1) were used. Prior to the experiment, the subjects performed a hearing threshold measurement.

Brain activity was measured using magnetoencephalography and electroencephalography while subjects listened to a specially composed piece of music. Segments of one, three or five different instruments in a pseudorandomised order reflected the three levels of sound complexity, with the transition from one level to another being fluent and, therefore, hardly noticeable. Afterwards, participants had to decide in a quiz for 30 of the segments whether one, three or five instruments were included to control for the ability to consciously assess the complexity.

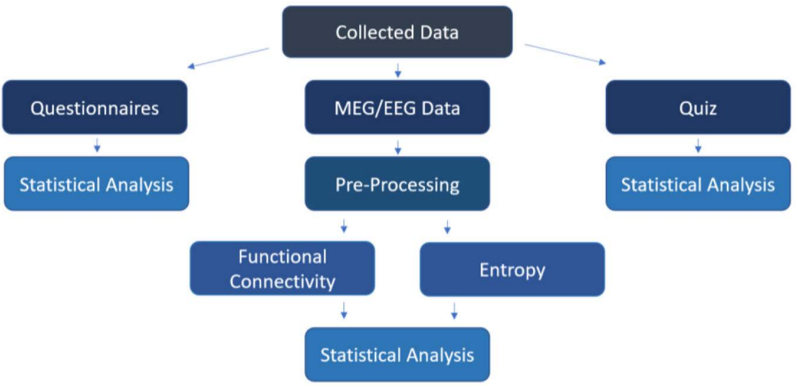

FIGURE 1
Methological steps of the analyses.

Results and discussion

Functional connectivity is assessed by coherence between signals from groups of sensors of different location. Additionally, modified multiscale entropy is used to assess dynamic changes in irregularities of temporal signals, which allows the evaluation of the signal's entropy over atypically longer periods of time. Fluctuation patterns in brain activity, which tend to repeat over time, are assigned a lower entropy, while more irregular, non-repetitive patterns yield higher entropy [13]. Parameters will be tested for statistical significance between the complexity levels. The Data is collected and is in the pre-processing stage right now, statistical analysis of the questionnaires and quiz is also in progress (Figure 1). The final analysis will be completed by the start of the conference.

Results will help to understand the processing of complexity in acoustic signals. This primary research can be a basis for clinical studies of patient care in which musical stimuli are used.

Based on this study's results further research is planned. Specifically, the effect of ketamine in combination with music for the therapy of treatment-resistant depression is to be investigated [14, 15, 16]. The ketamine's effect is expected to be altered by music [17, 18]. It is assumed that the complexity of the music also has an influence on this effect.

Acknowledgements
This work is funded by the interdisciplinary centre for clinical research Jena.

References

[1] M. Moerel, F. De Martino, K. Uğurbil et al., "Processing of frequency and location in human subcortical auditory structures," Scientific Reports, vol. 5, no. 1, pp. 1-15, 2015.

[2] D.N. Pandya, "Anatomy of the auditory cortex," *Revue Neurologique,* vol. 151, no. 8-9, pp. 486–494, 1995.

[3] G.G. Parras, J. Nieto-Diego, G.V. Carbajal et al., "Neurons along the auditory pathway exhibit a hierarchical organization of prediction error," *Nature Communications*, vol. 8, no. 1, pp. 1-17, 2017.

[4] M. Moerel, F. De Martino, E. Formisano, "An anatomical and functional topography of human auditory cortical areas," *Frontiers in Neuroscience*, vol. 8, p. 225, 2014.

[5] J. Davies, P.E. Gander, M. Andrews et al., "Auditory network connectivity in tinnitus patients: a resting-state fMRI study," *International Journal of Audiology*, vol. 53, no. 3, pp. 192–198, 2014.

[6] M. Lumaca, B. Kleber, E. Brattico et al., "Functional connectivity in human auditory networks and the origins of variation in the transmission of musical systems," *Elife,* vol. 8, p. e48710, 2019.

[7] K. Rosslau, D. Steinwede, C. Schröder et al. "Clinical investigations of receptive and expressive musical functions after stroke," *Frontiers in Psychology*, vol. 6, p. 768, 2015.

[8] A.J. Sihvonen, T. Särkämö, V. Leo et al. "Music-based interventions in neurological rehabilitation," *The Lancet Neurology,* vol. 16, no. 8, pp. 648-660, 2017.

[9] C. Kühner, C. Bürger, F. Keller et al. "[Reliability and validity of the Revised Beck Depression Inventory (BDI-II). Results from German samples]," *Nervenarzt,* vol. 78, no. 6, pp. 651-656, 2007.

[10] M.W. Johns "A New Method for Measuring Daytime Sleepiness: The Epworth Sleepiness Scale," *Sleep*, vol. 14, no. 6, pp. 540-545, 1991.

[11] D. Müllensiefen, B. Gingras, L. Stewart et. al "Goldsmiths Musical Sophistication Index (Gold-MSI) v1. 0: Technical Report and Documentation Revision 0.3," 2013.

[12] D. Müllensiefen, B. Gingras, J. Musil et al. "The Musicality of Non-Musicians: An Index for Assessing Musical Sophistication in the General Population," *PLOS ONE,* vol. 9, no. 2, p. e89642, 2014.

[13] J.Q. Kosciessa, N.A. Kloosterman, D.D. Garrett, "Standard multiscale entropy reflects neural dynamics at mismatched temporal scales: What's signal irregularity got to do with it?," *PLoS computational biology*, vol. 16, no. 5, p. e1007885, 2020.

[14] M. Scheidegger, M. Walter, M. Lehmann et al. "Ketamine Decreases Resting State Functional Network Connectivity in Healthy Subjects: Implications for Antidepressant Drug Action," *PLOS ONE,* vol. 7, no. 9, p. e44799, 2012.

[15] D.F. Ionescu, J.M. Felicione, A. Gosai et al. "Ketamine-associated brain changes: a review of the neuroimaging literature," *Harvard review of psychiatry,* vol. 26, no. 6, p. 320, 2018.

[16] N. B. Lundin, L. Sepe-Forrest, J. R. Gilbert et. al. "Ketamine Alters Electrophysiological Responses to Emotional Faces in Major Depressive Disorder," *Journal of Affective Disorders,* vol. 279, pp. 239-249, 2021.

[17] F.S. Barrett, K.H. Preller, M. Kaelen "Psychedelics and music: neuroscience and therapeutic implications," *International Review of Psychiatry,* vol. 30, no. 4, pp. 350-362, 2018.

[18] A. Kumar, A. Bajaj, P. Sarkaret et al. "The effect of music on ketamine induced emergence phenomena," *Anaesthesia,* vol. 47, no. 5, pp. 438-439, 1992.

Registration of thalamo-cortical tract-tracing experiments to the allen mouse common coordinate framework

Author
Mario Rubio-Teves – Department of Anatomy and Neuroscience, School of Medicine, Autónoma de Madrid University, Madrid, Spain
Nestor Timonidis – Radboud University Nijmegen, Donders Institute for Brain, Cognition and Behaviour, Department of Neuroinformatics, Nijmegen, The Netherlands
Carmen Alonso-Martínez – Department of Anatomy and Neuroscience, School of Medicine, Autónoma de Madrid University, Madrid, Spain
Rembrandt Bakker – Radboud University Nijmegen, Donders Institute for Brain, Cognition and Behaviour, Department of Neuroinformatics, Nijmegen, The Netherlands; Inst. of Neuroscience and Medicine (INM-6) and Inst. for Advanced Simulation (IAS-6) and JARA BRAIN Inst. I, Jülich, Germany
María García-Amado – Department of Anatomy and Neuroscience, School of Medicine, Autónoma de Madrid University, Madrid, Spain
César Porrero – Department of Anatomy and Neuroscience, School of Medicine, Autónoma de Madrid University, Madrid, Spain
Paul Tiesinga – Radboud University Nijmegen, Donders Institute for Brain, Cognition and Behaviour, Department of Neuroinformatics, Nijmegen, The Netherlands
Francisco Clascá – Department of Anatomy and Neuroscience, School of Medicine, Autónoma de Madrid University, Madrid, Spain

Citation
Rubio-Teves, M., Timonidis, N., Alonso-Martínez, C., Bakker, R., García-Amado, M., Porrero, C., Tiesinga, P., Clascá, F. Registration of thalamo-cortical tract-tracing experiments to the allen mouse common coordinate framework.

Introduction/Motivation

The thalamus is considered the gate for most sensory information on its way to the cortex. In the case of the somatosensory system, that role is played specifically by the ventral posterior complex (VP) [1]. The axonal projections from the neurons of these nuclei are extremely precise, and even when they are labeled as populations they manifest as column- and layer-specific. While tract-tracing experiments are the gold standard for revealing thalamocortical connectivity, only a few injections can be performed in a single brain. Therefore, studying the anatomical connectivity of the thalamocortical system requires the accurate registration of each experiment to a common atlas or reference space serving as an anatomical template.

The Human Brain Project has developed robust software tools for the registration of mouse brain sections to the Allen Common Coordinate Framework (CCF) [2]. Integrated as the QUINT workflow [3], they allow the registration of brain regions from the CCF to experimental sections to subsequently count labelled objects (somas and/or neurites) in each of the projected brain regions. Here we develop an alternative pipeline that inverts the first step of QUINT: it registers connectivity data to the CCF, and then counts the objects. The advantage is that the raw data becomes anchored to CCF space, ready for integration with other data or for use with updated brain parcellations. The pipeline is built as a Jupyter (Python) notebook and largely relies on the same tools as the QUINT workflow.

Methods

Our use case consists of series of evenly-spaced histological sections from the mouse brain, in which an anterograde tracer was injected in the somatosensory thalamus. This resulted in the labeling of 10-100 closely located cell bodies and their complete axonal arborizations. For each experiment, stacks of images covering whole sections were acquired at 10x magnification on a brightfield microscope (Neurolucida, MBF Bioscience). Minimum-intensity projection (MIP) images were produced from the stacks (Fig. 1A). The MIP images were segmented using Ilastik's Pixel Classification workflow (Fig. 1B) [4], to delineate the labeled neurites from the background.

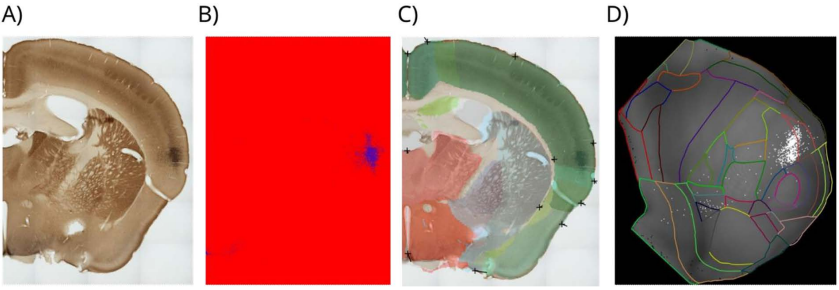

FIGURE 1

Illustration of the 3D registration pipeline presented in this work. **A**) An exemplar coronal slice highlighting a targeted axonal population labeled using anterograde tracing experiments. **B**) Segmentation of the population using the ilastik toolbox. **C**) Registration of the slice to the Allen CCF using a combination of the QuickNii, DeepSlice and VisuAlign tools (see Methods). **D**) The final output of registering all coronal slices of the experiment can be visually assessed using a dorsal flatmap in which anatomical boundaries have been delineated.

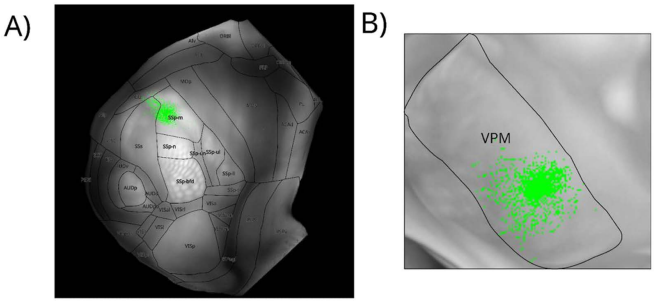

FIGURE 2

Illustration of 2D flatmaps developed for visualizing the registration of a population in CCF. The cells labeled in the ventral posterior medial nucleus (VPM) send their axons to the representation of the mouth in the primary somatosensory cortex (SSp-m). Therefore, the voxels within VPM labeled in this experiment can be identified in the CCF as part of the mouth representation at the thalamic level. **A**) Cortical flatmap. **B**) 2D plot of the VPM, in which maximum projection has been applied across the coronal plane for defining the anatomical boundaries, the intensity volume and the somatodendritic distribution. The gray intensity corresponds to the gray matter intensity, the green point-cloud corresponds to the distribution of axons (A) and somata/dendrites (B), and the black boundaries correspond to boundaries between different anatomically distinct sub-areas (A) and VPM (B).

In parallel, we performed linear registration of the MIP images using the QuickNii tool [5], assisted by the DeepSlice deep learning algorithm [6] and manual curation. We then applied the VisuAlign tool for non-linear refined registration based on manually placed histological landmarks over the atlas delineation (Fig. 1C). The computed inverse registration of the projection images to CCF was then applied to the segmented images, such that the labeled pixels were mapped to the 3D brain template (Fig 1D). Lastly, we produced 2D cortical and thalamic flatmaps [7] overlaid with anatomical boundaries to visually inspect the results prior to further statistical analyses (Fig. 2).

Results and discussion

The registration of this collection of experiments connects the ventral posterior nuclei and the somatosensory cortices within the CCF, via the spatial correlation between topographically organized somata in the former and their axonal termination patterns in the latter (Fig. 2). As a next step, we intend to analyze this topographical correlation and to identify different neuronal populations inside VP that preferentially target different layers within the same cortical column, or the same layer across different somatosensory regions.

Furthermore, registering the dataset allowed us to incorporate them to a virtual reference space that is to be shared and further improved by the whole neuroscientific community. The pipeline, compared to the QUINT workflow, requires some coding knowledge on part of the user. However, it also offers extensive customizable visualization options because of this, such as support for cortical flatmaps, 2D representations of subcortical nuclei and interactions with the Scalable Brain Atlas Composer 3D visualization tool [8]. Lastly, due to it sharing the same registration tools as QUINT, both workflows are fully compatible, allowing further analyses of previously registered datasets.

Acknowledgements

This work was supported by the FLAG-ERA grant NeuronsReunited, by NWO (680-91-318), by Spain's MICINN-AEI (PCI2019-111900-2), and by

the European Union's Horizon 2020 Framework Programme for Research and Innovation under Specific Grant Agreement No. 945539 (Human Brain Project SGA3).

References

[1] O'Reilly et al., 2021. Rodent somatosensory thalamocortical circuitry: Neurons, synapses, and connectivity. Neuroscience & Biobehavioral Reviews 126 (2021): 213-235.

[2] Wang et al., 2020. The allen mouse brain common coordinate framework: A 3d reference atlas. Cell, 181(4):936 – 953.

[3] Yates et al., 2019. QUINT: Workflow for Quantification and Spatial Analysis of Features in Histological Images From Rodent Brain. Frontiers in Neuroinformatics 13:1662-5196.

[4] Berg et al., 2019. ilastik: interactive machine learning for (bio)image analysis. Nat Methods 16:1226–1232.

[5] Puchades et al., 2019. Spatial registration of serial microscopic brain images to three-dimensional reference atlases with the QuickNII tool. PLOS ONE 14(5): e0216796.

[6] Carey et al., 2022. DeepSlice: rapid fully automatic registration of mouse brain imaging to a volumetric atlas. bioRxiv 2022.04.28.489953.

[7] Knox et al., 2018. High resolution data-driven model of the mouse connectome. Network Neuroscience. 3(1):217–236.

[8] Bakker, R., Tiesinga, P., and Kotter, R., 2015. The scalable brain atlas: Instant web-based access to public brain atlases and related content. Neuroinformatics, 13(3):353:366.

Brain simulation

NEST Desktop 3.2 - A front end moves towards young researchers

Author
Jens Bruchertseifer, Sebastian Spreizer, Benjamin Weyers– HCI, Universität Trier, Trier, Germany

Citation
Bruchertseifer, J., Spreizer, S., Weyers, B. NEST Desktop 3.2 - A front end moves towards young researchers

Introduction/Motivation

Simulators are invaluable tools for the daily work of computational neuroscientists. However, many persons in this field struggle to learn the scripting languages to control these simulators, as they do not have any programming experience and the simulators offer numerous options and commands. In order to flatten the learning curve, NEST Desktop offers a graphical user interface (GUI) presenting the concepts and the work steps together with the script code.

In the latest release, it has been extended significantly: On the one hand, connectors to numerous existing software suites were added, so that users can now also use it for more extensive scenarios. This provides greater practical relevance and should help to keep the motivation of students at a

higher level. On the other hand, new features relevant to scientific research have also been incorporated. This expands the target group, as researchers previously had to switch to other tools for such functions.

Methods

This abstract discusses the most recent advances of NEST Desktop, a web-based GUI which comprises graphical elements for creating and configuring network models, running simulations in a simulation tool, as well as visualizing and analyzing the results [2]. It allows students to explore important concepts in computational neuroscience without the need to learn a simulator control language beforehand. As a web-based tool, it has the advantage of being independent of the user's operating system, while still allowing the user to rely on the compute power of the simulator in the back-end. A local-only setup is also possible.

A central aspect of this work is the extension of the software's functions and methods through connectors to various other existing tool and software suites: As the initial use case of NEST Desktop - creating neuronal networks without extensive programming skills - is also helpful for other software tools, we aim for collaborations with multiple other projects. Many of them focus on the analysis of already executed simulations, but have the problem, that those simulation cannot be run by inexperienced users. Therefore, a connection to those tools would be of great interest, to create a cohesive tool landscape, welcoming to new users. In the following, we present the ones included in the 3.2 release of NEST Desktop. Some features, which are currently under development, are also included in that list, since we want to give an outlook on our future work as well:

- **Insite** (since v3.1): Insite is an in-situ pipeline which allows to visualize data sets from an ongoing simulation [3]. This enhances the interactivity for large simulations on HPC facilities and also extends the use case fundamentally.

- **ViSimpl** (since v3.2): ViSimpl is a tool that allows users to visualize spike data of simulations with NEST Simulator. Since the 3.2 release, NEST

Desktop is able to connect to ViSimpl and to provide the simulations for this tool [4], as seen in Figure 1.

- **NRP** (since v3.2): The Neurorobotics Platform is a very figurative use case of the NEST Simulator. However, the simulations still require neuronal networks, which were not so easy to create in the NRP software suite. The new connection from NEST Desktop to the NRP software suite allows also an straightforward creation as well as a better evaluation and visualization.

- **NESTML** (future release): NESTML is a python module allows user to construct an own neuron model which can be compiled and installed in NEST kernel code.

- **Elephant** (future release): Elephant is a very comprehensive tool for analysing simulation results of neuronal networks. Currently, we are investigating the possibilities to offer also a simple connection between NEST Desktop and Elephant.

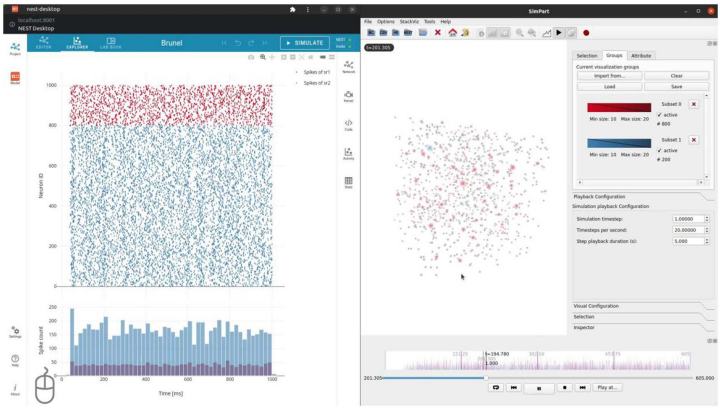

FIGURE 1
Coupling of NEST Desktop and ViSimpl in action.

- **HPC** (future release): Another use case for NEST Desktop would be the rapid construction of neuronal networks on high performance computers (HPC). This offers the possibility to create quickly more time- and resource-consuming simulations. The pitfalls in this project are the access restrictions on HPC systems, which offer only extremely limited possibilities for the communication between the back-end and the front-end.

For young researchers, NEST Desktop now offers the possibility to execute simulations for their daily research projects, use the created simulation data with numerous different tools, but also use the visualization capabilities of NEST Desktop to create high-resolution images for their work presentations.

In detail, NEST Desktop now offers the export option for network graphs as well as activity charts of spike activity (e.g. raster plot of spike activity, time histogram of spike times, distribution of inter-spike intervals (ISI)) and of analog

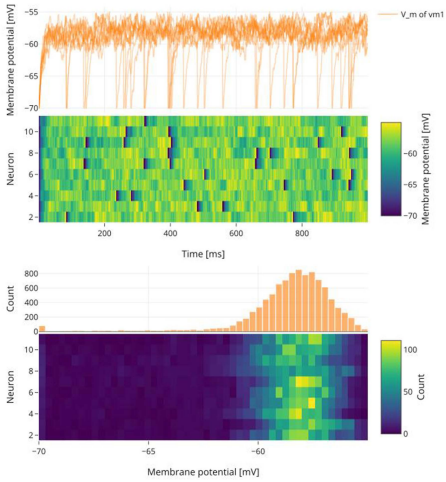

FIGURE 2
Visualization created with NEST Desktop.

signals (trace plot of analog signals for example membrane potential, different distributions of values, heat map of analog signals, two-dimensional histogram of analog signals), as seen in Figure 2. The raw data can also be inspected in files in comma-separated value (csv) format and is ready for use with other tools.

Another new aspect is the fundamentally improved model section: This allows the researcher to explore the concept and the behaviour of neuron or synapse models implemented in NEST Simulator. Since it is not always obvious how a newly defined or changed model behaves (especially for young researchers), this section provides valuable information for the daily work with neuron and synapse models.

Results and discussion

Since the releases introducing the collaborations with other software, NEST Desktop is no longer aiming solely at the classroom use-case, but rather able to simplify high-class research with cutting-edge technologies. With the extensions implemented in this GUI, experienced scientists have the possibility to use the scripting possibilities they are already familiar with, but extended by elements and visualizations that simplify their workflows considerably while providing an integration of other software suites. This supports the workflow of young researchers which need to produce simulation results quickly without requiring to invest a lot of time in learning the tool beforehand. It enables them to create sophisticated diagrams for scientific publications in their daily workflow without spending much time. This should lower the barrier for newcomers significantly and open this highly inter-disciplinary research area to a greater user base.

In order to give students, teachers, and researchers user-friendly access to the compute resources, the source code remains available under a free license. This gives the possibility to start NEST Desktop on the user's own devices and helps to grow a large community supporting the development in a long term perspective. This software is accompanied by a well-maintained documentation, which contains also video tutorials and examples for student courses [5]. These resources have been extended significantly in the recent times and are continuously updated along regular code releases.

Acknowledgements
This project has received funding from the European Union's Horizon 2020 Framework Programme for Research and Innovation under Specific Grant Agreement No. 785907 (Human Brain Project SGA2) and 945539 (Human Brain Project SGA3) and the Helmholtz Association Initiative and Networking Fund under project number SO-092 (Advanced Computing Architectures, ACA).

References

[1] NEST 3.3, Spreizer et al. 2022, [https://doi.org/10.5281/zenodo.6368024]

[2] NEST Desktop, Spreizer et al. 2021 [https://doi.org/10.1523/ENEURO.0274-21.2021]

[3] Insite: A Pipeline Enabling In-Transit Visualization and Analysis for Neuronal Network Simulations, Marcel Krüger et. al 2022 [to appear in Springer LNCS]

[4] ViSimpl: Multi-View Visual Analysis of Brain Simulation Data, Galindo et al, 2016 [https://doi.org/10.3389/fninf.2016.00044]

[5] NEST Desktop Official Documentation [ ]

GA computational model of early altered excitability in CA1 pyramidal neurons of the ventral hippocampus in Tg2576 AD mouse

Author
Elisabetta Giacalone – Institute of Biophysics, National Research Council, Palermo 90146, Italy
Carmen Alina Lupascu – Institute of Biophysics, National Research Council, Palermo 90146, Italy
Elena Spoleti – Faculty of Sciences and Technology, University Campus Bio-Medico, Rome 00128, Italy
Paraskevi Krashia – Faculty of Medicine and Surgery, University Campus Bio-Medico, Rome 00128, Italy; Department of Experimental Neurosciences, IRCCS Santa Lucia Foundation, Rome 00143, Italy
Livia La Barbera – Faculty of Sciences and Technology, University Campus Bio-Medico, Rome 00128, Italy; Department of Experimental Neurosciences, IRCCS Santa Lucia Foundation, Rome 00143, Italy
Annalisa Nobili – Faculty of Sciences and Technology, University Campus Bio-Medico, Rome 00128, Italy; Department of Experimental Neurosciences, IRCCS Santa Lucia Foundation, Rome 00143, Italy
Flavio Keller – Faculty of Medicine and Surgery, University Campus Bio-Medico, Rome 00128, Italy
Marcello D'Amelio – Faculty of Sciences and Technology, University Campus Bio-Medico, Rome 00128, Italy; Department of Experimental Neurosciences, IRCCS Santa Lucia Foundation, Rome 00143, Italy
Massimiliano Renzi – Department of Physiology and Pharmacology, Sapienza University, Rome 00185, Italy
Michele Migliore – Institute of Biophysics, National Research Council, Palermo 90146, Italy

Citation
Giacalone, E., Lupascu, C.A., Spoleti, E., Krashia, P., La Barbera, L., Nobili, A., Keller, F., D'Amelio, M., Renzi, M., Migliore, M. GA computational model of early altered excitability in CA1 pyramidal neurons of the ventral hippocampus in Tg2576 AD mouse

Introduction/Motivation

Alzheimer's disease (AD) is the most common cause of dementia characterized by gradual neurodegeneration leading to a decline in both cognitive and non-cognitive functions. The so-called amyloid hypothesis has been considered the main cause of the disease for more than 25 years but the AD's involvement in cellular and circuitry functions is still under intense investigation. To understand the key mechanisms underlying AD, extensive research is being conducted on AD's impact on early circuitry changes in the brain and cellular function modification [1,2]. In this context, the role of dopamine in hippocampal circuits during the progression of AD has been the subject of numerous studies in recent years, particularly as an initial sign of the disease [3,4]. This theory is supported by the finding of AD-related functional and behavioural abnormalities in the dorsal hippocampus of the Tg2576 AD mouse model (a well characterized mouse model of AD over-expressing the human amyloid precursor protein carrying the familial Alzheimer's disease genetic mutation) that are associated with premature degeneration of the dopaminergic system [5]. Early changes in firing characteristics and altered excitability were also observed experimentally in the ventral CA1 pyramidal neurons of Tg2576 mice.

In this poster, we show a computational model that is able to support experimental findings and offer experimentally testable predictions of the cellular mechanisms underlying functional change in ventral CA1 pyramidal neurons in the AD mouse model.

Methods

All simulations were carried out using the NEURON simulator (v8.0.0) [6].

For all simulations, we used a 3D reconstruction of a mouse hippocampal CA1 ventral pyramidal (morphology NMO_114635, [7]), downloaded from Neuromopho.org [8]. A 60 µm-long synthetic axon with a tapered diameter was added. The electrophysiological traces from a few representative neurons for each strain (WT and TG) and age (3 and 8 months) were used as reference to implement a set of biophysically detailed neuron models. In particular, we chose recordings from: six neurons of 3 months-old WT mice; seven neurons of 3 months-old Tg2576 mice; five neurons of 8 months-old WT mice; and six neurons of 8 months-old Tg2576 mice. Passive properties were manually tuned to match the observed input resistance and rheobase for each modelled neuron. Active properties included: a transient Na+ conductance; five types of K+ currents (Delayed Rectifier, KDR; A-type, KV7; one type of slow Calcium-dependent current, KCa; and a voltage and Ca2+ dependent current); a non-specific Ih current; N-, T- and L-type Ca2+ current; and a simple Ca2+-extrusion mechanism with a 100 ms time constant. Channel kinetics and distribution were from a previously published model for CA1 pyramidal neurons [9]. The kinetic parameters of Na+, delayed rectifier K+ and KV7-type K+ channels were modified to fit the specific experimental findings of this paper. To reproduce the depolarization block, we found that it was necessary to shift the Na+ activation [10]. The peak conductance of each channel type was manually tuned to fit, for each modelled neuron, the number of action potentials elicited experimentally as a function of the input current. To do this, we used a procedure aimed at identifying the minimal changes required to reproduce the experimental findings for each neuron population. The optimized values were compared using a Mann-Whitney Rank Sum Test.

Results and discussion

The model suggests that dysfunctional sodium and potassium conductances may be involved in the observed derailments of firing properties and neuronal changes, resulting in an in an anticipated depolarization-block of action

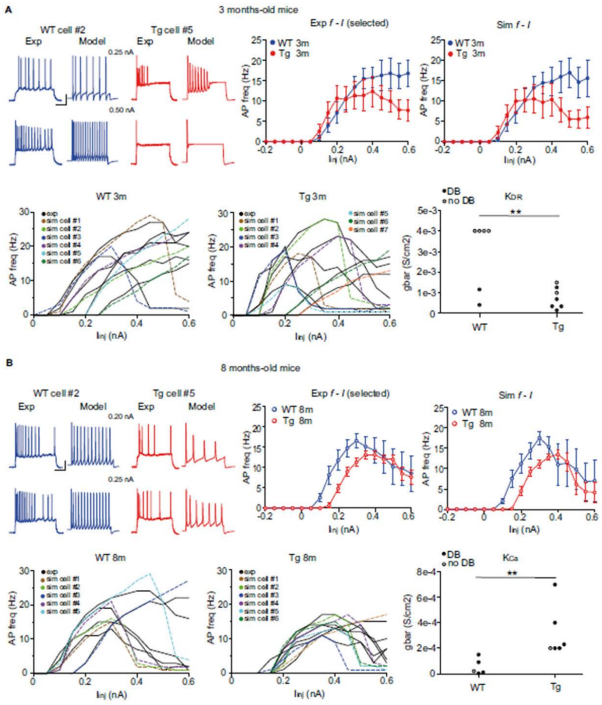

FIGURE 1

Computational modelling of electrophysiological features of ventral CA1 pyramidal neurons. A, Typical experimental and modelled somatic voltage response to current injections in neurons of 3 months-old WT or Tg mice (upper left; bars: 25 mV; 250 ms) and mean f - I relationships for selected neurons (upper right). f - I curves for each neuron (simulation vs recorded) are also shown, to depict modelling accuracy (lower left panels: black lines identify experimental data, colored dashed lines represent simulations). According to our computational analysis, the early appearance of depolarization block observed in CA1 neurons from 3-months old Tg mice could be ascribed to a significant decrease of conductance density for KDR channels in these neurons ($p < 0.001$ vs WT; lower right; open symbols depict neurons not entering the DB state; filled symbols, neurons entering DB). B, Same as in A, for neurons from 8 months-old WT or Tg mice. In this case, our computational analysis suggested that the different f - I relationships observed in Tg mice could be due to a significantly increased peak conductance for KCa channels ($p = 0.004$ vs WTs; lower right).

potential firing. In particular, we found that both a shift of sodium channel activation kinetics and the alteration of specific potassium conductances (KDr and KCa) were required to model the impaired excitability of these neurons during AD progression (Figure 1) . These results suggest that the AP firing behavior of Tg2576 ventral CA1 pyramidal neurons can be significantly altered by early changes in the expression and functional involvement of these ionic channels.

What is the nature of such initial perturbation? Interestingly, the early alterations found in the ventral CA1 of 3-month-old Tg2576 mice coincide with the first detectable degeneration of the VTA DA [11,12]. Notable, it has been shown that excitability, synaptic and behavioural deficits found in older Tg2576 animals could be rescued by administration of L-DOPA [12], suggesting that the loss of DA tone in the hippocampus following DA neuron degeneration is directly linked to excitability changes.

We thus hypothesize that reduction of homeostatic levels of extracellular DA plays a role in initial neuronal derailment eventually leading to hippocampal decline.

References

[1] Bateman, R.J., Xiong, C., Benzinger, T.L.S., Fagan, A.M., Goate, A., Fox, N.C., Marcus, D.S., Cairns, N.J., Xie, X., Blazey, T.M., et al., 2012. Clinical and biomarker changes in dominantly inherited Alzheimer's disease. N. Engl. J. Med. 367, 795–804.

[2] D'Amelio, M., Rossini, P.M., 2012. Brain excitability and connectivity of neuronal assemblies in Alzheimer's disease: from animal models to human findings. Prog. Neurobiol. 99, 42–60.

[3] Bethus, I., Tse, D., Morris, R.G.M., 2010. Dopamine and memory: modulation of the persistence of memory for novel hippocampal NMDA receptor-dependent paired associates. J. Neurosci. 30, 1610–1618.

[4] Broussard, J.I., Yang, K., Levine, A.T., Tsetsenis, T., Jenson, D., Cao, F., Garcia, I., Arenkiel, B.R., Zhou, F. M., De Biasi, M., et al., 2016. Dopamine regulates aversive contextual learning and associated in vivo synaptic plasticity in the hippocampus. Cell Rep. 14, 1930–1939.

[5] Nobili, A., Latagliata, E.C., Viscomi, M.T., Cavallucci, V., Cutuli, D., Giacovazzo, G., Krashia, P., Rizzo, F.R., Marino, R., Federici, M., et al., 2017. Dopamine neuronal loss contributes to memory and reward dysfunction in a model of Alzheimer's disease. Nat. Commun. 8, 14727.

[6] Hines, M.L., Carnevale, N.T., 1997 Aug. The NEURON simulation environment. Neural Comput 159 (6), 1179–1209. https://doi.org/10.1162/neco.1997.9.6.1179. PMID: 9248061.

[7] Ascoli, G.A., 2006. Mobilizing the base of neuroscience data: the case of neuronal morphologies. Nat. Rev. Neurosci. 7, 318–324.

[8] Ordemann, G.J., Apgar, C.J., Brager, D.H., 2019. D-type potassium channels normalize action potential firing between dorsal and ventral CA1 neurons of the mouse hippocampus. J. Neurophysiol. 121, 983–995.

[9] Migliore, R., Lupascu, C.A., Bologna, L.L., Romani, A., Courcol, J.-D., Antonel, S., Van Geit, W.A.H., Thomson, A.M., Mercer, A., Lange, S., et al., 2018. The physiological variability of channel density in hippocampal CA1 pyramidal cells and interneurons explored using a unified data-driven modeling workflow. PLoS Comput. Biol. 14, e1006423.

[10] Bianchi, D., Marasco, A., Limongiello, A., Marchetti, C., Marie, H., Tirozzi, B., Migliore, M., 2012. On the mechanisms underlying the depolarization block in the spiking dynamics of CA1 pyramidal neurons. J. Comput. Neurosci. 33, 207–225.

[11] La Barbera, L., Vedele, F., Nobili, A., Krashia, P., Spoleti, E., Latagliata, E.C., Cutuli, D., Cauzzi, E., Marino, R., Viscomi, M.T., et al., 2021. Nilotinib restores memory function by preventing dopaminergic neuron degeneration in a mouse model of Alzheimer's Disease. Prog. Neurobiol. 202, 102031.

[12] Nobili, A., Krashia, P., Cordella, A., La Barbera, L., Dell'Acqua, M.C., Caruso, A., Pignataro, A., Marino, R., Sciarra, F., Biamonte, F., et al., 2018. Ambra1 shapes hippocampal inhibition/excitation balance: role in neurodevelopmental disorders. Mol. Neurobiol. 55, 7921–7940.

Generating high performance simulations from a portable data format using arbor

Author
Thorsten Hater, Lennart P. L. Landsmeer – Jülich Supercomputing Center, Forschungszentrum Jülich, Jülich, Germany

Citation
Hater, T., Landsmeer, L.P.L. Generating high performance simulations from a portable data format using arbor.

Introduction/Motivation

Computational neuroscience is experiencing a steady growth in available simulation tools applicable to morphologically detailed cell descriptions [EDEN, NeuroGPU, Carl, Brian, ARB, NRN]. Researchers benefit from different specialisations and performance characteristics of these tools. Simulator developers likewise profit from the extended capabilities with respect to validation across tools. However, the development of models that are actually portable between simulators lags behind.

NeuroML2 is one of the few comprehensive approaches to portably describing whole simulations, but its reference implementation lacks in performance and scalability to larger simulations [NML2]. The NeuroML2 community has recently added an online database of cells and ion channels.

Our goal is to enable Arbor, a modern, performance-portable library for simulating morphologically detailed neurons to consume models in NeuronML2. However, the dynamic, object-oriented approach of NeuroML2 descriptions precludes a static implementation, as users can for example add arbitrary ion channels in their simulation design. Thus, our implementation has to match this extensibility. We choose to generate code for Arbor on a case-by-case basis.

We present nmlcc, a tool to generate optimised, full scale simulations in Arbor from a description in NeuroML2 [NMLCC]. It produces bespoke dynamics tailored to the input, resulting in speed-ups over the native NeuroML2 implementation comparable to hand-optimized code. Through Arbor, the generated simulation package is able to utilize modern hardware, including large-scale GPU clusters, scaling to millions of cells [ARB].

As a case study, we show how a single cell simulation based on [Hay] was ported to Arbor using nmlcc. Further more, we show the runtime performance of the produced model.

Methods

In essence, nmlcc is an optimising compiler from NeuroML2-conforming XML to inputs consumed by Arbor. We leverage the recently added capability of Arbor to interact with externally defined ion channel dynamics using a plugin interface. The cells' morphologies are described in standard file formats. Further, parameterization of dynamics and biophysical properties is handled via an Arbor-internal file format. These descriptions are combined together with the actual Arbor library in a Python script that also provides the network design and instantiates different cell types.

Since the ion channel dynamics are routinely the performance critical factor in simulations, we take special consideration when generating code for them. In addition to optimizations adapted from manual optimization, we add the capability to specialize to the concrete simulation, i.e. we replace all settable parameters by the actual values used and thus enable further optimizations.

Finally, we combine ion channel dynamics placed together on parts of the morphology, which further reduces overheads and uncovers more optimisation potential. Once generated, the simulation exists as a standalone bundle independent of nmlcc and only requires a recent version of Arbor and Python.

nmlcc itself is written in the high-performance, memory-safe language Rust, which offers convenient features for compiler development, e.g. Algebraic Data Types and pattern matching. The compiler is designed using a data driven approach and bootstrapped from the NeuroML2 XML schema definition. The backend is currently specific to Arbor's needs, but is designed to be swapped against another, if required, and could be adapted to cater to different simulators. Conversion and optimization from a NeuroML2 specification requires a simple command, so that users can become productive very fast.

nmlcc is an open source project under the GPL license developed at [NMLCC] and available on MacOS and Linux.

Results and discussion

To demonstrate the workflow of using Arbor in conjunction with nmlcc, we present the port of a single cell model from NeuroML2 to Arbor. We use a quite complex model taken from Hay *et al.* and describe the porting process [Hay]. Some features required upgrading to a pre-release version of Arbor, e.g. support for inhomogeneous parameters.

As an indication of the quality of nmlcc's output we study performance characteristics compared to hand-optimized ion channels in Arbor and jnml, the NeuroML2 reference implementation. jnml is likewise able to generate dynamics implementations compatible with Arbor, but as noted, performance is a critical factor. For simple dynamics like Hodgkin-Huxley, we routinely find a 3x improvement over jnml-generated output running in Arbor. These numbers are competitive with the highly optimized implementations Arbor provides as part of its built-in library.

Finally we sketch future plans on continued development and integration with the growing Arbor ecosystem.

References

[1] [EDEN] Panagiotou, S., Sidiropoulos, H., Soudris, D., Negrello, M., & Strydis, C. (2022). EDEN: A high-performance, general-purpose, NeuroML-based neural simulator. Frontiers in Neuroinformatics, 16.

[2] [NeuroGPU] Ben-Shalom, R., Ladd, A., Artherya, N., Cross, C., Kim, K., Sanghevi, H., Korngreen, A., Bouchard, K., & Bender, K. (2022). NeuroGPU: Accelerating multi-compartment, biophysically detailed neuron simulations on GPUs. Journal of Neuroscience Methods, 366, 109400.

[3] [Carl] Niedermeier, L., Chen, K., Xing, J., Das, A., Kopsick, J., Scott, E., Sutton, N., Weber, K., Dutt, N., & Krichmar, J. (2022). CARLsim 6: An Open Source Library for Large-Scale, Biologically Detailed Spiking Neural Network Simulation. In 2022 International Joint Conference on Neural Networks (IJCNN) (pp. 1–10).

[4] [Brian] Goodman, D., & Brette, R. (2009). The brian simulator. Frontiers in neuroscience, 26.

[5] [ARB] Abi Akar, N., Cumming, B., Karakasis, V., Kusters, A., Klijn, W., Peyser, A., & Yates, S. (2019). Arbor—a morphologically-detailed neural network simulation library for contemporary high-performance computing architectures. In 2019 27th euromicro international conference on parallel, distributed and network-based processing (PDP) (pp. 274–282).

[6] [NRN] Carnevale, N., & Hines, M. (2006). The NEURON book. Cambridge University Press.

[7] [NML2] Cannon, R., Gleeson, P., Crook, S., Ganapathy, G., Marin, B., Piasini, E., & Silver, R. (2014). LEMS: a language for expressing complex biological models in concise and hierarchical form and its use in underpinning NeuroML 2. Frontiers in neuroinformatics, 8, 79.

[8] [NMLCC] https://github.com/thorstenhater/nmlcc

[9] [Hay] Hay, E., Hill, S., Schürmann, F., Markram, H., and Segev, I. (2011). Models of Neocortical Layer 5b Pyramidal Cells Capturing a Wide Range of Dendritic and Perisomatic Active Properties, PLoS Comp Biol 2011

Computational modelling for non-invasive monitoring of intracranial pressure

Author
Fariba Karimi – Foundation for Research on Information Technologies in Society (IT'IS), Zurich, Switzerland; Department of Information Technology and Electrical Engineering, Swiss Federal Institute of Technology (ETH Zurich), Zurich, Switzerland
Esra Neufeld – Foundation for Research on Information Technologies in Society (IT'IS), Zurich, Switzerland
Arya Fallahi – Foundation for Research on Information Technologies in Society (IT'IS), Zurich, Switzerland; Department of Information Technology and Electrical Engineering, Swiss Federal Institute of Technology (ETH Zurich), Zurich, Switzerland
Andreas Spiegelberg – The Interface Group, Institute of Physiology, University of Zurich, Zurich, Switzerland
Andrea Boraschi – The Interface Group, Institute of Physiology, University of Zurich, Zurich, Switzerland
Jaco J.M. Zwanenburg – Department of Radiology, University Medical Center Utrecht, Utrecht, Netherlands
Vartan Kurtcuoglu – The Interface Group, Institute of Physiology, University of Zurich, Zurich, Switzerland
Niels Kuster – Foundation for Research on Information Technologies in Society (IT'IS), Zurich, Switzerland; Department of Information Technology and Electrical Engineering, Swiss Federal Institute of Technology (ETH Zurich), Zurich, Switzerland

Citation
Karimi, F., Neufeld, E., Fallahi, A., Spiegelberg, A., Boraschi, A., Zwanenburg, J.J.M., Kurtcuoglu, V., Kuster, N. Computational modelling for non-invasive monitoring of intracranial pressure.

Introduction/Motivation

Measuring intracranial pressure (ICP) is crucial for diagnosis, treatment and monitoring of craniospinal disorders. Non-invasive ICP measurement is still a grand challenge despite more than 60 years of research [1]. In this study, we tackle this challenge by computing the head impedance changes (ΔZ) during the cardiac cycles inspired by the work of Russegger and Ennemoser [2]. We use the results to establish correlations between the non-invasively measurable signal and features of brain pulsation, demonstrating its potential as non-invasive biomarker.

Methods

Exchanging the blood and cerebrospinal fluid (CSF) between cranial and spinal compartments during the cardiac cycle changes the geometry and dielectric properties of the head and thus its impedance (Z). Therefore, computing ΔZ between head-surface electrodes is a potential biomarker for non-invasive ICP measurement. Since ΔZ is very small compared to the impedance ($\Delta Z << Z$), computing it in the traditional manner – i.e., changing the geometry and dielectric properties of the head and computing its impedance by solving Maxwell equations for several time-steps during the cardiac cycle – is computationally huge and numerically challenging. To overcome these issues, we developed an accurate and efficient method based on the reciprocity theorem combined with verified physics-motivated approximations to computing transient $\Delta Z(t)$ for a given 3+1D brain deformation field, using a single electromagnetic simulation. The distribution of ΔZ-sensitivity to local interface-motion ('sensitivity map') computed as the functional derivate of ΔZ with respect to local displacements.

The proposed algorithm was verified in four different (semi-)analytic benchmarks and subsequently applied to an accurate head and neck anatomical model (MIDA model [3]). We then used 4D brain pulsation data from eight healthy young subjects to compute $\Delta Z(t)$ over the cardiac cycle [4]. After processing the deformation data (registration of the MIDA anatomy to the deformation data anatomy, preprocessing to remove the background error, masking of unreliable data in CSF and nearby regions, and

reconstruction of the missing data), we coupled this data to the sensitivity map and computed ΔZ for each subject. The method is also being validated using a prototype device (PEM1, Cephalotec, Horgen, Switzerland).

Using principal component analysis, correlations between the simulated non-invasively measurable signal and features (rotation, motion, volume change) of brain pulsation were extracted.

Results and discussion

1D, symmetric and asymmetric 2D, and 3D benchmarks were developed for verification (see Fig. 1). The relative error between the analytic solution and the proposed method is below 10% (worst-case), demonstrating the algorithm accuracy. The method was applied to the MIDA model and coupled to deformation data (see Fig. 2). Subsequently, the sensitivity map and processed deformation data were combined to compute ΔZ for all eight subjects. Figure 2 shows the electrode configuration, corresponding sensitivity map on the cortex, capacitance change (ΔC) and resistance change (ΔR) for one subject and the average for all eight subjects.

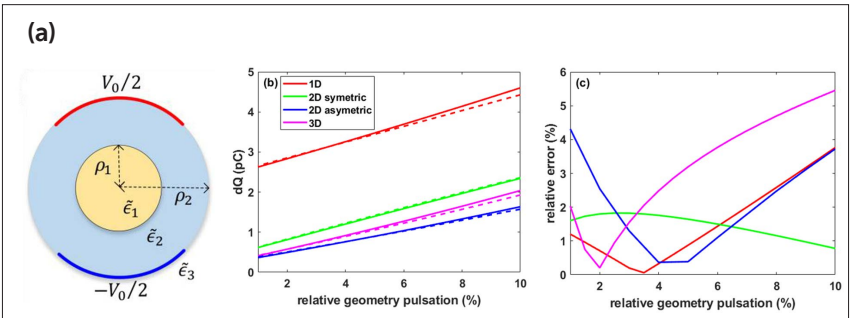

FIGURE 1

Verification results obtained for the 1D, 2D, and 3D benchmarks (dQ is the electric charge variation, which is trivially convertible to ΔZ). (**a**) Geometry of 2D symmetric benchmark (as an example), (**b**) dQ computed using the (semi)analytical solution (solid lines) vs dQ from the developed method (dashed lines), and (**c**) relative error between (semi)analytical solution and the proposed method.

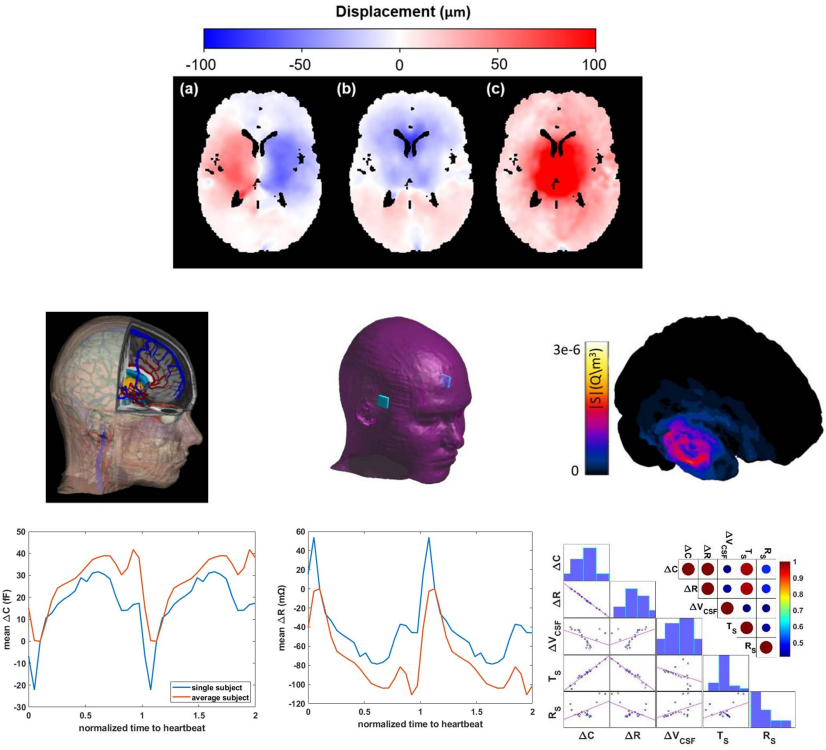

FIGURE 2

Top row: visualization of the processed deformation data; middle row: MIDA model, electrode configuration, and absolute value of the sensitivity map on the cortex; bottom row: ΔC (capacitance change) and ΔR (resistance change) for one subject and the average of all eight subjects together with the linear correlation coefficient and the correlation between ΔC and ΔR and the brain pulsation features (ΔV_{CSF}: CSF volume change, T_S: brain motion, R_S: brain rotation).

In this study, we developed an efficient and robust method for solving dynamic electromagnetic problems and verified it. We used the new method to compute transient ΔZ as a non-invasive ICP biomarker. Statistically

significant correlations between inter-subject differences in the (simulated) non-invasively measurable signal (i.e., capacitance and resistance change) and brain pulsation features demonstrating its potential as a non-invasive biomarker. This study paves the way toward experimental validation of the proposed method using the Cephalotec device.

Acknowledgements
The authors would like to thank the Swiss National Science Foundation (Grant no: 205321_182683) for providing financial support to this project.

References

[1] Evensen KB, Eide PK. Fluids and Barriers of the CNS. 2020;17(1), pp.1-33

[2] Russegger L, Ennemoser O. Wiener Klinische Wochenschrift. 1990; 102(18), pp.543-547.

[3] Iacono MI et al., PloS one. 2015; 10(4), p.e0124126.

[4] Adams AL et al., Neuroimage. 2020; 208, p.116466.

Estimation of microscale connectivity from spiking activity of macaque visuomotor cortices

Author
Aitor Morales-Gregorio – Institute of Neuroscience and Medicine (INM-6) and Institute for Advanced Simulation (IAS-6) and JARA-Institut Brain Structure-Function Relationships (INM-10), Jülich Research Centre, Jülich, Germany; Institute of Zoology, University of Cologne, Cologne, Germany
Robin Gutzen – Institute of Neuroscience and Medicine (INM-6) and Institute for Advanced Simulation (IAS-6) and JARA-Institut Brain Structure-Function Relationships (INM-10), Jülich Research Centre, Jülich, Germany; Theoretical Systems Neurobiology, RWTH Aachen University, Aachen, Germany
Paulina A. Dąbrowska– Institute of Neuroscience and Medicine (INM-6) and Institute for Advanced Simulation (IAS-6) and JARA-Institut Brain Structure-Function Relationships (INM-10), Jülich Research Centre, Jülich, Germany; Theoretical Systems Neurobiology, RWTH Aachen University, Aachen, Germany
Alper Yegenoglu – SDL Neuroscience, Jülich Supercomputing Centre (JSC), Institute for Advanced Simulation, JARA, Jülich Research Centre, Jülich, Germany; Institute of Geometry and Applied Mathematics, Department of Mathematics, RWTH Aachen University, Aachen, Germany
Sandra Diaz-Pier – SDL Neuroscience, Jülich Supercomputing Centre (JSC), Institute for Advanced Simulation, JARA, Jülich Research Centre, Jülich, Germany
Sarah Palmis – Institut de Neurosciences de la Timone (INT), CNRS & Aix-Marseille Université, Marseille, France
Sofia Paneri – Institute of Applied and Computational Mathematics, Foundation for Research and Technology Hellas, Heraklion, Greece; Department of Basic Sciences, Medical School, University of Crete, Heraklion, Greece
Alexandre René – Institute of Neuroscience and Medicine (INM-6) and Institute for Advanced Simulation (IAS-6) and JARA-Institut Brain Structure-Function Relationships (INM-10), Jülich Research Centre, Jülich, Germany; Department of Physics, University of Ottawa, Ottawa, Canada

Panagiotis Sapountzis – Institute of Applied and Computational Mathematics, Foundation for Research and Technology Hellas, Heraklion, Greece
Markus Diesmann – Institute of Neuroscience and Medicine (INM-6) and Institute for Advanced Simulation (IAS-6) and JARA-Institut Brain Structure-Function Relationships (INM-10), Jülich Research Centre, Jülich, Germany; Department of Psychiatry, Psychotherapy and Psychosomatics, School of Medicine, RWTH Aachen University, Aachen, Germany; Department of Physics, Faculty 1, RWTH Aachen University, Aachen, Germany
Sonja Grün – Institute of Neuroscience and Medicine (INM-6) and Institute for Advanced Simulation (IAS-6) and JARA-Institut Brain Structure-Function Relationships (INM-10), Jülich Research Centre, Jülich, Germany; Theoretical Systems Neurobiology, RWTH Aachen University, Aachen, Germany
Johanna Senk – Institute of Neuroscience and Medicine (INM-6) and Institute for Advanced Simulation (IAS-6) and JARA-Institut Brain Structure-Function Relationships (INM-10), Jülich Research Centre, Jülich, Germany
Georgia G. Gregoriou – Institute of Applied and Computational Mathematics, Foundation for Research and Technology Hellas, Heraklion, Greece; Department of Basic Sciences, Medical School, University of Crete, Heraklion, Greece
Bjørg E. Kilavik – Institut de Neurosciences de la Timone (INT), CNRS & Aix-Marseille Université, Marseille, France
Sacha J. van Albada – Institute of Neuroscience and Medicine (INM-6) and Institute for Advanced Simulation (IAS-6) and JARA-Institut Brain Structure-Function Relationships (INM-10), Jülich Research Centre, Jülich, Germany; Institute of Zoology, University of Cologne, Cologne, Germany

Citation
Morales-Gregorio, A., Gutzen, R., Dąbrowska, P.A., Yegenoglu, A., Diaz-Pier, S., Palmis, S., Paneri, S., René, A., Sapountzis, P., Diesmann, M., Grün, S., Senk, J., Gregoriou, G.G., Kilavik, B.E., van Albada, S.J. Estimation of microscale connectivity from spiking activity of macaque visuomotor cortices.

Introduction/Motivation

Connectivity structure is essential to understanding the activity and function of neuronal networks in the central nervous system. While the long-range

connectivity in the macaque cortex has been thoroughly studied [1, 2], little is known about the microscale connectivity within cortical areas and across cortical layers—"the microconnectome"— outside of the early sensory and primary motor areas. It has been hypothesized that the microconnectome follows a canonical motif across the cortex, but quantitative measurements to date are still insufficient to fully verify this claim. Here, we present a novel method to estimate the microconnectome from neuronal spiking activity across the visuo-parieto-frontal gradient and thus shed light on the extent to which it is canonical across the cortex.

Methods

We measured the resting-state activity from several cortical areas (V1, V4, M1, PMd, dlPFC) in macaque monkeys (*Macaca mulatta*) [3-6]. From the spike-sorted activity, we calculated several single-neuron summary statistics for 10 s data slices, quantifying the firing rates, irregularity, and correlations. Figure 1

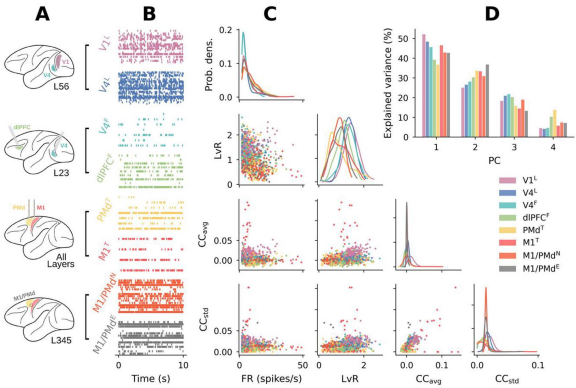

FIGURE 1

Overview of experimental data and summary statistics. **A)** Schematic representation of the data recording location [3-6]. **B)** Sample recordings of simultaneous spike trains from each dataset for a 10 s window. Superscripts refer to the subject name. **C)** Summary statistics of the single-unit spike trains. Each point in the scatter plot corresponds to a 10 s spike train of a single neuron. CC refers to the cross-correlations of the neuron with all other neurons in the recording. **D)** Variance explained by the first four principal components (PC) of the multi-dimensional summary statistics.

shows a summary of the spiking data and summary statistics for all the areas studied. The analysis was implemented using the NetworkUnit framework to ensure reproducibility and interoperability [7]. We then introduce a custom optimization algorithm [8]—a combination of random search, gradient descent, and genetic algorithms—which we use to estimate anatomical parameters from the multi-dimensional summary statistics. The optimization algorithm was implemented in the learning-to-learn (L2L) framework [8]. The cost function of the optimization algorithm is the Wasserstein distance between the multi-dimensional summary statistics of the experimental and model activity.

Results and discussion

To elucidate whether the resting-state activity is a unique signature of each cortical area, we test the differences of the multi-dimensional summary

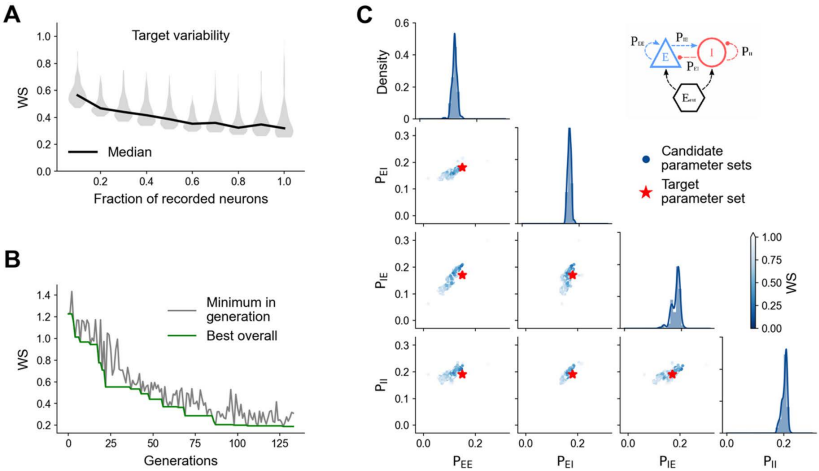

FIGURE 2

Proof of concept of the optimization algorithm using synthetic data from a random balanced spiking neuron network. **A)** Variability of the Wasserstein distance (WS) in the target simulation when recording only a certain fraction of the neurons in the model. **B)** Progress of the optimization algorithm, showing lowest WS overall and within each generation. **C)** Pairplot of estimated parameter sets.

statistics across areas and layers. Indeed, a multivariate analysis of variance (MANOVA) reveals significant differences between cortical areas within and across experiments.

Furthermore, we demonstrate the validity of our optimization method by first applying it to synthetic data. Our method can correctly estimate the connectivity parameters of a small balanced spiking neuron network, from the multi-dimensional summary statistics of spiking activity alone (Figure 2). Further work will include adapting the methods to larger models [9] and estimating the connectivity parameters from the experimental data.

Acknowledgements
This project has received funding from the DFG Priority Program (SPP 2041 "Computational Connectomics"); the EU's Horizon 2020 Framework under Grant Agreements No. 785907 and 945539 (HBP SGA2 and SGA3); the DFG (RTG 2416 "MultiSenses-MultiScales"); the CNRS Multidisciplinary Exploratory Projects initiative; and the FLAG-ERA grant PrimCorNet.

References

[1] Bakker et al. Frontiers in Neuroinformatics 6 (2012)

[2] Markov et al. Cerebral Cortex 24(1), 17-36 (2012)

[3] Xing*, Morales-Greogio* et al. Scientific Data 9(1), 77 (2022)

[4] Kilavik. Society for Neuroscience (2018)

[5] Brochier et al. Scientific Data 5(1), 180055 (2018)

[6] Sapountzis et al. PNAS 119 (40) e2202564119 (2022)

[7] Gutzen et al. Frontiers in Neuroinformatics 12:90 (2018); RRID:SCR_016543

[8] Yegenoglu et al. Frontiers in Computational Neuroscience 16, 885207 (2022)

[9] Potjans and Diesmann. Cerebral Cortex 24(3):785-806 (2014)

Backpropagation biases recurrent neural network models of the brain

Author
Thomas Schwarz, Meghana Gayatri Potta, Pau Vilimelis Aceituno, Benjamin F. Grewe – Institute of Neuroinformatics, University of Zürich and ETH Zürich, Zurich, Switzerland

Citation
Schwarz, T., Potta, M.G., Aceituno, P.V., Grewe, B.F. Backpropagation biases recurrent neural network models of the brain.

Introduction/Motivation

In neuroscience, recurrent neural networks (RNNs) are popular models for cortical neural networks. Machine learning training algorithms provide networks in terms of weights, from which task-relevant features are identified [Runyan et al. 2017], or the dynamics of latent features are studied [Mante & Sussillo 2014]. This process is very appealing because it allows neuroscientists to generate testable hypotheses before running costly experiments.

However, a neural network trained with machine learning tools might not provide the same solution as biology [Schaeffer et al. 2022]. This poses a problem, because it implies that we cannot generate hypotheses by blindly trying machine learning procedures. To address it, we need to find which types of solutions machine learning can find, and which are outside of its range, so that we can identify the solutions that are outside of its range.

We focus on Backpropagation Through Time (BPTT), the most common algorithm for training RNNs. We study its ability to learn to imitate the dynamics of a RNN in a simple setting where the solution can be characterized using tools from systems and control theory.

Methods

Teacher student training:

A key problem in neuroscience is that we usually do not know the underlying solution found by the brain. In this work we sidestep this problem by using a teacher-student setting, where a filter (the teacher) receives an input time

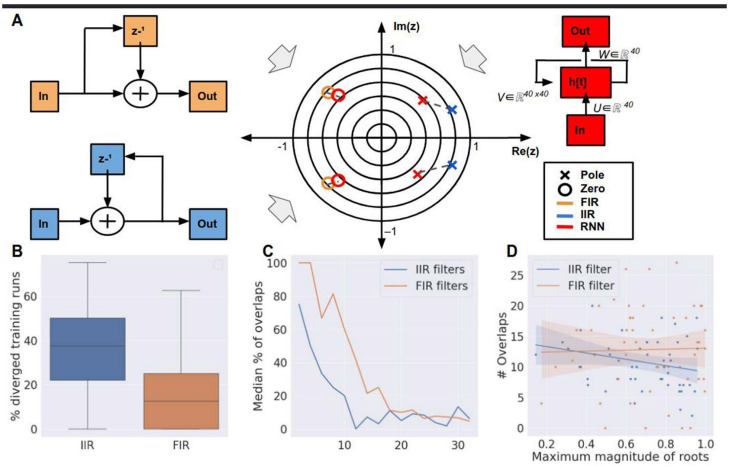

FIGURE 1

A) We generate training data from a FIR (top left) or IIR filter (bottom left), fit a single-layer linear RNN (top right) using BPTT and count the overlaps between their zeros or poles in the complex plane (middle). **B**) The training loss of RNNs imitating IIR filters diverges more often than for RNNs imitating FIR filters (not-significant). **C**) The zeros of the RNN overlap more often with the zeros of the FIR filter it imitates than do its poles with those of the IIR filter, across a range of filter orders. **D**) BPTT finds fewer poles as the largest pole of an IIR filter approaches the unit circle (the shaded envelopes correspond to the 95% CI of a bootstrapped linear regression).

series (Gaussian white noise), and generates an output (Fig1a). The student network can observe both the input and output to the teacher, and it is trained with BPTT to imitate the teacher. This setting allows us to know the dynamics of the teacher, which we can then use to evaluate how well the teacher and student align.

Characterizing Linear Systems

Even if we have a teacher-student setting, we need to be able to evaluate how different the student and the teacher are. This is not evident, as different networks can implement the same underlying computation with the same latent dynamics [Bishop 2006]. Here, we focus on linear systems like linear RNNs whose dynamics we can fully characterize in terms of the poles and the zeros [Oppenheim et al, 1996].

In linear RNNs, the poles of a filter correspond to its feedback architecture, while the zeros encode its feedforward structure. To investigate how well BPTT can characterize feedforward and feedback structures, we focus on two architectures:

- Finite Impulse Response (FIR) filters, which have only zeroes and are thus purely feedforward.

- Infinite Impulse Response (IIR) filters which have only poles and are thus purely feedback.

Comparison of the student RNN with the constructed filter

The zeros or poles of a student RNN can be estimated from its impulse response or the eigenvalues of its recurrent weight matrix [Kaufmann, 1973], respectively. This allows us to compare the dynamics of the filter and RNN in the complex plane, counting the overlaps of their poles or zeros within a small radius (less than the 5th percentile of distances between the filter's poles or zeros).

Results and discussion

BPTT finds the zeros of FIR filters more easily than the poles of the IIR filters (Fig1b). This trend is exacerbated as the order of IIR and FIR filters grows, with more complex models being harder to fit but with IIRs being notably harder (Fig1c). Since IIR filters represent the recurrent part of the dynamics, we hypothesize that a system that is more strongly driven by recurrent dynamics would be harder to fit. Indeed, BPTT imitates IIR filters more poorly as the largest pole approaches the unit circle (where recurrent dynamics are strongest; Fig1d). This suggests exploding gradients as the reason for which RNNs struggle to learn as the length of filters grows [Pascanu et al, 2012].

Problematically, finding only some of the poles of an IIR filter leads to poor out-of-distribution generalization (Fig2a). In this case, an RNN may still imitate the filter's response to input from the data distribution on which it was trained (Gaussian white noise; Fig2b) but fail to do so in response to data outside this distribution is fed into the RNN imitates (impulse; Fig2c).

Our work suggests that BPTT is biased towards feed-forward solutions. In particular, as feedforward structures - like FIR filters - can be specified using

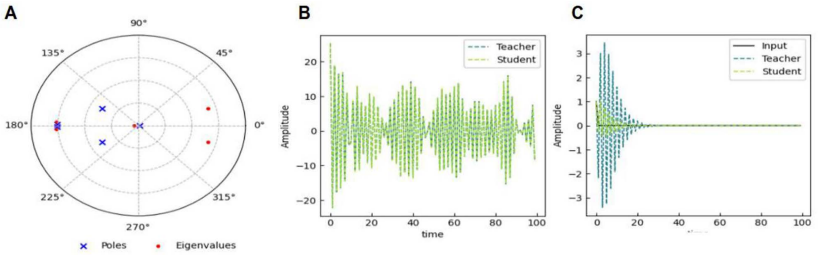

FIGURE 2

A) the eigenvalues (i.e. poles) of the RNN partially overlap with the poles of the imitated IIR filter. The output of the RNN and the corresponding IIR filter are similar when supplying Gaussian white noise as an input (**B**) but differ when inputting a single impulse (**C**).

only zeros (no poles), BPTT discovers them more easily than strong recurrent structures – like IIR filters.

This bias raises concerns about the applicability of BPTT in modeling neural circuits that are often close to the instability threshold [Wilting and Priesemann, 2019; Cocci et al 2017].

Future work should characterize the failure of BPTT to find the right network structure for other tasks and non-linear networks, potentially by combining dynamical systems with statistical learning theory [Boussange et al, 2022]. Another line of research is to study other algorithms that can be used to train RNNs or design variants of BPTT that could alleviate the current problems.

References

Runyan, C. A., Piasini, E., Panzeri, S., & Harvey, C. D. (2017). Distinct timescales of population coding across cortex. Nature, 548(7665), 92-96.

Mante V, Sussillo D, Shenoy KV, Newsome WT. Context-dependent computation by recurrent dynamics in prefrontal cortex [Internet]. Vol. 503, Nature. Springer Science and Business Media LLC; 2013. p. 78–84. Available from: http://dx.doi.org/10.1038/nature12742

Schaeffer, Rylan, et al. "No Free Lunch from Deep Learning in Neuroscience: A Case Study through Models of the Entorhinal-Hippocampal Circuit." 2022, https://doi.org/10.1101/2022.08.07.503109.

Bishop C. Pattern Recognition and Machine Learning. Springer; 2006.

Oppenheim A, Willsky A, Nawab H. Signals and Systems. Prentice-Hall 1996

Kaufman, Ilia. "On poles and zeros of linear systems." IEEE Transactions on Circuit Theory 20.2 (1973): 93-101.

Pascanu R, Mikolov T, Bengio Y. On the difficulty of training Recurrent Neural Networks [Internet]. arXiv; 2012. Available from: https://arxiv.org/abs/1211.5063

Cocchi, Luca, et al. "Criticality in the Brain: A Synthesis of Neurobiology, Models and Cognition." Progress in Neurobiology, vol. 158, 2017, pp. 132–152., https://doi.org/10.1016/j.pneurobio.2017.07.002.

Wilting, J, and V Priesemann. "Between Perfectly Critical and Fully Irregular: A Reverberating Model Captures and Predicts Cortical Spike Propagation." Cerebral Cortex, vol. 29, no. 6, 2019, pp. 2759–2770., https://doi.org/10.1093/cercor/bhz049.

Boussange, Victor, and Loïc Pellissier. "Eco-Evolutionary Model on Spatial Graphs Reveals How Habitat Structure Affects Phenotypic Differentiation." Communications Biology, vol. 5, no. 1, 2022, https://doi.org/10.1038/s42003-022-03595-3

Incremental awake-NREM-REM learning cycles: Cognitive and energetic effects in a multi-area thalamo-cortical spiking model

Author
Leonardo Tonielli – Istituto Nazionale di Fisica Nucleare (INFN) Sezione di Roma, Rome, Italy
Chiara De Luca – PhD Behavioural Neuroscience at La Sapienza University of Rome, Rome, Italy; Istituto Nazionale di Fisica Nucleare (INFN) Sezione di Roma, Rome, Italy
Bruno Golosio – Istituto Nazionale di Fisica Nucleare (INFN) Sezione di Cagliari, Cagliari, Italy; Dipartimento di Fisica, Università di Cagliari, Italy
Gianmarco Tiddia – Istituto Nazionale di Fisica Nucleare (INFN) Sezione di Cagliari, Cagliari, Italy; Dipartimento di Fisica, Università di Cagliari, Italy
Irene Bernava – Istituto Nazionale di Fisica Nucleare (INFN) Sezione di Roma, Rome, Italy
Cristiano Capone – Istituto Nazionale di Fisica Nucleare (INFN) Sezione di Roma, Rome, Italy
Davide Cipollini – Bernoulli Institute for Mathematics, Computer Science and Artificial Intelligence, University of Groningen, The Netherlands
Giulia De Bonis – Istituto Nazionale di Fisica Nucleare (INFN) Sezione di Roma, Rome, Italy
Cosimo Lupo – Istituto Nazionale di Fisica Nucleare (INFN) Sezione di Roma, Rome, Italy
Elena Pastorelli – Istituto Nazionale di Fisica Nucleare (INFN) Sezione di Roma, Rome, Italy
Francesco Simula – Istituto Nazionale di Fisica Nucleare (INFN) Sezione di Roma, Rome, Italy
Pier Stanislao Paolucci – Istituto Nazionale di Fisica Nucleare (INFN) Sezione di Roma, Rome, Italy

Citation
Tonielli, L., De Luca, C., Golosio, B., Tiddia, G., Bernava, I., Capone, C., Cipollini, D., De Bonis, G., Lupo, C., Pastorelli, E., Simula, F., Paolucci, P.S. Incremental awake-NREM-REM Learning Cycles: Cognitive and energetic effects in a multi-area thalamo-cortical spiking model

Introduction/Motivation

The alternation of wakefulness and sleep supports the brain energetic and cognitive efficiency in a large variety of high-level functions: among them, the capability of fast incremental learning from a few noisy examples, as well as the ability to associate similar memories in autonomously-created categories, to combine contextual hints with sensory perceptions and to maintain the metabolic cost of brain functions within a budget notwithstanding the progressive increment in knowledge and performance[1][2]. Sleep is known to be essential for a performance, but the mechanisms underlying its role in supporting learning and energetic management are still to be clarified. This work leverages the recent experimentally driven hypotheses of apical isolation and apical drive[3][4] principles to induce in a model some of the favourable energetic and cognitive effects associated to NREM and REM sleep, reconciling the experimental observation of [5][6]. Also, we follow the apical amplification[7] concept to combine context and perception during awake learning. This way, we added REM to the brain states accessible to the thalamo-cortical spiking model [1][2] that demonstrated the effects of incremental awake-NREM learning cycles. Specifically, we investigate both the effects of sleep on the internal synaptic structure of the network and on its neural activity in a two-area model. We demonstrate the homeostatic effect of slow-wave and dreaming-like phases of sleep on cortico-cortical synapses performing multiple sleep cycles and we show the consequent beneficial energetic consumption effects while keeping the sleep-induced cognitive effects.

Methods

In this work, we improved to REM simulation the data-driven thalamo-cortical spiking model[1][2] that was already able to carry out cognitive tasks (such as object recognition or decision-making), while expressing realistic brain dynamics in different brain states (AWAKE and NREM). In particular, the model now is able to experience AWAKE NREM and REM cycles through the modulation of adaptation, synaptic asymmetry and inhibitory conductance parameters. Specifically, we implemented a multi-area thalamo-cortical spiking model in NEST[8] made of adaptive exponential conductance based excitatory and inhibitory neurons: the thalamic layer projects into the cortical layer through feed-forward synaptic connections. The cortical layer, in turn, is organized into two areas recurrently and reciprocally connected, as depicted in Figure 1A. Also, the cortex project towards the thalamic layer through top-down back-ward connections. During the awake phase, a visual input[9] is encoded into the thalamic layer and projected to the cortical one: each area in the cortex has access to a different portion of the visual input with a region of overlapping. Plastic synapses are updated in the training and sleeping phase through a STDP (Spike-timing-dependent plasticity) synaptic rule. The training of the network is implemented with a combination of lateral contextual and perceptual signals to correctly sculpt the synaptic weight encoding for the learnt examples, analogously as in [1], in accordance with an Apical Amplification situation[7]. The training protocol is unsupervised, meaning that no information concerning the perception class is provided to the cortex. During the classification phase, on the other hand, the network is provided with a perceptual signal only. In the sleeping phase, the network is not exposed to any perceptual signal and is stimulated by a random lateral signal. During REM sleep the network adaptation is decreased with respect to the awake state [12] while all cortico-cortical connections are active and plastic, in particular those connecting the two areas, implementing an Apical Drive-like situation[3,4]. To emulate the NREM sleep, on the other hand, the adaptation is increased [12] and inter-area cortico-cortical connections are cut, in accordance with the Apical Isolation principle[3,4].

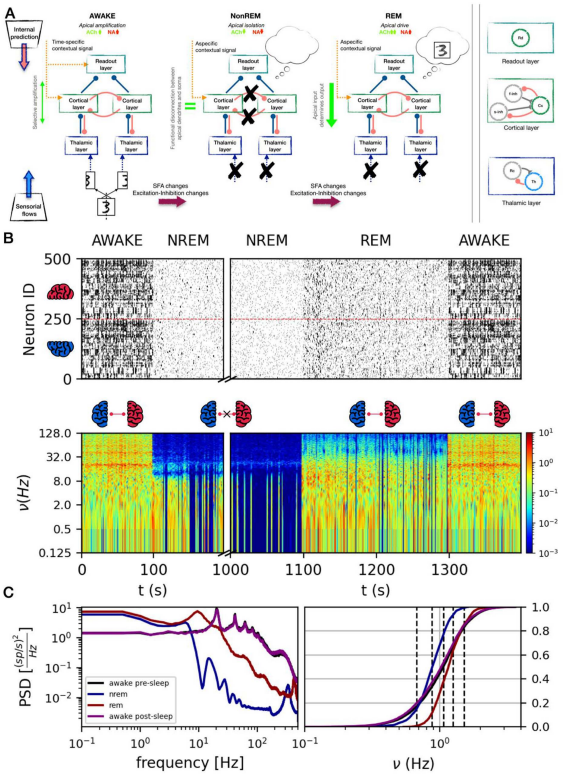

FIGURE 1

Awake-NREM-REM cycle. **A)** Network structure: two-area thalamo-cortical model with interconnected cortical populations in awake, nrem and rem phases (Apical Amplification[7], Apical Isolation and Apical Drive principles [3,4]) **B)** Rastergram (upper) and Spectrogram (lower)of network cortical activity across one awake-NREM-REM cycle. The dashed horizontal red line separates neurons belonging to different areas; Coloured brain hemispheres icons depict whether inter-areal connections are active or not during simulated brain states **C)** Network's Power Spectral Density (left) and Neuron Mean Firing Rate (right) in awake, NREM, REM stages. The dashed vertical lines indicate awake pre-sleep distribution sextiles. Results are comparable with what experimentally observed[11,5].

Results and discussion

First, we show the network is able to perform one AWAKE-NREM-REM cycle and to reproduce rhythms comparable with experimental data (Fig1B-C), then we studied the effects of two sleep cycles on both classification performances and energy consumption (fig2A-B). To show such effects on the network cognitive tasks, we tested the classification performances when classifying the

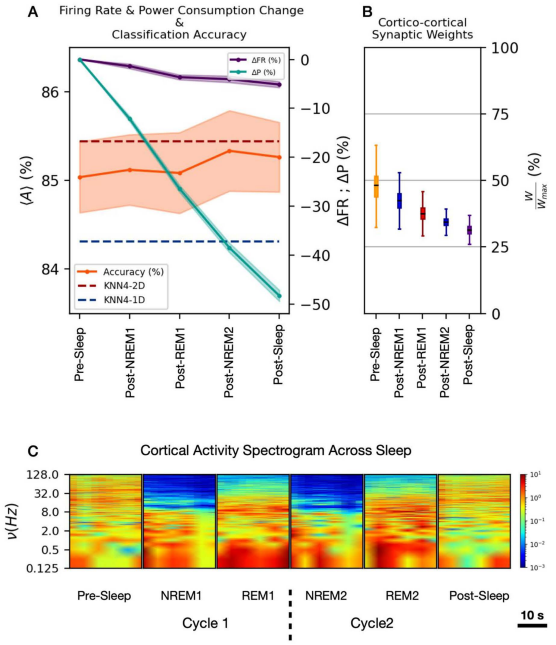

FIGURE 2

Effects of sleep on synaptic structure and network performance. **A)** Network Mean Firing Rate (purple) and Power Consumption (light-blue) change and Classification Accuracy (orange). Horizontal dashed lines make the comparison with monocular (red) and binocular-like (blue) K-Nearest-Neighbour 4 algorithm **B)** Homeostatic effects of sleep: box-plots describing the cortico-cortical synaptic weights distribution dynamics across two awake-nrem-rem cycles. **C)** Spectrogram of the cortical network activity during 2 sleep cycles. Only the first 25 seconds of the activity of each stage are reported here.

MNIST[9] dataset after a balanced training over 5 examples belonging to 10 classes (averages shown in the graphs are performed considering 40 training subsets). The firing rate cumulative distribution and power spectra of the network activity during awake classification, NREM and REM stages (shown in Figure 1B-C) are comparable with what is expected by experimental biological recordings [5,11]. In Figure 2B we show the homeostatic effect of sleep on cortical synapses leading to a general reduction of the cortico-cortical synaptic weights and the sharpening of the distribution. This is reflected on the classification and energetics network performance: as depicted in Figure 2A classification accuracy is assessed stable across sleep, close to the theoretical upper-limit imposed by a binocular-like K-Nearest-Neighbour algorithm (KNN4-2D, Fig2A). Whereas, network mean firing rate and power consumption show a significant decrease (about 5%, 50% respectively). Last in Figure 2C we show in detail the spectrogram of the cortical activity during each state experienced by the network, in order to highlight the different oscillatory behaviour of each brain state.

Acknowledgements
This work has been supported by the European Union Horizon 2020 Research and Innovation program under the FET Flagship Human Brain Project (grant agreement SGA3 n. 945539) and by the INFN APE Parallel/ Distributed Computing laboratory. D. Cipollini contributed to this work during his master thesis research project at La Sapienza University of Rome.

References

[1] Golosio, B., De Luca, C., Capone, C., Pastorelli E, Stegel G, Tiddia G, et al. (2021) "Thalamo-cortical spiking model of incremental learning combining perception, context and NREM-sleep", PLoS Comput Biol 17(6): e1009045. https://doi.org/10.1371/journal.pcbi.1009045

[2] Capone, C., Pastorelli, E., Golosio, B. et al. Sleep-like slow oscillations improve visual classification through synaptic homeostasis and memory association in a thalamo-cortical model. Sci Rep 9, 8990 (2019). https://doi.org/10.1038/s41598-019-45525-0

[3] Aru, J., Suzuki, M., Larkum, M.E. (2020) "Cellular Mechanisms of Conscious Processing", Trends in Cognitive Sciences 24(10) https://doi.org/10.1016/j.tics.2020.07.006

[4] Aru, J. Siclari, F., Phillips, W.A., Storm, J.F. (2020) "Apical drive - A cellular mechanism of dreaming?" Neuroscience and Biobehavioral Reviews, 119 p.440-445 https://doi.org/10.1016/j.neubiorev.2020.09.018

[5] B. O. Watson et al. "Network Homeostasis and State Dynamics of Neocortical Sleep." https://doi.org/10.1016/j.neuron.2016.03.036

[6] Giulio Tononi, Chiara Cirelli. Sleep and the Price of Plasticity: From Synaptic and Cellular Homeostasis to Memory Consolidation and Integration. Neuron, 2014; 81 (1): 12 DOI: 10.1016/j.neuron.2013.12.025

[7] Larkum, M. (2013) "A cellular mechanism for cortical associations: an organizing principle for the cerebral cortex" Trends in neuroscience, 36(3) https://doi.org/10.1016/j.tins.2012.11.006

[8] Fardet, T. et al. Vennemo, Stine Brekke, Mitchell, Jessica, Mørk, Håkon, Graber, Steffen, Hahne, Jan, Spreizer, Sebastian, Deepu, Rajalekshmi, Trensch, Guido, Weidel, Philipp, Jordan, Jakob, Eppler, Jochen Martin, Terhorst, Dennis, Morrison, Abigail, Linssen, Charl, Antonietti, Alberto, Dai, Kael, Serenko, Alexey, Cai, Binghuang, ... Plesser, Hans Ekkehard. (2021). NEST 2.20.2 (2.20.2). Zenodo. https://doi.org/10.5281/zenodo.5242954

[9] Y. LeCun, L. Bottou, Y. Bengio, and P. Haffner. "Gradient-based learning applied to document recognition." Proceedings of the IEEE, 86(11):2278-2324, November 1998. [on-line version]

[10] H.R. Colten, B.M. Altevogt. "Sleep Disorders and Sleep Deprivation: An Unmet Public Health Problem" Institute of Medicine (US) Committee on Sleep Medicine and Research. Washington (DC): National Academies Press (US) (2006) 10.17226/11617

[11] González, J. et al. (2019) "Decreased electrocortical temporal complexity distinguishes sleep from wakefulness." Scientific Reports 9: 18457 https://doi.org/10.1038/s41598-019-54788-6

[12] Krishnan, G.P. et al. "Cellular and neurochemical basis of sleep stages in the thalamocortical network." eLife 2016;5:e18607 10.7554/eLife.18607

Ethics and society

Key ethical and legal principles for global brain data governance

Author
Paschal Ochang, Bernd Carsten Stahl, Damian Eke – Centre for Computing and Social Responsibility, De Montfort University, Leicester, UK

Citation
Ochang, P., Stahl, B.C., Eke, D. Key ethical and legal principles for global brain data governance.

Introduction/Motivation

The advancement of neuroscience is currently generating big brain data and brain datasets (Fothergill et al., 2019)large-scale data collection and analysis enabled by novel and emergent technologies. Each step of this work involves aspects of ethics, ranging from concerns for adherence to informed consent or animal protection principles and issues of data re-use at the stage of data collection, to data protection and privacy during data processing and analysis, and issues of attribution and intellectual property at the data-sharing and publication stages. Significant dilemmas and challenges with far-reaching implications are also inherent, including reconciling the ethical imperative for openness and validation with data protection compliance and considering future innovation trajectories or the potential for misuse of research results. Furthermore, these issues are subject to local interpretations within different ethical cultures applying diverse legal systems emphasising different aspects. Neuroscience big data require a

concerted approach to research across boundaries, wherein ethical aspects are integrated within a transparent, dialogical data governance process. We address this by developing the concept of \"responsible data governance,\" applying the principles of Responsible Research and Innovation (RRI which are used for various purposes and also exist in various collaborative platforms which have been developed as standards for neuroscientists to share, use, build analysis tools, and store brain data (Teeters et al., 2015). These brain data and datasets are generated and reside in various brain projects across various jurisdictions, therefore are governed using various ethical and legal principles (Rommelfanger et al., 2018; Eke et al., 2021). Ethical and legal principles serve as tools to enhance the efficient management of data to depict data governance and are considered to reflect societal expectations, public values, and norms. The importance of ethical and legal principles has been highlighted in the field of brain data through the development of neuroethics which provides a set of ethical tools for informing the design and conduct of neuroscience research (Illes and Bird, 2006; Stahl et al., 2018). These highlights the ethical, legal, and social implications of brain data research as brain data is considered to be neuroexceptional (Hallinan et al., 2021) there have been significant advances in the sciences concerned with the brain and its functions. As science has advanced, the scientific and practical utility of neurodata – data concerning the nervous system's nature, structure and function – has also grown. This expansion in utility, however, has brought with it ever increasing ethical and legal scrutiny on the legitimate use of neurodata. There is every reason to believe that the expansion in the scientific and practical utility of neurodata, as well as the increased attention given to attendant ethical and legal concerns, will continue apace. It seems likely that many of the forthcoming legal discussions will concern questions as to whether the collection and use of neurodata should be subject to specific and novel legal, ethical considerations: questions of neuroexceptionalism. In order for such discussions to take place in a structured and logical manner, a framework, in the form of an elaborated set of boundary conditions, for what constitutes a legitimate neuroexceptionalist position, is necessary. Unfortunately, no such framework has hitherto been elaborated. This paper attempts to fill this gap by elaborating such a

framework in the form of relevant boundary conditions in relation to: i and the neglect of ethical and legal principles in the generation of data may prevent successful collaboration between brain research projects (Stahl et al., 2018).

However, despite the need for collaboration among neuroscientists the application of brain data across different jurisdictions for a variety of purposes present various challenges to researchers and collaborations (Minielly, Hrincu and Illes, 2020; Esther Landhuis, 2017) giving rise to ethical, legal, and social concerns in an era where data sharing and collaborative research is depicted as a catalyst for scientific discovery (Lefaivre et al., 2019). Some of these challenges may be due to varying ethical, legal, cultural, or even scientific standards which vary across jurisdictions and may influence the usage and application of brain data. Furthermore, despite an agreement that brain data research should be ethical and legal, there is a debate about what ethical and legal requirements, principles and best practices should be attained to achieve its realisation which will promote the governance of brain data globally (Eke et al., 2021). Therefore, this justifies the main objective of this research which is to identify legal and ethical principles related to brain data and to understand how these legal and ethical principles influence brain data governance.

Methods

For our methodology we adopted a systematic scoping review and thematic analysis of 89 sources focused on biomedical, neuro and brain data governance to identify the ethical and legal principles which shape the current brain data governance landscape. To promote reproducibility, we adopted the Preferred Reporting Items for Systematic reviews and Meta-Analyses (PRISMA) 2020 framework which is a reporting guideline or framework designed to address poor reporting of reviews which are systematic in nature. The following inclusion and exclusion criteria were used

Inclusion criteria:

- PubMed and Scopus
- Papers on data governance principles but solely focused on biomedical data, brain data or neuro data.

Exclusion criteria:

- Not substantially about principles of data governance, i.e., data governance is not the topic of investigation, but referenced and relevant empirical research involving data governance but focused on other topics not related to brain data, neuro data or biomedical data
- Papers on data structure and ontologies
- Not in English Language

A search strategy was developed using the Pubmed and Scopus databases which initially generated 230 publications. After applying our inclusion and exclusion criteria also with the removal of duplicate results, 89 articles which met the inclusion criteria were exported to Nvivo 12 (*NVivo Data Analysis Software*, 2021) for analysis. One cycle of manual coding and one cycle of code mapping was carried out within the Nvivo qualitative data analysis software. Before the coding cycle a top-level coding scheme was developed to deductively and inductively capture the themes pre-empted by the focus of our study. The deductive strategy focused on the use of well-known ethical and legal principles as guided by neuroethical literature, while the inductive strategy focused on identifying ethical and legal principles which were induced by the analysis and therefore emerged from the coding process. For the theming of ethical and legal principles two iterations of theming were carried out and we relied on prior knowledge (deductively) and on knowledge induced by the analysis (inductive) but rooted in normative ethical literature. These includes baseline ethical principles used in data ethics, data governance, and biomedical ethics.

Results and discussion

Out of the 89 articles analysed only four provided a definition of data governance. This highlights the contribution of this study and shows that there is need for more contribution to the definition of data governance in the context of brain data. A total of twenty-four overarching ethical and legal principles emerged from the analysis as illustrated in Table 1.

Discussions were highly focused on consent and privacy which shows that researchers are highly influenced by ethical and legal issues around consent and privacy. Discussions around consent focused on the different types of consent such as specific or traditional, general or blanket or broad or dynamic, and altruistic consent. Issues around opt-in and opt out models were also the focus of discussions around consent. While in terms of privacy the focus was on privacy by design, physical privacy, informational privacy, decisional privacy, and proprietary privacy. The results also revealed that there is currently a large variation of how the principles are presented and

TABLE 1: Ethical and legal principles identified from the analysis

Ethical and Legal Principles	Level of Visibility
Consent, Privacy	**Very high**
Accountability, Anti-Discrimination, Autonomy, Beneficence and Non-Maleficence, Bias, Confidentiality, Dignity and Respect for Persons, Fairness, Integrity, Justice, Proportionality, Protection and Security, Transparency, Trust, Solidarity, Independence, Responsibility, Engagement, Ownership, Legal basis	Medium
Neurorights, Retention and Destruction	Very Low

discussions around the terms are very multidimensional with different definitions and recommendations. Some of the principles are still at their infancy and are barely visible in current discussions most especially the principle of neurorights and the principle of retention and destruction of data as these had only one reference in the coding cycle. This is important because countries like Chile have enacted a fully functional neurorights law and data management plans have established life cycle guidelines for data use in brain projects.

This research provides a key contribution to neuroscience research and innovation by providing additional insights into the foundational principles that can shape the practice and implementation of data governance in the context of brain data. The study will inform researchers and research institutions, brain research initiatives and projects, governmental and intergovernmental organizations, funding organisations and other relevant stakeholders involved in the advancement of brain data and neuroscience research. With the application of brain data in the development of neurotechnologies such as direct to consumer neuro-wearables gaining momentum, this study also brings important ethical and legal discussions under the radar of industry leaders at the forefront of brain data related technologies.

Further research is currently being carried out as part of the overall research to understand the ethical and legal perceptions of key stakeholders (neuroscientists) in different brain projects on a global scale around the identified principles. Understanding the ethical and legal principles that influence key actors in different projects will provide the framework for understanding how ethical and legal principles are applied in different projects and how ethical and legal principles influence data governance in neuroscience.

Acknowledgements
This work was supported by the European Union's Horizon 2020 Framework Programme for Research and Innovation under the Specific Grant Agreements No. 945539 (HBP SGA3).

References

Eke, D.O. *et al.* (2021) 'International data governance for neuroscience', *Neuron*, 0(0). Available at: https://doi.org/10.1016/j.neuron.2021.11.017.

Fothergill, B.T. *et al.* (2019) 'Responsible Data Governance of Neuroscience Big Data.', *Frontiers in neuroinformatics*, 13, p. 28. Available at: https://doi.org/10.3389/fninf.2019.00028.

Hallinan, D. *et al.* (2021) *Neuroexceptionalism: Framing an emergent debate*. SSRN Scholarly Paper ID 3909816. Rochester, NY: Social Science Research Network. Available at: https://doi.org/10.2139/ssrn.3909816.

Illes, J. and Bird, S.J. (2006) 'Neuroethics: a modern context for ethics in neuroscience', *Trends in neurosciences (Regular ed.)*, 29(9), pp. 511–517. Available at: https://doi.org/10.1016/j.tins.2006.07.002.

NVivo Data Analysis Software (2021). Available at: https://www.qsrinternational.com/nvivo-qualitative-data-analysis-software/about/nvivo (Accessed: 11 November 2021).

Rommelfanger, K.S. *et al.* (2018) 'Neuroethics Questions to Guide Ethical Research in the International Brain Initiatives', *Neuron (Cambridge, Mass.)*, 100(1), pp. 19–36. Available at: https://doi.org/10.1016/j.neuron.2018.09.021.

Stahl, B.C. *et al.* (2018) 'The role of ethics in data governance of large neuro-ICT projects.', *Journal of the American Medical Informatics Association : JAMIA*, 25(8), pp. 1099–1107. Available at: https://doi.org/10.1093/jamia/ocy040.

Human brain organisation

tACS and dynamic functional connectivity for a potential treatment of Alzheimer's Disease - A pilot study (tACS)

Author
Martín Carrasco-Gómez – Center for Cognitive and Computational Neuroscience, Universidad Complutense de Madrid, Madrid, Spain; Universidad Politécnica de Madrid, Madrid, Spain; Biomedical Research Networking Center in Bioengineering Biomaterials and Nanomedicine (CIBER-BBN), Madrid, Spain
Alberto del Cerro León – Center for Cognitive and Computational Neuroscience, Universidad Complutense de Madrid, Madrid, Spain
Jesús Cabrera Álvarez – Center for Cognitive and Computational Neuroscience, Universidad Complutense de Madrid, Madrid, Spain; Complutense University of Madrid, Madrid, Spain
Fernando Maestú – Center for Cognitive and Computational Neuroscience, Universidad Complutense de Madrid, Madrid, Spain; Biomedical Research Networking Center in Bioengineering Biomaterials and Nanomedicine (CIBER-BBN), Madrid, Spain; Complutense University of Madrid, Madrid, Spain

Citation
Carrasco-Gómez, M., del Cerro León, A., Álvarez, J.C., Maestú, F. tACS and dynamic functional connectivity for a potential treatment of Alzheimer's Disease - A pilot study (tACS)

Introduction/Motivation

Alzheimer's Disease (AD) is a neurodegenerative disorder which produces a progressive alteration in the patient's physiology. One of its most characterized electrophysiological biomarkers is an increased static functional connectivity (sFC) in the default mode network (DMN), which has been linked to a excitation/inhibition balance dysfunction [1] and to a further progression in the AD spectra [2]. This electrophysiological activity emerges in the brain while in a resting state, meaning that the individual is not engaged in any specific task, and can be detected as a pathological increase in phase synchronicity estimators such as phase locking value (PLV) in neural activity in the alpha band (8-12 Hz) [1, 2]. Thus, restoring this basic psychophysiological phenomenon could help improve the performance of related functional networks and, consequently, the cognitive state in AD patients.

In this regard, transcranial alternate current stimulation (tACS) seems to be a promising tool. tACS is a technique that consists in introducing alternating currents on the brain through disc or pad electrodes placed on the scalp of the head, and it entrains neural activity at a particular frequency in a non-invasive fashion. This means we might be able to modulate both inter and intra sFC, by facilitating neural activity at a specific frequency in one or more brain areas.

Additionally, most research on functional connectivity has been based on static descriptions of this phenomena, and only in the last years a growing body of literature has taken advantage of the information contained in its temporal features, building the concept of dynamic functional connectivity (dFC). dFC has been demonstrated to have an important role in arousal and consciousness state [3], attention modulation [4], and even in development of dementia and neurodegenerative disorders [5]. Regarding dFC in Alzheimer's Disease, a recent study observed a dFC generalized decrease in AD patients, which might be related to alterations of GABAergic receptor subunits, the depression of cholinergic inhibitory activity, the decrease in inhibitory neurotransmission or the enhancement of excitatory glutamatergic receptor activity [5], alluding again to an E/I imbalance [1]. While tACS effects

on power have been widely demonstrated, the effect of tACS on both static and dynamic FC is still unknown, which this study investigates.

Given that tACS recruits neural populations activity around one specific frequency, we expect to find a local increase of sFC and a decrease of dFC over the stimulated areas, pinpointing a possible future treatment for AD patients.

Methods

Healthy controls with ages ranging from 25 to 54 years had their magnetoencephalographic (MEG) activity registered in a 5-minute resting eyes-closed recording in an Elekta Neuromag MEG system, twice before and once after 20 minutes of tACS verum/sham stimulation at their individual alpha-peak frequency (IAF) as showed in Figure 1, measured from the pre-stimulation MEG recordings at parietooccipital sensors. The device used for applying tACS was a NeuroConn DC-Stimulator Plus, and sponge electrodes were placed over Cz and Oz (Figure 2). Verum stimulation intensity was set to 3mA peak-to-peak, while those undergoing sham stimulation only received stimulation during the fade-in and fade-out periods (30 seconds each). After MEG cleaning, pre-processing, and source reconstruction, functional connectivity was estimated through PLV with a 4-seconds long sliding window, and intrarregional change in PLV () as well as change of

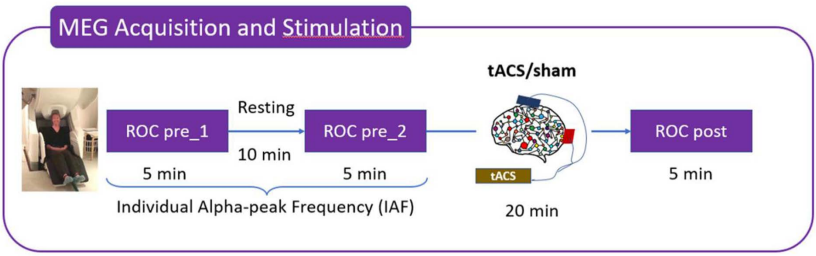

FIGURE 1
MEG recording and tACS stimulation protocol.

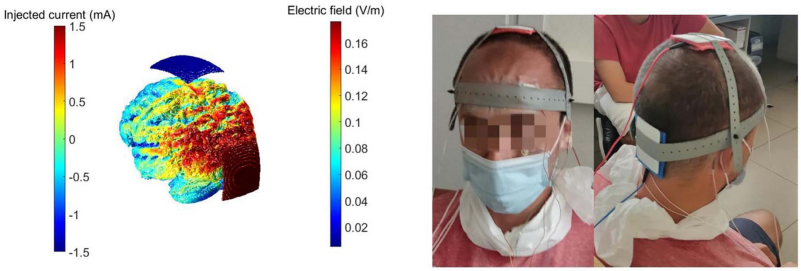

FIGURE 2
In the left, electric field elicited by tACS over the MNI, calculated with ROAST [7]. On the right, an example of the tACS stimulation setting on a participant.

standard deviation of PLV () in the areas directly below stimulation electrodes (Precuneus and Calcarine fissure), where the effects were supposed to be strongest, was statistically compared between groups.

Results and discussion

To our surprise, no intraregional sFC changes were observed between groups in the Precuneus (= 0.3240). However, a significant increase in variability was found (= 0.0373). On the other hand, the Calcarine fissure showed an almost significant change in intrarregional sFC (= 0.0534), and a significant decrease in standard deviation (= 0.0431) as seen in Figure 3. No significant changes were observed in the sham group. While not meeting our expectations, we think that our diverging results might explain the extent of our capability to entrain different brain areas with tACS. Firstly, we were not able to change sFC at the Precuneus, but we could do so at the Calcarine fissure. Secondly, the direction of the change in intraregional standard deviation of FC might be linked to these facts. According to Jesus et al. [6], highly connected areas, such as the Precuneus, might be harder to entrain than less connected brain areas. Is might explain why we were not able to change the mean FC in the precuneus, but were able to increase the variability of FC, by pulling the frequency away from its natural oscillation frequency at limited times. The calcarine fissure, having its mean FC almost significantly changed, was

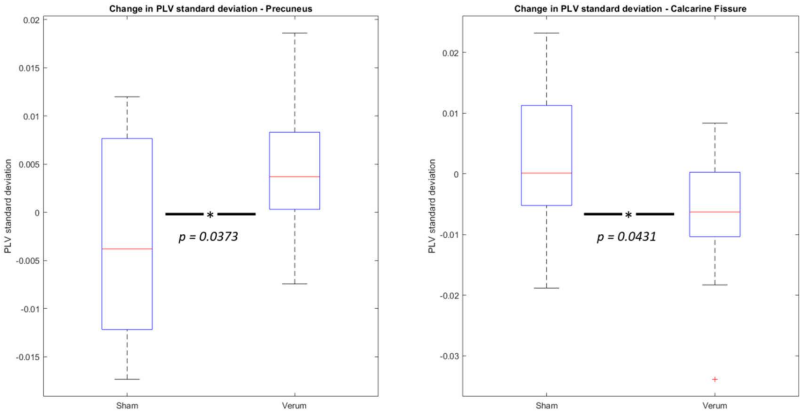

FIGURE 3

Boxplots showing the change in PLV standard deviation in both Precuneus (right), and Calcarine Fissure (left).

highly entrained to the external stimuli, thus decreasing the variability of its FC. Another reason behind these results might be the adjustment of the frequency of stimulation and the natural oscillating frequency of these two brain areas, which we will investigate in the future. There is still so much more work to do, so we encourage research to further investigate around this topic.

References

[1] Ramírez-Toraño F, Bruña R, de Frutos-Lucas J, Rodríguez-Rojo IC, Marcos de Pedro S, Delgado-Losada ML, Gómez-Ruiz N, Barabash A, Marcos A, López Higes R, Maestú F. Functional connectivity hypersynchronization in relatives of Alzheimer's disease patients: An early E/I balance dysfunction?. Cerebral Cortex. 2021 Feb;31(2):1201-10.

[2] Pusil S, López ME, Cuesta P, Bruna R, Pereda E, Maestu F. Hypersynchronization in mild cognitive impairment: the 'X'model. Brain. 2019 Dec 1;142(12):3936-50.

[3] Naro, A., Bramanti, A., Leo, A., Cacciola, A., Manuli, A., Bramanti, P., & Calabrò, R. S. (2018). Shedding new light on disorders of consciousness diagnosis: The dynamic functional connectivity. Cortex, 103, 316-328.

[4] Fong, A. H. C., Yoo, K., Rosenberg, M. D., Zhang, S., Li, C. S. R., Scheinost, D., ... & Chun, M. M. (2019). Dynamic functional connectivity during task performance and rest predicts individual differences in attention across studies. NeuroImage, 188, 14-25.

[5] Núñez, P., Poza, J., Gómez, C., Rodríguez-González, V., Hillebrand, A., Tola-Arribas, M. A., ... & Hornero, R. (2019). Characterizing the fluctuations of dynamic resting-state electrophysiological functional connectivity: reduced neuronal coupling variabil44ity in mild cognitive impairment and dementia due to Alzheimer's disease. Journal of neural engineering, 16(5), 056030.

[6] Cabrera-Álvarez J, Susi G, Sánchez-Claro J, Carrasco M, del Cerro A, Maestú F, Mirasso C. A computational model to guide the functional decoupling of two brain regions with transcranial alternating current stimulation. Brain Stimulation: Basic, Translational, and Clinical Research in Neuromodulation. 2021 Nov 1;14(6):1613.

[7] Huang Y, Datta A, Bikson M, Parra LC. Realistic volumetric-approach to simulate transcranial electric stimulation—ROAST—a fully automated open-source pipeline. Journal of neural engineering. 2019 Jul 30;16(5):056006.

Cortical reorganization in patients with deafferentiation pain after brachial plexus avulsion or amputation

Author
Hanna Koehler – Department of Neurology, Jena University Hospital, Jena, Germany; Biomagnetic Center, Jena University Hospital, Jena, Germany; Department of Clinical Psychology, Friedrich Schiller University Jena, Jena, Germany
Jennifer Ernst – Department of Trauma Surgery, Orthopaedics, and Plastic Surgery, Universitätsmedizin Göttingen, Göttingen, Germany; Department for Trauma Surgery Hannover Medical School, Hannover, Germany
Frauke Musial – National Research Center in Complementary and Alternative Medicine, Department of Community Medicine, UiT, The Arctic University of Norway, Tromsø, Norway
Nadine Wanke – Fakultät Life Sciences, Hamburg University of Applied Sciences, Hamburg, Germany
Meike Wilke – Fakultät Life Sciences, Hamburg University of Applied Sciences, Hamburg, Germany
Thomas Weiss – Department of Clinical Psychology, Friedrich Schiller University Jena, Jena, Germany

Citation
Koehler, H., Ernst, J., Musial, F., Wanke, N., Wilke, M., Weiss, T. Cortical reorganization in patients with deafferentiation pain after brachial plexus avulsion or amputation

Introduction/Motivation

After losing a limb, up to 87% of amputees suffer from painful sensations in the now missing limb [11]. One explanation for the origin of such

phantom limb pain (PLP) is that after amputation, the area in the primary somatosensory cortex (S1) representing the missing limb is now deprived of sensory input leading to cortical reorganization, such that somatotopically adjacent brain areas shift or enlarge into the affected region - a maladaptive process leading to pain [4]. Several studies confirmed a correlation between the intensity of PLP and a reduced distance between the estimated representation of the phantom hand and the representation of the lip of the affected side compared to the healthy side in S1 in upper-limb amputees [e.g., 4,5,7] and therapies have been developed to reverse this effect [e.g., 3]. However, sensory deprivation occurs not only after amputation but also after brachial plexus avulsion (BPA). Although studies show that patients with BPA report similar sensations to amputees in the affected limb [8] and the number of publications concerning BPA rapidly increased over the past 10 years [9], only few studies investigated a link between pain and reorganization in such patients [2]. However, if sensory deprivation in S1 leads to maladaptive plasticity, these maladaptive changes should also be present in patients suffering from pain after BPA. Accordingly, the present study aims at a) ascertaining the extent of cortical reorganization in S1 in patients with BPA and PLP-like pain, b) investigating a possible link between the amount of reorganization and pain intensity and c) comparing the phenomenon between patients with BPA and amputees.

Methods

3 patients with BPA and 3 patients with transradial amputation were included in the study. All patients reported pain in the affected limb for more than 3 months. Somatosensory evoked fields during air-puff stimulation of both corners of the lower lip and the phalanx of the healthy thumb were measured using magnetoencephalography to estimate the respective representation in S1. Source reconstruction was conducted under the assumption of equivalent current dipoles. As the affected thumb could not be stimulated, its cortical representation was estimated by mirroring the location of the healthy thumb along the longitudinal fissure. A reduced distance between the center of gravity of the lip and thumb representation in the hemisphere contralateral to the injury compared to the distance in the ipsilateral hemisphere depicts

a cortical reorganization. To avoid reliance on the estimation of the affected thumb representation, a second method to assess cortical reorganization was used in which, after mirroring the representation of the healthy lip along the longitudinal fissure, the center of gravity of lip representations were compared. In healthy participants, a distance of less than 6 mm between lip representations is found [10]. Hence, a distance greater than 6 mm between lip representations indicates a shift of the lip in the hemisphere contralateral to the affected side and, therefore, cortical reorganization. For pain assessment, patients were asked to describe the intensity of acute pain in the affected limb directly before and after measurement using a 0 (no pain at all) to 10 (worst imaginable pain) numeric rating scale (NRS). For a deeper comparison of symptoms between groups, pain was additionally assessed in detail using the German version of the neuropathic pain symptom inventory (NPSI) and the German short-form of the McGill Pain Questionnaire (MPQ). Spearman's rank correlation was used to assess the relationship between cortical reorganization and pain.

Results and discussion

Results show a reduced distance between the estimated lip and thumb representation on the affected side compared to the healthy side and a distance greater than 6 mm between lip representations in all participants, indicating cortical reorganization in all patients irrespective of group membership (Figure 1). Likewise, participants in both groups show little differences in pain characteristics. However, no correlation between pain and amount of cortical reorganization was found, possibly due to little variance in pain and small sample size (Table 1). Results of the present study suggest similar underlying mechanisms of pain in patients with BPA compared to amputees. An adaptation of therapies aiming at reducing PLP through cortical retro-reorganization might be possible. The study helps to expand these considerations and thus improve the treatment of pain in the context of BPA, which is particularly relevant given that such injuries occur primarily in young people in their prime working years [6] and an increasing number of patients with BPA over the past years [1].

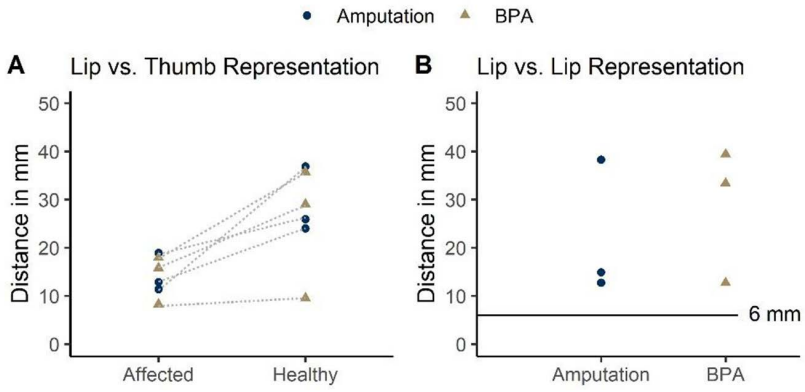

FIGURE 1

A. Cortical reorganization measured by the distance between lip and thumb representation. All participants show a smaller distance in the hemisphere contralateral to the affected side than in the hemisphere contralateral to the healthy side, indicating cortical reorganization. **B**. Cortical reorganization measured by the distance between the representation of both lips. A maximum distance of 6 mm is expected in healthy individuals [10], which is exceeded by all patients in the present sample, indicating cortical reorganization.

TABLE 1: Minimum, maximum, mean and standard deviation pain values assessed using the numeric rating scale (Mean between pre- and post-measurement assessment of momentary pain), the German version of the neuropathic pain symptom inventory (total score) and the German short-form of the McGill Pain Questionnaire (total score). Spearman's rank correlation was computed to assess the relationship between pain measures and cortical reorganization measured by a) the difference in the distance of lip and thumb representations on the healthy compared to the affected side (higher values indicate greater reorganization) and b) the distance between lip representations (higher values indicate greater reorganization). As a positive correlation was expected, a one-sided test was computed. No correlation reached significance

					Difference between distances on healthy and affected side		**Distance between lip representations**	
	Min	Max	M	SD	rho	p	rho	p
NRS	2.00	3.30	2.77	0.50	-0.58	.885	-0.52	.853
NPSI	13.00	57.00	29.33	15.73	0.37	.249	0.66	.088
MPQ	14.00	30.00	21.83	6.18	0.03	.500	0.49	.178

Acknowledgements
The current work has been supported by the German Federal Ministry of Education and Research (BMBF) grant "PROMPT" given to Jennifer Ernst, Thomas Weiss, and Meike Annika Wilke [FKZ: 13GW00xx A-x].

References

[1] Dy CJ, Peacock K, Olsen MA, Ray WZ, Brogan DM. Incidence of surgically treated brachial plexus injury in privately insured adults under 65 years of age in the USA. HSS J. 2020;16:339–43.

[2] Ernst J, Weiss T, Wanke N, Frahm J, Felmerer G, Farina D, Schilling AF, Wilke MA. Case Report: Plasticity in Central Sensory Finger Representation and Touch Perception After Microsurgical Reconstruction of Infraclavicular Brachial Plexus Injury. Front. Neurosci. 2022;16.

[3] Flor H, Denke C, Schaefer M, Grüsser S. Effect of sensory discrimination training on cortical reorganisation and phantom limb pain. The Lancet 2001;357(9270):1763–4.

[4] Flor H, Elbert T, Knecht S, Wienbruch C, Pantev C, Birbaumer N, Larbig W, Taub E. Phantom-limb pain as a perceptual correlate of cortical reorganization following arm amputation. Nature 1995;375(6531):482–4.

[5] Flor H, Elbert T, Mühlnickel W, Pantev C, Wienbruch C, Taub E. Cortical reorganization and phantom phenomena in congenital and traumatic upper-extremity amputees. Experimental brain research 1998;119(2):205–12.

[6] Kaiser R, Waldauf P, Ullas G, Krajcová A. Epidemiology, etiology, and types of severe adult brachial plexus injuries requiring surgical repair: systematic review and meta-analysis. Neurosurg. Rev. 2020;43(2):443–52.

[7] Knecht S, Henningsen H, Elbert T, Flor H, Höhling C, Pantev C, Taub E. Reorganizational and perceptional changes after amputation. Brain 1996;119(4):1213–9.

[8] Pazzaglia M, Leemhuis E, Giannini AM, Haggard P. The Homuncular Jigsaw: Investigations of Phantom Limb and Body Awareness Following Brachial Plexus Block or Avulsion. J. Clin. Med. 2019;8(2):182.

[9] Santana Chagas AC de, Wanderley D, Oliveira Ferro JK de, Alves de Moraes A, Morais de Souza FH, Da Silva Tenório A, Araújo de Oliveira D. Physical therapeutic treatment for traumatic brachial plexus injury in adults: A scoping review. PM&R 2021;14(1):120–50.

[10] Schaefer M, Nöennig N, Karl A, Heinze H-J, Rotte M. Reproducibility and Stability of Neuromagnetic Source Imaging in Primary Somatosensory Cortex. Brain Topography 2004;17(1):47–53.

[11] Stankevicius A, Wallwork SB, Summers SJ, Hordacre B, Stanton TR. Prevalence and incidence of phantom limb pain, phantom limb sensations and telescoping in amputees: A systematic rapid review. EJP 2021;25(1):23–38.

Relation between functional and structural brain networks using Magnetoencephalography (MEG) and Tensor Diffusion Images (DTI): A preliminary study

Author
María Sevilla García, Federico Ramírez Toraño, Pablo Cuesta Prieto – Center for Cognitive and Computational Neuroscience, Universidad Complutense de Madrid, Madrid, España

Citation
García, M.S., Toraño, F.R., Prieto, P.C. Relation between functional and structural brain networks using Magnetoencephalography (MEG) and Tensor Diffusion Images (DTI): A preliminary study

Introduction/Motivation

The brain is a highly complex structure that fulfills essential functions for life and whose study can be approached from multiple perspectives: psychological, anatomical, functional, molecular, etc. In this project we focused on the anatomical and functional perspectives. Functional connectivity (FC) quantifies the statistical interdependence between two or more brain activity signals recorded simultaneously (Garcés et al., 2016) and is used to define different brain networks, while structural connectivity (SC) studies the structural interconnections through white matter fibers between neural populations (Ramírez, 2021). We have hypothesized that both connectivities, structural and functional, had to be related.

FC was studied using magnetoencephalography (MEG) recordings, focusing on the default mode network (DMN) and its activity in the alpha frequency band (predominant when the brain is at rest). SC was evaluated by diffusion-weighted images (DWI), obtained in the same patients who carried out the MEG recordings, have been used. These images have been processed to calculate diffusion tensor images (DTI). Finally, once both connectivities have been obtained, the correlation between them has been studied, both at the individual and population levels. Additionally, the way in which this relationship affects the structure of the DMN itself has been examined.

In the first approach, the relationship between FC and SC in participants with non-pathological aging has been studied, however, in the database we have records and images of participants with mild cognitive impairment (MCI) and relatives of Alzheimer's patients. The main idea of the project is to continue with the analysis and study the two remaining groups, in order to later be able to evaluate the possible differences between these three groups.

Methods

Participants

To ensure working with a sample of non-pathological aging, we selected those participants who were over 50 years old, who did not show any signs of cognitive impairment, that is, a Mini-Mental score of more than 26, and who had optimal SC and FC recordings. After the selection, the resulting database consisted of 164 control participants.

T1, DWI and DTI

Before the analysis, a preprocessing of the T1 anatomical images and DWI images had to be done, and the DTI images had to be calculated from the information contained in the DWI. The steps followed were:

1. DWI images preprocessing

2. T1 images preprocessing and segmentation

3. 5TT images calculation (only the dimension that represented the line that separates the gray matter from the white matter was selected)

4. T1 (segmented) and 5TT images (only the dimension mentioned above) registration

5. Estimation of the GM, the WM and the cerebrospinal fluid response functions

6. The probabilistic fiber orientation map was generated by calculating the Fiber Orientation Distribution (FOD)

7. Finally, the tractography was calculated

MEG

For the MEG signals recordings, the participants remained seated in a chair with their eyes closed in a state of rest for 4 minutes.

After the signals acquisition, it was necessary to eliminate the noise present in the MEG. MEG data were automatically reviewed for eye, muscle, or jump artifacts. After that, the artifact-free data were divided into 4-second segments. Before source reconstruction, MEG time series were filtered in an Alpha frequency band. After the preprocessing, the signals were reconstructed in the source space, which was carried out independently for each participant. Finally, for each source, the Phase-Locking Value (PLV) was estimated as a measure of FC.

Using as reference the Automated Anatomical Labeling (AAL) atlas (Tzourio-Mazoyer et al., 2002), the DMN is formed by 22 cortical areas. Therefore, only the sources that were part of one of these 22 cortical areas were selected. The estimated PLV of each cortical area was calculated as the average PLV of all the sources belonging to that area. The result for each subject is a matrix of 22x22 PLV values.

Statistical analysis

Analysis I: the existing correlation between SC and FC is studied for all the connections between the 22 ROIs involved in the DMN (relationships between the SC and FC values of the 231 links (22 x 21/2) of the DMN). This correlation was calculated using Spearman's correlation coefficient and was carried out first at the population level (231 x 164 values) and subsequently studying the distribution of the mean correlation values obtained for each participant.

Analysis II: the correlation between SC and FC was evaluated for each link (e.g., right hippocampus connection - left cingulate gyrus) at the population level. This analysis allowed us to check if subnetworks emerged within the DMN based on the structure of their relationship between SC and FC connectivities. Again, correlation was calculated using Spearman's correlation coefficient.

Results and discussion

The results of the first approach carried out only with participants with non-pathological aging showed that there is a strong positive correlation between the two types of connectivity. The significant correlation (Spearman) showed a result of $\rho = 0.485$, as shown in Figure 1.

For the second analysis, the correlations were grouped according to the sign of the corresponding rho. In this way, two brain subnetworks were obtained; one composed of those links with significant inverse correlations and another with those links with significant direct correlations. Both subnetworks are shown in Figure 2. The inverse significant correlations subnetwork is a network whose topology strongly resembles the DMN itself. Instead, the subnetwork made up of the links with significant positive correlations is made up of only three links, which basically map two anteroposterior connections without interhemispheric crossover.

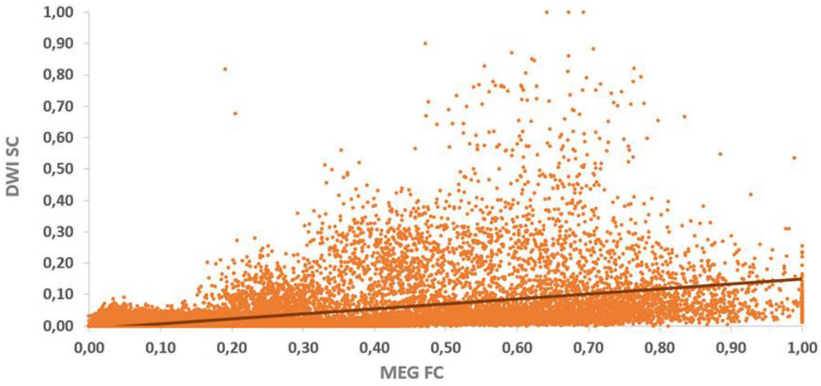

FIGURE 1
Significant correlation for inter ROIs connections: ρ = 0.485.

Once the results of these analyzes have been obtained, it has been possible to conclude that there is indeed a relationship between these two connectivities in the non-pathological aging people's brain, this being a positive relationship. In addition, it has been found that the SC-FC relationship can be used to disaggregate the DMN into subnetworks depending on the sign of the correlation found.

In short, this was the initial phase of a project in which the analyzes will be deepened and will be carried out in different populations in order to understand these connections and to observe if there are any changes between the brains of healthy people or brains with some type of cognitive impairment.

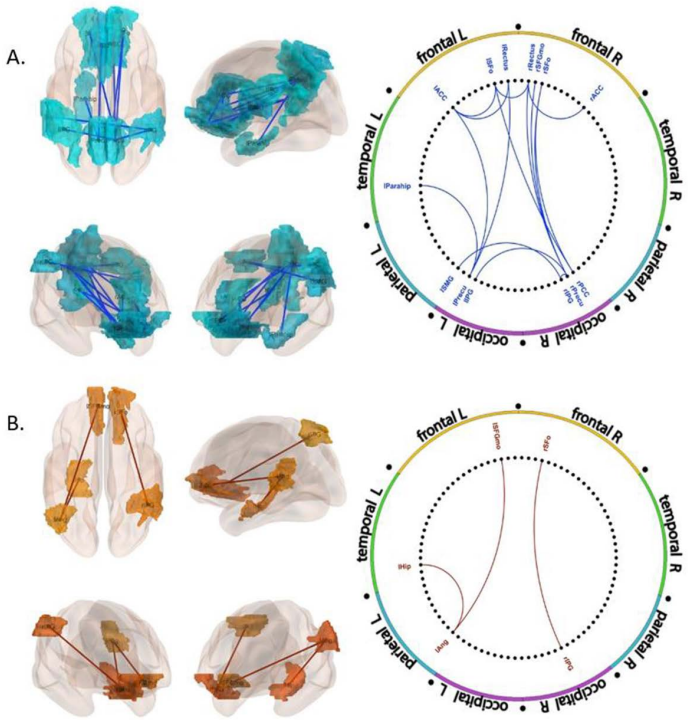

FIGURE 2

DMN´s subnetwork made up of the links whose FC and SC showed an inverse significant correlation (A) and a direct significant correlation (B). lParahip: Left parahipocampus . lSMG: Left Supramarginal gyrus. lPrecu: Left Precuneus. lIPG: Left Inferior Parietal gyrus. lRectus: Left Gyrus Rectus. lSFo: Left Superior Frontal gyrus, Orbital. lACC: Left Cingulate gyrus, Anterior part. lAng: Left Angular gyrus. lHip: Left Hippocampus. rIPG: Right Inferior Parietal gyrus. rPrecu: Right Precuneus. rPCC: Right Cingulate gyrus, Posterior part. rACC: Right Cingulate gyrus, Anterior part. rSFo: Right Superior Frontal gyrus, Orbital. rSFGmo: Right Superior Frontal gyrus, Medial Orbital. rRectus: Right Gyrus Rectus.

References

Andrews-Hanna JR, Snyder AZ, Vincent JL, Lustig C, Head D, Raichle MEE, Buckner RL (2007) Disruption of Large-Scale Brain Systems in Advanced Aging. Neuron 56:924–935.

Betzel RF, Byrge L, He Y, Goñi J, Zuo XN, Sporns O (2014) Changes in structural and functional connectivity among resting-state networks across the human lifespan. Neuroimage 102:345–357.

Dale AM, Fischl B, Sereno MI (1999) Cortical Surface-Based Analysis I. Segmentation and Surface Reconstruction. Available at: http://www.idealibrary.com

Damoiseaux JS (2017) Effects of aging on functional and structural brain connectivity. Neuroimage 160:32–40.

Dhollander, T., & Connelly, A. (2016). A novel iterative approach to reap the benefits of multi-tissue CSD from just single-shell (+b=0) diffusion MRI data. In 24th International Society of Magnetic Resonance in Medicine. Singapore.

Elam JS, Glasser MF, Harms MP, Sotiropoulos SN, Andersson JLR, Burgess GC, Curtiss SW, Oostenveld R, Larson-Prior LJ, Schoffelen JM, Hodge MR, Cler EA, Marcus DM, Barch DM, Yacoub E, Smith SM, Ugurbil K, van Essen DC (2021) The Human Connectome Project: A retrospective. Neuroimage 244.

Fischl B, Sereno MI, Tootell RBH, Dale AM (1999) High-Resolution Intersubject Averaging and a Coordinate System for the Cortical Surface. Available at: http://www.nmr.mgh.harvard.edu.

Ségonne F, Pacheco J, Fischl B (2007) Geometrically accurate topology-correction of cortical surfaces using nonseparating loops. IEEE Transactions on Medical Imaging 26:518–529

Garcés P, Ángel Pineda-Pardo J, Canuet L, Aurtenetxe S, López ME, Marcos A, Yus M, Llanero-Luque M, Del-Pozo F, Sancho M, Maestú F (2014) The Default Mode Network is functionally and structurally disrupted in amnestic mild cognitive impairment-A bimodal MEG-DTI study. NeuroImage: Clinical 6:214– 221.

Oostenveld R, Fries P, Maris E, Schoffelen J-M (2011) FieldTrip: Open-source software for advanced analysis of MEG, EEG, and invasive electrophysiological data. Comput Intell Neurosci 2011:156869.

Raffelt, D., Dhollander, T., Tournier, J. D., Tabbara, R., Smith, R. E., Pierre, E., & Connelly, A. (2017). Bias Field Correction and Intensity Normalisation for Quantitative Analysis of Apparent Fibre Density. In 25th International Society of Magnetic Resonance in Medicine. Honolulu.

Ramírez, F. (2021). Caracterización de personas con alto riesgo para el desarrollo de demencia mediante técnicas de neuroimagen. Universidad Politécnica de Madrid

Smith RE, Tournier JD, Calamante F, Connelly A (2012) Anatomically-constrained tractography: Improved diffusion MRI streamlines tractography through effective use of anatomical information. Neuroimage 62:1924–1938.

Tzourio-Mazoyer N, Landeau B, Papathanassiou D, Crivello F, Etard O, Delcroix N, Mazoyer B, Joliot M (2002a) Automated anatomical labeling of activations in SPM using a macroscopic anatomical parcellation of the MNI MRI single-subject brain. Neuroimage 15:273–289.

Van Veen BD, van Drongelen W, Yuchtman M, Suzuki A, Veen BD Van, Drongelen W Van, Yuchtman M, Suzuki A (1997) Localization of brain electrical activity via linearly constrained minimum variance spatial filtering. IEEE Trans Biomed Eng 44:867–880.

Transdiagnostic EEG microstate analysis in schizophrenia and autism spectrum disorder – can microstate parameters aid the differential diagnosis of the two dysconnectivity disorders?

Author
Ágota Vass, Gábor Csukly, Máté Baradits, Kinga Farkas – Department of Psychiatry and Psychotherapy, Semmelweis University, Budapest, Hungary

Citation
Vass, Á., Csukly, G., Baradits, M., Farkas, K. Transdiagnostic EEG microstate analysis in schizophrenia and autism spectrum disorder – can microstate parameters aid the differential diagnosis of the two dysconnectivity disorders?.

Introduction/Motivation

Schizophrenia (SCZ) and autism spectrum disorder (ASD) are clinically differentiable disorders with heterogeneous symptom manifestation. However, it is argued that these disorders overlap at several levels of organization such as defective neural processing (Pinkham et al., 2008), cognitive deficits (Nilsson et al., 2020), and perceptual anomalies (Lanillos et al., 2020) hindering differential diagnosis (Figure 1). While the aetiology of the two disorders is currently unknown, at a deeper level, both SCZ and

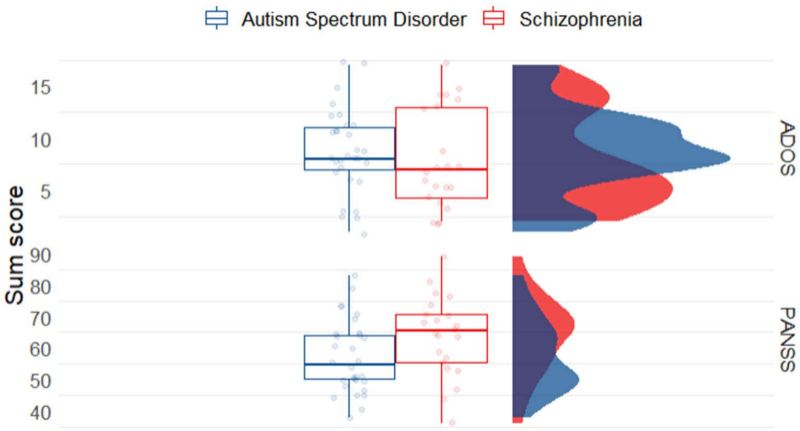

FIGURE 1
Autism Diagnostic Observation Schedule (ADOS) and Positive and Negative Syndrome Scales (PANSS) sum scores of patients diagnosed with ASD (N=33), and SCH (N=25) in our study.

ASD can be understood as disorders of connectivity between components of large-scale brain-networks (Friston, 1999; Frith, 2004). SCZ has been conceptualised as a "Disconnection Syndrome" (Friston, 1999), and ASD has also been referred to as a disconnection disorder (Frith, 2004).

Microstates are global patterns of scalp potential topographies that remain quasi-stable for 60–120ms (Mackintosh et al., 2020), and they are often referred to as the "atoms of thought" (Lehmann et al., 1998). As microstates have been associated with known large-scale neural networks in simultaneous EEG-fMRI studies such as the Default Mode Network (Britz et al., 2010), alterations in microstate parameters are believed to offer a novel method to investigate the integrity of brain networks at the subseconds-level (Michel & Koenig, 2018). This makes it a promising tool to uncover crucial underlying neural mechanisms of SCZ and ASD where the dysfunction of brain networks

has been hypothesized to be of central importance. We aim to investigate how EEG microstate parameters are altered in schizophrenia and autism spectrum disorder, respectively, and whether these alterations can be linked to alterations at higher levels of organisation such as cognition and behaviour.

Methods

We have recruited SCZ patients (N = 25), ASD patients (N = 33), and controls (N = 26). Patients were diagnosed with schizophrenia and autism spectrum disorder based on the DSM-5 diagnostic criteria (American Psychiatric Association, 2013) prior to recruitment and have been recruited from the outpatient units of the Department of Psychiatry and Psychotherapy, Semmelweis University. Healthy controls who are gender-, education level- and age-matched to both patient samples have been recruited on social media and were screened for any psychiatric or neurological diseases. All participants completed a battery of standardized cognitive tests assessing a variety of cognitive functions including working memory, executive functions and implicit memory. Subsequently, participants performed 2 minutes of resting state with eyes closed and 2 minutes of resting state with eyes open. We recorded a 64-channel-EEG and we performed the preprocessing and aim to perform the microstate analysis of the EEG data in Matlab (EEGLAB). For participants both with ASD and SCZ, symptom severity was measured by Positive and Negative Symptom Scale (PANSS) and Autism Diagnostic Observation Schedule (ADOS). The statistical analyses such as group comparison of various microstate parameters (mean duration, time coverage, and frequency of occurrence of microstate A, B, C, D), and their association with clinical scores will be undertaken in R.

Results and discussion

While the final evaluation of our results is currently in progress, based on previous results in the literature, we are able to establish firm hypotheses. Based on a recent meta-analysis, SCZ is associated with increase in the occurrence and time coverage of microstate C and decreased duration and time coverage of microstate D (da Cruz et al., 2020). These findings seem so robust that changes to the temporal metrics of microstate C and D have

been referred to as a potential endophenotype of SCZ (da Cruz et al., 2020). With regards to ASD, B microstate was found to occur more frequently, and also had a higher time coverage, while microstate C was found to occur less frequently (D'Croz-Baron et al., 2019). In another study, microstate A and C were found to have lower duration, while microstate B occurred more frequently and lasted longer, and microstate D occurred more frequently in patients with ASD (Jia & Yu, 2019). Here, we aim to investigate the changes in microstate parameters associated with SCZ and ASD transdiagnostically with the same methodology, which will be an important step towards empirically testing the disconnection hypothesis of these disorders, and towards mapping out neural markers that aid differential diagnosis of disorders that overlap in symptoms and behaviour.

Note(s): ADOS is a standardized diagnostic tool of ASD (Lord, 1999) and PANSS provides a representation of positive and negative symptoms that are prevalent in SCH (Kay et al., 1987). There is a significant overlap of symptoms in the ASD and SCH groups when assessed by ADOS, but symptoms assessed by PANSS can also be detected in both groups. This is in line with the theory that ASD and SCH show several similarities in terms of behaviour. This makes differential diagnosis challenging and underscores the need to find neural markers that reliably distinguish between the two conditions.

Acknowledgements
Supported by the ÚNKP-22-3-I New National Excellence Program of the Ministry for Culture and Innovation from the source of the National Research, Development and Innovation Fund.

References

American Psychiatric Association. (2013). Diagnostic and Statistical Manual of Mental Disorders (Fifth Edition). American Psychiatric Association. https://doi.org/10.1176/appi.books.9780890425596

Britz, J., Van De Ville, D., & Michel, C. M. (2010). BOLD correlates of EEG topography reveal rapid resting-state network dynamics. *NeuroImage*, *52*(4), 1162–1170. https://doi.org/10.1016/j.neuroimage.2010.02.052

da Cruz, J. R., Favrod, O., Roinishvili, M., Chkonia, E., Brand, A., Mohr, C., Figueiredo, P., & Herzog, M. H. (2020). EEG microstates are a candidate endophenotype for schizophrenia. *Nature Communications*, *11*(1), Article 1. https://doi.org/10.1038/s41467-020-16914-1

D'Croz-Baron, D. F., Baker, M., Michel, C. M., & Karp, T. (2019). EEG Microstates Analysis in Young Adults With Autism Spectrum Disorder During Resting-State. *Frontiers in Human Neuroscience*, *13*. https://doi.org/10.3389/fnhum.2019.00173

Friston, K. J. (1999). Schizophrenia and the disconnection hypothesis. *Acta Psychiatrica Scandinavica*, *99*(s395), 68–79. https://doi.org/10.1111/j.1600-0447.1999.tb05985.x

Frith, C. (2004). Is autism a disconnection disorder? *The Lancet Neurology*, *3*(10), 577. https://doi.org/10.1016/S1474-4422(04)00875-0

Jia, H., & Yu, D. (2019). Aberrant Intrinsic Brain Activity in Patients with Autism Spectrum Disorder: Insights from EEG Microstates. *Brain Topography*, *32*(2), 295–303. https://doi.org/10.1007/s10548-018-0685-0

Kay, S. R., Fiszbein, A., & Opler, L. A. (1987). The Positive and Negative Syndrome Scale (PANSS) for Schizophrenia. Schizophrenia Bulletin, 13(2), 261–276. https://doi.org/10.1093/schbul/13.2.261

Lanillos, P., Oliva, D., Philippsen, A., Yamashita, Y., Nagai, Y., & Cheng, G. (2020). A review on neural network models of schizophrenia and autism spectrum disorder. *Neural Networks*, *122*, 338–363. https://doi.org/10.1016/j.neunet.2019.10.014

Lehmann, D., Strik, W. K., Henggeler, B., Koenig, T., & Koukkou, M. (1998). Brain electric microstates and momentary conscious mind states as building blocks of spontaneous thinking: I. Visual imagery and abstract thoughts. *International Journal of Psychophysiology*, *29*(1), 1–11. https://doi.org/10.1016/S0167-8760(97)00098-6

Lord, C., Rutter, M., DiLavore, P., & Risi, S. (1999). Autism diagnostic observation schedule: Manual. Los Angeles: Western Psychological Services.

Mackintosh, A. J., Borgwardt, S., Studerus, E., Riecher-Rössler, A., de Bock, R., & Andreou, C. (2020). EEG Microstate Differences in Medicated vs. Medication-Naïve First-Episode Psychosis Patients. *Frontiers in Psychiatry*, *11*. https://www.frontiersin.org/articles/10.3389/fpsyt.2020.600606

Michel, C. M., & Koenig, T. (2018). EEG microstates as a tool for studying the temporal dynamics of whole-brain neuronal networks: A review. *NeuroImage*, *180*, 577–593. https://doi.org/10.1016/j.neuroimage.2017.11.062

Nilsson, M., Arnfred, S., Carlsson, J., Nylander, L., Pedersen, L., Mortensen, E. L., & Handest, P. (2020). Self-Disorders in Asperger Syndrome Compared to Schizotypal Disorder: A Clinical Study. *Schizophrenia Bulletin*, *46*(1), 121–129. https://doi.org/10.1093/schbul/sbz036

Pinkham, A. E., Hopfinger, J. B., Pelphrey, K. A., Piven, J., & Penn, D. L. (2008). Neural bases for impaired social cognition in schizophrenia and autism spectrum disorders. *Schizophrenia Research*, *99*(1), 164–175. https://doi.org/10.1016/j.schres.2007.10.024

Medical informatics and clinical neurosciences

The influence of Pavlovian conditioning-induced hallucinations on MMN amplitude

Author
Inés Abalo-Rodríguez – Department of Experimental Psychology, Complutense University of Madrid, Spain; Center of Cognitive and Computational Neuroscience, Complutense University of Madrid, Spain
Alejando Santo-Mayos – Department of Experimental Psychology, Complutense University of Madrid, Spain; Center of Cognitive and Computational Neuroscience, Complutense University of Madrid, Spain
Stephan Moratti – Department of Experimental Psychology, Complutense University of Madrid, Spain; Center of Cognitive and Computational Neuroscience, Complutense University of Madrid, Spain

Citation
Abalo-Rodríguez, I., Santo-Mayos, A., Moratti, S. The influence of Pavlovian conditioning-induced hallucinations on MMN amplitude.

Introduction/Motivation

The mismatch negativity (MMN) is an evoked potential that indexes auditory regularity violations [1,2]. Since the 90's, an aberrant modulation of this brain activity in schizophrenia has been consistently reported [3,4]. Recently, this

alteration has been related to the presence of auditory hallucinations (AH) rather than the schizophrenia diagnostic per se [5-6]. However, making this attribution is rather complicated due to the high heterogeneity of symptoms in schizophrenia [7].

Methods

In an attempt to isolate AH influences on the MMN amplitude from other cofounding variables, we artificially induced AHs in a non-clinical population by applying a Pavlovian conditioning paradigm [8, 9]. Thereby, a visual cue predicted consistently a tone. During the course of the experiment the number of trials with a visual cue only (without presenting a tone) increased. After each trial the participants (N = 33) had to rate if they experience a tone or not and rate their confidence in their judgements. High confident "yes" responses were recorded as induced AHs. Before and after conditioning, all participants faced an oddball paradigm that elicited a MMN that was recorded with a 64-electrode EEG system. This paradigm creates a regularity by presenting an auditory stimulus multiple times (standard), which is later broken by presenting a distinct stimulus (deviant) which will evoke the MMN. Two different types of deviants were presented: a frequency and a duration deviant, as the MMN alteration seems to be especially associated with AHs with duration deviants. In order to compare whether experiencing conditioned AHs exert any influence on MMN amplitudes, the number of experienced AHs served as a regressor to predict changes of the MMN amplitude at each EEG electrode. The multiple comparisons problem was controlled for by using a non-parametric cluster-based permutation procedure.

Results and discussion

Firstly, our results show the typical MMN shape for frequency and duration deviant, with no significant differences between pre and post conditions (Figure 1). Moreover, our results show that the reduction of the duration-deviant related MMN significantly correlates with the number of AH experienced during the conditioning paradigm (Figure 2). A lack of correlation between the MMN amplitude and induced AHs before conditioning makes plausible to attribute the MMN reductions to the learning

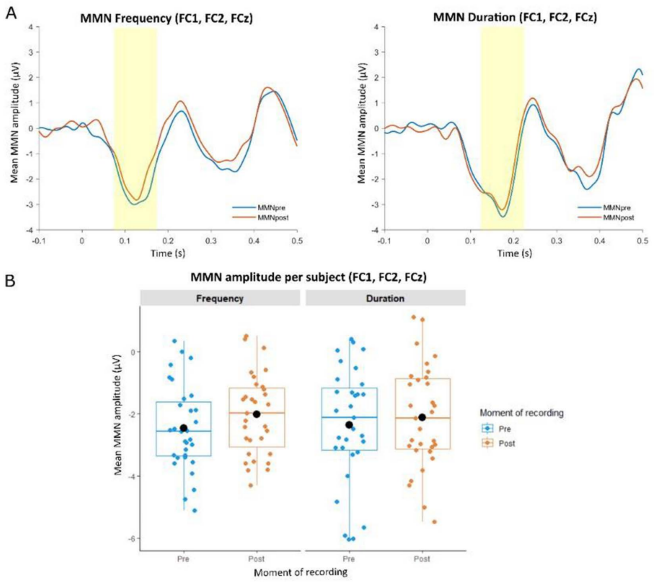

FIGURE 1

MMN mean amplitude for Pre and Post Conditions. (**A**) The time course of the mean MMN amplitudes across FC1, FC2, FCz electrodes for pre- and post-conditioning and the frequency and duration deviants are shown. As there were no significant clusters for the main effect Moment of Recording and the interaction Moment of Recording and Deviant Type the FC1 FC2, FCz electrodes were chosen as they best reflect the MMN component (see also the main effect of Deviant Type). Left panel: frequency deviant; right panel: duration deviant. The temporal window that will be averaged to show the mean MMN amplitude in B is highlighted in yellow. (**B**) Box plot for the mean MMN amplitude (averaged across the electrodes FC1, FC2, FCz, and the time interval 0.074 s to 0.174 s for frequency and 0.124 s to 0.224 s for duration) is shown. The small dots represent MMN amplitudes of single participants and the bold black dots the mean amplitude across subjects. The horizontal lines represent the median of the corresponding distributions. The range of the data is indicated by the vertical lines.

effects due to the conditioning procedure. Moreover, we found a significant correlation between AH proneness (likelihood of experiencing AH in real life, measured with the Launay-Slade Hallucination Scale [10]) and the number of AH experienced during the paradigm. In sum, our study allows to

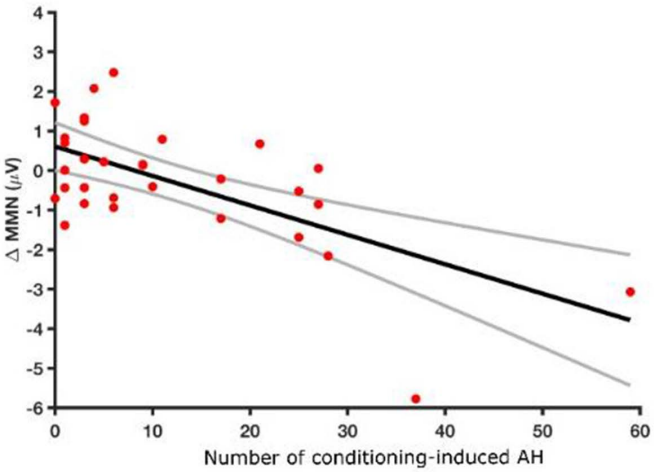

FIGURE 2
Scatter plot of the number of conditioning-induced AHs versus the MMN change at electrode C5 and at 0.150 s (where the strongest effect was observed). The best fitting regression line is adjusted to the data. The grey lines depict the 95% confidence kernel.

study processes underlying hallucinations without the clinical confounding variables and show that AHs can be conditioned and exert similar effects on MMN modulation in healthy participants as in schizophrenia. In addition to the results provided in pre-print version, we will discuss these findings within the predictive coding framework, highlighting the change of the weights of priors during the conditioning paradigm.

References

[1] Näätänen, R., Kujala, T., & Light, G. (2019). Mismatch negativity: A window to the brain. Oxford University Press

[2] Naatanen R, Paavilainen P, Rinne T, Alho K (2007): The mismatch negativity (MMN) in basic research of central auditory processing: A review. Clin Neurophysiol 118:2544–2590

[3] Erickson, M. A., Ruffle, A., & Gold, J. M. (2016). A Meta-Analysis of Mismatch Negativity in Schizophrenia: From Clinical Risk to Disease Specificity and Progression. Biological Psychiatry, 79(12), 980-987. https://doi.org/10.1016/j.biopsych.2015.08.025

[4] Shelley, A. M., Ward, P. B., Catts, S. V., Michie, P. T., Andrews, S., & McConaghy, N. (1991). Mismatch negativity: an index of a preattentive processing deficit in schizophrenia. Biological psychiatry, 30(10), 1059-1062.

[5] Fisher, D. J., Labelle, A., & Knott, V. J. (2012). Alterations of mismatch negativity (MMN) in schizophrenia patients with auditory hallucinations experiencing acute exacerbation of illness. Schizophrenia Research, 139(1-3), 237-245. https://doi.org/10.1016/j.schres.2012.06.004

[6] McCleery, A., Wynn, J. K., & Green, M. F. (2018). Hallucinations, neuroplasticity, and prediction errors in schizophrenia. Scandinavian Journal of Psychology, 59(1), 41-48. https://doi.org/10.1111/sjop.12413

[7] Berrios, G. E. (2006). Classifying Madness: A Philosophical Examination of the Diagnostic and Statistical Manual of Mental Disorder.

[8] Ellson, D. G. (1941). Hallucinations produced by sensory conditioning. 20.

[9] Powers, A. R., Mathys, C., & Corlett, P. R. (2017). Pavlovian conditioning–induced hallucinations result from overweighting of perceptual priors. Science, 357(6351), 596-600.

[10] Launay, G., & Slade, P. (1981). The measurement of hallucinatory predisposition in male and female prisoners. Personality and Individual Differences, 2(3), 221-234. https://doi.org/10.1016/01918869(81)90027-1

Modelling amyotrophic lateral sclerosis in vitro by direct cell reprogramming approaches

Author
Víctor Álvaro-Sánchez – Molecular, Cellular and Developmental Neurobiology Department. Cajal Institute – CSIC (Madrid, Spain)
Amel Falco – Molecular, Cellular and Developmental Neurobiology Department. Cajal Institute – CSIC (Madrid, Spain)
Lucía Gallego – Molecular, Cellular and Developmental Neurobiology Department. Cajal Institute – CSIC (Madrid, Spain)
Miriam Segura – Molecular and cellular neurobiotechnology | IBEC (Barcelona, Spain)
José Antonio del Río – Molecular and cellular neurobiotechnology | IBEC (Barcelona, Spain)
Alberto García-Redondo – Neurology Department, ALS Unit, CIBERER U-723, Health Research Institute, October 12th Hospital "IIS I+12" (Madrid, Spain)
Sergio Gascón – Molecular, Cellular and Developmental Neurobiology Department. Cajal Institute – CSIC (Madrid, Spain)

Citation
Álvaro-Sánchez, V., Falco, A., Gallego, L., Segura, M., del Río, J.A., García-Redondo, A., Gascón, S. Modelling amyotrophic lateral sclerosis in vitro by direct cell reprogramming approaches

Introduction/Motivation

Neuromuscular disorders (NDs) are conditions in which motor neurons (MNs) and/or skeletal muscle cells are functionally impaired. Either if the neuronal, the muscular or both components are affected, such diseases normally lead to the disruption of the neuromuscular junctions (NMJs),

the functional connections between them. In this regard, MNs and skeletal muscle cells (myotubes -MTs-) derived from iPSC have been used, for years, to study several NDs, such as Amyotrophic Lateral Sclerosis (ALS). However, a promising alternative is to obtain these induced cells by direct lineage conversion approaches, which, unlike iPSC reprogramming, (1) do not imply cell rejuvenation [1], being more reliable to study degenerative diseases that normally manifest in old onsets. (2) It is more affordable in terms of time and resources [2]. Therefore, this work's goal is to set up a model of human NMJs *in vitro* by applying direct cell reprogramming approaches. Thus, induced MNs (iMNs) and induced MTs (iMTs) were obtained through direct reprogramming led by the expression of neurogenic and myogenic factors respectively, in human fibroblasts (HF). By the combination of both cell types, we are testing the possibility to achieve a NMJ. And even more, if we accomplish a successful reprogramming of patient-derived fibroblasts into iMNs and iMTs, we can obtain powerful disease models, in which we could test the efficiency of different drugs in reversing the pathological characteristics of NDs.

Methods

In this study, control donor and ALS patient HFs were separately exposed to retroviral vectors encoding the neurogenic transcription factors Neurog2 and Isl1, together with Bcl2, to induce MNs, and the myogenic determinant MyoD, co-expressing Bcl2 or not, to induce MTs. After 48 h, transduced cells from both lineages were re-seeded in coculture conditions, allowing them to achieve conversion, maturation and thereafter, functional interaction. We evaluated the effect of Bcl2 and the presence of different feeder cells, such as murine astrocytes, macrophages and neural stem cells (NSC), in the conversion efficiency. To establish the best conditions, we determined the number of transduced cells that were immunoreactive for β-III-tubulin, HB9, Isl2 and Peripherin, in the case of iMNs, and Myosin, Phalloidin and number of cells with sarcomeres, in iMTs.

Once the reprogramming conditions were established, we cocultured MNs and iMTs together but in microfluidic devices that have two different

chambers connected by microchannels which allow only axons to project from the neuronal' to the muscle's compartments. In these cultures, NMJ formation is being analysed through bungarotoxin staining. In the current

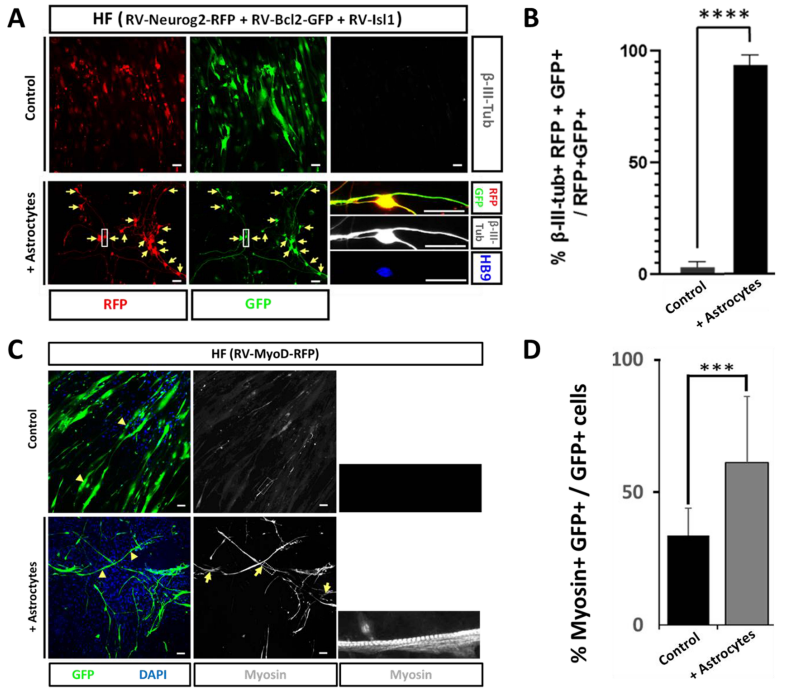

FIGURE 1

Direct neuronal and myogenic reprogramming experiments. (**A**) Fluorescent micrographs show iMNs (yellow arrows) obtained through retroviral expression of Neurog2, Isl1 and Bcl2 in HF. (**B**) Quantitative analysis shows that astrocytes increase the % of iMNs 45 days post-transduction (DPT) (highly significant differences: ****p≤0,0001). (**C**) Fluorescent micrographs show iMTs obtained through retroviral expression of MyoD in HF. Yellow arrowheads mark the nucleus of a multinucleated cell (typical characteristic of MTs) and yellow arrows point sarcomeres. (**D**) Quantitative analysis shows that astrocytes increase the % of iMTs 21DPT (highly significant differences: ***p≤0,001). // Scale bar: 40μm.

experiments, we are investigating functionality by monosynaptic tracing using modified rabies virus, and by patch-clamp approaches.

Results and discussion

We demonstrated that HF can be directly converted into iMNs by retroviral expression of Neurog2 and Isl1 [3]. In this context, co-expression of Bcl2 highly improved neuronal conversion efficiency. Despite Bcl2 being an anti-apoptotic factor, it facilitates the acquisition of the oxidative metabolism required by neurons to obtain energy [4]. Considering this, and focusing on fibroblast-to-muscle conversion, we asked whether this model would also benefit from the expression of this gene. Indeed, Bcl2 increased the proportion of iMTs and sarcomere formation compared with the control condition (without Bcl2). To improve further the muscle conversion, we also tested the effect of a mutant MyoD (CT 4S-A), which is known to hold higher myogenic activity during embryonic development [5]. Although iMTs are visually more mature in terms of the sarcomere organization (they are easier to identify through microscopy), quantitative analysis is being performed, and results will be presented in the final version of the poster. Next, we studied the influence of the cellular environment in the neuronal and myogenic reprogramming paradigms. We found that astrocytes were crucial for fibroblast-to-neuron conversion and, interestingly, their presence in a fibroblast-to-myotube conversion model highly increased the conversion efficiency in terms of myosin expression (~85% of myosin positive cells compared with ~40% in the control; see Figure 1), while NSC and macrophages benefited the process just slightly (~50-55% respectively). The molecular mechanism by which astrocytes improve conversion efficiency in both models is still unknown. However, we are using transwell inserts which allow us to coculture astrocytes with transduced HF without physical interaction, so we can evaluate if the effect is due to soluble molecules or by direct cell-to-cell contact.

Additionally, we evaluated the capability of these iMTs to establish functional connections with MNs. We cocultured murine primary MNs with iMTs in the previously presented microfluidic devices (see methods). We demonstrated that fibroblast-to-myotube conversion can be accomplished in these

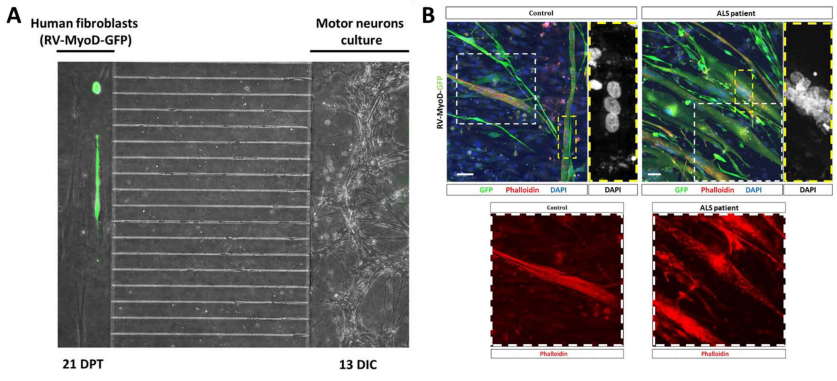

FIGURE 2
(**A**) Live cell imaging combining bright-field and green fluorescence. On the left, we found HF infected with RV-MyoD-GFP 21DPT. On the right, it is shown the primary culture of MNs 13 days in culture (DIC). Projections of these MNs crossing microgrooves can be seen. (**B**) Phenotypic differences between iMTs obtained by the conversion of HF from control donors and ALS patients.

devices, and cocultured MNs extended axons through the microgrooves toward the myotube chamber (Figure 2A). The formation of NMJs is currently being analysed.

Finally, we accomplished a successful reprogramming of HFs from ALS patients, and we found some alterations in these induced cells compared to those obtained from control donors. Regarding fibroblast-to-myotube conversion, we found immunoreactive cells for myosin which showed disorganization of the cytoskeleton (observed with phalloidin staining) and abnormal accumulation of nuclei (Figure 2B). Moreover, we could not find sarcomeric structures. Differences regarding ALS-iMNs are still being analyzed but to date, we have seen differences in the size of the soma.

Acknowledgements
This work was funded by 5 grants: 1) the grant PID2021-128796OB-I00, Ministry of Science and Innovation, 2) Fundación La Caixa LCF/PR/

HA21/52350003, Instituto Cajal, Madrid (Spain) 3) the grant RTI2018-099345-B-I00, Ministry of Science and Innovation, 4) the grant MAIV01EK1611A, Federal Ministry of Education and Research (BMBF-Germany) and 5) the Network of Excellence "Synaptic Role in Cognitive Disabilities" SAF2017–90664-REDT, Ministry of Science, Innovation and Universities (Spain).

References

[1] Mertens J, Marchetto MC, Bardy C, Gage FH (2016) Evaluating cell reprogramming, differentiation and conversion technologies in neuroscience. Nat Rev Neurosci. 17:424–437.

[2] Mertens J, Reid D, Lau S, Kim Y, Gage FH (2018) Aging in a Dish: iPSC-Derived and Directly Induced Neurons for Studying Brain Aging and Age-Related Neurodegenerative Diseases. Annu Rev Genet. 52:271-293.

[3] Falco A, Bartolomé-Cabrero R, Gascón S (2021) Bcl-2-assisted Reprogramming of Mouse Astrocytes and Human Fibroblasts into Induced Neurons. Methods in Mol Biol. 2352:57-71.

[4] Gascón S, Murenu E, Masserdotti G, Ortega F, Russo GL, Petrik D, Deshpande A, Heinrich C, Karow M, Robertson SP, Schroeder T, Beckers J, Irmler M, Berndt C, Angeli JP, Conrad M, Berninger B, Götz M (2016) Identification and Successful Negotiation of a Metabolic Checkpoint in Direct Neuronal Reprogramming. Cell Stem Cell. 18(3):396-409.

[5] Hardwick LJ, Davies JD, Philpott A (2016) MyoD phosphorylation on multiple C terminal sites regulates myogenic conversion activity. Biochem Biophys Res Commun. 481(1-2):97-103.

Electroconvulsive therapy changes functional brain connectivity and TNF-α blood levels in depressed patients

Author
Nadia Falhani, Caroline Nothdurfter, Jens Schwarzbach – Department of Psychiatry and Psychotherapy, University of Regensburg, Regensburg, Germany

Citation
Falhani, N., Nothdurfter, C., Schwarzbach, J. Electroconvulsive therapy changes functional brain connectivity and TNF-α blood levels in depressed patients.

Introduction/Motivation

Depression is characterized by a range of symptoms including persistent low mood, loss of interest or pleasure, and fatigue. Moreover, depressed patients experience this state as chronic and difficult to escape. Notably, 30% of cases are resistant to treatment and this poses a severe challenge to patient care efforts[1]. For such cases, a chance of relief is provided by electroconvulsive therapy (ECT), a non-pharmacological treatment consisting of an electrical stimulation of the brain which triggers a generalized seizure[2]depression severity, psychotic and melancholic features for ECT response and remission in major depression. Method A meta-analysis was conducted according to the PRISMA statement. A literature search identified recent studies that reported on at least one of the potential predictors. Results Of the 2193 articles screened, 34 have been included for metaanalysis. Presence of

psychotic features is a predictor of ECT remission (odds ratio (OR. Although beneficial, the precise mechanisms of ECT remain to be determined. Based on previous knowledge, ECT induces an acute inflammatory immune response that might reinforce neurotrophins expression[3,4]. Here we aim to unveil the potentially beneficial role of inflammation observed during ECT. We also hypothesize that ECT induces changes in brain network communication, as indirect result of changes in metabolism. In fact, it has been suggested that depression can be better conceptualized as the inability to switch from a negative mood state to a non-negative one, rather than the depressive state itself[5], i.e. that depression may be a disorder of brain dynamics. Hence, studying brain functional connectivity (FC) is of great importance to understand the pathophysiological mechanisms of ECT.

Methods

Inpatients (N=8) at the District Hospital of Regensburg diagnosed with depressive episode (ICD-10 F31, F32, F33; HAMD-21: 18-30) underwent three ECT sessions per week for a total of 16 sessions on average (Fig. 1). Functional magnetic resonance imaging (fMRI) was performed before starting the therapy and once a week for four weeks to investigate functional graph theoretical measures of brain connectivity. According to graph theory, the complex structure and function of the brain can be described as a graph which is defined as a set of nodes (brain regions) linked by edges (connections). After extracting regional time course activity using an atlas-based parcellation of the brain, we computed pairwise Pearson's correlation between time courses.

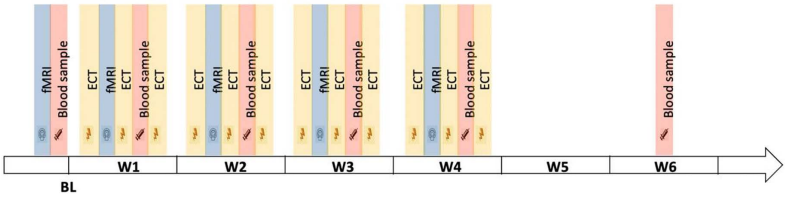

FIGURE 1

Study design. Patients receive three ECT sessions per week. fMRI is performed and blood samples are collected every week. Follow-up measurements take place in week six.

We created brain graphs from adjacency matrices (thresholded FC matrices), and we measured how each region is connected to other regions using degree metric (i.e., number of connections of each region).

We documented the clinical course using Hamilton Depression Rating Scale (HAMD-21) and Beck Depression Inventory (BDI) and we collected blood samples before starting the therapy and during the following six weeks (Fig. 1). Serum was separated from cellular components to assess inflammatory biomarkers levels in peripheral blood using ELISA (V-PLEX Proinflammatory Panel 1 Human Kit).

Results and discussion

Clinical outcome

Six patients out of eight responded to the therapy, leading to a response rate of 75%. Responsiveness was defined as reduction of at least 50% of the baseline score for both HAMD and BDI scores.

Brain graph measures

fMRI data analysis revealed that several regions included in default mode (DMN), cognitive control (CC) and somatomotor (SM) networks change the number of connections (degree) during four weeks of therapy. In particular, the degree of SM regions (PreCG) and CC regions (IFG, MFG) decreases from week one to week two and increases again in week three (Fig. 2). Interestingly, these changes mostly occur between the first and the third week, suggesting that the main effect of ECT on brain connectivity takes place at very early stages of the therapy, although the first effects on the clinical outcome emerge only later around week four. Those regions have been associated with regulation of emotion expression, decision making, language and semantic memory processing; all functions known to be affected in depression6,7. Altogether our results are compatible with a reorganisation of brain connections as a consequence of ECT.

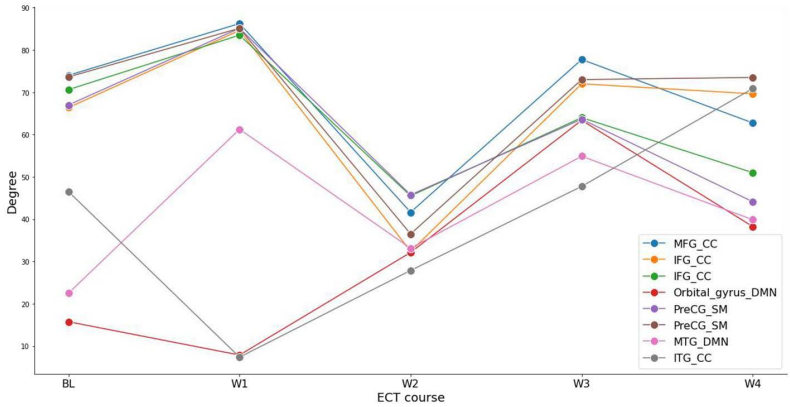

FIGURE 2

Degree measure in regions in CC, DM and SM networks during the course of ECT (BL= baseline, W1= week 1, W2= week 2, W3= week 3, W4= week 4). Degree decreases from W1 to W2 and increases again at W3. *p < .05, Bonferroni corrected.

Inflammatory state

Among eight inflammatory cytokines (IFN-γ, IL-1β, IL-2, IL-4, IL-6, IL-8, IL-10, TNF-α) measured in serum, only TNF-α levels increased from baseline to week three, and from baseline to week four. This result is consistent with previous literature stating an increase of TNF-α after ECT[8]few studies have addressed the functioning of the immune system in relation to electroconvulsive therapy (ECT. We did not find any changes in other cytokines levels, although some of them (e.g. IL-6, IL-1ß) have been suggested as potential state markers of depression and antidepressant therapy[9,10].

PreCG = Precentral Gyrus; IFG = Inferior Frontal Gyrus; MFG = Medial Frontal Gyrus

Acknowledgements
This work has been supported by the German Research Council (DFG) within GRK2174.

References

1. Al-Harbi, K. S. Treatment-resistant depression: therapeutic trends, challenges, and future directions. *Patient Prefer. Adherence* **6**, 369–388 (2012).

2. Van Diermen, L. *et al.* Prediction of electroconvulsive therapy response and remission in major depression: Meta-analysis. *British Journal of Psychiatry* vol. 212 71–80 (2018).

3. van Buel, E. M. *et al.* Immune and neurotrophin stimulation by electroconvulsive therapy: is some inflammation needed after all? *Translational psychiatry* vol. 5 e609 (2015).

4. Yrondi, A. *et al.* Electroconvulsive therapy, depression, the immune system and inflammation: A systematic review. *Brain Stimul.* **11**, 29–51 (2018).

5. Holtzheimer, P. E. & Mayberg, H. S. Stuck in a rut: Rethinking depression and its treatment. *Trends in Neurosciences* vol. 34 1–9 (2011).

6. Liakakis, G., Nickel, J. & Seitz, R. J. Diversity of the inferior frontal gyrus—A meta-analysis of neuroimaging studies. *Behav. Brain Res.* **225**, 341–347 (2011).

7. Talati, A. & Hirsch, J. Functional Specialization within the Medial Frontal Gyrus for Perceptual Go/No-Go Decisions Based on "What," "When," and "Where" Related Information: An fMRI Study. *J. Cogn. Neurosci.* **17**, 981–993 (2005).

8. Freire, T. F. V., Rocha, N. S. da & Fleck, M. P. de A. The association of electroconvulsive therapy to pharmacological treatment and its influence on cytokines. *J. Psychiatr. Res.* **92**, 205–211 (2017).

9. Tuglu, C., Kara, S. H., Caliyurt, O., Vardar, E. & Abay, E. Increased serum tumor necrosis factor-alpha levels and treatment response in major depressive disorder. *Psychopharmacology (Berl).* **170**, 429–433 (2003).

10. Zincir, S., Öztürk, P., Emrah Bilgen, A. & Zci 4 Cihad Yükselir, F. I. levels of serum immunomodulators and alterations with electroconvulsive therapy in treatment-resistant major depression. (2016) doi:10.2147/NDT.S106652.

Longitudinal functional connectivity changes in individuals at risk of Alzheimer's disease

Author
Alejandra García-Colomo – Center for Cognitive and Computational Neuroscience, Complutense University of Madrid, 28223, Pozuelo de Alarcón, Spain; Departament of Experimental Psychology, Cognitive Psychology and Speech & Language Therapy, Complutense University of Madrid, 28223, Pozuelo de Alarcón, Spain
Alberto Nebreda Pérez – Center for Cognitive and Computational Neuroscience, Complutense University of Madrid, 28223, Pozuelo de Alarcón, Spain; Departament of Experimental Psychology, Cognitive Psychology and Speech & Language Therapy, Complutense University of Madrid, 28223, Pozuelo de Alarcón, Spain
Martín Carrasco – Center for Cognitive and Computational Neuroscience, Complutense University of Madrid, 28223, Pozuelo de Alarcón, Spain; Departament of Electronical Engineering, Polytechnic University of Madrid, 28040, Madrid, Spain
Jaisalmer de Frutos – Center for Cognitive and Computational Neuroscience, Complutense University of Madrid, 28223, Pozuelo de Alarcón, Spain; Departament of Experimental Psychology, Cognitive Psychology and Speech & Language Therapy, Complutense University of Madrid, 28223, Pozuelo de Alarcón, Spain
Federico Ramírez-Toraño– Center for Cognitive and Computational Neuroscience, Complutense University of Madrid, 28223, Pozuelo de Alarcón, Spain; Departament of Experimental Psychology, Cognitive Psychology and Speech & Language Therapy, Complutense University of Madrid, 28223, Pozuelo de Alarcón, Spain
Ricardo Bruña – Center for Cognitive and Computational Neuroscience, Complutense University of Madrid, 28223, Pozuelo de Alarcón, Spain; Departament of Radiology, Rehabilitation, and Physiotherapy, Complutense University of Madrid, 28040, Madrid, Spain; Instituto de Investigación Sanitaria San Carlos (IdISSC), 28040, Madrid, Spain
Fernando Maestú – Center for Cognitive and Computational Neuroscience, Complutense University of Madrid, 28223, Pozuelo de Alarcón, Spain; Departament of Experimental Psychology, Cognitive Psychology and Speech & Language Therapy, Complutense University of Madrid, 28223, Pozuelo de Alarcón, Spain

Citation
García-Colomo, A., Pérez, A.N., Carrasco, M., de Frutos, J., Ramírez-Toraño, F., Bruña, R., Maestú, F. Longitudinal functional connectivity changes in individuals at risk of Alzheimer's disease.

Introduction/Motivation

Alzheimer's disease (AD) is the most common form of dementia. However, there is no available treatment capable of preventing its appearance. The reason behind this is that an AD diagnosis is only given in the presence of cognitive and functional impairment; however, the underlying neurological damage and dysfunction are vast and extensive, and the processes behind said degeneration have been going on for years, even decades. Consequently, recent research has been focused on the identification of early biomarkers of AD that can help detect individuals at risk of developing the disease, and on the creation of intervention programs that help prevent the development of AD or, at the very least, delay its course (Jack et al., 2018).

AD is characterized by the presence of insoluble aggregates of amyloid-beta (Aβ), neurofibrillary tangles of hyperphosphorylated tau protein and synaptic degeneration. Recent findings show that soluble species of Aβ are toxic for GABAergic neurons and reduce the reuptake of glutamate from the extracellular space, leading to an excitation/inhibition neuronal imbalance (Busche & Konnerth, 2016). This initially manifests as neuronal hyperexcitability that has been shown to contribute to the trans-synaptic transmission of hyperphosphorylated tau, in a prion-like fashion (Busche & Hyman, 2020). Subsequently, the prolonged state of hyperexcitability leads to neuronal excitotoxicity and neuronal loss, which, in turn, manifests as hypoexcitability (Busche & Hyman, 2020).

For the current study, we used magnetoencephalography (MEG) to measure early changes in neuronal activity of healthy and cognitively unimpaired adults (50-80 years of age) at different levels of risk of developing AD, given their family history. We also measured plasma levels of p-tau231, a novel

biomarker known to increase very early in the pathological continuum of the disease (Ashton et al., 2021). Both measures are minimally invasive.

The main objective of the study was to evaluate longitudinal changes in the connectivity of three regions known to be affected in the progression of AD, and which, according to previous studies, exhibit hyperconnectivity in subjects at greater risk of developing the disease (Ramírez-Toranõ et al., 2021). These regions include the left and right precuneus, and the left anterior cingulate cortex.

Methods

The sample consisted of 69 subjects with family history (FH+) of AD and 28 individuals with no history (FH-). Two longitudinal, eyes-closed, resting state MEG recordings were obtained from each individual, three years apart. Blood extractions and p-tau231 determinations were performed following the second MEG visit.

The aforementioned areas were designated as seeds in a cluster-based permutation test (CBPT) to find clusters with connectivity values which significantly differ between the first and second MEG recording. These analyses were performed for the FH+ and FH- groups separately to assess whether each group showed different trends of longitudinal change. Only the CBPT clusters that survived FDR were considered.

Results and discussion

The FH+ results show significant clusters of longitudinal change that closely resemble those obtained by Ramírez-Toranõ et al. (2021), sharing up to 94% of sources in the case of the right precuneus. All three clusters present greater connectivity values in the second MEG recording. Additionally, a significant positive correlation was found between the connectivity values at the second MEG recording and p-tau231 in the left precuneus. The same positive trend was found for right precuneus and left anterior cingulate.

To our knowledge, this is the first longitudinal study performed on cognitively unimpaired subjects, addressing connectivity changes and studying the relationship between those values and plasma biomarkers. The precuneus is one of the areas that accumulates early damage due to the pathology of AD. We believe that the hyperconnectivity found in both precuneus can be considered an early biomarker of AD risk; not only did the FH+ group show greater connectivity in very similar clusters as those found by the Ramírez-Toranõ et al. (2021), we also found a relationship between those values and plasma levels of p-tau231, a biomarker of pathology that increases very early in the continuum of the disease and shows a tight association with Aβ accumulation, even at preclinical levels. Therefore, we believe the hyperconnectivity we observe might be caused by the hyperexcitability produced due to the increase of Aβ levels in subjects who might be entering the AD continuum.

References

Ashton, N. J., Pascoal, T. A., Karikari, T. K., Benedet, A. L., Lantero-Rodriguez, J., Brinkmalm, G., Snellman, A., Schöll, M., Troakes, C., Hye, A., Gauthier, S., Vanmechelen, E., Zetterberg, H., Rosa-Neto, P., & Blennow, K. (2021). Plasma p-tau231: a new biomarker for incipient Alzheimer's disease pathology. Acta Neuropathologica, 141(5), 709–724. https://doi.org/10.1007/s00401-021-02275-6

Busche, M. A., & Hyman, B. T. (2020). Synergy between amyloid-β and tau in Alzheimer's disease. In Nature Neuroscience (Vol. 23, Issue 10, pp. 1183–1193). Nature Research. https://doi.org/10.1038/s41593-020-0687-6

Busche, M. A., & Konnerth, A. (2016). Impairments of neural circuit function in Alzheimer's disease. In Philosophical Transactions of the Royal Society B: Biological Sciences (Vol. 371, Issue 1700). Royal Society of London. https://doi.org/10.1098/rstb.2015.0429

Jack, C. R., Bennett, D. A., Blennow, K., Carrillo, M. C., Dunn, B., Haeberlein, S. B., Holtzman, D. M., Jagust, W., Jessen, F., Karlawish, J., Liu, E., Molinuevo, J. L., Montine, T., Phelps, C., Rankin, K. P., Rowe, C. C., Scheltens, P., Siemers, E., Snyder, H. M., … Silverberg, N. (2018). NIA-AA Research Framework: Toward a biological definition of Alzheimer's disease. In Alzheimer's and Dementia (Vol. 14, Issue 4, pp. 535–562). Elsevier Inc. https://doi.org/10.1016/j.jalz.2018.02.018

Ramírez-Toranõ, F., Brunã, R., de Frutos-Lucas, J., Rodríguez-Rojo, I. C., Marcos De Pedro, S., Delgado-Losada, M. L., Gómez-Ruiz, N., Barabash, A., Marcos, A., López Higes, R., & Maestú, F. (2021). Functional Connectivity Hypersynchronization in Relatives of Alzheimer's Disease Patients: An Early E/I Balance Dysfunction? Cerebral Cortex, 31(2), 1201–1210. https://doi.org/10.1093/cercor/bhaa28

RNA sequencing analyses in bipolar families with multiple affected individuals

Author
Inés García-Ortiz – Centre for Molecular Biology Severo Ochoa UAM/CSIC, Madrid, Spain
Miriam Martínez-Jiménez – Centre for Molecular Biology Severo Ochoa UAM/CSIC, Madrid, Spain
Tomas Kavanagh – Brain and Mind Centre, School of Medical Sciences, University of Sydney, NSW, Australia; Garvan Institute of Medical Research, Sydney, NSW, Australia
Lee Marshall – Garvan Institute of Medical Research, Sydney, NSW, Australia
Anna Heath – Neuroscience Research Australia, Sydney, NSW, Australia
Philip B Mitchell – Discipline of Psychiatry and Mental Health, University of New South Wales, Sydney, NSW, Australia; Black Dog Institute, Prince of Wales Hospital, Sydney, NSW, Australia
Peter R Schofield – Neuroscience Research Australia, Sydney, NSW, Australia; School of Medical Sciences, University of New South Wales, Sydney, NSW, Australia
Antony A Cooper – Garvan Institute of Medical Research, Sydney, NSW, Australia; St Vincent's Clinical School, University of New South Wales, Sydney, NSW, Australia
Janice M Fullerton – Neuroscience Research Australia, Sydney, NSW, Australia; School of Medical Sciences, University of New South Wales, Sydney, NSW, Australia
Claudio Toma – Centre for Molecular Biology Severo Ochoa UAM/CSIC, Madrid, Spain; Neuroscience Research Australia, Sydney, NSW, Australia; School of Medical Sciences, University of New South Wales, Sydney, NSW, Australia

Citation
García-Ortiz, I., Martínez-Jiménez, M., Kavanagh, T., Marshall, L., Heath, A., Mitchell, P.B., Schofield, P.R., Cooper, A.A., Fullerton, J.M., Toma, C. RNA sequencing analyses in bipolar families with multiple affected individuals

Introduction

Bipolar disorder (BD) is a complex psychiatric disorder characterized by episodes of mania and depression, with a prevalence of approximately 1% in the general population (1). BD patients are often associated with psychotic events and suicidal behaviours. Family studies have established a large genetic component in BD, despite most of genetic risk variants still remain largely unknown. Genetic studies have also established complex mechanisms of inheritance that include common variants of small effects identified through genome-wide association studies (GWAS) (2), and rare variants of higher penetrance identified via next-generation sequencing (NGS) (3-5). Our group has completed whole-exome and whole-genome sequencing (WES and WGS) in large Australian families with multiple affected individuals with BD, revealing potential susceptibility genes carrying rare variants (3-5). Recently, we combined different sequencing technologies performing both RNA sequencing (RNA-seq) and WGS in nine multiplex bipolar families comprising 4-7 members across two generations, aiming to unveil genes and pathways implicated in this psychiatric disease. Here, we present results from the data of RNA-seq identifying differential expressed genes (DEGs) and networks between affected and unaffected individuals from these families.

Methods

We selected nine nuclear families with multiple individuals across two generations who had been diagnosed with bipolar disorder I (N=15), bipolar disorder II (N=6), schizoaffective disorder-manic type (N=6), and recurrent unipolar disorder (N=5). The selection also included unaffected parents (N=14) and siblings (N=9). All individuals were clinically assessed with the "Family Interview for Genetic Studies" (FIGS) and the "Diagnostic Interview for Genetic Studies" (DIGS) (6,7). Whole genome sequencing and initial variant calling was performed at Kinghorn Centre for Clinical Genomics (KCCG) at Garvan Institute (Sydney, Australia) on 48 individuals (28 BD cases, 20 unaffected). RNA-seq was performed on total mRNA extracted from lymphoblastoid cell lines from 31 individuals at KCCG (15 BD cases, 16 unaffected relatives). Libraries were prepared with the Illumina Tru-seq stranded mRNA library kit, and amplified using the KAPA HiFi HotStart Library

Amplification Kit (Roche). Raw reads were quality checked using FastQC (http://www.bioinformatics.babraham.ac.uk/projects/fastqc/), trimmed using Trimmomatic (8), and then re-checked for QC. Trimmed reads were mapped to the GRCh38.p13 reference genome from Ensembl (https://www.ensembl.org) using HISAT2 aligner (9). Mapped bams were then sorted and indexed with samtools (version 1.9) (10), and quantified with HTSeq (11). The DESeq2 package was used to perform DEGs analysis between BD patients and their unaffected relatives (12), using sex, family ID, and age as covariates. Gene set enrichment analysis (GSEA), Ingenuity Pathway Analysis (IPA), and weighted gene co-expression network analysis (WGCNA) are underway to detect pathways or network of genes with plausible role in BD (13). Polygenic Priority Score (PoPS; 14) that incorporates data from an extensive set of public bulk and single-cell expression datasets, curated biological pathways, and predicted protein-protein interactions will be used for gene prioritization, leveraging MAGMA gene-based signals from GWAS summary statistics in BD (41,917 BD cases and 371,549 controls) (2,15).

Results and discussion

Gene quantification was carried out for 61,806 genes. A first filter for genes with low count reads ($\leq$10) was applied and 33,281 genes were removed from the analysis. The remaining 28,525 genes were used for DEGs analysis. A second QC procedure using independent filtering, which is based on normalized count means, removed another set of 13,293 genes. Finally, 15,232 genes were considered for this analysis. Our results showed 61 genes differentially expressed between BD patients and unaffected relatives (adjusted P-values <0.05), and 31 of those genes had $|\log_2$ fold change$|$ > 0.3 (Figure 1). Comparison of the 16 most significant DEGs (adjusted P-value<0.01) between BD and unaffected individuals is shown in the heat map and grouped by hierarchal clustering (Figure 2).

The most significant differentially expressed gene is *LINC01237*, a long non-coding RNA (lncRNA) on chromosome 2, which is over-expressed in BD. Interestingly, this lncRNA has been recently associated to BD from two independent DNA methylation studies (16,17). In one study *LINC01237* is one

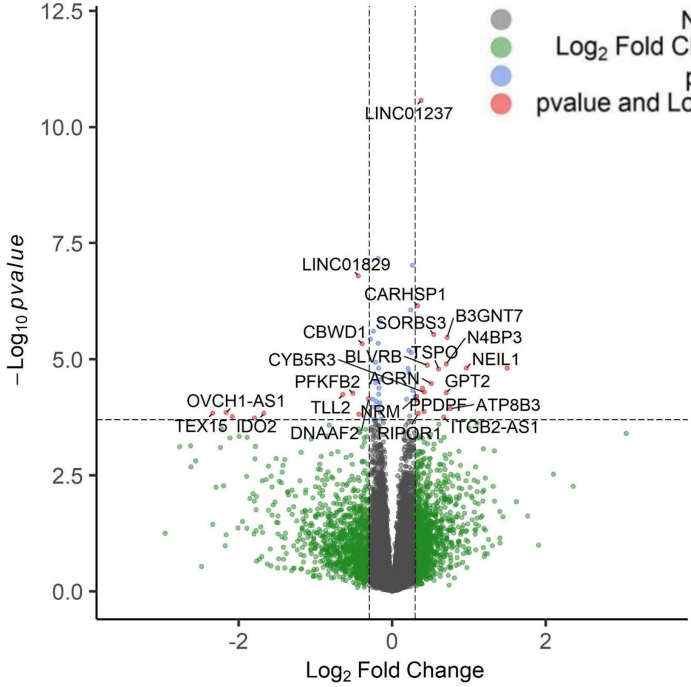

FIGURE 1
Volcano plot shows 15,232 genes out of 61,806 after QC in DEGs analysis. Genes with a raw P-value<0.0002 are represented by red and blue dots. Only those genes with $|\log_2$ fold change$| > 0.3$ and adjusted P-value < 0.05 (FDR 10%) were considered significant (red dots).

of the seven differentially methylated regions (DMRs) between excellent-responders and non-responders to lithium, the most effective drug used to treat BD symptoms (16). In a second study, this gene is found as the most significant DMRs between BD cases and controls (17). Other lncRNAs have been already associated to BD, in particular with the response to lithium (18).

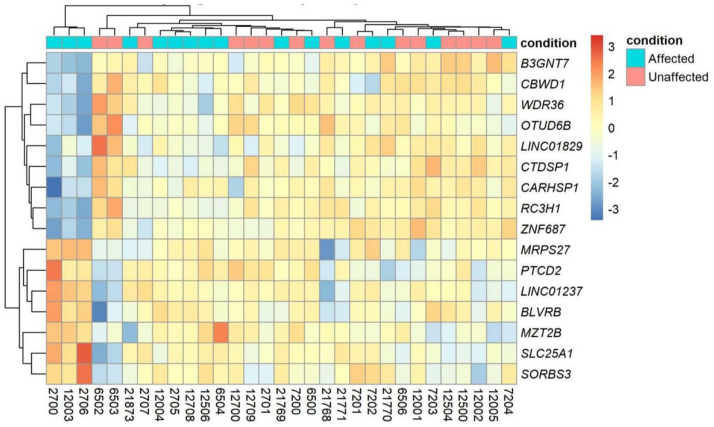

FIGURE 2

Heatmap showing the most significant DEGs (adjusted P-value < 0.01). Gene names are indicated on the right in italics, individual participants are shown along the bottom. Hierarchical clustering is shown for both genes and affection status (pale blue for "Affected", pink for "Unaffected) with individual ID on the bottom of the figure. Red and blue indicate relative over- or under-expression of genes, respectively, based on log2 normalized counts.

These RNAseq results will be comprehensively analysed with WGS data pinpoint genes and pathways implicated in the disorder.

Acknowledgments

NAB Foundation "Stronger Minds" grant: "Identification of mutant genes that contribute to bipolar disorder" (CIs: A Cooper, JM Fullerton)

MLC Community Foundation grant: "Whole Genome Sequencing of families with mental illness: 9 nuclear families with bipolar disorder" (CI: A Cooper; Collaborator: JM Fullerton)

NHMRC project grant APP1063960 "Unravelling the genetic causes of bipolar disorder: lessons from rare but highly penetrant variants in very heritable forms of illness" (CIA: JM Fullerton, CIB: PR Schofield)

Ministerio de Ciencia e Innovación: "Advances in understanding bipolar disorder through the combination of digital phenotyping and genome-wide approaches" (PI: C Toma; Collaborator: JM Fullerton)

References

[1] Mitchell, P. B. et al. Bipolar disorder in a national survey using the World Mental Health Version of the Composite International Diagnostic Interview: the impact of differing diagnostic algorithms. Acta Psychiatr. Scand. 2013; 127, 381–393

[2] Mullins et al. (2021) Genome-wide association study of more than 40,000 bipolar disorder cases provides new insights into the underlying biology. Nature Genetics 53:817-829

[3] Toma et al. (2018) An examination of multiple classes of rare variants in extended families with bipolar disorder. Transl Psychiatry 8(1):65-77

[4] Toma et al. (2020) De Novo Gene Variants and Familial Bipolar Disorder. JAMA Network Open 3: e203382-e203382

[5] Toma et al. (2021) A linkage and exome study of multiplex families with bipolar disorder implicates rare coding variants of ANK3 and additional rare alleles at 10q11-q21. J Psychiatry Neurosci 46:E247-E257

[6] NIMH Genetics Initiative: Family Interview for Genetic Studies (FIGS). Rockville (MD): National Institute of Mental Health; 1992.

[7] Nurnberger JI Jr, et al. Diagnostic interview for genetic studies. Rationale, unique features, and training. NIMH Genetics Initiative. Arch Gen Psychiatry 1994;51:849-59, discussion 63-4.

[8] Bolger, A. M., Lohse, M., & Usadel, B. (2014). Trimmomatic: A flexible trimmer for Illumina Sequence Data. Bioinformatics, btu170.

[9] Kim D, Langmead B, Salzberg SL. HISAT: a fast spliced aligner with low memory requirements. Nat Methods. 2015 Apr;12(4):357-60. doi: 10.1038/nmeth.3317. Epub 2015 Mar 9. PMID: 25751142; PMCID: PMC4655817.

[10] Li H, et al. The Sequence alignment/map (SAM) format and SAMtools, Bioinformatics (2009) 25(16) 2078-9

[11] Putri G et al (2022) Analyzing high-throughput sequencing data in Python with HTSeq 2.0. doi: https://doi.org/10.1093/bioinformatics/btac166

[12] Love M I et al (2014). Moderated estimation of fold change and dispersion for RNA-seq data with DESeq2. Genome Biol 15, 550 (2014). https://doi.org/10.1186/s13059-014-0550-8

[13] Peter Langfelder & Steve Horvath. WGCNA: an R package for weighted correlation network analysis. BMC Bioinformatics 2008; 9:559.

[14] Weeks EM et al. (2020) Leveraging polygenic enrichments of gene features to predict genes underlying complex traits and diseases. medRxiv 2020.09.08.20190561; doi: https://doi.org/10.1101/2020.09.08.20190561

[15] De Leeuw CA, et al. MAGMA: generalized gene-set analysis of GWAS data. PLOS Comput Biol 2015;11:e1004219

[16] Marie-Claire, C., Lejeune, F.X., Mundwiller, E. et al. A DNA methylation signature discriminates between excellent and non-response to lithium in patients with bipolar disorder type 1. Sci Rep 10, 12239 (2020). https://doi.org/10.1038/s41598-020-69073-0

[17] Gaine ME, Seifuddin F, Sabunciyan S, Lee RS, Benke KS, Monson ET, Zandi PP, Potash JB, Willour VL. Differentially methylated regions in bipolar disorder and suicide. Am J Med Genet B Neuropsychiatr Genet. 2019 Oct;180(7):496-507. doi: 10.1002/ajmg.b.32754. Epub 2019 Jul 27. PMID: 31350827; PMCID: PMC8375453.

[18] Hou L et al. (2016) Genetic variants associated with a response to lithium treatment in bipolar

[19] disorder: a genome-wide association study. Lancet 387: 1085-1093.

Analyses of *DMRT* gene family susceptibility across psychiatric disorders

Author
Jose Ignacio Gomez-Blanco – Centro de Biología Molecular Severo Ochoa, Universidad Autónoma de Madrid/CSIC, Madrid, Spain
Rafael Casado-Navarro, Sergio Espartero-Boza – Centro de Biología Molecular Severo Ochoa, Universidad Autónoma de Madrid/CSIC, Madrid, Spain
Esther Serrano-Saiz – Centro de Biología Molecular Severo Ochoa, Universidad Autónoma de Madrid/CSIC, Madrid, Spain
Claudio Toma – Centro de Biología Molecular Severo Ochoa, Universidad Autónoma de Madrid/CSIC, Madrid, Spain; Neuroscience Research Australia, Sydney, NSW 2031, Australia; School of Medical Sciences, University of New South Wales, Sydney, NSW 2052, Australia

Citation
Gomez-Blanco, J.I., Casado-Navarro, R., Espartero-Boza, S., Serrano-Saiz, E., Toma, C. Analyses of *DMRT* gene family susceptibility across psychiatric disorders.

Introduction/Motivation

In recent years, members of the DMRT (Doublesex and Mab-3 Related Transcription factors) gene family have emerged as evolutionary conserved sexual effectors, both at gonadal and brain levels [1,2]. In mammals, DMRTA1 and DMRTA2 are involved in cortical development regulating homeobox genes for correct positional information of cortical progenitors [3]. DMRTA2 is also involved in the generation of Cajal-Retzius cells, which are responsible for the secretion of reelin (RELN), leading the correct corticogenesis [4].

Homozygous mutations in DMRTA2 are responsible for a rare and severe condition characterized by microcephaly and lissencephaly, similarly to Mendelian conditions reported for RELN, LIS1 and TUBA1A [5]. All these genes responsible for human conditions associated to lissencephaly have been also suggested to play a role into susceptibility to psychiatric disorders, such as attention-deficit hyperactive disorder (ADHD), autism spectrum disorder (ASD) or bipolar disorder [6, 7]. The role of DMRT genes in early brain development, their implication in brain sexual differentiation and the recent reported human phenotype caused by DMRTA2 mutations, indicate that DMRT genes are good candidates to be investigated in psychiatric diseases, especially considering the sex skewing observed between male and female populations. In this study, we investigated the seven DMRT genes (DMRT1, DMRT2, DMRT3, DMRTA1, DMRTA2, DMRTB1, and DMRTC2) using the largest datasets currently available from the Psychiatric Genomics Consortium, and we found genetic risk variants in DMRTA1 and DMRTA2. Additionally, we performed in situ hybridization and immunofluorescence techniques in mice models to study the expression and role of Dmrta2 and Dmrta1 in midbrain dopaminergic neurons.

We hypothesized that genetic variants in DMRTA1 and DMRTA2 lead to expression changes that may increase susceptibility to specific psychiatric phenotypes.

Methods

We used GWAS summary statistics data of ten psychiatric disorders from the Psychiatric Genomics Consortium (PGC) [8-18] to assess the effect of single nucleotide polymorphisms (SNPs) for seven *DMRT* genes for each psychiatric disorder. Each GWAS dataset has summary statistics for ~8 million SNPs for about 20,000 to 60,000 patients and from 30,000 to 350,000 controls. We extracted data from summary statistics GWAS using PLINK (plink/v1.07), and after filtering for imputation scores (R2>0.6), we performed a gene based analysis using MAGMA software (magma/v1.09). Additionally, we performed a meta-analysis using Z scores to evaluate the impact for each gene across psychiatric disorders. To study the linkage disequilibrium

(LD) patterns of *DMRTA1* and *DMRTA2* we used data from populations of the "1000 genomes Project" (404 samples) using Haploview (v4.2). We used Locus Zoom (http:://locuszoom.org/) to represent SNPs and P-values from significant associations. We also estimated LD patterns of *DMRTA1* promoter for a Spanish population of 91 individuals genotyping rs2247403, rs2247404, rs2671622, rs655497. We performed variant prediction using SNPinfo Web Server (https:://snpinfo.niehs.nih.gov/).

We also performed *in situ* hybridization on mouse midbrain sections at embryonic stages and adulthood as previously described by Di Meglio *et al.*, 2013 [19], and to do that we used riboprobes for *Dmrta1* and *Dmrta2* [4,20].

Results and discussion

Gene-based analysis showed association for *DMRTA2* in ADHD (P= 0.008749; Perm-P=0.0102) and bipolar disorder (P=0.006227; Perm-P=0.0084), and additionally for *DMRTA1* in ADHD (P= 0.001679; Perm-P=0.0014) (Table 1). *DMRTA1* associated single nucleotide variants (SNPs) in ADHD were found in a LD block of 1 kb at the promotor region, mapping along several transcription factors binding sites (TFBS); whereas *DMRTA2* associated SNPs were within its promotor region, overlapping with a lncRNA (AL049637.1). The analysis by sex group in male and female populations showed potential sex effects in ADHD for associated SNPs of *DMRTA1* and *DMRTA2*. The analysis of LD pattern using genotypes data from non-Finnish European populations from the 1000 genomes project showed that the associated SNPs in ADHD are in a LD block of 1 kb at the promoter region of the gene. This LD block of four SNPs has three highly associated variants with ADHD (Figure 1) and constitute four haplotypes (frequency>0.01). The rarer haplotype (GGCG) was the risk haplotype for ADHD. An analysis of 91 Spanish subjects confirmed the LD patterns and haplotype frequencies found in 1000 genomes. The SNPs at this block are predicted to be transcription factors binding sites, suggesting a potential role in the regulation of gene expression of *DMRTA1*.

TABLE 1: P-values and Permuted P-values (PermP) from gene-based analysis for DMRT members for each psychiatric phenotype. Significant associations are in bold (P<0.05) and italics (P<0.01)

Gene-based P (PermP)	DMRT1	DMRT2	DMRT3	DMRTA1	DMRTA2	DMRTB1	DMRTC2
Attention-deficit hyperactive disorder	0.00553 (0.0148)	0.68944 (0.6836)	0.050635 (0.0525)	0.001679 (0.0014)	0.008749 (0.0102)	0.30166 (0.3037)	0.70287 (0.6852)
Eating Disorder	0.88819 (0.871)	0.77318 (0.7558)	0.16033 (0.1466)	0.043627 (0.0458)	0.6203 (0.6122)	0.37779 (0.3793)	0.55452 (0.5557)
Alcohol Dependence	0.49788 (0.4852)	0.54931 (0.5394)	0.47752 (0.4622)	0.93794 (0.9314)	0.55744 (0.5561)	0.55653 (0.5437)	0.61481 (0.5983)
Autism Spectrum Disorder	0.54382 (0.629)	0.72307 (0.7059)	0.57195 (0.5553)	0.17341 (0.1676)	0.09627 (0.0944)	0.79893 (0.8133)	0.13409 (0.1278)
Bipolar Disorder	0.117 (0.1141)	0.23739 (0.2361)	0.72334 (0.7133)	0.022515 (0.0234)	0.006227 (0.0084)	0.16982 (0.1639)	0.30155 (0.2958)
Major depressive disorder	0.81545 (0.9125)	0.289 (0.2711)	0.97368 (0.9754)	0.67932 (0.6649)	0.023431 (0.0254)	0.014975 (0.0183)	0.1502 (0.1468)
Obsessive compulsive disorder	0.74843 (0.8564)	0.76718 (0.7736)	0.48494 (0.4681)	0.18845 (0.1845)	0.43058 (0.4252)	0.23264 (0.2229)	0.56038 (0.5619)
Schizophrenia	0.71894 (0.6778)	0.53615 (0.5195)	0.078165 (0.0738)	0.26298 (0.2562)	0.038137 (0.036)	0.31565 (0.3023)	0.11534 (0.1088)
Tourette síndrome	0.84959 (0.8281)	0.42625 (0.4071)	0.64364 (0.6358)	0.3806 (0.3668)	0.92616 (0.9104)	0.69158 (0.683)	0.96722 (0.9562)
Post-traumatic stress disorder	0.20138 (0.2096)	0.30933 (0.2875)	0.46867 (0.4581)	0.78454 (0.7826)	0.68057 (0.6735)	0.66468 (0.6515)	0.45427 (0.4642)
Meta-analysis	0.39914	0.33606	0.67886	0.049278	0.000443	0.039068	0.12951

In mice, we found that *Dmrta1* and *Dmrta2* display different temporal dynamics in their expression in mice midbrains. *Dmrta2* is continuously expressed in the posterior hypothalamic area and midbrain from progenitors until adulthood [21]. In wild-type conditions, *Dmrta1* is expressed in post-mitotic midbrain dopaminergic (mDA) neurons but only transiently and was not observed in mDA progenitors. However, in *Dmrta2* knock-out mice [4] at E14.5, it is also expressed ectopically in midbrain progenitors. *Dmrta2*

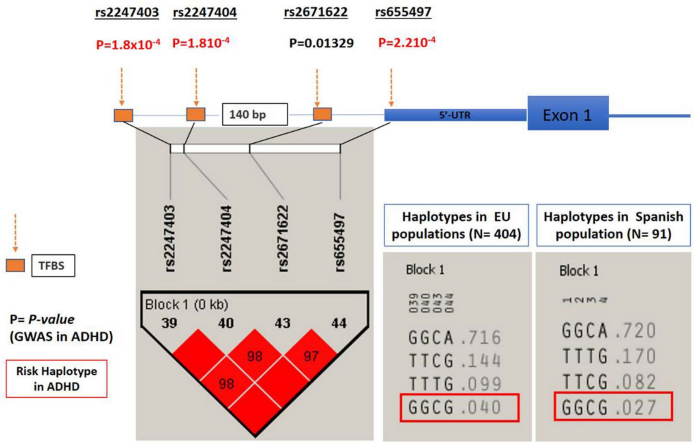

FIGURE 1
Linkage disequilibrium patterns with the four SNPs at *DMRTA1* promoter (<1 kb). The four variants identify four possible haplotypes in non-Finnish European populations. The risk haplotype found in ADHD is also the rarer haplotype in general population. It is shown both haplotype frequencies and samples for individuals in 1000 genomes and an in-house sample of 91 Spanish individuals.

could act repressing *Dmrta1* in this brain region. Ectopic *Dmrta1* expression could compensate an early role for *Dmrta2* in progenitors (at the peak of embryonic testosterone). Interestingly, midbrain dopaminergic neurons alterations have been related to ADHD [22, 23].

We are currently generating constructs to assess gene expression changes associated to the four different haplotypes at *DMRTA1* promoter using Luciferase assay in neuroblastome cell lines. Additionally, *in vivo* studies are underway to assess the effect of the risk haplotype through *in utero* electroporation in mice.

Acknowledgements
Ministerio de Ciencia e Innovación: "Advances in understanding bipolar disorder through the combination of digital phenotyping and genome-wide approaches" (PI: C Toma; Collaborator: JM Fullerton).

This work was supported by Grant PGC2018-101751-A100, by MCIN/AEI /10.13039/501100011033/ and by ERDF "A way of making Europe". RC-N was supported by Ministerio de Universidades - FPU19/02352. ES-S was supported by Grant RYC-2016-20537 funded by MCIN/AEI/10.13039/501100011033 and ESF "Investing in your future".

References

[1] Kopp A. (2012). Dmrt genes in the development and evolution of sexual dimorphism. Trends in genetics: TIG, 28(4), 175–184.

[2] Zarkower D. (2001). Establishing sexual dimorphism: conservation amidst diversity?. Nature reviews. Genetics, 2(3), 175–185.

[3] Kikkawa, T., & Osumi, N. (2021). Multiple Functions of the Dmrt Genes in the Development of the Central Nervous System. Frontiers in neuroscience, 15, 789583.

[4] Saulnier, A., et al (2013). The doublesex homolog Dmrt5 is required for the development of the caudomedial cerebral cortex in mammals. Cerebral cortex (New York, N.Y. : 1991), 23(11), 2552–2567.

[5] Urquhart, J. E., et al (2016). DMRTA2 (DMRT5) is mutated in a novel cortical brain malformation. Clinical genetics, 89(6), 724–727.

[6] Ishii, K., et al (2016). Reelin and Neuropsychiatric Disorders. Frontiers in cellular neuroscience, 10: 229.

[7] Kumar, S., et al (2019). Impaired neurodevelopmental pathways in autism spectrum disorder: a review of signaling mechanisms and crosstalk. Journal of neurodevelopmental disorders, 11(1), 10.

[8] Demontis, D., Walters, R. K., Martin, J., Mattheisen, M., Als, T. D., Agerbo, E., Baldursson, G., Belliveau, R., Bybjerg-Grauholm, J., ... Neale, B. M. (2019). Discovery of the first genome-wide significant risk loci for attention deficit/hyperactivity disorder. Nature genetics, 51(1), 63–75.

[9] Watson HJ, Yilmaz Z, Thornton LM, Hübel C, Coleman JR, Gaspar HA, et al. Genome-wide association study identifies eight risk loci and implicates metabo-psychiatric origins for anorexia nervosa. Nat Genet 2019;51(8):1207-1214.

[10] Walters, R. K., Polimanti, R., Johnson, E. C., McClintick, J. N., Adams, M. J., Adkins, A. E., Aliev, F., Bacanu, S. A., Batzler, A., ... Agrawal, A. (2018). Transancestral GWAS of alcohol dependence reveals common genetic underpinnings with psychiatric disorders. Nature neuroscience, 21(12), 1656–1669.

[11] Grove, J., Ripke, S., Als, T. D., Mattheisen, M., Walters, R. K., Won, H., Pallesen, J., Agerbo, E., Andreassen, O. A., Anney, R., ... Børglum, A. D. (2019). Identification of common genetic risk variants for autism spectrum disorder. Nature genetics, 51(3), 431–444.

[12] Mullins N, Forstner AJ, O'Connell KS, Coombes B, Coleman JR, Qiao Z, et al. Genome-wide association study of more than 40,000 bipolar disorder cases provides new insights into the underlying biology. Nat Genet 2021:1-13.

[13] Howard, D. M., Adams, M. J., Clarke, T. K., Hafferty, J. D., Gibson, J., Shirali, M., Coleman, J., Hagenaars, S. P., Ward, J., Wigmore, E. M., ... McIntosh, A. M. (2019). Genome-wide meta-analysis of depression identifies 102 independent variants and highlights the importance of the prefrontal brain regions. Nature neuroscience, 22(3), 343–352.

[14] International Obsessive Compulsive Disorder Foundation Genetics Collaborative (IOCDF-GC) and OCD Collaborative Genetics Association Studies (OCGAS) (2018). Revealing the complex genetic architecture of obsessive-compulsive disorder using meta-analysis. Molecular psychiatry, 23(5), 1181–1188.

[15] Ripke S, Walters JT, O'Donovan MC, Schizophrenia Working Group of the Psychiatric Genomics Consortium. Mapping genomic loci prioritises genes and implicates synaptic biology in schizophrenia. MedRxiv 2020.

[16] Yu, D., Sul, J. H., Tsetsos, F., Nawaz, M. S., Huang, A. Y., Zelaya, I., Illmann, C., Osiecki, L., Darrow, S. M., Hirschtritt, M. E., Greenberg, E., ... Tourette Association of America International Consortium for Genetics, the Gilles de la Tourette GWAS Replication Initiative, the Tourette International Collaborative Genetics Study, and the Psychiatric Genomics Consortium Tourette Syndrome Working Group (2019). Interrogating the Genetic Determinants of Tourette's Syndrome and Other Tic Disorders Through Genome-Wide Association Studies. The American journal of psychiatry, 176(3), 217–227.

[17] Nievergelt, C. M., Maihofer, A. X., Klengel, T., Atkinson, E. G., Chen, C. Y., Choi, K. W., Coleman, J., Dalvie, S., Duncan, L. E., ... Koenen, K. C. (2019). International meta-analysis of PTSD genome-wide association studies identifies sex- and ancestry-specific genetic risk loci. Nature communications, 10(1), 4558.

[18] Martin, J., Walters, R. K., Demontis, D., Mattheisen, M., Lee, S. H., Robinson, E., Brikell, I., Ghirardi, L., Larsson, H., Lichtenstein, P., Eriksson, N., 23andMe Research Team, Psychiatric Genomics Consortium: ADHD Subgroup, iPSYCH–Broad ADHD Workgroup, Werge, T., Mortensen, P. B., Pedersen, M. G., Mors, O., Nordentoft, M., Hougaard, D. M., ... Neale, B. M. (2018). A Genetic Investigation of Sex Bias in the Prevalence of Attention-Deficit/Hyperactivity Disorder. Biological psychiatry, 83(12), 1044–1053.

[19] Di Meglio, T., Kratochwil, C. F., Vilain, N., Loche, A., Vitobello, A., Yonehara, K., Hrycaj, S. M., Roska, B., Peters, A. H., Eichmann, A., Wellik, D., Ducret, S., & Rijli, F. M. (2013). Ezh2 orchestrates topographic migration and connectivity of mouse precerebellar neurons. Science (New York, N.Y.), 339(6116), 204–207.

[20] Konno, D., Iwashita, M., Satoh, Y., Momiyama, A., Abe, T., Kiyonari, H., & Matsuzaki, F. (2012). The mammalian DM domain transcription factor Dmrta2 is required for early embryonic development of the cerebral cortex. PloS one, 7(10), e46577.

[21] Gennet, N., Gale, E., Nan, X., Farley, E., Takacs, K., Oberwallner, B., Chambers, D., & Li, M. (2011). Doublesex and mab-3-related transcription factor 5 promotes midbrain dopaminergic identity in pluripotent stem cells by enforcing a ventral-medial progenitor fate. Proceedings of the National Academy of Sciences of the United States of America, 108(22), 9131–9136.

[22] Montarolo F, et al. NURR1 Impairment in Multiple Sclerosis. Int J Mol Sci 2019;20(19).

[23] Razoki B. Neurofeedback versus psychostimulants in the treatment of children and adolescents with attention-deficit/hyperactivity disorder: a systematic review. Neuropsychiatr Dis Treat 2018;14:2905-13

Ischemic stroke & Artificial networks - network performance depending on the use of expert or non-expert training data

Author
Sophia Hemm – Department of Neurology, Jena University Hospital, Germany; Biomagnetic Center, Jena University Hospital, Germany; Else Kröner Graduate School for Medical Students 'JSAM', Jena University Hospital, Germany
Franziska Wagner – Department of Neurology, Jena University Hospital, Germany; Biomagnetic Center, Jena University Hospital, Germany; Clinician Scientist Program OrganAge, Jena University Hospital, Germany
Carsten M. Klingner – Department of Neurology, Jena University Hospital, Germany; Biomagnetic Center, Jena University Hospital, Germany;
Stefan Brodoehl – Department of Neurology, Jena University Hospital, Germany; Biomagnetic Center, Jena University Hospital, Germany

Citation
Hemm, S., Wagner, F., Klingner, C.M., Brodoehl, S. Ischemic stroke & Artificial networks - network performance depending on the use of expert or non-expert training data

Introduction/Motivation

Stroke is one of the deadliest diseases worldwide and was the second-leading cause of death in 2019 [1],[2]. Diagnosing an acute stroke from non-contrast-enhanced CT (NC-CT) images is often a challenge even for experienced physicians. However, there is an opportunity to counteract this problem: Artificial Intelligence and in particular Neural Networks, which show

already promising results in this context [3],[4],[5]. Nevertheless, preparing a lot of high-quality processed data for the training of stroke-detecting networks is time-consuming and only a few experts can provide it.

Therefore, we asked to what extent the stroke detection performance of a network is dependent on the experience of the person preparing the training data: what is the difference in performance between a network trained with data processed by a non-expert (e.g., a medical student) and one trained with data processed by an expert (e.g., an experienced neurologist). Furthermore, we aimed to understand whether the performance of a network trained with expert data can be improved by augmenting its training data with additional non-expert-generated data. Besides, the agreement in detecting potential strokes in NC-CT images was compared between a non-expert and an expert.

Methods

For this purpose, 108 NC-CT images of a total of 50 stroke patients were processed independently by both an expert (a specialist for neurology) and a non-expert (a medical student) according to a pipeline established during the project. The pipeline focused mainly on the following: Stroke yes/no, drawing

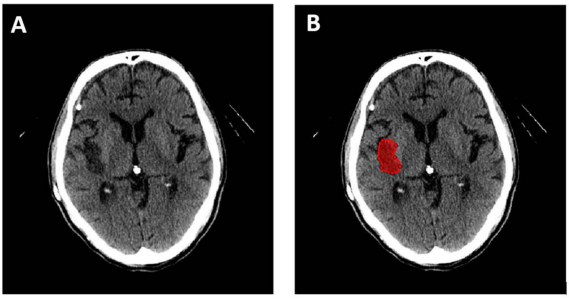

FIGURE 1

Processing pipeline: marking of a lesion

A: The rater was presented with an NC-CT image to detect a potentially present stroke

B: Acute MCA stroke right, detected and marked by the rater

in the lesion, if necessary (refer to Fig.1), defining the location of the lesion. Afterward, this processed data was used for training three Neural Networks according to a well-known and well-established network architecture (*DenseNet121*, provided by the PyTorch-based framework 'MONAI' (https://monai.io/index.html; last visited on 05.11.2022)): an Expert Network (EN), a Non-Expert Network (N-EN), and an Extended Expert Network (E-EN).

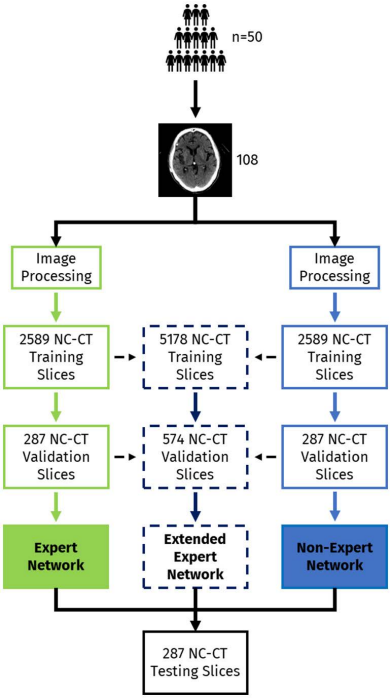

FIGURE 2
Network configuration and training
Green: Expert Network's training
Light blue: Non-Expert Network's training
Dark blue: Extended Expert Network's training

While the EN was trained with the image data processed only by the expert, the N-EN was trained with those processed only by the non-expert, and the E-EN with the expert training set augmented by the non-expert image data (refer to Fig.2). The aim of the network training was not to determine the location of the lesion and/or the associated affected arteries, but to differentiate between 'NC-CT image with stroke' (=*strokes*) and 'NC-CT image without stroke' (=*non-strokes*). To compare the performance of the trained networks, three measures frequently used in this context were assessed: *Precision* (≙ positive predictive value), *Recall* (≙ sensitivity), and *F1-Score* (≙ weighted average of Precision and Recall). To determine the agreement in detecting potential strokes in NC-CT images between the non-expert and the expert, *Cohen's kappa coefficient* κ was calculated.

Results and discussion

First, we found a high level of agreement in stroke detection between the non-expert and the expert (κ= .834, P<.05, [6]).

Second, particularly as measured by comparison of the median F1-Score (=$Mdn_{\text{F1-Score}}$), the EN performed better than the N-EN in correctly detecting both *non-strokes* and *strokes* (***non-strokes*:** $Mdn_{\text{F1-ScoreEN}}$ = 0.866 vs. $Mdn_{\text{F1-ScoreN-EN}}$ = 0.825; ***strokes***: $Mdn_{\text{F1-ScoreEN}}$ = 0.857 vs. $Mdn_{\text{F1-ScoreN-EN}}$ = 0.788).

Third, and of paramount importance, we found that the E-EN outperformed the pure EN (***non-strokes:*** $Mdn_{\text{F1-ScoreE-EN}}$ = 0.880 vs. $Mdn_{\text{F1-ScoreEN}}$ =0.866; ***strokes***: $Mdn_{\text{F1-ScoreE-EN}}$ = 0.869 vs. $Mdn_{\text{F1-ScoreEN}}$ = 0.857).

We chose this network architecture, which can be assigned to so-called 'Densely Connected Convolutional Networks' and thus to Deep Learning, due to, in contrast to classical Machine Learning techniques, the possibility of using unstructured, complex, and raw data as network input. Furthermore, the probability of a potential information loss is lower than in classical Convolutional Networks [7] and therefore this architecture seemed the most suitable for our study.

Our data show that the performance divergence between an EN and an N-EN is very small but more important, that an EN can be improved by training it additionally with non-expert data: heterogeneity of training data seems to be a very relevant and performance-determining factor.

Consequently, our results suggest that the use of data labeled and processed by non-experts introduces new possibilities to generate new and improve existing training data for the automated detection of strokes as well as further applications. This could lead to overall better, faster, and more accurate care for patients with stroke, thus positively influencing their survival and individual outcome.

References

[1] World Health Organization W, Organization WH. 2020. 'The Top 10 Causes of Death'.

[2] Collaborators, G. B. D. Stroke. 2021. 'Global, Regional, and National Burden of Stroke and Its Risk Factors, 1990-2019: A Systematic Analysis for the Global Burden of Disease Study 2019'. Lancet Neurol 20(10):795–820. doi: 10.1016/S1474-4422(21)00252-0.

[3] Lo, C. M., P. H. Hung, and D. T. Lin. 2021. 'Rapid Assessment of Acute Ischemic Stroke by Computed Tomography Using Deep Convolutional Neural Networks'. J Digit Imaging 34(3):637–46. doi: 10.1007/s10278-021-00457-y.

[4] Qiu, W., H. L. Kuang, E. Teleg, J. M. Ospel, S. I. Sohn, M. Almekhlafi, M. Goyal, M. D. Hill, A. M. Demchuk, and B. K. Menon. 2020. 'Machine Learning for Detecting Early Infarction in Acute Stroke with Non-Contrast-Enhanced CT'. Radiology 294(3):638–44. doi: 10.1148/radiol.2020191193.

[5] Soun, J. E., D. S. Chow, M. Nagamine, R. S. Takhtawala, C. G. Filippi, W. Yu, and P. D. Chang. 2021. 'Artificial Intelligence and Acute Stroke Imaging'. AJNR Am J Neuroradiol 42(1):2–11. doi: 10.3174/ajnr.A6883.

[6] Landis, J. R., and G. G. Koch. 1977. 'The Measurement of Observer Agreement for Categorical Data'. Biometrics 33(1):159–74.

[7] G. Huang, Z. Liu, L. Van Der Maaten, and K. Q. Weinberger. 2017. 'Densely Connected Convolutional Networks'. Pp. 2261–69 in 2017 IEEE Conference on Computer Vision and Pattern Recognition (CVPR).

Altered functional organization of iPSCs-derived neuronal networks in major depressive disorder

Author
Rahaf Issa*, Simon Wein, Vladimir Milenkovic, Christian Wetzel, Jens Schwarzbach – Department of Psychiatry and Psychotherapy, University of Regensburg, Regensburg, Germany

Citation
Issa, R., Wein, S., Milenkovic, V., Wetzel, C., Schwarzbach, J. Altered functional organization of iPSCs-derived neuronal networks in major depressive disorder.

Introduction/Motivation

The brain is a complex network with distinctive functional topology that reflects optimized network integrity and information transfer [1]. Such architecture allows for an efficient integration of information across distant parts of the network while still maintaining a level of segregation in which effective local neural communication and functional specialization is feasible [2]. Several brain imaging studies have demonstrated that these functional network properties are disrupted in clinical disorders like major depression disorders (MDD), giving rise to clinical symptoms such as depressed mood and anhedonia [3, 4]. However, whether network alterations in depression are detectable on a smaller spatial scale of cultured neural networks is still unknown. In this study, we investigated whether neurons derived from

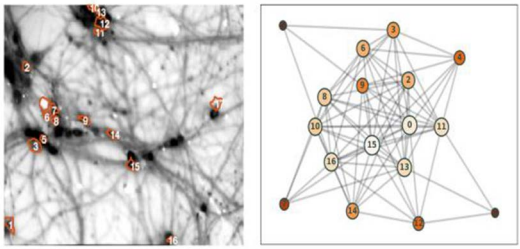

FIGURE 1
Neuronal Network illustrated as a graph. On the left, the field of view from one neuronal culture with the active cells contoured in orange. On the right, the corresponding graph where the nodes represent the active neurons and the edges represent the pairwise correlation of their activity.

induced human pluripotent stem cells (hiPSCs) [5] already show altered network properties compared to controls when their spontaneous activity is observed *in-vitro*. Such alterations, if present, would reflect inherently disturbed network properties in depression, even at the early stages of network formation and maturation. Network properties could be examined by means of graph theory, a mathematical framework that allows for modelling neuronal networks as graphs composed of nodes (representing active neurons) connected by edges (representing inter-regional functional relation) (Fig. 1) [6].

Methods

We derived hiPSCs from somatic cells of 9 MDD patients and their matched controls, which we then reprogrammed into neural progenitor cells (NPCs). In a later step, we differentiated NPCs into neurons as described in [7]. Next, we loaded the mature neuronal cultures with a calcium-sensitive fluorescent dye and recorded 20 minutes of their spontaneous activity *in-vitro* by means of calcium imaging. We motion corrected the videos and extracted time courses of regions of interest (active cells) in each recording and computed their pairwise correlations to obtain connectivity matrices. We studied the binarized adjacency matrices as undirected graphs consisting of nodes (segmented active cells) and edges (statistical dependencies between the

cells' time courses) and probed their network topology within the framework of graph theory. To examine differential global and local functional network architecture in cultures of depressed patients and controls, we computed a number of graph measures that included global efficiency, local efficiency, and clustering coefficient. To account for the variability of the number of cells, we randomly sampled 500 combinations of 5 to up to 60 cells in each video and computed graph measures averaged across respective sample sizes. It is worth noting that the functional topology of the constructed graph is heavily dependent on the choice of the threshold used to create the adjacency matrices. Therefore, we computed graph measures for all thresholds between ± 0.1 and ± 0.8. The significance of the difference in graph measures between patients and control was tested at each number of cells for every threshold using Monte Carlo permutation test. We shuffled group labels and computed a t-test 5000 times to create the null-distribution of t-values and used it to assess the observed t value of group difference. A group difference was considered significant if the Monte Carlo p-value was ≤ 0.05. Furthermore, we investigated the Pearson correlation between depression severity and graph measures for depressed patients where the correlation was considered significant at a p-value ≤ 0.05.

Results and discussion

Neuronal cultures of MDD patients showed lower global efficiency compared to controls which was significantly different for most thresholds (except for 0.3 and 0.4) and for numbers of cells ranging from 26-53. The reduced global efficiency in MDD neurons reflects reduced effectiveness in parallel information transfer across the entirety of the network and reduced network capacity to globally integrate information (Fig. 2). On the regional level, local efficiency was also decreased in patient-derived neuronal networks indicating a local disruption of information transfer within the subnetworks of neighbouring neurons (p-value < 0.05 for thresholds 0.1 and 0.2 and number of cells between 26 and 53). Clustering coefficient followed the same pattern with patient-derived neurons exhibiting lower clustering tendencies (p-value <0.05 for all thresholds (except 0.3 and 0.4) and for cell numbers 15-28 and 38-53). The diminished local efficiency and clustering coefficient in

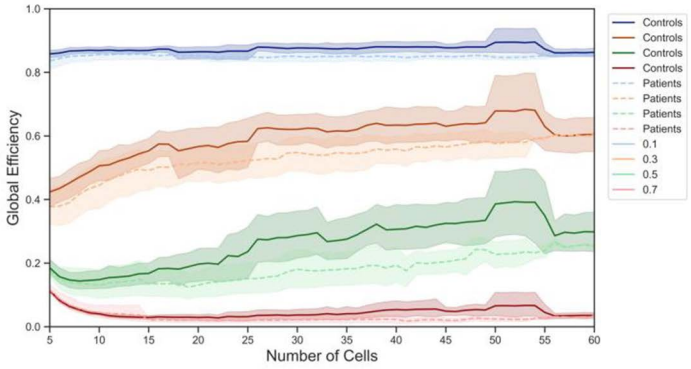

FIGURE 2
Global efficiency was reduced in graphs of depressed patients (dashed lines) compared to controls (solid lines). This difference persisted regardless of the network size or the threshold used to compute adjacency matrices (shown in different colours). Global efficiency was computed for all thresholds ranging from ± 0.1 – 0.8. For the sake of clarity, results of only four thresholds are show here. Shaded area represents the 95% confidence interval.

patient networks point to reduced network propensity to segregate and form specialized modules Finally, no correlation was found between depression severity and any of the graph measures. Our findings suggest a reduced integration and segregation properties of *in-vitro,* micro-scale neuronal networks of depressed patients and that such alterations are detectable in a small-scale topology of iPSCs-derived neurons. This might suggest a genetic predisposition for the network in depression to develop disrupted functional organization. hiPSC-derived neuronal cultures may thus provide a promising model to explore and perturb network properties in depression.

References

[1] Sporns, O. (2011). The human connectome: a complex network. *Annals of the New York Academy of Sciences*, 1224(1), 109-125.

[2] Sporns, O., Tononi, G., & Edelman, G. M. (2000). Connectivity and complexity: the relationship between neuroanatomy and brain dynamics. Neural networks, 13(8-9), 909-922.

[3] Gong, Q., & He, Y. (2015). Depression, neuroimaging and connectomics: a selective overview. *Biological psychiatry*, 77(3), 223-235.

[4] Fornito, A., & Bullmore, E. T. (2012). Connectomic intermediate phenotypes for psychiatric disorders. *Frontier in psychiatry*, 3, 32.

[5] Nishikawa, S. I., Goldstein, R. A., & Nierras, C. R. (2008). The promise of human induced pluripotent stem cells for research and therapy. *Nature reviews Molecular cell biology*, 9(9), 725-729.

[6] Bullmore, E., & Sporns, O. (2009). Complex brain networks: graph theoretical analysis of structural and functional systems. *Nature reviews neuroscience*, 10(3), 186-198.

[7] Triebelhorn, J., Cardon, I., Kuffner, K., Bader, S., Jahner, T., Meindl, K., ... & Wetzel, C. H. (2022). Induced neural progenitor cells and iPS-neurons from major depressive disorder patients show altered bioenergetics and electrophysiological properties. *Molecular Psychiatry*, 1-11.

Acoustic and visual mismatch negativity as potential biomarkers in schizophrenia

Author
Hajnalka Molnár, Csilla Marosi, Kinga Farkas, Gábor Csukly – Department of Psychiatry and Psychotherapy, Semmelweis University, Budapest, Hungary

Citation
Molnár, H., Marosi, C., Farkas, K., Csukly, G. Acoustic and visual mismatch negativity as potential biomarkers in schizophrenia

Introduction/Motivation

Mismatch negativity (MMN) is an event-related potential (ERP), elicited to a visual or acoustic oddball paradigm, in which repeated standard stimuli are disrupted by deviants [1]. The signal latency and amplitude varies according to the stimulus characteristics [2]. For the registration of the MMN signal, participants' attention is not needed [3], therefore it can be elicited by stimuli, that is unrelated to the task [4]. Previous pharmaceutical studies found that NMDA-receptor antagonists, such as ketamine can trigger positive, negative and cognitive symptoms of schizophrenia. These drugs also caused the decrease of the auditory MMN signal in healthy volunteers, proving the link to NMDA-receptor function [5]. Both visual and auditory MMN are widely investigated in schizophrenia, as promising biomarkers, but until now, the two modalities were always examined separately. Our aim was to examine auditory and visual mismatch negativity in schizophrenia and their correlation with the patients' clinical and demographical data.

Methods

Altogether 39 patients with schizophrenia and 39 healthy controls matched in age, gender, and education were enrolled in the study. EEG was recorded in eight experimental blocks, using a 64 channel quikcap. As acoustic stimuli, we presented 100 and 200 ms long beeping sounds. As visual stimuli, 6 and 12 vane windmill patterns were presented to the subjects. Mismatch responses were obtained by subtracting responses to standard from the physically identical deviant stimuli. We defined three regions of interest for auditory MMN (right and left frontal, frontocentral) and four regions of interest for visual MMN (left, right and midline occipital, frontal). The recorded EEG data was analysed with a mixed linear model. The correlations were analysed by Pearson and Spearman correlation.

Results and discussion

In the control group, a significant MMN signal was detected to both acoustic stimuli, in all regions of interest, while no mismatch signal was detected in the patient group. The between group difference was significant. The short stimulus had the largest effect size among all stimuli, in the left frontal region (Cohen's d=0.69). *Figure 1* presents the line plots of this region and the topoplots of the short acoustic stimulus. The 12 vane windmill pattern evoked MMN in both study groups but in different regions. The 6 vane windmill pattern evoked MMN only in the patient group. Interestingly, the between group difference was not significant for the visual stimuli. No correlation was found between the MMN amplitude and the demographical variables, illness duration, symptom severity (PANSS score) or the antipsychotic medication dosage (in the terms of chlorpromazine (CPZ) equivalent). According to our results, acoustic stimulus processing tends to be impaired more in schizophrenia compared to visual processing. Considering the robust between group difference and the larger effect size, acoustic mismatch negativity is a more promising candidate for biomarker in schizophrenia. Glutamatergic transmission is still a promising drug target in schizophrenia, while MMN is connected to NMDA function, which connection makes it a potential biomarker for monitoring drug efficacy.

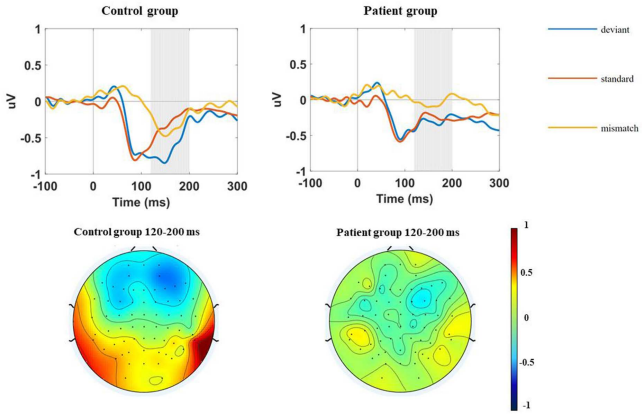

FIGURE 1
Line plots and topoplots of the short acoustic stimulus.

References

1. Kremláček, J., et al., Visual mismatch negativity (vMMN): A review and meta-analysis of studies in psychiatric and neurological disorders. Cortex, 2016. 80: p. 76-112.

2. Fitzgerald, K. and J. Todd, Making Sense of Mismatch Negativity. Front Psychiatry, 2020. 11: p. 468.

3. Stefanics, G., J. Kremláček, and I. Czigler, Visual mismatch negativity: a predictive coding view. Frontiers in human neuroscience, 2014. 8: p. 666-666.

4. Garrido, M.I., et al., The mismatch negativity: A review of underlying mechanisms. Clinical Neurophysiology, 2009. 120(3): p. 453-463.

5. Catts, V.S., et al., A quantitative review of the postmortem evidence for decreased cortical N-methyl-d-aspartate receptor expression levels in schizophrenia: How can we link molecular abnormalities to mismatch negativity deficits? Biological Psychology, 2016. 116: p. 57-67.

Early magnetoencephalography power alterations in individuals at risk for Alzheimer's disease during the retrieval phase of a working memory task with faces

Author

Alberto Nebreda – Center for Cognitive and Computational Neuroscience, Complutense University of Madrid, 28223, Pozuelo de Alarcón, Spain; Departament of Experimental Psychology, Cognitive Psychology and Speech & Language Therapy, Complutense University of Madrid, 28223, Pozuelo de Alarcón, Spain
Alejandra García-Colomo – Center for Cognitive and Computational Neuroscience, Complutense University of Madrid, 28223, Pozuelo de Alarcón, Spain; Departament of Experimental Psychology, Cognitive Psychology and Speech & Language Therapy, Complutense University of Madrid, 28223, Pozuelo de Alarcón, Spain
Martín Carrasco – Center for Cognitive and Computational Neuroscience, Complutense University of Madrid, 28223, Pozuelo de Alarcón, Spain; Departament of Electronical Engineering, Polytechnic University of Madrid, 28040, Madrid, Spain
Jaisalmer de Frutos – Center for Cognitive and Computational Neuroscience, Complutense University of Madrid, 28223, Pozuelo de Alarcón, Spain; Departament of Experimental Psychology, Cognitive Psychology and Speech & Language Therapy, Complutense University of Madrid, 28223, Pozuelo de Alarcón, Spain
Ricardo Bruña – Center for Cognitive and Computational Neuroscience, Complutense University of Madrid, 28223, Pozuelo de Alarcón, Spain; Department of Radiology, Rehabilitation, and Physiotherapy, Complutense University of Madrid, 28040, Madrid, Spain; Instituto de Investigación Sanitaria San Carlos (IdISSC), 28040, Madrid, Spain
Federico Ramírez-Toraño – Center for Cognitive and Computational Neuroscience, Complutense University of Madrid, 28223, Pozuelo de Alarcón, Spain; Departament of Experimental Psychology, Cognitive Psychology and Speech & Language Therapy, Complutense University of Madrid, 28223, Pozuelo de Alarcón, Spain

Fernando Maestú – Center for Cognitive and Computational Neuroscience, Complutense University of Madrid, 28223, Pozuelo de Alarcón, Spain; Departament of Experimental Psychology, Cognitive Psychology and Speech & Language Therapy, Complutense University of Madrid, 28223, Pozuelo de Alarcón, Spain

Citation
Nebreda, A., García-Colomo, A., Carrasco, M., de Frutos, J., Bruña, R., Ramírez-Toraño, F., Maestú, F. Early magnetoencephalography power alterations in individuals at risk for Alzheimer's disease during the retrieval phase of a working memory task with faces.

Introduction/Motivation

The first pathological signs of Alzheimer's disease (AD) appear decades before a diagnosis can be made. By the time the first diagnosable cognitive symptoms appear, deterioration at the neurological level is already very extensive (Sperling et al., 2011). This fact could be one of the main reasons why an effective treatment has not yet been found. Therefore, it is of utmost importance to find biomarkers that can predict AD in its early stages, opening the door to the study of early pharmacological treatments that act on the brain when it is not yet so damaged, or to the development of preventive interventions, in areas such as cognitive training, nutrition or physical exercise, that can try to delay the progression of the disease as long as possible. Furthermore, the updated research framework for AD, proposed by the National Institute of Aging-Alzheimer's Association (NIA-AA) Work Group, defines AD as a biological construct and emphasizes the importance of incorporating biomarkers in AD research (Jack et al., 2018).

Electrophysiological techniques such as electroencephalography (EEG) or magnetoencephalography (MEG) have several advantages for studying the dynamic activities of the brain during cognitive tasks. Since most cognitive processes are fast and occur within tens to hundreds of milliseconds, these

methods, which have temporal resolution in the order of milliseconds, can capture cognitive dynamics in the same time frame in which cognition occurs (Cohen, 2011).

Using magnetoencephalography, differential patterns have been found for various stages prior to Alzheimer's dementia. Differences have been found between mild cognitive impairment (MCI) and healthy subjects both in resting state (Nakamura et al., 2018) and during cognitive tasks (Serrano et al., 2020). MEG signatures have even been previously used as a biomarker to correctly identify MCI by means of a predictive model (Amezquita-Sanchez et al., 2016). Differences have also been found using this technique in patients with subjective cognitive decline (SCD), proposed as an even earlier indicator of preclinical AD (López-Sanz et al., 2016). Recently, it has been shown that MEG can also detect alterations in subjects with a high risk of developing the disease, even before any clinical symptoms are present (Ramírez-Toraño et al., 2021). However, thus far, these studies have been limited to analyses in resting state. This study aims to analyze electrophysiological alterations in subjects at high risk of developing AD during the performance of a face memorization task, specifically, during the period of visualization of the second face in the retrieval phase. To our knowledge, this is the first study finding differences in this kind of sample during a cognitive task.

Methods

The sample consisted of 235 healthy subjects, 166 with a family history of AD and 69 without a family history, who underwent a comprehensive evaluation, including magnetoencephalography (MEG), magnetic resonance imaging (MRI) and genotyping, among others. A subsample of 53 subjects aged 50 to 80 years was selected, maximizing the difference in genetic risk: 26 with no family history and low genetic risk (non-carriers of allele 4 of the APOE gene); and 27 with family history and high genetic risk (carriers of allele 4 of the APOE gene).

Artifact-free epochs, relative to the retrieval period (1 second corresponding to the presentation of the second face), were analysed in the time-frequency

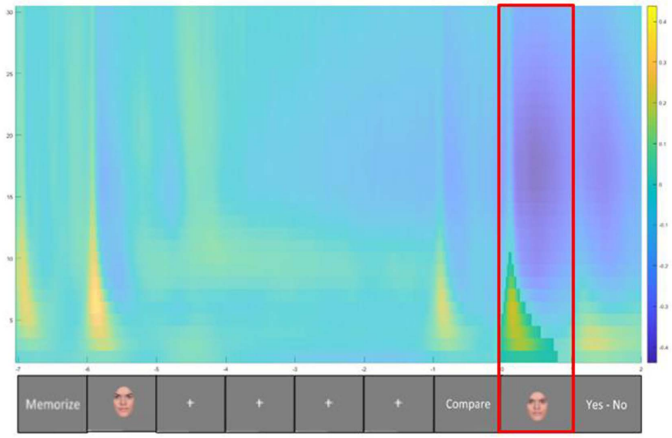

FIGURE 1

Average Time-Frequency Representation with task pictures and chosen window for analyses.
The Y-axis represents the frequency in Hertz. The X-axis represents the time in seconds (0 corresponds to the presentation of the second face). The color code represents the power at each time-frequency step.

domain using 5-cycle Gaussian Morlet wavelets, from 2Hz to 30Hz in 1Hz frequency steps and 10ms time steps.

To specify the window of interest in which to perform the analyses, an average of the time-frequency activity was calculated for all subjects, and specific time-frequency steps related to visual activation were chosen for further analyses (Fig. 1).

Subsequently, a cluster-based permutation test (CBPT) was performed to correct for the multiple comparisons problem, comparing the low-risk group with the high-risk group. This analysis was performed both in sensor space, and after a source reconstruction using beamformer, specifically in the calcarine and in fusiform areas.

For comparison, the same analyses were repeated in the encoding period (1 second corresponding to the presentation of the first face).

Results and discussion

Subjects with higher genetic risk presented a cluster with greater relative power in the visual activation window during the presentation of the second face, in the retrieval period. Significant clusters were found both in sensor space (Fig. 2) and in the left and right fusiform gyri after source reconstruction. A cluster with the same positive trend was found in the calcarine cortex, but it did not reach significance.

When performing the same analysis, but during the presentation of the first face, in the encoding period, no significant clusters were found in any of the aforementioned spaces.

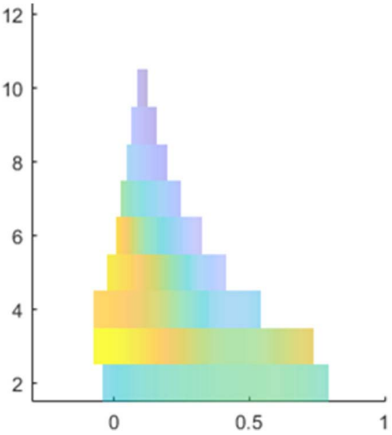

FIGURE 2

Cluster of significant activation differences between high-risk and low-risk group in sensor space (p = 0.0062). The Y-axis represents the frequency in Hertz. The X-axis represents time in seconds. The color code represents the power at each time-frequency step. The colored steps are those on which the CBPT analysis was performed, corresponding to those shown activated in Figure 1.

These results could indicate an early affection of the visual system, which is compatible with previous findings we have made relating ophthalmologic measures and MEG power (Nebreda et al., under review). However, given that the effects are more prevalent in the fusiform gyri than in the calcarine cortex, and that they appear only during the retrieval period, and not during the encoding stage, this could indicate abnormalities in cognitive, and not purely sensory activity.

The main interest of these results, besides the solely theoretical one of being able to better understand the preclinical stages of AD, or the differences based on the genetic risk of suffering from it, is to be able to use the clusters found as a biomarker, which, in combination with others, could be used in the generation of models to predict whether the subject is in the continuum of AD and has started to develop neurological signs of it, with minimal invasiveness.

In this sense, artificial intelligence (AI) models that attempt to do this often have a limited number of subjects, and a huge amount information and possible variables, so they can benefit greatly from having specific sets of information to use as *a priori* targets for their models.

References

Amezquita-Sanchez, J. P., Adeli, A., & Adeli, H. (2016). A new methodology for automated diagnosis of mild cognitive impairment (MCI) using magnetoencephalography (MEG). *Behavioural Brain Research*, *305*, 174–180. https://doi.org/10.1016/j.bbr.2016.02.035

Cohen, M. X. (2011). It's about time. In *Frontiers in Human Neuroscience* (Issue JANUARY, pp. 1–16). Frontiers Media S. A. https://doi.org/10.3389/fnhum.2011.00002

Jack, C. R., Bennett, D. A., Blennow, K., Carrillo, M. C., Dunn, B., Haeberlein, S. B., Holtzman, D. M., Jagust, W., Jessen, F., Karlawish, J., Liu, E., Molinuevo, J. L., Montine, T., Phelps, C., Rankin, K. P., Rowe, C. C., Scheltens, P., Siemers, E., Snyder, H. M., … Silverberg, N. (2018). NIA-AA Research Framework: Toward a biological definition of Alzheimer's disease. In *Alzheimer's and Dementia* (Vol. 14, Issue 4, pp. 535–562). Elsevier Inc. https://doi.org/10.1016/j.jalz.2018.02.018

López-Sanz, D., Brunã, R., Garcés, P., Camara, C., Serrano, N., Rodríguez-Rojo, I. C., Delgado, M. L., Montenegro, M., López-Higes, R., Yus, M., & Maestú, F. (2016). Alpha band disruption in the AD-continuum starts in the Subjective Cognitive Decline stage: A MEG study. *Scientific Reports*, *6*. https://doi.org/10.1038/srep37685

Nakamura, A., Cuesta, P., Fernández, A., Arahata, Y., Iwata, K., Kuratsubo, I., Bundo, M., Hattori, H., Sakurai, T., Fukuda, K., Washimi, Y., Endo, H., Takeda, A., Dlers, K., Bajo, R., Maestú, F., Ito, K., & Kato, T. (2018). Electromagnetic signatures of the preclinical and prodromal stages of Alzheimer's disease. *Brain*, *141*(5), 1470–1485. https://doi.org/10.1093/brain/awy044

Ramírez-Toranõ, F., Brunã, R., de Frutos-Lucas, J., Rodríguez-Rojo, I. C., Marcos De Pedro, S., Delgado-Losada, M. L., Gómez-Ruiz, N., Barabash, A., Marcos, A., López Higes, R., & Maestú, F. (2021). Functional Connectivity Hypersynchronization in Relatives of Alzheimer's Disease Patients: An Early E/I Balance Dysfunction? *Cerebral Cortex*, *31*(2), 1201–1210. https://doi.org/10.1093/cercor/bhaa286

Serrano, N., López-Sanz, D., Bruña, R., Garcés, P., Rodríguez-Rojo, I. C., Marcos, A., Crespo, D. P., & Maestú, F. (2020). Spatiotemporal Oscillatory Patterns during Working Memory Maintenance in Mild Cognitive Impairment and Subjective Cognitive Decline. *International Journal of Neural Systems*, *30*(1). https://doi.org/10.1142/S0129065719500199

Sperling, R. A., Aisen, P. S., Beckett, L. A., Bennett, D. A., Craft, S., Fagan, A. M., Iwatsubo, T., Jack, C. R., Kaye, J., Montine, T. J., Park, D. C., Reiman, E. M., Rowe, C. C., Siemers, E., Stern, Y., Yaffe, K., Carrillo, M. C., Thies, B., Morrison-Bogorad, M., … Phelps, C. H. (2011). Toward defining the preclinical stages of Alzheimer's disease: Recommendations from the National Institute on Aging-Alzheimer's Association workgroups on diagnostic guidelines for Alzheimer's disease. *Alzheimer's & Dementia*, *7*(3), 280–292. https://doi.org/10.1016/J.JALZ.2011.03.003

Spectral analysis of after-discharges elicited by intracranial 50 Hz stimulation of epileptic patients

Author
Johanna-Petra Szabó – Epilepsy Unit, National Institute of Mental Health, Neurology and Neurosurgery, Budapest, Hungary; János Szentágothai Doctoral School of Neurosciences, Semmelweis University, Budapest, Hungary
Boglárka Hajnal – Epilepsy Unit, National Institute of Mental Health, Neurology and Neurosurgery, Budapest, Hungary; János Szentágothai Doctoral School of Neurosciences, Semmelweis University, Budapest, Hungary
Sákovics Anna – Epilepsy Unit, National Institute of Mental Health, Neurology and Neurosurgery, Budapest, Hungary; János Szentágothai Doctoral School of Neurosciences, Semmelweis University, Budapest, Hungary
Loránd Erőss – Department of Functional Neurosurgery, National Institute of Mental Health, Neurology and Neurosurgery, Budapest, Hungary
Dániel Fabó– Epilepsy Unit, National Institute of Mental Health, Neurology and Neurosurgery, Budapest, Hungary

Citation
Szabó, J.-P., Hajnal, B., Anna, S., Erőss, L., Fabó, D. Spectral analysis of after-discharges elicited by intracranial 50 Hz stimulation of epileptic patients.

Introduction/Motivation

Patients with drug-resistant epilepsy (DRE) might benefit from surgical treatment only when the epileptic focus is focalized and if the resected brain

area does not overlap with functionally eloquent regions. For this reason, DRE patients are submitted to detailed presurgical evaluation, including video-EEG monitoring, MRI imaging and neuropsychological assessment. In some cases, where the epileptic focus cannot be determined by non-invasive measures, resection is preceded by the implantation of diagnostic electrodes, such as stereo-electroencephalographic (SEEG) and electrocorticographic (ECoG) electrodes. These tools offer the possibility to perform functional mapping of eloquent and symptomatogenic areas by sending electrical pulses to the cortex through invasive electrodes, using either single pulse- or high frequency (50 Hz) stimulation protocol [1]. Beside seizures and auras elicited by the stimulation, rhythmic stimulation-induced discharges, known as after-discharges (AD), might also convey information on the epileptogenic network. ADs were described and related to epileptic processes almost a century ago [2,3] and clinicians routinely use them to aid the localization of the epileptogenic zone (EZ). Nevertheless, ADs appear in both epileptogenic and non-epileptogenic areas and present high inter- and intrasubject variability [4,5]. Hence, the latent neuronal processes, as well as its exact relationship with the EZ are still poorly understood. Our goal is to delineate spectral characteristics of ADs derived from macro- and microelectrode recordings. Additionally, we aim to differentiate measures predicting their appearance and correlation with the EZ.

Methods

Our study examines the data of 12 patients undergoing presurgical evaluation with intracerebral depth - or subdural grid electrodes, presenting prominent ADs in the course of a 50 Hz stimulation protocol. Simultaneously with diagnostic macroelectrodes, laminar multielectrode arrays (LME) have been also implanted in the hypothesized EZ. ADs are visually identified on the macroelectrode recordings of all patients. Stimulation artifacts are removed using spline interpolation between each stimulus peak (1. Figure). Spectral characteristics of the detected events are calculated and AD containing epochs are compared with AD-free stimulation periods (2. Figure). Patients with LMEs placed near an AD-presenting electrode (at 0.5-1.5 cm distance), are selected for further analysis (analysis of LME data still in progress).

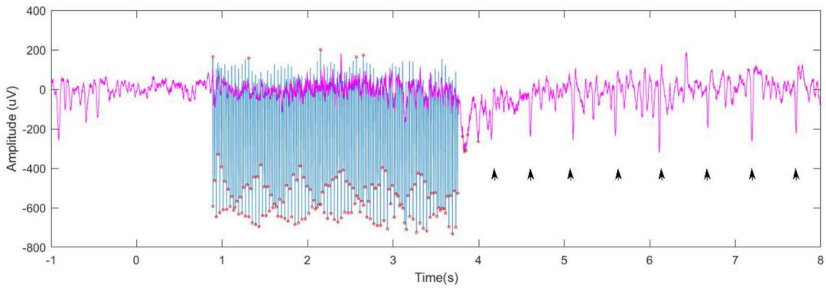

FIGURE 1

Correction of stimulation artifacts

Raw signal on a channel adjacent to stimulation channels (blue curve), presenting prominent ADs (black arrows). Spline interpolation was applied in 14 ms window around individual peaks (red dots) of stimulation artifact, resulting in a corrected signal (pink curve).

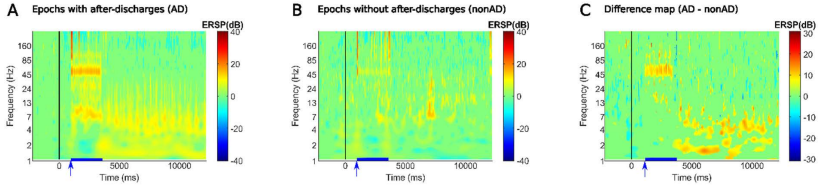

FIGURE 2

Comparison of AD and non-AD containing epochs

Averaged time-frequency maps of an example patient. The blue arrow and line show the start and extent of stimulation. A) Average of AD containing epochs. B) Average of epochs without ADs. C) Difference map, resulting from the subtraction: A) - B). Regions not significantly different are masked with green. Bootstrap statistical test was used with false discovery rate (FDR) to correct for multiple comparison.

We intend to correlate the spectral pattern observed on microelectrode recording with macroelectrode data during ADs identified on SEEG and ECoG recordings. Additionally, we also plan to apply current-source density and multiunit activity analysis on LME data. All analyses are performed using custom-written MatLab algorithms and publicly available software suites (EEGLAB [6]).

Results and discussion

ADs detected on macroelectrode recordings have proven to be very localized, mostly involving only the stimulating contacts and in few cases one or two adjacent channels. Not even LMEs located at ~1 cm have been able to register visible discharges, although changes in the spectral pattern have been observed.

Our preliminary results on spectral changes observed on macroelectrode recordings show that ADs around hypothesized EZ contain prominent high delta (1-4 Hz), theta (4-7 Hz) and beta (13-30 Hz) frequency components, accompanied by decrease in low delta (<1 Hz). During stimulation, AD epochs seem to be characterized by increased gamma (>30 Hz) oscillations, while pre-stimulation periods show increased low delta power compared to epochs with no ADs (2. Figure).

Stimulation periods preceding ADs have been marked by increased gamma oscillation, which is in line with previous research [7]. Using methods of network analysis, Bellistri et al. showed that 60-80 Hz activity during stimulation is associated with brain regions responsible for generation and propagation of seizures. Although in this case the emergence of ADs has not been considered, it can be hypothesized that neural processes underlying ADs also engage a wider network, even if visible discharges can be detected only at localized channels.

High-frequency currents are thought to result in repetitive depolarization [8] of cortical neurons, associated with gamma oscillation on the scale of local field potentials (LFP). Thus, enhanced gamma hints on the over-excitability of epileptic brain regions. Stimulation period is followed by a state of depression, i.e. decreased activity of local neurons. Based on our preliminary analysis, this depressed state is accompanied by low delta LFP, resembling cortical down state. It has been presumed that high-frequency stimulation weakens the activity of inhibitory neurons relative to excitatory neurons in the cortex, producing enhanced synchronization among a group of cortical columns around stimulation site, leading to very localized ADs

[8]. For this reason, it would be of great interest to compare the activity of localized neural populations measured by microelectrodes with respect to LFP measured during AD, a question not investigated yet.

We expect that our results will contribute to the better understanding of ADs and its relationship with EZ. Specific spectral measures associated with ADs, both on a micro- and macroscopic level, might support successful EZ localization, thus improving surgical outcome.

References

[1] Suller Marti, A., et al. Extraoperative electrical stimulation mapping in epilepsy presurgical evaluation: a proposal and review of the literature. Clin Neurol Neurosurg 214, 107170 (2022).

[2] Adrian, E.D. The spread of activity in the cerebral cortex. J Physiol 88, 127-161 (1936).

[3] Li, H., et al. Disparate properties of afterdischarges elicited by electric cortical stimulation in MRI lesional epilepsy patients with different surgical outcomes. Clin Neurol Neurosurg 212, 107034 (2022).

[4] Gollwitzer, S., et al. Afterdischarges elicited by cortical electric stimulation in humans: When do they occur and what do they mean? Epilepsy Behav 87, 173-179 (2018).

[5] Baier, G., Taylor, P.N. & Wang, Y. Understanding Epileptiform After-Discharges as Rhythmic Oscillatory Transients. Frontiers in Computational Neuroscience 11(2017).

[6] Delorme, A. & Makeig, S. EEGLAB: an open source toolbox for analysis of single-trial EEG dynamics including independent component analysis. J Neurosci Methods 134, 9-21 (2004).

[7] Bellistri, E., et al. Fast Activity Evoked by Intracranial 50 Hz Electrical Stimulation as a Marker of the Epileptogenic Zone. Int J Neural Syst 25, 1550022 (2015).

[8] Kalamangalam, G.P., Tandon, N. & Slater, J.D. Dynamic mechanisms underlying afterdischarge: a human subdural recording study. Clin Neurophysiol 125, 1324-1338 (2014).

Evidence of different contributions of correlations and anticorrelations to network structure in AD

Author
Ignacio Taguas– Centre for Cognitive and Computational Neuroscience (C3N), Madrid, Spain;Department of Experimental Psychology, Cognitive Processes and Speech Therapy, Complutense University of Madrid, Madrid, Spain
Sandra Doval – Centre for Cognitive and Computational Neuroscience (C3N), Madrid, Spain;Department of Experimental Psychology, Cognitive Processes and Speech Therapy, Complutense University of Madrid,
Madrid, Spain
Fernando Maestú – Centre for Cognitive and Computational Neuroscience (C3N), Madrid, Spain;Department of Experimental Psychology, Cognitive Processes and Speech Therapy, Complutense University of Madrid, Madrid, Spain; Department of Radiology, Complutense University of Madrid, Madrid, Spain
David López-Sanz – Centre for Cognitive and Computational Neuroscience (C3N), Madrid, Spain; Department of Experimental Psychology, Cognitive Processes and Speech Therapy, Complutense University of Madrid, Madrid, Spain

Citation
Taguas, I., Doval, S., Maestú, F., López-Sanz, D. Evidence of different contributions of correlations and anticorrelations to network structure in AD.

Introduction/Motivation

Alzheimer's Disease (AD) is an incurable neurodegenerative disease that accounts for about two-thirds of dementia cases [1]. Its earliest

neuronal dysfunction signs take place ten to fifteen years before any clinical symptoms manifest [2]. Thus, the assessment of neuronal function, through the study of brain networks, is a potential marker for the early detection of AD. Accordingly, the study of its prodromal stage, Mild Cognitive Impairment (MCI), is of great interest.

Brain networks are commonly studied through Functional Connectivity (FC), defined as the statistical dependence through time between physiological signals from different brain regions [3]. The FC between two neural substrates can be positive or negative.

A higher level of analysis uses graph theory to study the topology of brain networks, representing them as a set of nodes (neural substrates) connected by links (FC values). This allows us to study each neural substrate's importance (measured by centrality in graph theory) in the network. However, the existing articles have conflicting findings [4]. Recently, it has been suggested that the dissimilar results between studies might be influenced by the fact that frequency-specific functional networks are studied in isolation and suggested using a more integrative approach. A recent study concluded that cross-frequency graphs reveal information that cannot be extracted by studying the frequency networks separately [5].

Typically, when assessing FC and centrality changes in AD, the Default Mode Network (DMN) areas are among the most affected [6]. Since the DMN is known to have high anticorrelations with task-positive networks, studying neg-correlations might be of great importance in AD. The graph theory approach, however, does not allow negative FC values, which are usually taken as positive values (e.g., [5], [7]). Therefore, their influence is rarely studied. In the present study, we used magnetoencephalography (MEG) to study the impact of pos- and neg-correlations on the centrality changes observed in MCI, using a cross-frequency approach.

Methods

The sample consisted of 172 healthy controls and 105 amnestic MCI patients. Recordings were obtained using a 306-channel Vectorview MEG system,

under eyes-closed resting-state conditions. The electrophysiological data analysis was performed using the Fieldtrip toolbox [8].

For the construction of the cross-frequency graphs, the five classical frequency bands were considered. FC was calculated between every pair of sources on every band using corrected Amplitude Envelope Correlation [9], [10]. The Pearson correlation coefficients obtained were arranged in the form of correlation matrices. Three matrices were constructed for each subject: one with the absolute values and no zeros (abs-correlation matrix), one with just the absolute value of negative values and zeros (neg-correlation matrix), and one with only the positive values and zeros (pos-correlation matrix). These correlation matrices were then used as the adjacency macoloredtrices for the graphs, which were constructed following the method explained in [11], except for 1210 cortical sources being used instead of brain regions. As a result, each graph had 6050 nodes (1210 sources x 5 bands).

Three graph measures were used as centrality indicators, each one reflecting slightly different aspects of network centrality: strength, eigenvector centrality, and betweenness centrality. The three were merged into one, termed *centrality score*, by calculating the z-score of each centrality measure, and then averaging the three.

The results were compared between the control and MCI groups. The statistical analysis performed was a three-way factorial ANOVA, using age and ages of education as covariables setting the alpha level at 0'05. The ANOVA analysis was non-parameterized by using 10.000 permutations. The multiple comparison test used was the two-sided cluster-based permutation test [12].

Results and discussion

To stress the fact that each band includes the links to nodes in the same band, but also to the nodes in other bands, the names given to the results are Band Cross-Frequency Coupling.

The results for the abs-correlations case are shown in Fig. 1. A single cluster was found in each band: in the delta and theta bands, positive clusters were present (and , respectively). On the other side, alpha, beta and gamma bands had a negative cluster each (and , respectively).

The results for the pos-correlations case are shown in Fig. 2A. In delta and theta, positive clusters were present (and , respectively). On the other side, beta and gamma had a negative cluster each (and , respectively), while no cluster was found in alpha. Contrarily, the neg-correlations case (Fig. 2B) only showed a positive cluster in delta (), and negative clusters in theta, alpha and gamma (and , respectively).

The abs-correlations case shows a centrality increase in MCIs in low-frequency bands in anterior brain regions and a decrease in high-frequency

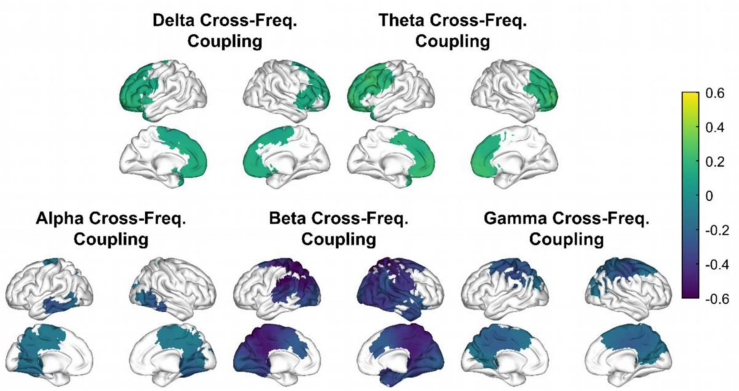

FIGURE 1

FC disruption assessed through the centrality score in the complete graphs. The colored regions indicate significative clusters: blue colors represent negative clusters (the centrality measure is higher in the control group), while green colors represent positive clusters (the MCI group has an increased centrality).

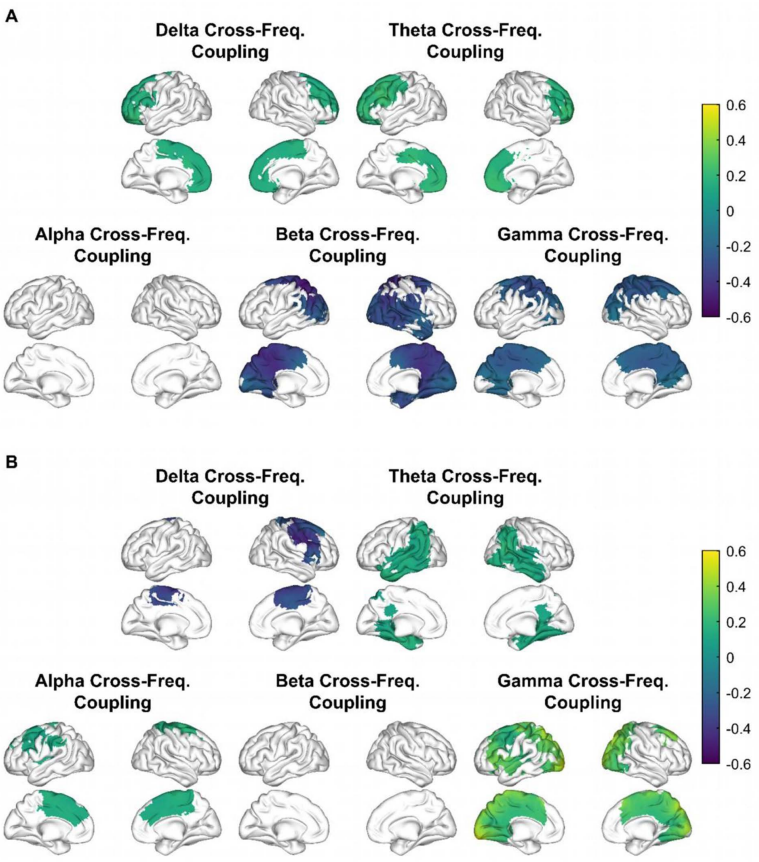

FIGURE 2

FC disruption assessed through the centrality score in the pos-correlation (A) and neg-correlation (B) graphs. The color code is the same as in Fig. 1.

bands in posterior areas. These results are congruent with FC changes reported in previous studies [13]–[15], and also with the pathophysiology of AD (Aβ depositions are associated with neuronal hyperexcitability, while tau causes neuronal death) [16]. The pos-correlations case shows a very similar pattern, which is to be expected as the positive FC values are about four-fifths of the total. Both cases include the main areas of the DMN (prefrontal cortex, cingulate, hippocampus, parahippocampus, and precuneus). The neg-correlations case, however, has quite different behavior, displaying chiefly centrality increases even in high-frequency bands and anterior aspects of the brain. Nonetheless, the areas of the DMN are once again affected, although in a different manner.

Thus, here we prove that neg-correlations have different disruption patterns than pos-correlations, and therefore the biological meaning of such changes should be addressed independently of correlations. Furthermore, it should be studied how the anticorrelations between the task-negative and task-positive networks are affected in AD and its implications on cognitive performance.

References

[1] S. Duong, T. Patel, and F. Chang, "Dementia: What pharmacists need to know," *Canadian Pharmacists Journal*, vol. 150, no. 2, 2017, doi: 10.1177/1715163517690745.

[2] M. Khanahmadi, D. D. Farhud, and M. Malmir, "Genetic of Alzheimer's Disease: A Narrative Review Article," 2015. [Online]. Available: http://ijph.tums.ac.ir

[3] K. J. Friston, "Functional and Effective Connectivity: A Review," *Brain Connect*, vol. 1, no. 1, pp. 13–36, 2011, doi: 10.1089/brain.2011.0008.

[4] L. Kucikova *et al.*, "Resting-state brain connectivity in healthy young and middle-aged adults at risk of progressive Alzheimer's disease," *Neuroscience and Biobehavioral Reviews*, vol. 129. Elsevier Ltd, pp. 142–153, Oct. 01, 2021. doi: 10.1016/j.neubiorev.2021.07.024.

[5] M. Yu *et al.*, "Selective impairment of hippocampus and posterior hub areas in Alzheimer's disease: An MEG-based multiplex network study," *Brain*, vol. 140, no. 5, pp. 1466–1485, May 2017, doi: 10.1093/brain/awx050.

[6] M. Grieder, D. J. J. Wang, T. Dierks, L. O. Wahlund, and K. Jann, "Default Mode Network Complexity and Cognitive Decline in Mild Alzheimer's Disease," *Front Neurosci*, vol. 12, 2018, doi: 10.3389/fnins.2018.00770.

[7] I. Sintini *et al.*, "Tau and Amyloid Relationships with Resting-state Functional Connectivity in Atypical Alzheimer's Disease," *Cerebral Cortex*, vol. 31, no. 3, 2021, doi: 10.1093/cercor/bhaa319.

[8] R. Oostenveld, P. Fries, E. Maris, and J. M. Schoffelen, "FieldTrip: Open source software for advanced analysis of MEG, EEG, and invasive electrophysiological data," *Comput Intell Neurosci*, vol. 2011, 2011, doi: 10.1155/2011/156869.

[9] M. J. Brookes, M. W. Woolrich, and G. R. Barnes, "Measuring functional connectivity in MEG: A multivariate approach insensitive to linear source leakage," *Neuroimage*, vol. 63, no. 2, pp. 910–920, Nov. 2012, doi: 10.1016/j.neuroimage.2012.03.048.

[10] M. J. Brookes *et al.*, "Measuring functional connectivity using MEG: Methodology and comparison with fcMRI," *Neuroimage*, vol. 56, no. 3, pp. 1082–1104, Jun. 2011, doi: 10.1016/j.neuroimage.2011.02.054.

[11] M. J. Brookes *et al.*, "A multi-layer network approach to MEG connectivity analysis," *Neuroimage*, vol. 132, pp. 425–438, May 2016, doi: 10.1016/j.neuroimage.2016.02.045.

[12] E. Maris and R. Oostenveld, "Nonparametric statistical testing of EEG- and MEG-data," *J Neurosci Methods*, vol. 164, no. 1, pp. 177–190, Aug. 2007, doi: 10.1016/j.jneumeth.2007.03.024.

[13] K. G. Ranasinghe *et al.*, "Neurophysiological signatures in Alzheimer's disease are distinctly associated with TAU, amyloid-β accumulation, and cognitive decline," *Sci Transl Med*, vol. 12, no. 534, Mar. 2020, doi: 10.1126/scitranslmed.aaz4069.

[14] S. J. Ruiz-Gómez, R. Hornero, J. Poza, A. Maturana-Candelas, N. Pinto, and C. Gómez, "Computational modeling of the effects of EEG volume conduction on functional connectivity metrics. Application to Alzheimer's disease continuum," *J Neural Eng*, vol. 16, no. 6, Oct. 2019, doi: 10.1088/1741-2552/ab4024.

[15] C. T. Briels *et al.*, "Reproducibility of EEG functional connectivity in Alzheimer's disease," *Alzheimers Res Ther*, vol. 12, no. 1, Jun. 2020, doi: 10.1186/s13195-020-00632-3.

[16] J. W. Vogel *et al.*, "Four distinct trajectories of tau deposition identified in Alzheimer's disease," *Nat Med*, vol. 27, no. 5, pp. 871–881, May 2021, doi: 10.1038/s41591-021-01309-6.

Mouse brain organisation

Deciphering the role of miR-148a in the brain development

Author
Rocío Bartolomé-Cabrero – Department of Biochemistry, Instituto de Investigaciones Biomédicas Alberto Sols, Madrid, Spain; Department of Cell, Molecular and Developmental Neurobiology, Cajal Institute, Madrid, Spain
Elisa Murenu – Department of Pharmacy, Ludwig Maximilian University, Munich, Germany
Alicia González-Martín – Department of Biochemistry, Instituto de Investigaciones Biomédicas Alberto Sols, Madrid, Spain
Sergio Gascón – . Department of Cell, Molecular and Developmental Neurobiology, Cajal Institute, Madrid, Spain

Citation
Bartolomé-Cabrero, R., Murenu, E., González-Martín, A., Gascón, S. Deciphering the role of miR-148a in the brain development.

Introduction/Motivation

microRNAs (miRNAs) are endogenous non-coding RNAs that play crucial roles in post-transcriptional regulation of gene expression. Mature miRNAs are incorporated into the RNA-induced silencing complex and bind to the 3' UTR region of the target mRNA. This results in gene silencing by degradation of the transcript or suppression of protein translation1. miR-148a has been described as a key regulator in important biological and pathological processes such as immunity, lipid metabolism, or cancer 2–4. Recent studies

suggest that miR-148a might also play an important role in the mammal brain: miR-148a is expressed in the central nervous system of rodents, and it has been associated with febrile seizures, age-related cognitive decline, or Alzheimer's Disease 5–7. Despite these advances, the physiological function of miR-148a in the brain is still unknown. In this study we, therefore, aim to determine the expression pattern and the role of miR-148a in the mouse brain.

Methods

miR-148a expression was detected through a Taqman assay in the mouse brain at different timepoints of the brain development and aging: embryonic day 14 and 17 (E14, E17), postnatal day 0 and 5 (P0, P5), 2 months old (adult) and 1 year old (old). *In situ* hybridization (ISH) was performed in sagittal slices of E14 and adult mice brains to confirm our qPCR results and stablish the spatial expression pattern of miR-148a in the mouse brain. Magnetic Resonance Imaging (MRI) analysis was performed to investigate the effect of the deletion of miR-148a *in vivo.* To reveal possible anatomical differences between miR-148a-KO and WT brains, we segmented and measured the volume of different brain structures, starting with the lateral ventricles, from adult and old mice. These analyses assessed the spatial and temporal distribution of the miR-148a in the brain, and its function in the development of the lateral ventricles as well as their adjacent structures. To determine the function of miR-148a in single specific neurons, we used an *in vitro* model of primary cultured cortical neurons from E14 mice. These neurons were transfected with a vector carrying four copies of miR-148a or a neutralizing sponge, that would lead to either increase or reduce the miRNA expression, respectively. After 14 days in culture, neurons were fixed, and the expression of different neuronal hallmarks was determined by immunocytochemistry. In addition, Sholl analysis was used to register the number of neurite intersections at 0, 25, 50 and 100 µm from the soma, thus revealing possible differences in the arbour complexity of the WT and KO neurons. These approaches revealed roles of the miR-148a on neurite growth and distribution.

Results and discussion

Taqman assay results revealed miR-148a expression increases progressively from E14 and reaches a peak in the adult stage, decreasing again in old mice. ISH experiments showed miR-148a is expressed in different areas of the adult brain. At this timepoint, miR-148a expression in cortex was restricted to neurons from layers 2/3, 5 and 6. It also showed a heterogeneous distribution along the anteroposterior axis, with higher expression in the somatomotor and somatosensory areas, and no detectable expression in the visual area. miR-148a expression could be also detected in other brain regions such as the mitral layer of the olfactory bulb, the CA2 and CA3 region of the hippocampus, or the Purkinge layer in the cerebellum, regions characterized by the presence of neurons with long axons. No expression of miR-148a was detected in the E14 embryo, confirming our qPCR results.

A line of miR-148a-KO mice was stablished to investigate the role of miR-148a *in vivo.* MRI analysis allowed us to detect any anatomic changes caused by the deletion of miR-148a in the brain. miR-148a-KO adult mice showed alterations in the distribution and volume of the lateral ventricles, without changes in the total volume of the brain. These changes were caused by an increase in the size of the ventricles in the frontal brain, matching with the regions where the miR-148a is highly expressed in the cortex. This effect was exacerbated in miR-148a KO old mice, which also showed an anteriorization of the lateral ventricles. These observations suggest that the loss of miR-148a expression in the cortex leads to alterations in its structure, which in turn causes a compensating growth of the adjoining lateral ventricles. A complementary anatomical analysis of the cortex or brain commissures would be required to validate this hypothesis.

Knowing that the miR-148a is expressed in the cortex, we set to investigate the role of miR-148a in single cortical neurons in culture. Altering miR-148a levels in cortical neurons *in vitro* led to significant morphological changes (Fig 1). Overexpression of miR-148a induced a decrease in the number and complexity of neurites, with an increase in the axon number and length, while its downregulation caused a reduction in neurite length, suggesting miR-148a might be involved in axonal growth.

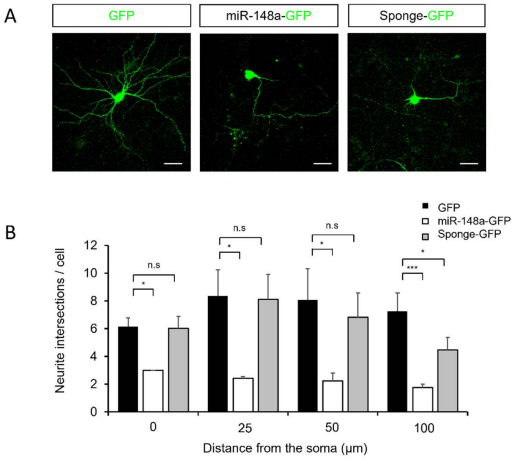

FIGURE 1

miR-148a is involved in neurite growth and distribution. (**A**) Cortical neurons were cultured and transfected with a plasmid carrying GFP, miR-148a-GFP or sponge-GFP to overexpress or knock down the expression of miR-148a (Scale bar = 50 um). (**B**) Sholl analysis revealed overexpressing or blocking the expression of miR-148a in neuron in vitro causes alterations in neurite number and length, leading to an impairment in the normal neurite development.

Considering the temporal and neuronal expression pattern described for miR-148a, and the effects its loss causes in the brain and specific neurons, it seems likely that miR-148a is involved in processes associated with neurite development such as axonal maturation, myelination or synaptogenesis. Furthermore, miR-148a predicted targets include multiple genes involved in neuronal morphology and plasticity such as FMR1 or PTEN but the pathways mediating this function are yet to be investigated. Overall, these results highlight the importance of miR-148a importance in the brain function.

Acknowledgements

This work was funded by the following grants: 1) the grant PID2021-128796OB-I00, Ministry of Science and Innovation, 2) Fundación La Caixa LCF/PR/HA21/52350003, Instituto Cajal, Madrid (Spain) 3) the grant

RTI2018-099345-B-I00, Ministry of Science and Innovation, 4) the grant MAIV01EK1611A, Federal Ministry of Education and Research (BMBF-Germany) and 5) the Network of Excellence "Synaptic Role in Cognitive Disabilities" SAF2017-90664-REDT, Ministry of Science, Innovation and Universities (Spain), granted to Sergio Gascón; 6) RTI2018-100008-A-I00 by MCIN/AEI/10.13039/501100011033 and FEDER, 7) RyC-21155 funded by MCIN/AEI/10.13039/501100011033 and FSE "El FSE invierte en tu futuro" granted to Alicia Gonzalez-Martín.; and FPI-UAM scholarship of the Autónoma University of Madrid (Spain) granted to Rocío Bartolomé-Cabrero.

References

1. O'Brien, J., Hayder, H., Zayed, Y. & Peng, C. Overview of microRNA biogenesis, mechanisms of actions, and circulation. *Frontiers in Endocrinology* vol. 9 402 (2018).

2. Gonzalez-Martin, A. *et al.* The microRNA miR-148a functions as a critical regulator of B cell tolerance and autoimmunity. *Nat. Immunol.* **17**, 433–440 (2016).

3. Wang, X. X., Zhang, H. & Li, Y. Preliminary study on the role of miR-148a and DNMT1 in the pathogenesis of acute myeloid leukemia. *Mol. Med. Rep.* **19**, 2943–2952 (2019).

4. Shi, C. *et al.* Obesity-associated miR-148a is regulated by cytokines and adipokines via a transcriptional mechanism. *Mol. Med. Rep.* **14**, 5707–5712 (2016).

5. Xu, J. *et al.* MicroRNA expression profiling after recurrent febrile seizures in rat and emerging role of miR-148a-3p/SYNJ1 axis. *Sci. Rep.* **11**, (2021).

6. Islam, M. R. *et al.* A microRNA signature that correlates with cognition and is a target against cognitive decline. *EMBO Mol. Med.* **13**, e13659 (2021).

7. Zeng, L. *et al.* Implications of miR-148a-3p/p35/PTEN signaling in tau hyperphosphorylation and autoregulatory feedforward of Akt/CREB in Alzheimer's disease. *Mol. Ther. - Nucleic Acids* **27**, 256–275 (2022).

The cellular and molecular basis of COVID-19 effects in the retina and brain

Author
Fabián Lombillo Alfonso – Laboratory of Neurodevelopment and Neurodegeneration, Institute of Biomedical Sciences, Federal University of Rio de Janeiro, Rio de Janeiro, Brazil
Carlos Franciney Moreira Vasconcelos – Laboratory of Neurodevelopment and Neurodegeneration, Institute of Biomedical Sciences, Federal University of Rio de Janeiro, Rio de Janeiro, Brazil
Bruna B. Lins – Department of Immunology, Institute of Biomedical Sciences, University of Sao Paulo, Sao Paulo, Brazil
Momtchillo Russo – Department of Immunology, Institute of Biomedical Sciences, University of Sao Paulo, Sao Paulo, Brazil
Lucianna C. Mirotti – Institute of Science and Technology in Biomodels, Oswaldo Cruz Foundation, Rio de Janeiro, Brazil
Rodrigo Martins – Laboratory of Neurodevelopment and Neurodegeneration, Institute of Biomedical Sciences, Federal University of Rio de Janeiro, Rio de Janeiro, Brazil

Citation
Alfonso, F.L., Vasconcelos, C.F.M., Lins, B.B., Russo, M., Mirotti, L.C., Martins, R. The cellular and molecular basis of COVID-19 effects in the retina and brain.

Introduction/Motivation

The novel coronavirus disease 2019 (COVID-19) is caused by the severe acute respiratory syndrome coronavirus 2 (SARS-CoV-2) and is an absolute priority of the global health agenda. Although the predominant clinical presentation is respiratory disease, it is now clear that COVID-19 is a systemic

disease, and neurological manifestations and retinal findings have been described [1]. In humans, the retina and other tissues of the central nervous system (CNS) are affected by COVID-19 during the symptomatic phase and after recovery. Is now evident that SARS-CoV-2 infection presents with neurological symptoms that include early hyposmia, ischemic stroke, meningitis, delirium and falls, even after viral clearance [2]. This may suggest chronic or permanent changes to the neurons, glial cells, and/or brain vasculature in response to SARS-CoV-2 infection or COVID-19. Although the modality of neurological impairments associated with COVID-19 has not been thoroughly investigated, the latest studies have observed that SARS-CoV-2 induces neuroinflammation and may have severe long-term consequences depending on affected brain region [3].

However, the cellular basis of retinal and brain manifestations and the long-term consequences of COVID-19 to these brain regions are not fully understood [4]. That is why our prior motivation was to study the acute effects of SARS-CoV-2 infection and its consequences to the specific tissues of the CNS. We hypothesize that the effects of acute COVID-19 in the retina and brain are mediated by cytokine expression associated with neuroinflammation, which may be brain region-specific and could depends on the SARS-CoV-2 variant.

Methods

Imaging, histopathological and gene and expression studies were performed to understand cellular and molecular basis of neuroinflammation in different regions of the brain. We addressed these questions performing intranasal infection of the K18-ACE2 transgenic mice with three strains of SARS-CoV-2: Ancestral (Wuhan), Gamma, Delta. SARS-CoV2-infected mice were euthanized at 2 or 4 days after infection.

Different cytokines expression was evaluated by qPCR in the brain and the eye, to detect and quantitate a neuroinflammatory profile produced by microglial activation or peripheral immune response caused by infection. We also performed confocal microscopy bioimaging techniques for evaluation of the microglial activation pattern for each experimental group.

Results and discussion

We observed an up-regulation of the gene expression for cytokines being crucial for the neuroinflammatory burst caused by SARS-Cov-2, in K18-hACE2 mice model, comparing between controls and infected group in four days post infection. TNF-α, IL-1β, and IL-6 cytokines are strongly upregulated in the olfactory bulb, different than hippocampus and cortex where they were mildly upregulated. IL-6 was strongly upregulated in the eye (Figure1).

Nevertheless, we could observe an increased expression for the tree cytokines in all studied brain areas, mostly for animals infected with the ancestral strain, followed by the gamma strain (4 dpi). Our results,

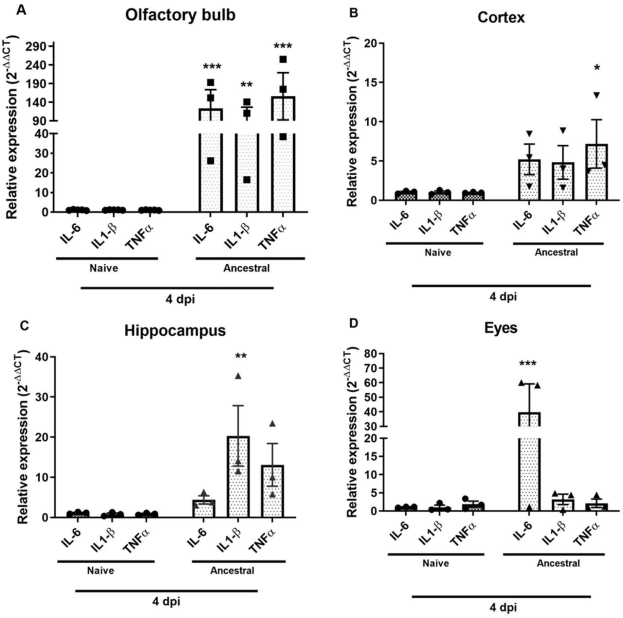

FIGURE 1
Neuroinflammatory cytokine expression genes are expressed differentially in brain areas and retina of K18-hACE2 mice (4 dpi). **A**: Olfactory bulb, **B**: Cortex, **C**: Hippocampus, **D**: Eye (retina).

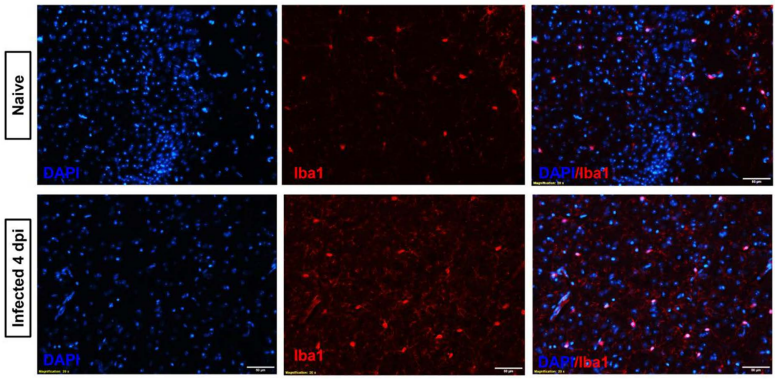

FIGURE 2
Representative immunofluorescence images of microglial Iba1+ cells labeling (in red) comparing slices from K18-hACE2 mice naive and infected with the ancestral strain of SARS-Cov-2 four days post infection (4 dpi). The cell nuclei are labelled with DAPI (blue).

regarding microglial activation in different brain areas, were performed by immunofluorescence assay. We can observe, by the representative images for Iba1+ cells, that there was a considerable difference between the naive group compared with the animals infected with the SARS-Cov-2 ancestral strains four days post infection (4 dpi), mostly in the hippocampus, the cortex, and the cerebellum. In the olfactory bulb, we hadn't observed the same difference of the above-mentioned brain areas (Figure 2).

The results showed that several of the studied brains evidenced morphological changes in neural cells, an increase in microglial activation, and change in spatial distribution of neurons in the pyramidal and granular layer. It was also demonstrated that COVID-19 altered the morphological characteristics and distribution of astrocyte and microglia cells.

Immunohistological studies for Iba1+ cells evidenced morphological changes in microglial cells, suggesting microglial activation state. Observation based on decreasing of number of processes and changes to ameboid round

shape, when we compared against not infected control animals in four days post infection.

Acknowledgements
This research was supported by The International Retinal Research Foundation (IRRF), which upholds a mission to provide financial support for vision research directly and is committed to sustaining targeted research efforts. We thank our colleagues from University of São Paulo who provided insight and expertise that greatly assisted the research.

References

[1] Joseph W. Golden, Catherine V. Badger, Jay W. Hooper: Human angiotensin-converting enzyme 2 transgenic mice infected with SARS-CoV-2 develop severe and fatal respiratory disease Published August 25, 2020, JCI Insight. 2020;5(19):e142032. https://doi.org/10.1172/jci.insight.142032.

[2] Yinda CK, Port JR, Bushmaker T, Offei Owusu I, Purushotham JN, Avanzato VA, et al. (2021) K18-hACE2 mice develop respiratory disease resembling severe COVID-19. PLoS Pathog 17(1): e1009195. https://doi.org/10.1371/journal.ppat.1009195

[3] Oladunni FS, Park JG, Pino PA, Gonzalez O, Akhter A, Allué-Guardia A, Olmo-Fontánez A, Gautam S, Garcia-Vilanova A, Ye C, Chiem K, Headley C, Dwivedi V, Parodi LM, Alfson KJ, Staples HM, Schami A, Garcia JI, Whigham A,

Platt RN 2nd, Gazi M, Martinez J, Chuba C, Earley S, Rodriguez OH, Mdaki SD, Kavelish KN, Escalona R, Hallam CRA, Christie C, Patterson JL, Anderson TJC, Carrion R Jr, Dick EJ Jr, Hall-Ursone S, Schlesinger LS, Alvarez X, Kaushal D, Giavedoni LD, Turner J, Martinez-Sobrido L, Torrelles JB. Lethality of SARS-CoV-2 infection in K18 human angiotensin-converting enzyme 2 transgenic mice. Nat Commun. 2020 Nov 30;11(1):6122. doi: 10.1038/s41467-020-19891-7. PMID: 33257679; PMCID: PMC7705712.

[4] Li YP, Ma Y, Wang N, Jin ZB. Eyes on coronavirus. Stem Cell Res. 2021 Mar;51:102200. doi: 10.1016/j.scr.2021.102200. Epub 2021 Jan 27. PMID: 33535156; PMCID: PMC7838582.

Ultrastructural comparison of VPM/Po layer-specific thalamocortical afferents into somatosensory cortices

Author
Pablo J. Martin-Correa – Department of Anatomy & Neuroscience, School of Medicine, Autonoma de Madrid University, 28029 Madrid (28029), Spain
Javier Rodriguez-Moreno – Department of Anatomy & Neuroscience, School of Medicine, Autonoma de Madrid University, 28029 Madrid (28029), Spain
Astrid Rollenhagen – Institute of Neuroscience and Medicine INM-10, Research Centre Jülich GmbH, 52425 Jülich, Germany
Brigitte Marshallsay – Institute of Neuroscience and Medicine INM-10, Research Centre Jülich GmbH, 52425 Jülich, Germany
Joachim Lübke – Institute of Neuroscience and Medicine INM-10, Research Centre Jülich GmbH, 52425 Jülich, Germany
Francisco Clasca – Department of Anatomy & Neuroscience, School of Medicine, Autonoma de Madrid University, 28029 Madrid (28029), Spain

Citation
Martin-Correa, P.J., Rodriguez-Moreno, J., Rollenhagen, A., Marshallsay, B., Lübke, J., Clasca, F. Ultrastructural comparison of VPM/Po layer-specific thalamocortical afferents into somatosensory cortices.

Introduction

Thalamocortical synapses are key cellular links in sensory, motor and cognitive information processing. In rodents, ventral posteromedial thalamic nucleus (VPM) axons innervate layer 4 cells of the vibrissal

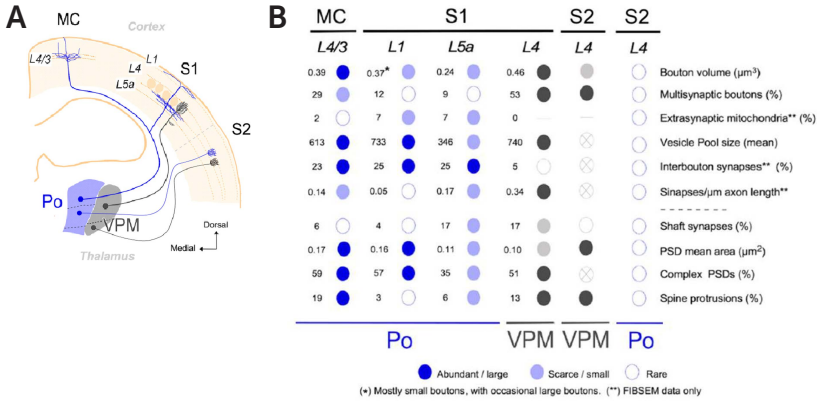

FIGURE 1

Graphic summary of relevant structural differences between Po and VPM axon synapses in cerebral cortex. (A) Outline of a coronal mouse brain section, the trajectories and cortical arborizations from Po cell axons (blue) and a VPM cell axons (gray)**. (B)** Salient differences in synaptic structure between Po boutons in MC-L4/3, S1–L1, and S1–L5a (blue) and on the right values measured in S1–L4 and S2–L4 VPM synapses (gray) as well as S2–L4 Po synapses**.** S2 data is currently being added so as to get higher statistical power. Further information of previous datasets from our lab can be found in [4,5].

primary somatosensory cortex (S1) but also layer 4 cells of the secondary somatosensory cortex (S2) [1] (Fig. 1A). The posterior thalamic nucleus (Po) projects to the same somatosensory areas but acting as a "higher order" nucleus [2] (Fig. 1A). Because of the "primary" and "secondary" functional characterization of these two areas [3], it is unknown If differences exist in VPM and/or Po axon synapse structure and/or their postsynaptic target elements in secondary cortices [4,5]. Here, we set out to 3D measure and compare the ultrastructure (volume, mitochondrial volume, vesicle pool size, active zone size and shape) of VPM and Po synapses on these two areas and compared as well with previous datasets from our lab [4,5] (Fig. 1B).

Methods

We microinjected adult male C57B/L6 mice iontophoretically with biotinylated dextran amine (BDA) in different regions of VPM and Po to

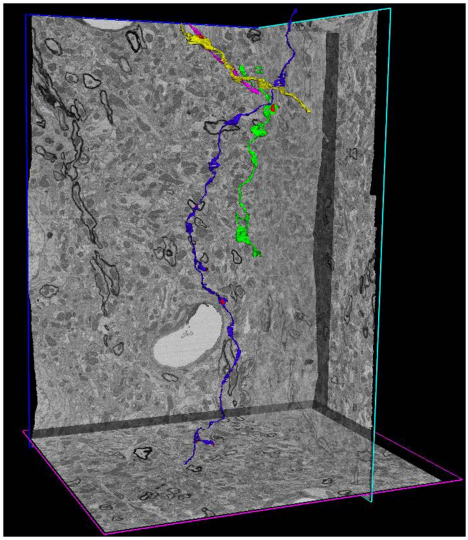

FIGURE 2
3D FIB/SEM reconstruction of VPM-S2L4 labeled thalamocortical axon segments shown in different colors on a 3-axis projection of the neuropil. Scale bar = 3000 nm

selectively label thalamocortical axon arborizations of interest. Following a 5 day survival, mice were perfused, and their brains sectioned (50µm) on a vibratome into two parallel series of coronal sections. BDA-labeled axon arborizations were carefully located on a light microscopy series of counter-stained cytochrome oxidase sections. Adjacent sections were stained for BDA and included for electron microscopy. Area and layer-specific serial image samples of interest were obtained with either serial sectioning TEM or FIB/SEM electron microscopy. Using TrakEM2 [6] and OpenCAR [7] software labeled boutons were 3D reconstructed and measured (Fig. 2).

Results and discussion

Our preliminary results are consistent with previous evidence that VPM axon synapses are mostly located (>90%) on spiny cell dendrites, and very few on

smooth, spineless dendrites (putative interneurons). Samewise, VPM to S2L4 thalamocortical synaptic boutons are significantly smaller than VPM-S1L4, but still maintain a similar percentage of multi-synaptic boutons (Fig. 1B). This suggests differences in synaptic efficacy and its roles in somatosensory processing. We are currently investigating how such differences relate to the same thalamocortical projections emerging from Po, VPM's "higher order" nucleus counterpart [2]. Progress in the proper description of synaptic circuitry in such areas has a direct impact in cortical areas interaction models.

References

[1] Pierret, T., Lavallée, P., & Deschênes, M. (2000). Parallel Streams for the Relay of Vibrissal Information through Thalamic Barreloids. The Journal Of Neuroscience, 20(19), 7455-7462.

[2] Casas-Torremocha, D., Rubio-Teves, M., Hoerder-Suabedissen, A., Hayashi, S., Prensa, L., & Molnár, Z. et al. (2022). A combinatorial input landscape in the "higher-order relay" posterior thalamic nucleus. The Journal Of Neuroscience, JN-RM-0698-22.

[3] Hubatz, S., Hucher, G., Shulz, D., & Férézou, I. (2020). Spatiotemporal properties of whisker-evoked tactile responses in the mouse secondary somatosensory cortex. Scientific Reports, 10(1).

[4] J. Rodriguez-Moreno, A. Rollenhagen, J. Arlandis, A. Santuy, A. Merchan-Pérez, J. DeFelipe, J. H. R. Lübke and F. Clasca. Quantitative 3D Ultrastructure of Thalamocortical Synapses from the "Lemniscal" Ventral Posteromedial Nucleus in Mouse Barrel Cortex. Cerebral Cortex, Volume 28(9):3159–3175, 2018.

[5] Rodriguez-Moreno, J., Porrero, C., Rollenhagen, A., Rubio-Teves, M., Casas-Torremocha, D., & Alonso-Nanclares, L. et al. (2020). Area-Specific Synapse Structure in Branched Posterior Nucleus Axons Reveals a New Level of Complexity in Thalamocortical Networks. The Journal Of Neuroscience, 40(13), 2663-2679.

[6] Cardona, A., Saalfeld, S., Schindelin, J., Arganda-Carreras, I., Preibisch, S., & Longair, M. et al. (2012). TrakEM2 Software for Neural Circuit Reconstruction. Plos ONE, 7(6), e38011.

[7] Saetzler, K. (2001). 3-D Rekonstruktion von Serienschnitten. In Forschung und wissenschaftliches Rechnen, Beiträge zum Heinz-Billing-Preis 2000 (pp. 31-47). GWDG.

Understanding the contributions of voltage gated potassium channels to neuronal excitability by integrating transcriptomics with detailed ion channel kinetics

Author
Anukrati Nigam – Krembil Centre for Neuroinformatics, Centre for Addiction and Mental Health, Toronto, Ontario, Canada; Institute of Medical Science, Temerty Faculty of Medicine, University of Toronto, Toronto, Ontario, Canada
Dr. Rajnish Ranjan – Blue Brain Project, Ecole Polytechnique Fédérale de Lausanne, Geneva, Switzerland
Dr. Enrico Scantamburlo – Blue Brain Project, Ecole Polytechnique Fédérale de Lausanne, Geneva, Switzerland
Dr. Shreejoy Tripathy – Krembil Centre for Neuroinformatics, Centre for Addiction and Mental Health, Toronto, Ontario, Canada; Institute of Medical Science, Temerty Faculty of Medicine, University of Toronto, Toronto, Ontario, Canada
Dr. Sean L. Hill – Krembil Centre for Neuroinformatics, Centre for Addiction and Mental Health, Toronto, Ontario, Canada; Institute of Medical Science, Temerty Faculty of Medicine, University of Toronto, Toronto, Ontario, Canada

Citation
Nigam, A., Ranjan, R., Scantamburlo, E., Tripathy, S., Hill, S.L. Understanding the contributions of voltage gated potassium channels to neuronal excitability by integrating transcriptomics with detailed ion channel kinetics.

Introduction/Motivation

Neuronal excitability is a core phenomenon where large and rapid changes in membrane potential occur in response to a small stimulus (1); having implications virtually across all neurological and neuropsychiatric disorders. Ion channels are the major players involved in its regulation among which, voltage gated potassium channels (Kv) on their own are part of a diverse family. The dysfunction in Kv channels is involved in channelopathy, epilepsy, schizophrenia and multiple other neurological and neuropsychiatric disorders (1,2). Here, we want to focus on understanding the generic principles for Kv channels, in terms of synergy, degeneracy, pleiotropy, and the functional overlap as hypothesized (3). By diving into the gene expression and electrophysiological properties of both current clamp and voltage clamp features of voltage gated potassium ion channels, we aim to identify key insights of potassium channels, including how they work together to contribute to neuronal excitability.

Methods

We use the deeply characterized homomeric ionic channels data from the Channelpedia database for kinetic characteristics (4)extensive research has been carried out to characterize the molecular, structural and biophysical properties of ion channels. This research has begun to elucidate the role of ion channels in neuronal function and has subsequently led to the development of computational models of ion channel function. Although there have been substantial efforts to consolidate these findings into easily accessible and coherent online resources, a single comprehensive resource is still lacking. The success of these initiatives has been hindered by the sheer diversity of approaches and the variety in data formats. Here, we present "Channelpedia" (http://www.Channelpedia.net and the mouse visual cortex patch-seq dataset (5)physiological, or genetic attributes. To better constrain the definition of neuronal cell types, we characterized the transcriptomes and intrinsic physiological properties of over 4,200 mouse visual cortical GABAergic interneurons and reconstructed the local morphologies of 517 of those neurons. We find that most transcriptomic types (t-types for transcriptomics and cellular electrophysiology to study Kv genes. We can

study at the single cell and the population level resolution of how the Kv channels work from gene expression to protein function. Hierarchical clustering is performed to integrate these three modalities. Based on the transcriptomics data from the mouse visual cortex, we used cell state analysis in combination with hierarchical clustering to analyze the combinatorial expression of the 15 Kv genes in each subclass.

Results and discussion

The clusters obtained from the correlation matrix of Kv gene expression and electrophysiology features revealed that channels can be categorized broadly into multiple clusters when looking at gene co-expression (six), gene expression-electrophysiological feature associations (six), and genes with their kinetic characterization (three). These clusters are further analyzed to observe the similarities and the differences between these Kv ion channels. The clusters obtained from the correlation matrices of gene co-expression and gene expression-electrophysiology properties indicate high correlation of gene expression of certain Kv channels with fast neuronal spiking properties. Further, observing the voltage ranges of activation and inactivation and their association with electrophysiology features and gene expression has resulted in clusters of Kv genes corresponding to timescales (slow, medium, and fast) (Figure 1).

Each cell was denoted with a cell state depending upon the binary expression of the Kv genes. Each subclass has a signature of a combination of such cell states. Hierarchical clustering of these cell states results in identification of Kv genes that are ubiquitous expressed together in some subclasses. In certain subclasses, their expression varies across cell states in AND, OR, and NONE combinations highlighting the importance of that Kv gene in the sustenance of the cell viability.

Consolidating the information from the hierarchical clustering and cell state analysis, we put forward the following principles governing regulation of ion channel expression and function - Functional Pleiotropy, Functional Overlap, Functional Redundancy, Functional Degeneracy, Functional Antagonism,

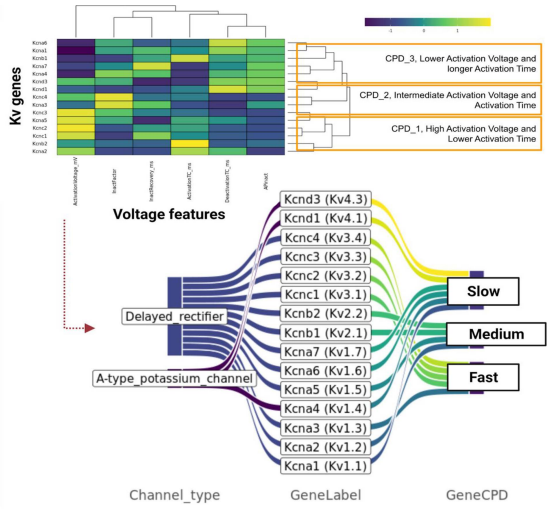

FIGURE 1

Represents the hierarchical clustering of the 15 Kv genes with their kinetic features. Three hierarchical clusters of Kv genes are observed indicating Kv genes corresponding to different timescales.

and Transcriptomics substitution. These principles are defined based on the correlation of the electrophysiology, gene co-expression or the kinetics of these Kv channels. Examples of Kv genes following the above mentioned principles were present in most subclasses with certain exceptions.

Integrating these multiple modalities has highlighted principles of how Kv channels work together to regulate neuronal excitability. Here, we define an approach to study the fundamental principles underlying ion channel function in 15 Kv genes. We want to further look at all the voltage gated ion channels to understand the fundamental associations. Eventually, we aim to understand these relationships between genes, transcripts, and alterations in neuronal excitability in brain disorders and neuropsychiatric illnesses.

Acknowledgements
We acknowledge the generous support from the CAMH Discovery Fund, Krembil Foundation, Kavli Foundation, McLaughlin Foundation, Natural Sciences and Engineering Research Council of Canada (RGPIN-2020-05834 and DGECR-2020-00048), and Canadian Institutes of Health Research (NGN-171423 and PJT-175254) and the Simons Foundation Autism Research Initiative.

References

[1] Wijesinghe R, Camp AJ. Intrinsic neuronal excitability: implications for health and disease. Biomol Concepts. 2011 Aug 1;2(4):247–59.

[2] Crabtree GW, Sun Z, Kvajo M, Broek JAC, Fénelon K, McKellar H, et al. Alteration of Neuronal Excitability and Short-Term Synaptic Plasticity in the Prefrontal Cortex of a Mouse Model of Mental Illness. J Neurosci. 2017 Apr 12;37(15):4158–80.

[3] Goaillard JM, Marder E. Ion Channel Degeneracy, Variability, and Covariation in Neuron and Circuit Resilience. Annu Rev Neurosci. 2021 Jul 8;44(1):335–57.

[4] Ranjan R, Khazen G, Gambazzi L, Ramaswamy S, Hill SL, Schürmann F, et al. Channelpedia: An Integrative and Interactive Database for Ion Channels. Front Neuroinformatics [Internet]. 2011 [cited 2020 Aug 28];5. Available from: http://www.frontiersin.org/articles/10.3389/fninf.2011.00036/full

[5] Gouwens NW, Sorensen SA, Baftizadeh F, Budzillo A, Lee BR, Jarsky T, et al. Integrated Morphoelectric and Transcriptomic Classification of Cortical GABAergic Cells. Cell. 2020 Nov 12;183(4):935-953.e19.

Neuroinformatics

Hierarchical Optimal Sampling (HOS): A tool for managing and manipulating wide-field imaging datasets

Author
Irene Bernava – Istituto Nazionale di Fisica Nucleare (INFN), Sezione di Roma, Rome, Italy
Chiara De Luca – Ph.D. Program in Behavioural Neuroscience, "Sapienza" University of Rome, Rome, Italy; Istituto Nazionale di Fisica Nucleare (INFN), Sezione di Roma, Rome, Italy
Giulia De Bonis – Istituto Nazionale di Fisica Nucleare (INFN), Sezione di Roma, Rome, Italy
Francesco Simula – Istituto Nazionale di Fisica Nucleare (INFN), Sezione di Roma, Rome, Italy
Francesco Resta – European Laboratory for Non-linear Spectroscopy (LENS), University of Florence, Florence, Italy
Elena Montagni – European Laboratory for Non-linear Spectroscopy (LENS), University of Florence, Florence, Italy
Anna Letizia Allegra Mascaro – European Laboratory for Non-linear Spectroscopy (LENS), University of Florence, Florence, Italy; Istituto di Neuroscienze, CNR, Pisa, Italy
Francesco Saverio Pavone – European Laboratory for Non-linear Spectroscopy (LENS), University of Florence, Florence, Italy
Pier Stanislao Paolucci – Istituto Nazionale di Fisica Nucleare (INFN), Sezione di Roma, Rome, Italy

Citation
Bernava, I., De Luca, C., De Bonis, G., Simula, F., Resta, F., Montagni, E., Mascaro, A.L.A., Pavone, F.S., Paolucci, P.S. Hierarchical Optimal Sampling (HOS): A tool for managing and manipulating wide-field imaging datasets

Introduction/Motivation

Recent developments of new and powerful recording techniques of brain activity allow studying the brain with unprecedented spatial resolution, as the one achieved with wide-field calcium imaging data [1]. The main issue arising from this innovative experimental setting is to enhance the signal-to-noise ratio for each pixel, for a given phenomenon of interest.

Aiming at addressing the needs of the neuroscience community, we present a tool able to automatically identify the optimal spatial resolution that preserves and emphasizes the most of the information, by recurrently scanning the high number of fluorescence signal sources in a calcium imaging dataset. The method relies only on the spatial distribution of channels, and consists in evaluating the signal-to-noise ratio according to a user-defined acceptance rule. As a result, from raw images made of thousands of pixels with native resolution reaching linear dimensions of 24µm, inhomogeneous gridding of the field of view can be obtained and enabled. Strengths of the algorithm are its adaptability to different data types and its intrinsic modularity.

Methods

The idea behind the method (illustrated in Fig. 1) is to give up homogeneous sampling, i.e. a regular grid of channels, in favor of a sampling where spatial resolution is different at different sites. The optimal sampling is defined by maximizing the signal-to-noise ratio according to the values of a chosen observable and of an exit condition. Indeed, when the same downsampling factor is applied indiscriminately along the cortex, important information could be lost. HOS method allows maintaining native resolution at recording sites where the signal-to-noise ratio is large enough that no averaging processes are needed (Figure 2.B). In general, HOS allows identifying the best recording sites, thus reducing the quantity, meanwhile increasing the quality of the retained information in noisy datasets. For example, in the situation illustrated in Figure 2.A some information seems to be lost, however the method itself ensures that what is actually discarded is noise, or more specifically what is identified as noise resulting from the chosen test.

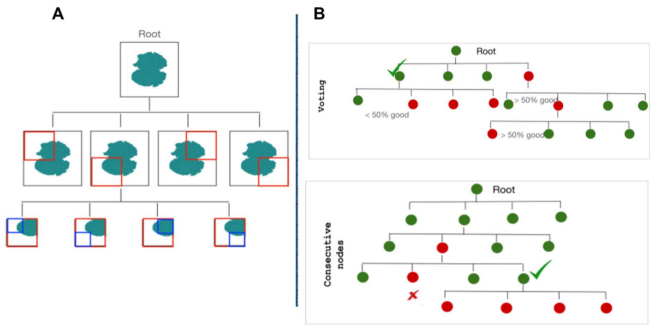

FIGURE 1

Hierarchical Optimal Sampling (HOS): methods A. Tree structure of the algorithm: iterative division of the original data into substructures. **B.** Graphical illustration of the two exit conditions implemented so far, namely voting (upper) and consecutive nodes (lower).

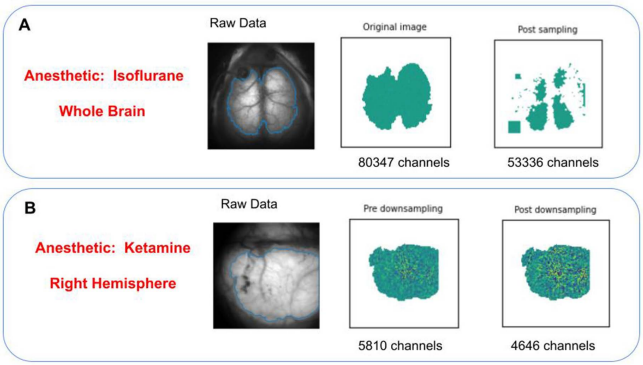

FIGURE 2

Hierarchical Optimal Sampling (HOS): applications A. Hierarchical Optimal Sampling applied to data consisting in recording cortical activity (bi-hemispheric) from anesthetized mice under isoflurane anesthesia; the data-driven inhomogeneous sampling of the original frame is evident.
B. Application of HOS on calcium imaging wide-field data recording cortical activity from single hemisphere of anesthetized mice (under ketamine anesthesia).

The structure of the algorithm is hierarchical; at each layer, the dataset is iteratively divided into substructures and the observable of interest (test value) is assessed. The iteration ends when the exit condition is met. As the backbone of the algorithm is independent of the quality test and exit condition, it is highly customizable, in response to different scientific questions. The current implementation, driven by the context of analysing spatio-temporal patterns of slow waves in anesthetized cortex, adopts a p-value test for bimodality as a quality test. Currently, the user can choose between two exit conditions, namely 'voting' and 'consecutive'. The former (Figure 1B upper) relies on whether a sufficient fraction of 'children' of the upper layer satisfies the quality test to decide whether to go deeper in the tree branch: if the condition is met, the algorithm keeps investigating deeper layers; otherwise, the parent node becomes a leaf, and the search for that specific branch is stopped. The alternative option, the 'consecutive' exit condition (Figure 1B lower), relies on setting a threshold number of consecutive rejected nodes in a single branch: if the condition is met for all children the search is stopped and the parent node becomes a leaf, otherwise, if only one child meets the condition, the specific branch is discarded and the search keeps running on the remaining ones.

The method described above can either be used stand-alone, as a diagnostic tool for experimental datasets, or as a block in an analysis pipeline providing inputs for further processing steps, enabling data-driven setting of analysis parameters. Indeed, the method has been designed as part of the CoBraWAP[2] , a collaborative analysis pipeline developed for the study of cortical wave dynamics, and it is fully integrated into the pipeline which provides the software framework for its execution.

Results and discussion

As to validate the Hierarchical Optimal Sampling (HOS), the method has been applied on two different datasets, both recording cortical activity of mice under anesthesia through wide-field calcium imaging (GCaMP6f indicator).

The impact of HOS can be appreciated when applied to a dataset consisting of images from the whole brain cortex of a mouse under isoflurane anesthetic [3], where the native spatial resolution is 24 μm with a sampling rate of acquisition of fluorescence frames of 40 Hz. As shown in Figure (2A), the application of the HOS method allows retaining a very fine spatial resolution in some specific areas. On the other hand, the retention of an equivalent spatial resolution obtained by performing a homogeneous downsampling would be collaterally accompanied by the introduction of a considerable amount of noise.

As to validate the efficacy of the method, it has been also applied to a dataset consisting of images related to a portion of a single hemisphere of mouse cortex under ketamine anesthesia acquired with native spatial resolution of 50 μm (sampling rate 25 Hz) . This dataset has been previously analysed in [4] and [5], where a uniform spatial 2x2 downsampling was performed. Despite the low-noise nature of this dataset does not make essential an inhomogeneous spanning of the grid, however the application of the hierarchical optimal sampling method allows recovering native resolution for most of the recording sites and thus increasing the number of significative channels up to 4646 channels, to be compared with 1470 channels obtained when performing an homogeneous spatial downsampling by averaging on 2x2 pixels (Fig2B).

Acknowledgements
This work has been supported by the European Union Horizon 2020 Research and Innovation program under the FET Flagship Human Brain Project (grant agreement SGA3 n. 945539 and grant agreement SGA2 n. 785907) and by the INFN APE Parallel/Distributed Computing laboratory.

References

[1] Chi Ren et al. "Characterizing Cortex-Wide Dynamics with Wide-Field Calcium Imaging". In: J Neurosci. 2021 May 12;41(19):4160-4168. doi: 10.1523/JNEUROSCI.3003-20.2021.

[2] https://github.com/INM-6/cobrawap

[3] Montagni Elena et al. "Wide-field imaging of cortical response to sensory stimulation in GCaMP6f mice at different brain states"[Dataset](2021). EBRAINS. https://doi.org/10.25493/2GDR-AKY

[4] Marco Celotto et al. "Analysis and model of cortical slow waves acquired with optical techniques". In: Methods and protocols 3.1 (2020), p. 14 10.3390/mps3010014

[5] Cristiano Capone et al. "Simulations Approaching Data: Cortical Slow Waves in Inferred Models of the Whole Hemisphere of Mouse". In arXiv (2021) 10.48550/ARXIV.2104.07445

A statistical approach for validating neuron segmentation from confocal microscopy images

Author
Ester Bruno – University of Pisa, Centro di Ricerca "E. Piaggio", Pisa, Italy
Simone Cauzzo – University of Pisa, Centro di Ricerca "E. Piaggio", Pisa, Italy
Miriam Basile – University of Pisa, Centro di Ricerca "E. Piaggio", Pisa, Italy
Alejandro Callara – University of Pisa, Centro di Ricerca "E. Piaggio", Pisa, Italy
Chiara Magliaro – University of Pisa, Centro di Ricerca "E. Piaggio", Pisa, Italy
Lydia Danglot – Institute of Psychiatry & Neuroscience of Paris, Inserm 1266, University of Paris, Paris, France
Arti Ahluwalia – University of Pisa, Centro di Ricerca "E. Piaggio", Pisa, Italy
Nicola Vanello – University of Pisa, Centro di Ricerca "E. Piaggio", Pisa, Italy

Citation
Bruno, E., Cauzzo, S., Basile, M., Callara, A., Magliaro, C., Danglot, L., Ahluwalia, A., Vanello, N. A statistical approach for validating neuron segmentation from confocal microscopy images.

Introduction/Motivation

The three-dimensional reconstruction of isolated neurons at micro- and nano scale is crucial for characterizing cell types and for detecting morphological abnormalities associated to neuropathies [1][2]. Despite the important progresses in tissue processing and optical imaging, mapping the connectome, i.e., neurons and their connections in their native environment, is still a challenge in neuroscience [3]. Specifically, the analysis of images

from ex-vivo clarified samples allows the structural characterization of neurons through segmentation algorithms, but it deals with well-known issues, such as the dense-packed organization of neurons and the low contrast to noise ratio, which severely impair the visual detection of the thinnest structures such as distal dendritic arborizations. As a result, manual segmentation may fail to provide high-quality results. Nonetheless, although highly demanding in terms of time and expertise, it is still regarded as the gold standard for testing segmentation algorithms. Semi-automatic software, such as Neutube [4] and NeuroLucida® (MicroBrightField, Inc.), that are often used as alternative gold standards, Still rely on the visual assessment of the user, may fail as well in the detection of thin branches in dense images.

In this context, a validation approach is needed that does not rely on the user expertise, nor on image quality. The approach must be easily accessible, implementable and objective. We propose a new paradigm for testing the validity of the obtained segmentations using measures available in literature. These measures quantitatively describe the 3D neuronal structures available from public repositories [5][6], overcoming limitations of the most common morphological complexity descriptor, i.e., Sholl analysis, which might fail in differentiating among simple and complex dendritic patterns [7][8]. We test this approach in the validation of our new segmentation algorithm SENPAI [9].

Methods

1-mm thick cerebellum slices from transgenic L7GFP mice are clarified with CLARITY protocol to isolate Purkinje Cells (PCs) expressing Green Fluorescent Protein (GFP) [10]. Two different datasets are acquired with confocal microscopy (Nikon A1 equipped with a 40x objective) and segmentations on 27 PCs are performed and analyzed.

To segment these cells, SENPAI implements a k-means clustering using the information on image intensity and on spatial second derivatives computed along the three main axes. Class selection is performed according to negative mean second order derivatives and high intensity, which describe neural structures. We employed a watershed transform to split the segmentation of dense images into separate whole-neuron structures [11].

To provide a standard validation, we compare on the same set of isolated neurons, segmentations obtained with SENPAI against manual segmentations performed with ManSegTool [12] (majority voting across six operators) and against semi-automatic tracings obtained with Neutube.

The proposed validation approach is based on the comparison between topological features estimated from segmented structures and those based on a priori knowledge. Specifically, we retrieved from literature [13] a statistical description of six types of neurons, including Purkinje cells, from high resolution single cell imaging. The description is based on the centripetal Horton-Strahler Ordering (SO), a descriptor of fractal complexity As a function of SO, we extract nine topological measures Strahler Number (SN), i.e., the maximal SO assigned to a segment in the neuronal tree, the Branch Bifurcation Ratio and Normalized Number of Segments , Normalized Number of Branches, Normalized Topological Subtree Size, Normalized Branch Diameter, Total Normalized Dendritic Length, Normalized Average Segment Length, Normalized Average Branch Length. Each neuron type is described by a characteristic range of such parameters. We thus propose to use such features to compared segmentations provided by SENPAI with the same statistics for Purkinje cells found in literature.

Results and discussion

By comparing manual segmentations with those obtained with NeuTube or SENPAI (Figure 1), it is evident that the former clearly fails in competing with semi-automatic tools. Therefore, we decided to limit the application of the proposed validating approach to the results of SENPAI and NeuTube. SENPAI segmentations are shown to be in line with results from high resolution single cell imaging in terms of statistical fractal descriptors (Figure 2). Taking as reference a subset of the results described in Vormberg et al., SENPAI achieved segmentations having the same SN mode as the one found for Purkinje cells. Considering the normalized number of segments, SENPAI neurons matched a steep decay (slope=-1.20) found for PCs in the reference work. Regarding the slope for the normalized number of branches, SENPAI achieves values in the range reported by Vomberg et al. and provide

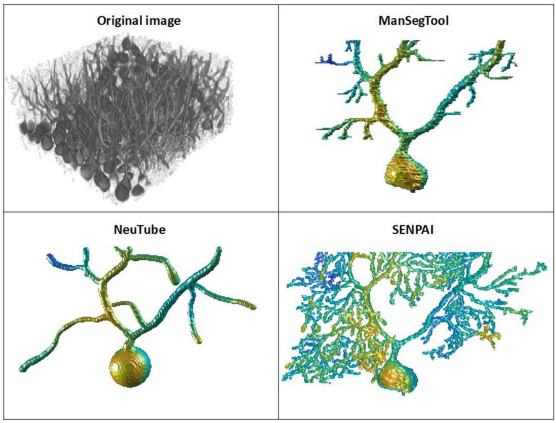

FIGURE 1
3D visualization of original confocal dataset and comparison of the segmentation performed by ManSegTool (manual), the semi-automatic tracing performed by Neutube and the automatic segmentation performed by SENPAI.

Purkinje-like Branch Bifurcation Ratio. Instead, for the topological subtree size, our algorithm performs slightly below the reference range.

Overall, SENPAI shows a good agreement with the Purkinje cells statistics of Vormberg et al.. On the other hand, the semi-automatic segmentations performed with Neutube often provide poor results due to the inability to capture thinner structures, such as dendritic branches.

Our validation approach allows to quantify the quality of SENPAI and NeuTube segmentations exploiting available knowledge on Purkinje cells morphology. Moreover, it may represent a new approach for segmentation algorithm validation when manual segmentation may not represent the gold standard. Currently, this approach is limited by the low availability of SO-based statistics on neurons from ex-vivo samples. We could not find works similar to Vormberg et al.. For Purkinje cells, the statistics are based on only

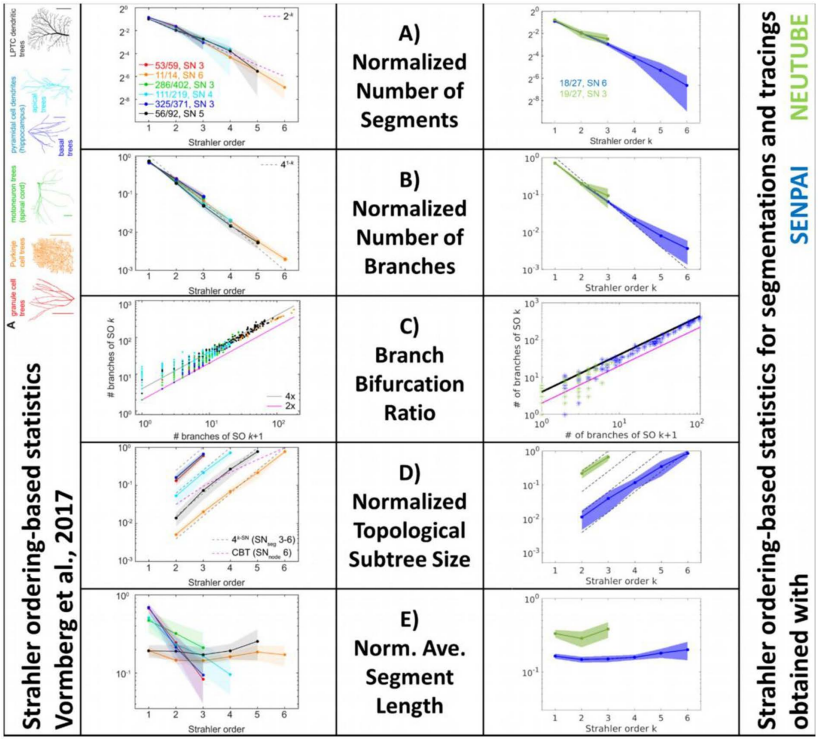

FIGURE 2

Graphical comparison of the SO of Purkinje cells found in literature and measured on the neurons segmented with SENPAI and with NeuTube.

14 neurons. In addition, statistic-based approaches cannot be regarded as ground-truth as they only provide a quantification of fitness within a model.

In future advances, we plan to extend the validation approach to the comparison of multiple automatic segmentation algorithms and to the

analysis of different types of cells. This approach would surely benefit from new publications on topological features extracted from larger samples.

References

[1] BROWN K, GILLETTE T, ASCOLI G (2008): Quantifying neuronal size: Summing up trees and splitting the branch difference. Seminars in Cell & Developmental Biology 19:485–493. doi: 10.1016/j.semcdb.2008.08.005.

[2] Magliaro C, Callara AL, Vanello N, Ahluwalia A (2019): Gotta Trace 'em All: A Mini-Review on Tools and Procedures for Segmenting Single Neurons Toward Deciphering the Structural Connectome. Frontiers in Bioengineering and Biotechnology 7. doi: 10.3389/fbioe.2019.00202.

[3] Alivisatos AP, Chun M, Church GM, Greenspan RJ, Roukes ML, Yuste R (2012): The Brain Activity Map Project and the Challenge of Functional Connectomics. Neuron 74:970–974. doi: 10.1016/j.neuron.2012.06.006.

[4] Feng L, Zhao T, Kim J (2015): neuTube 1.0: A New Design for Efficient Neuron Reconstruction Software Based on the SWC Format. eneuro 2:ENEURO.0049-14.2014. doi: 10.1523/ENEURO.0049-14.2014.

[4] Ledderose J, Sención L, Salgado H, Arias-Carrión O, Treviño M (2014): A software tool for the analysis of neuronal morphology data. International Archives of Medicine 7:6. doi: 10.1186/1755-7682-7-6.

[6] Nanda S, Bhattacharjee S, Cox DN, Ascoli GA (2020): Distinct Relations of Microtubules and Actin Filaments with Dendritic Architecture. iScience 23:101865. doi: 10.1016/j.isci.2020.101865.

[7] Rowland C, Harland B, Smith JH, Moslehi S, Dalrymple-Alford J, Taylor RP. Investigating Fractal Analysis as a Diagnostic Tool That Probes the Connectivity of Hippocampal Neurons. Front Physiol. 2022 Jun 23;13:932598. doi: 10.3389/fphys.2022.932598. PMID: 35812343; PMCID: PMC9260144.

[8] Jelinek, H., Elston, N., Zietsch, B. (2005). Fractal Analysis: Pitfalls and Revelations in Neuroscience. In: Losa, G.A., Merlini, D., Nonnenmacher, T.F., Weibel, E.R. (eds) Fractals in Biology and Medicine. Mathematics and Biosciences in Interaction. Birkhäuser Basel. https://doi.org/10.1007/3-7643-7412-8_8

[9] S. Cauzzo, M. Basile, E. Bruno, A. Callara, L. Danglot, A. Ahluwalia, C. Magliaro, N. Vanello (2022), "SENPAI: SEgmentation of Neurons using PArtial derivatives Information. A tool for neuronal segmentation from confocal microscopy using K-means and topological information", Federation of European Neuroscience Societies, FENS Forum 2022, Paris, France, 9-13 July 2022

[10] Magliaro C, Callara AL, Mattei G, Morcinelli M, Viaggi C, Vaglini F and Ahluwalia A (2016): Clarifying CLARITY: Quantitative Optimization of the Diffusion Based Delipidation Protocol for Genetically Labeled Tissue. Front. Neurosci. 10:179. doi: 10.3389/fnins.2016.00179

[11] S. Cauzzo, M. Basile, E. Bruno, A. Callara, L. Danglot, A. Ahluwalia, C. Magliaro, N. Vanello (2022), "Parcellation of binary segmentations in microscopy images of ex-vivo clarified neurons via morphological reconstruction and watershed transform", Federation of European Neuroscience Societies, FENS Forum 2022, Paris, France, 9-13 July 2022

[12] Magliaro C, Callara AL, Vanello N, and Ahluwalia A (2017): A manual segmentation tool forthree-dimensional neuron datasets". Frontiers in neuroinformatics. doi: 10.3389/fninf.2017.00036.

[13] Vormberg A, Effenberger F, Muellerleile J, Cuntz H (2017a): Universal features of dendrites through centripetal branch ordering. Ed. Boris S. Gutkin. PLOS Computational Biology 13:e1005615. doi: 10.1371/journal.pcbi.1005615.

The Scientific Liaison Unit of EBRAINS from science to infrastructure

Author
Marissa Pier Diaz, Claudia Bachmann, Wouter Klijn – Jülich Supercomputer Centre (JSC), Institute for Advance Simulation (IAS), Jülich Research Centre, Jülich, Germany

Citation
Diaz, M.P., Bachmann, C., Klijn, W. The Scientific Liaison Unit of EBRAINS from science to infrastructure

EBRAINS comprises more than 130 European research organizations, each with a large number of scientists, programmers, and technical coordinators. Developing, operating, and using an immense infrastructure such as EBRAINS is a complex task that bears the risk of an individual scientist getting lost in details. The Scientific Liaison Unit (SLU) was founded to provide a helping hand in navigating the complexity of EBRAINS services and science.

SLU has a series of tools and processes designed to help you identify your needs and make a concrete description that will guide you into how to homogenize your data, use other information sources, and asses your computational needs. Also, EBRAINS members can provide standardized workflows that you can use to implement your models and test your ideas and compare them with other published work. The middle section of our poster shows how we use a Structured formalization process.

The objective of this poster is to show you an example of how the processes developed by the SLU can support scientific cases in defining a roadmap that consists of all the necessary descriptions to assess the needs of the research and how to achieve its objectives in a Fair science scenario ensuring reproducibility, availability, and visibility of the work.

Methods

We introduce a descriptive template [1] that guides the scientist through a couple of steps: from a scientific description of her/his science case at the beginning, followed by a progressively technical presentation of it. The technical representation also includes a diagram with symbols organized according to specific rules that allow us to identify commonalities between different scientific cases and infer major scientific needs.

To achieve this description the case is submitted to a structured formalization process fig.1 that transforms in a co-design manner a free form description of a science use case into technical specifications.

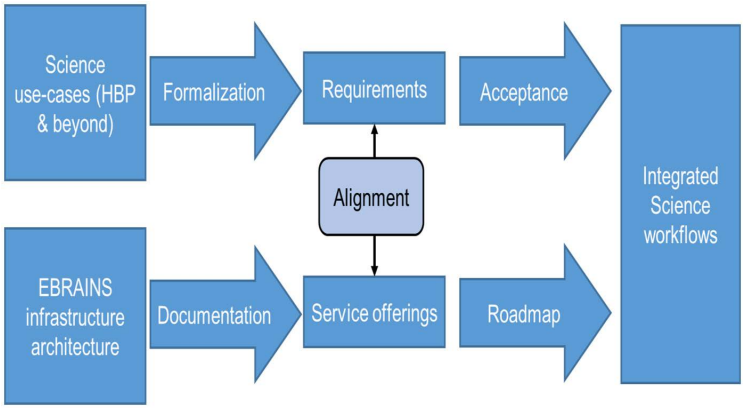

FIGURE 1
Science Use case & Workflow Description and Specification.

Benefits:

a) Find the essential parts of the project.

b) Early identification of inconsistencies in your scientific workflow.

c) Early identification of potential problems and possible solutions.

d) Easier communication with technical support and other internal and external collaborators.

e) A standardized format helps us to identify similar technical requirements across different.

f) Science cases -> higher prioritization of your technical needs.

Collaborative:

The document will typically be written in an iterative manner, with the document bouncing from scientist to developer getting more detailed on each iteration.

Living document:

Details of the project can and will change over time, components might be hard to implement and trade-offs might be made depending on the availability of resources and technical limitations.

Reuse of effort:

The material created during this process is your property and will not be made public. It can be reused for a later publication.

Results

Based on an example of the hyper-parameter optimization framework ([2], Fig.2) we demonstrate how the structure of the document leads the reader from a scientific description to a technical requirement analysis. In this way, potential project challenges as well as opportunities for extensions and interaction are identified early on.

Discussion

The poster gives an overview of the different areas of responsibility that the SLU has. In particular, it explains our strategies for identifying and prioritizing the needs of the scientific community and their formulation into technical requirements based on scientific cases in a systematic and standardized way.

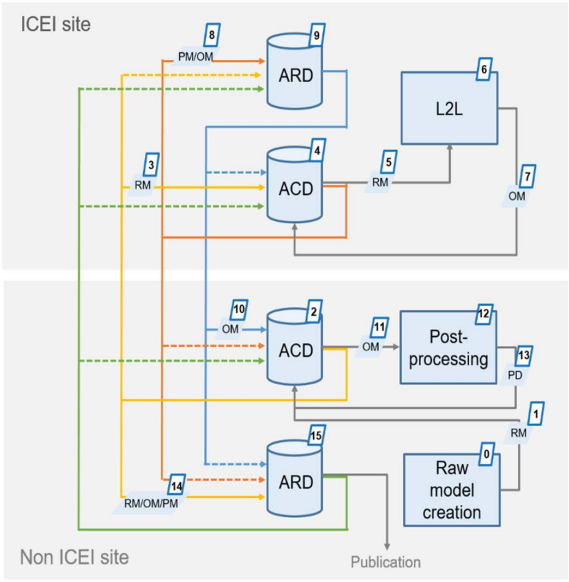

FIGURE 2
Diagrammatic description of the hyper-parameter optimization workflow.

Acknowledgements
This research was supported by the EBRAINS research infrastructure, funded by European Union's Horizon 2020 Framework Program for Research and Innovation under the Specific Grant Agreement No. 945539 (Human Brain Project SGA3)

References

[1] https://drive.ebrains.eu/f/2d30a9a6284f4cc0b8c9/

[2] https://meta-optimization.github.io/L2L/

Poster Link

[3] https://drive.ebrains.eu/f/d7a272dff57c415ba1a1/

Aging myeloid cells associated with Blood-Brain barrier dysfunction favors brain diseases

Author
Marta Caamaño-Moreno, Sara Hiller-Vallina, Lucía Mondéjar-Ruescas, Ricardo Gargini, Berta Segura-Collar – Instituto de investigaciones Biomédicas I+12, Hospital 12 de Octubre, Madrid, Spain

Citation
Caamaño-Moreno, M., Hiller-Vallina, S., Mondéjar-Ruescas, L., Gargini, R., Segura-Collar, B. Aging myeloid cells associated with Blood-Brain barrier dysfunction favors brain diseases.

Introduction/Motivation

The world population aging is increasing, particularly in developed countries. Consequently, an increase in the comorbidity of age-related diseases has occurred. For this reason, it is important to study the correlation between aging and the susceptibility to suffer certain pathologies that rarely occur in young age. At the brain-cognitive level, during aging, some individuals experience a series of progressive changes characterized by the loss of physiological brain functions, such as loss of brain volume, a state of chronic inflammation or increased permeability of the Blood-Brain Barrier (BBB), leading to an increased infiltration of different cell types (myeloid suppressors or lymphocytes) (1). These cases have been directly related to the development of certain pathologies of neuronal dysfunction (2). Physiologically, the brain is in a situation of immune privilege controlled by the BBB. Its disruption allows the entry of immune molecules and infiltrates, causing neuroinflammation induced by proinflammatory cytokines.

This process alters the brain microenvironment (3) leading to neuronal dysfunction and the consequent appearance of cognitive-behavioral problems.

Taken together, the data obtained in our laboratory indicate that the aging process leads to BBB dysfunction that allows the entry of immunosuppressive myeloid cells into the brain such as $TREM2^{+}/TIM3^{+}$ determined in our laboratory, a finding that could favor the progression of different neuropathologies developed in the same age range such as Alzheimer's disease and glioma. These results could help us to understand the progression of brain pathologies and, therefore, to improve therapies.

Methods

In silico analyses: UCSC Xena-Browser and GTEx database were used for gene expression correlation analyses in specific regions: hippocampus, cerebral cortex, anterior cingulate cortex, frontal cortex. Quantitative Real Time-PCR: To obtain the different gene signatures expression qRT-PCR was performed. Immunofluorescence: Co-expression of TREM2/TIM3, CD68/TREM2/TIM3 and CD8/PD-1 were analysed by immunofluorescence using specific antibodies.

Results and discussion

Dysfunctional BBB during aging allows pro-pathogenic immune system cells infiltration.

In silico analyses showed a progressive loss of the synapse signature correlated with an increase in BBB dysfunction genes (**Figure 1a)**. Moreover, a BBB dysfunction and synapse loss related with age increase was described (**Figure 1b**), these data were supported by the results obtained *in vivo* (**Figure 1c**). The BBB dysfunction leads to the loss of brain immunoprivilege causing therefore the entry of different molecules and cells of the immune system, provoking inflammatory processes associated with different brain pathologies. Using the inflammatory processes, we established two gene signatures: one of neuroinflammation and the other of myeloid suppressor

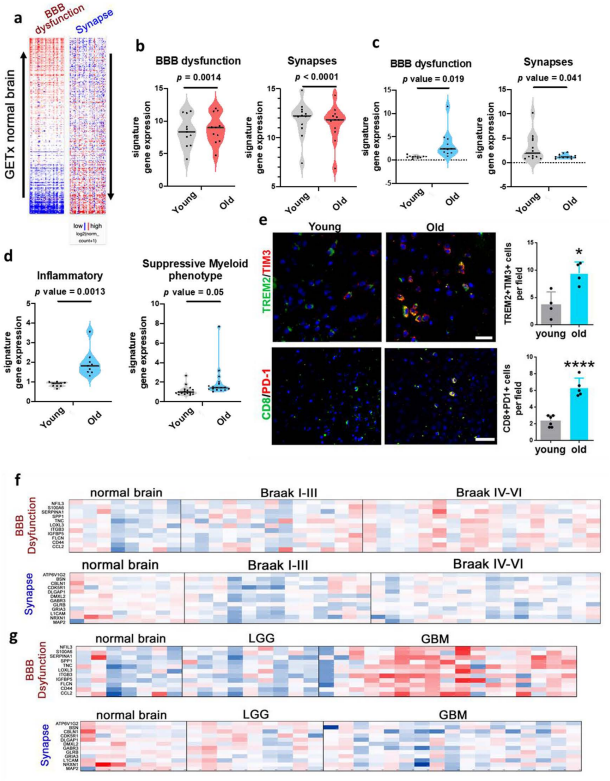

FIGURE 1

a. GTEx In silico synapse and BBB dysfunction signatures analyses representing high (blue) and low expression (red) **b.** GTEx In silico synapse and BBB dysfunction signatures according to age analyses. **c.** Quantitative real time-PCR (qRT-PCR) of BBB dysfunction and synapses signatures in 3-month (young) and 13-month (old) C57/BL6 mice. **d.** Quantitative real time-PCR of inflammatory and suppressive myeloid phenotype signatures in 3-month (young) and 13-month (old) C57/BL6 mice. **e.** Representative immunofluorescence for TREM2/TIM3 and PD-1/CD8 co-expression in young and old mouse brain tissue besides its quantification. **f-g** Synapses and BBB dysfunction gene expression signatures representing high blue) and low expression (red) obtained by qRT-PCR in normal brain tissue (n=7), AD Braak I-III (n=13), AD Braak IV-V (n=16), LGG (n=7) and GBM (n=17).

cells associated with the TREM2 gene. Thus, we observed an increment in the expression signature of inflammatory and suppressor myeloid phenotype in old individuals (**Figure 1d**). Then, immunofluorescence studies corroborated that myeloid cells labeled with TREM2+ co-expressed with TIM3+ -a potent immunosuppressor. In addition, it was also associated an infiltrate increase in CD8+/PD-1+ labeled immune cells in old mice, compromising the non-inflammatory brain environment (**Figure 1e**).

Immune cell infiltration cause by BBB dysfunction in different neuropathologies such as glioma and AD.

In order to corroborate whether the phenotype observed in aging is involved in the development and malignancy of various brain pathologies, we decided to analyze both processes, BBB dysfunction and immunosuppressive myeloid cell infiltration in glioma and AD.

By qRT-PCR the expression of BBB dysfunction and synapse signature genes in our own cohort of glioma and AD patients was studied, for that normal tissue from healthy patients was used as control (**Figure 1f-g**). Previously, based on the degree of glioma malignancy, we stratified patients into two subgroups: low-grade gliomas (LGG) and high-grade gliomas, named glioblastoma (GBM). Patients with AD were divided using the Braak staging system (4), low Braak (including grade I, III and III Braak) and high Braak (grade IV, V and VI).

In both pathologies, an inverse patterns followed by gene expression signature was observed (**Figure 1f-g**). In patients with glioblastoma a strong induction of BBB dysfunction genes expression comparing to patients with less aggressive tumors was described, simultaneously presenting more increased levels regarding to normal tissue (**Figure 1f**). Similarly, in the Alzheimer's cohort, increased expression of BBB dysfunction genes was observed in more advanced stages of the disease (Figure 1g). In contrast, the synapse signature presented a reverse pattern (**Figures 1f-g**).

Furthermore, when we analyzed by qRT-PCR the previously mentioned cohorts, the expression of gene signatures related to the inflammatory process and the immunosuppressive myeloid phenotype presented a pronounced increase in both processes and pathologies (**Figure 2a**).

Taking into account the above data set, where we observed an increase in BBB dysfunction and progression of both pathologies, the infiltration of pro-pathogenic immune cells labeled with TREM2 and TIM3 was studied in our cohort of glioma and Alzheimer's patients. Thus, the expression of TREM2 and TIM3 was analyzed performing correlation analysis. In addition to **Figure 2c**, where a positive correlation between these genes was determined, in **Figure 2d-e** a positive and significant correlation in patients with glioblastoma and Alzheimer's disease (Braak IV-VI) was also observed, where a BBB dysfunction was previously described (**Figure 1f-g**).

In addition, a histologically analysis was performed by triple immunofluorescence in glioma and AD patient tissue, evaluating the infiltration of immunosuppressive myeloid cells co-expressing TREM2 and TIM3 with macrophage marker CD68. As can be seen in **Figure 2f**, glioma and Alzheimer's patients presented a large number of CD68+ myeloid cells expressing TREM2, as well as TIM3 marker. Therefore, as happens at the gene expression level (**Figure 2c-e**).

In conclusion, we can establish that the loss of BBB integrity observed in the brain leads to the entry of myeloid cells that generate an inflammatory process linked to an immunosuppression profile. These cells can be defined with TREM2 labeling, which has an macrophage M2 expression profile, as well as the TIM3 marker, related in previous work to myeloid dysfunction associated with tumorigenesis (5).

Concerning the future, due to the encouraging results obtained in this project, we strongly believe that therapeutical approaches against these targets would be interesting to address.

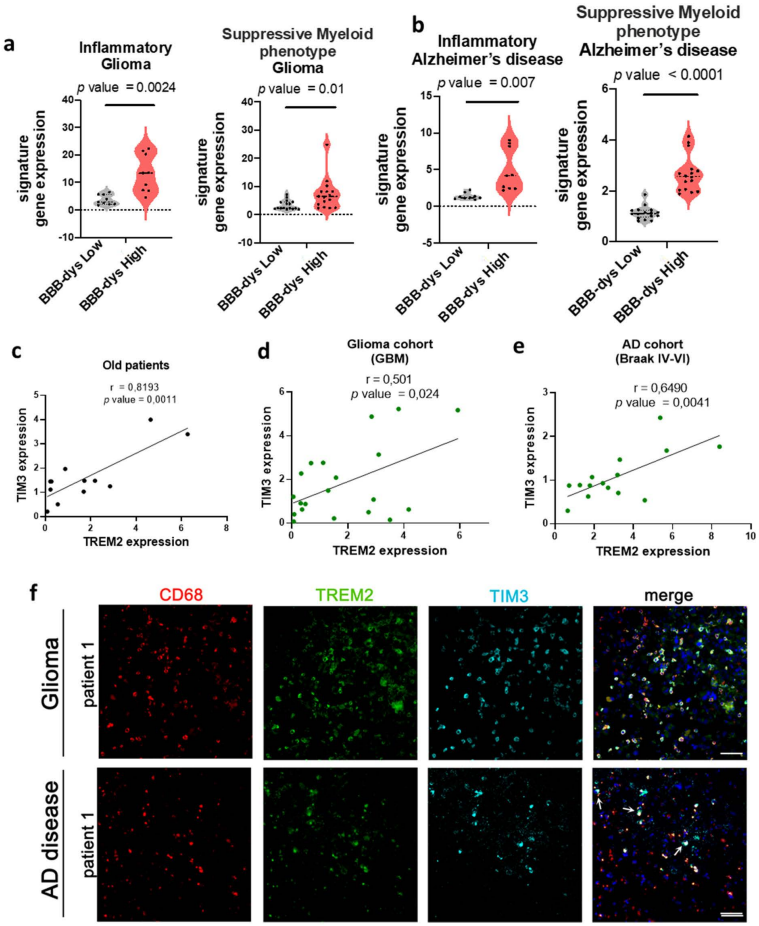

FIGURE 2

a-b. Inflammatory and suppressive myeloid phenotype signatures obtained by qRT-PCR in glioma (n=26) and AD (n=29). **c-e.** Pearson correlation analyses for TIM3/TREM2 expression in old patients (n=12), GBM (n=20) and AD cohort (n=16), respectively. **f.** Representative immunofluorescence for CD68/TREM2/TIM3 co-expression in glioma and AD brain tissue.

References

(1) Erdő, F., Denes, L., & de Lange, E. (2017). Age-associated physiological and pathological changes at the blood–brain barrier: a review. Journal of Cerebral Blood Flow & Metabolism, 37(1), 4-24.

(2) Segura-Collar B, Mata-Martínez P, Hernández-Laín A, Sánchez-Gómez P, Gargini R. Blood-Brain Barrier Disruption: A Common Driver of Central Nervous System Diseases. Vol. 28, Neuroscientist. SAGE Publications Inc.; 2022. p. 222–37.

(3) Gargini R, Segura-Collar B, Sánchez-Gómez P. Cellular plasticity and tumor microenvironment in gliomas: The struggle to hit a moving target. Vol. 12, Cancers. MDPI AG; 2020. p. 1–24.

(4) Braak H, Braak E. Acta H ' pathologica Neuropathological stageing of Alzheimer-related changes. Vol. 82, Acta Neuropathol. 1991.

(5) Wolf, Y., Anderson, A. C., & Kuchroo, V. K. (2020). TIM3 comes of age as an inhibitory receptor. Nature Reviews Immunology, 20(3), 173-185.

Application of unsupervised machine learning methodologies for the detection of electrophysiological factors predisposing to heavy alcohol consumption in teenagers

Author
Marcos Uceta – Center for Cognitive and Computational Neuroscience (C3N), University Complutense of Madrid (UCM), 28223, Madrid, Spain
Luis Antón-Toro – Center for Cognitive and Computational Neuroscience (C3N), University Complutense of Madrid (UCM), 28223, Madrid, Spain; Department of Psychology, Faculty of health, University Camilo José Cela (UCJC), 28692, Madrid, Spain
Alberto Del Cerro-León – Center for Cognitive and Computational Neuroscience (C3N), University Complutense of Madrid (UCM), 28223, Madrid, Spain; Department of Pharmacology and Toxicology, Complutense University of Madrid (UCM), 28040, Madrid, Spain
Danylyna Shpakivska – Center for Cognitive and Computational Neuroscience (C3N), University Complutense of Madrid (UCM), 28223, Madrid, Spain; Department of Psychobiology and Methodology in Behavioral Sciences, Complutense University of Madrid (UCM), 28040, Madrid, Spain
Fernando Maestú – Center for Cognitive and Computational Neuroscience (C3N), University Complutense of Madrid (UCM), 28223, Madrid, Spain; Department of Experimental Psychology, Complutense University of Madrid (UCM), 28223, Madrid, Spain
Luis Miguel García-Moreno – Department of Psychobiology and Methodology in Behavioral Sciences, Complutense University of Madrid (UCM), 28040, Madrid, Spain

Citation
Uceta, M., Antón-Toro, L., Cerro-León, A.D., Shpakivska, D., Maestú, F., García-Moreno, L.M. Application of unsupervised machine learning methodologies for the detection of electrophysiological factors predisposing to heavy alcohol consumption in teenagers.

Introduction

Binge Drinking (BD) has emerged as a widespread pattern of consumption among teenagers. It is characterized by the intake of large amounts of alcohol (more than 4 drinks per session) within shorts periods of time (2 hours), with a period of abstinence between episodes (Courtney K. et al., 2009). This type of consumption entails several social and sanitary risks, altering the integrity and development of the nervous system, particularly vulnerable during adolescence (Blakemore S. et al., 2006). Beyond these neuroanatomical and neurofunctional alterations, there is a raising concern regarding predisposing factors that might prone teenagers to such harmful lifestyle. Behavioral factors like impulsivity, sensation seeking, or executive control has been reported as potentially risky towards BD development (Ohannessian C. et al., 2007; Verdejo-García A. et al., 2008; Antón-Toro et al., 2021); neuroanatomically, a decreased grey matter volume in prefrontal and parietal regions were proposed as good indicators of a predisposition to BD (Brumback et al., 2016; Squeglia et al., 2017). In neurofunctional studies, altered BOLD activity (Spear, 2018) as well as altered electrophysiological connectivity predating BD (Antón Toro et al., 2021; Antón-Toro et al., 2022) were shown. However, by the time, there is a scarcity of works with the advantages from the newcoming Machine Learning (ML) approaches combined with those neuroimage data. This work represents an innovative approach to techniques previously used as exploratory methods, from the Unsupervised Learning branch of Machine Learning.

Methods

In this longitudinal study, we recruited 99 students from different high schools of the Community of Madrid, Spain, aged around 14 years

(± 0.9 years). All subjects reported no previous alcohol intake, measured by means of the Alcohol Use Disorder Identification Test (AUDIT) and semi-structured interview. Participants did not report any familiar history of alcohol misuse, and no psychiatric or neurological disorders. We recorded resting-state electrophysiological activity by means of Magnetoencephalography (MEG), and individual brain morphology using a magnetic resonance imaging (MRI). Two years later, they fulfilled the AUDIT test and a semi-structured interview to measure their alcohol consumption habits. According to this information, we subdivided the sample into two groups: control group (N= 40; less than 2 drinks per session) and BD group (N = 59; more than 4 drinks per session); the division was made in line with the previous work in the field, mentioned above.

We conducted a source-space spectral power analysis for 78 cortical regions (based on AAL atlas), in four frequency bands: theta (4-8 Hz), alpha (8-12 Hz), beta (12-20 Hz), and gamma (30-45 Hz). Next, we analyze and clusterize the normalized power data using Unsupervised ML techniques, using Python packages like SciPy, Scikit-learn and Matplotlib. To ascertain the most efficient number of groups our data was divided into, we performed a preliminary K-nearest neighbors (KNN) model (K between 1-10). Metrics like the Sum of Squared Within (SSW) or the Calinski-Harabasz coefficient were used to measure the cohesion and coherence of the clusters. Once the most efficient number of clusters is obtained, the Unsupervised Learning model is developed. The similarity between ROIs' power is obtained using a Pearson's correlation matrix, which, later, is discretize by mutual information (Ferreira A. et al., 2015); this distance between points (being the similarity between points an inverse measure of its distance) was used to create hierarchical clusterisation, in the form of dendrograms, using Ward's method with Euclidean distance between points (Murtagh F. et al., 2014). The results obtained this way in control groups were then compared with the BD ones, analyzing the differences between them.

Results

The obtained results showed a different clusterisation in alpha and theta bands between groups. In alpha band, we found a clusterisation

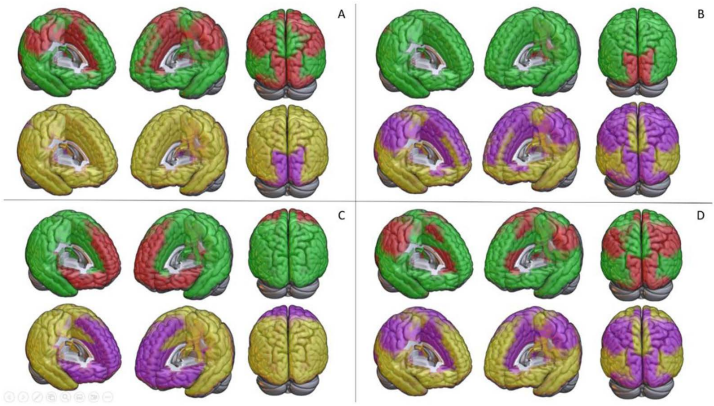

FIGURE 1
Detailed cortical distribution of the different clusters within the four frequency bands of interest. In green and red, the clusters for control groups; in yellow and purple, the clusters for BD groups. A) Theta. B) Alpha. C) Beta. D) Gamma.

encompassing regions from the default mode network (DMN) in the BD group, while in the control group only a portion of the occipital lobe was clusterize. Regarding the theta band, we found the inverse pattern of clusterisation, with control groups clustering regions from the DMN in theta band, while the BD group only clustering in an occipital region. The results found in beta and gamma bands showed similar pattern between control and BD participants (focused on the frontal lobe in beta band; and on parieto-occipital areas in gamma band) (see Figure 1 for detailed cortical distribution of different clusters). The quantitative differences are shown in Figure 2, with a general reduction in power in BD groups in theta band, and an augment of power in BD in beta band. The distribution of quantitative differences in both alpha and gamma band is more heterogeneous, with hotspots of difference found in areas related to the DMN.

Discussion and Conclusions

The results shown demonstrate the capabilities of ML techniques, especially unsupervised learning algorithms, historically used for preliminary exploratory

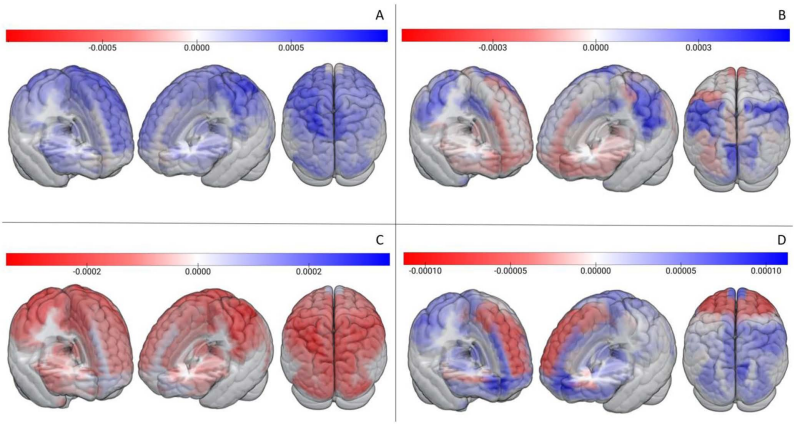

FIGURE 2
Quantitative differences, result of the subtraction between control and BD groups (Control Group Power – BD Group Power), in the different frequency bands of interest. **A**) Theta Band Differences; **B**) Alpha Band Differences; **C**) Beta Band Differences; D) Gamma Band Differences. Red and blue denotes an increase/decrease in BD group's mean power respectively.

purpose. The distinctive patterns found between control and BD groups, especially in Alpha and Theta bands, might be used to understand brain organizations associated with BD predisposition, probably derived from different neuromaturation patterns. The qualities of MEG, with its significant temporal resolution, coupled with the capacities and sensibility of ML techniques, have been shown as excellent tools to analyze neurofunctional data. In this case, focusing on Alpha and Theta bands, we found an inverse pattern of power between control and BD groups. This pattern, which is very similar to a DMN-like distribution, links with a decrease in theta and alpha bands' power in BD and control groups. In this vein, some studies have reported a progressive increment of the oscillatory frequency after puberty onset (Shulman E. *et al.*, 2016). The similar clusterisation of control and BD groups in different frequency bands may concord with this "pseudomadurative" hypothesis, pointing to an early maturational process in the BD groups, with an altered oscillatory activity related to the DMN areas.

In the other hand, quantitative differences seems to show a widespread increased activity in fast frequency band in future BD, probably reflecting a neurobiological hyperexcitability profile.

References

Antón-Toro L et al. (2021). Abnormal organization of inhibitory control functional networks in future binge drinkers. Drug and alcohol dependence, 108401, 218. https://doi.org/10.1016/j.drugalcdep.2020.108401

Antón-Toro, L. F., Bruña, R., Del Cerro-León, A., Shpakivska, D., Mateos-Gordo, P., Porras-Truque, C., García-Gómez, R., Maestú, F., & García-Moreno, L. M. (2022). Electrophysiological resting-state hyperconnectivity and poorer behavioural regulation as predisposing profiles of adolescent binge drinking. Addiction biology, 27(4), e13199. https://doi.org/10.1111/adb.13199

Blakemore, S. J., & Choudhury, S. (2006). Development of the adolescent brain: implications for executive function and social cognition. Journal of child psychology and psychiatry, and allied disciplines, 47(3-4), 296–312. https://doi.org/10.1111/j.1469-7610.2006.01611.x

Brumback T et al. (2016). Neural predictors of alcohol use and psychopathology symptoms in adolescents. Development and Psychopathology, 1209-1216, 28(4). https://doi.org/10.1017/S0954579416000766

Courtney, K. E., & Polich, J. (2009). Binge drinking in young adults: Data, definitions, and determinants. Psychological bulletin, 135(1), 142–156. https://doi.org/10.1037/a0014414

Ferreira A, Figueiredo M (2015). Feature discretization with relevance and mutual information criterio. Advances in Intelligent Systems and Computing, (2015), 101-118. https://doi.org/10.1007/978-3-319-12610-4_7

Meltzer, J. A., Negishi, M., Mayes, L. C., & Constable, R. T. (2007). Individual differences in EEG theta and alpha dynamics during working memory correlate with fMRI responses across subjects. Clinical neurophysiology: official journal of the International Federation of Clinical Neurophysiology, 118(11), 2419–2436. https://doi.org/10.1016/j.clinph.2007.07.023

Murtagh F, Legendre P (2014). Ward's Hierarchical Agglomerative Clustering Method: Which Algorithms Implement Ward's Criterion? Journal of Classification, 274-295, 31(3). https://doi.org/10.1007/s00357-014-9161-z

Ohannessian C, Hesselbrock V (2007). Do personality characteristics and risk taking mediate the relationship between paternal substance dependence and adolescent substance use? Addictive behaviors, 1852-62, 32(9). https://doi.org/jaddbeh.2006.12.017

Oostenveld R, Fries P, Maris E, Schoffelen J-M (2011). FieldTrip: Open-Source Software for Advanced Analysis of MEG, EEG, and Invasive Electrophysiological Data. Comput. Intell. Neurosci.; 2011:1–9. https://doi.org/10.1155/2011/156869

Spear LP (2018). Effects of adolescent alcohol consumption on the brain and behaviour. Nat Rev Neurosci.; 19(4):197-214. doi: 10.1038/nrn.2018.10.

Shulman, E. P., Smith, A. R., Silva, K., Icenogle, G., Duell, N., Chein, J., & Steinberg, L. (2016). The dual systems model: Review, reappraisal, and reaffirmation. *Developmental Cognitive Neuroscience*, *17*, 103–117. https://doi.org/10.1016/j.dcn.2015.12.010

Squeglia L et al. (2017). Neural predictors of initiating alcohol use during adolescence. American Journal of Psychiatry, 172-185, 174(2). https://doi.org/10.1176/appi.ajp.2016.15121587

Tzourio-Mazoyer N et al. (2002). Automated Anatomical Labelling of Activations in SPM Using a Macroscopic Anatomical Parcellation of the MNI MRI Single-Subject Brain. Neuroimage; 15(1):273–89. https://doi.org/10.1006/nimg.2001.0978

Van Veen BD, Van Drongelen W, Yuchtman M, Suzuki A (1997). Localization of brain electrical activity via linearly constrained minimum variance spatial filtering. IEEE Trans. Biomed. Eng.; 44(9):867–80. https://doi.org/10.1109/10.623056

Verdejo-García A, Lawrence A, Clark L (2008). Impulsivity as a vulnerability marker for substance-use disorders: review of findings from high-risk research, problem gamblers and genetic association studies. Neuroscience and biobehavioral reviews, 777-810, 32(4). https://doi.org/10.1016/j.neubiorev.2007.11.003

Towards a fully automatic method for dendritic spine segmentation

Author
Isabel Vidaurre-Gallart[1]* – VG-LAB, Universidad Rey Juan Carlos, Móstoles, Spain
Isabel Fernaud-Espinosa[2,3] – Instituto Cajal, Consejo Superior de Investigaciones Científicas (CSIC), Madrid, Spain; Laboratorio Cajal de Circuitos Corticales, Centro de Tecnología Biomédica, Universidad Politécnica de Madrid, Madrid, Spain
Nicusor Cosmin-Toader[1] – VG-LAB, Universidad Rey Juan Carlos, Móstoles, Spain
Ruth Benavides-Piccione[2,3]* – Instituto Cajal, Consejo Superior de Investigaciones Científicas (CSIC), Madrid, Spain; Laboratorio Cajal de Circuitos Corticales, Centro de Tecnología Biomédica, Universidad Politécnica de Madrid, Madrid, Spain
Luis Pastor[1,4] – VG-LAB, Universidad Rey Juan Carlos, Móstoles, Spain; Research Center for Computational Simulation (CCS), Madrid, Spain
Javier DeFelipe[2,3] – Instituto Cajal, Consejo Superior de Investigaciones Científicas (CSIC), Madrid, Spain; Laboratorio Cajal de Circuitos Corticales, Centro de Tecnología Biomédica, Universidad Politécnica de Madrid, Madrid, Spain
Marcos García-Lorenzo[1,4]* – VG-LAB, Universidad Rey Juan Carlos, Móstoles, Spain; Research Center for Computational Simulation (CCS), Madrid, Spain

Citation
Vidaurre-Gallart, I., Fernaud-Espinosa, I., Cosmin-Toader, N., Benavides-Piccione, R., Pastor, L., DeFelipe, J., García-Lorenzo, M. Towards a fully automatic method for dendritic spine segmentation.

Introduction/Motivation

Dendritic spines (for simplicity, spines) play a fundamental role in modulating the transmission of excitatory information in the pyramidal cells of the cerebral cortex. They are key structures in learning, memory, and cognition

[1,2,3,4,5]. Despite their importance and the efforts put on their study, the morphological analysis of dendritic spines is a challenging task. Current techniques still rely on experts for accurate segmentation [6,7]. This process is tedious and time-consuming; therefore, expensive.

In 2022, we presented a solution based on Deep Learning (DL)[8]. In that work, we tested some of the most popular DL architectures for semantic segmentation in the field of medical imaging. Our previous work opens the door to fully automatic segmentation, but still has some limitations.

In the biomedical field, DL-based techniques have proven to be effective in image segmentation [9]. However, they require a high-quality dataset to train DL models with guarantees. In this regard despite having one of the largest data sets available in the literature [10], we suffer from overfitting problems. For this reason, we could not implement more complex models, such as deeper or instance segmentation-based architectures.

There is currently no software solution for segmenting dendritic spines based on neural networks. Therefore, we have designed and implemented a graphical user interface (GUI) application that segments dendritic spines automatically from confocal microscopy images using the DL model proposed in [8]. Our tool allows users to improve the quality of the confocal image before segmentation and correct the results provided by the DL model. Our goal is to store the user's corrections to improve the ground truth (GT), allowing us to train more complex and efficient DL models shortly.

Methods

We developed our GUI application with two main goals: (i) to accelerate the reconstruction of dendritic spines and (ii) to gather a new high-quality GT without wasting the experts' time.

Neuromorphologists can use our tool to reconstruct new data for their studies. In most cases, the DL model segments spines and dendritic shafts adequately. Users must only correct a limited number of spines. User corrections are stored to improve the GT transparently to the user.

The main functionalities of our tool are listed in Table 1. Figure 1 shows the designed user workflow.

TABLE 1: Main functionalities of our system

Functionalities	Description	Options
Load/save 3D images and meshes	Users can load confocal microscopy images and 3D reconstruction of the dendritic shafts and spines. The data is hierarchically stored in a tree graph, similarly to Imaris (Bitplane AG, Zurich, Switzerland). The data can be exported into different data file formats for its analysis.	Load: - All data (proprietary format) - Images (.tiff) - Meshes (.obj, .stl) Save: - All data (proprietary format) - Images (.tiff) - Meshes (.obj, .stl) - Data tables (.csv)
Viewers	We implemented several widgets for exploring, analyzing, and comparing the confocal images and 3D meshes.	Basic 3D image viewer, 3D image multiprojection viewer.
Image editors	Confocal images can suffer from different problems such as noise, low contrast, etc. Our tool offers different image-enhancing options, to improve the automatic segmentation process.	ROI selector, Contrast/brightness, Scaling, Gamma correction, Log correction, Sigmoid correction, Equalization, Adaptative equalization, and Contrast stretching.
Automatic segmentation	Users can perform fully automatic segmentation.	User can choose between 3 different DL models.
Semiautomatic correction	The automatic segmentation may present some problems: noise, misclassification, unconnected components, and overlapping spines. We designed several automatic and user-supervised algorithms to address them.	Noise filtering, manual misclassification correction, automatic correction of unconnected components, and separation of overlapping spines.
3D reconstruction	Users can reconstruct the dendritic shafts and spines automatically	3D surface mesh viewer.

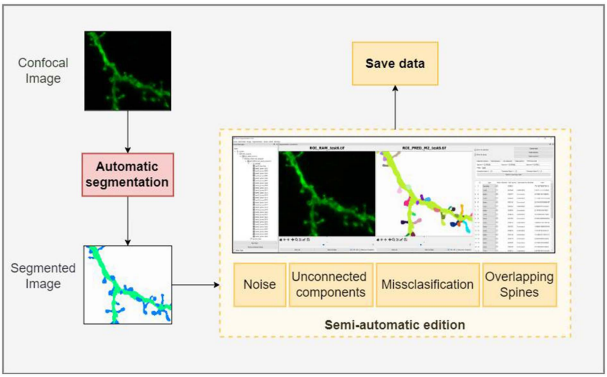

FIGURE 1
Automatic segmentation and postprocessing workflow. First, our CNN model provides a fully automatic segmentation. Users can then correct the CNN prediction through our GUI, if necessary. Finally, the corrected data are saved to augment the GT.

Results and discussion

Our GUI application is shown in Figure 2. The software was implemented in Python, Qt and VTK, following a flexible and modular plugin-based architecture. It was released under an open-source license and can be found in this repository:

https://gitfront.io/r/user-4306573/be116855b22f779ae17fb981f89fbd138ac27133/DeepSpineNet-GUI/

Our previous work opens the door to automate the reconstruction of dendritic spines using DL. Although current solutions are not flawless yet, the combination of DL models and our application reduces the time spent by the user without any segmentation quality compromise. Neuroscientists could use our solution to correct the automatic reconstructions. At the same time, this data can be used to gather a larger and higher quality GT. This GT can be used by the community to retrain current models or even develop new and

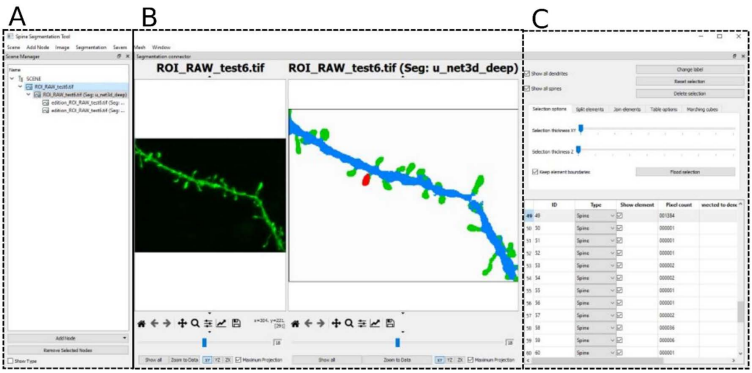

FIGURE 2

*The GUI allows the user to organize the scene in a hierarchical manner. (**A**) Users can select between several data view widgets. (**B**) shows a view of the confocal and segmented images. (**C**) allows users to configure the different correction algorithms.*

more complex neural networks. Current semantic segmentation models are especially sensitive to overlapping spines. The instance-based segmentation models [11] may perform better in these cases. Increasing the size of our current GT is mandatory for this approach to be feasible.

We created a prototype GUI to test our automatic segmentation and user-supervised correction algorithms. Once we have proven the usefulness of this approach, the implemented algorithms could be integrated into other tools such as ImageJ [12]. The ImageJ plugin system makes this application an ideal candidate to include our algorithms. Additionally, in our future research, we plan to automatically feed our current DL models with the users' corrections, improving the model performance transparently to the user.

Acknowledgements

The research leading to these results has received funding from the following entities:

The Spanish Government under grants FPU18/05304, PRE2018-085403, PID2020-113013RB-C21 (MEDAVI), and the European Union's Horizon 2020 Framework under the Specific Grant Agreement No. 945539 (HBP SGA3).

The authors gratefully acknowledge the computer resources at Artemisa, funded by the European Union ERDF and Comunitat Valenciana as well as the technical support provided by the Instituto de Física Corpuscular, IFIC (CSIC-UV).

References

[1] Harris, K. M., and Kater, S. B. (1994). Dendritic spines: cellular specializations imparting both stability and flexibility to synaptic function. Ann. Rev. Neurosci. 17, 341–371.

[2] Bourne, J., and Harris, K. M. (2007). Do thin spines learn to be mushroom spines that remember? Curr. Opin. Neurobiol. 17, 381–386. doi: 10.1016/j.conb.2007.04.009

[3] Spruston, N (2008). Pyramidal neurons: dendritic structure and synaptic integration. Nat. Rev. Neurosci. 9, 206–221. doi: 10.1038/nrn2286

[4] Yuste, R (2010). Dendritic Spines. Cambridge, MA: MIT Press.

[5] Kandel, E. R., Dudai, Y., and Mayford, M. R. (2014). The molecular and systems biology of memory. Cell 157, 163–186. doi: 10.1016/j.cell.2014.03.001

[6] Zhang, Y., Chen, K., Baron, M., Teylan, M. A., Kim, Y., Song, Z., et al. (2010). A neurocomputational method for fully automated 3D dendritic spine detection and segmentation of medium-sized spiny neurons. NeuroImage 50, 1472–1484. doi: 10.1016/j.neuroimage.2010.01.048

[7] Mukai, H., Hatanaka, Y., Mitsuhashi, K., Hojo, Y., Komatsuzaki, Y., Sato, R., et al. (2011). Automated analysis of spines from confocal laser microscopy images: Application to the discrimination of androgen and estrogen effects on spinogenesis. Cereb. Cortex 21, 2704–2711. doi: 10.1093/cercor/bhr059

[8] Vidaurre-Gallart I, Fernaud-Espinosa I, Cosmin-Toader N, Talavera-Martínez L, Martin-Abadal M, Benavides-Piccione R, Gonzalez-Cid Y, Pastor L, DeFelipe J and García-Lorenzo M (2022) A Deep Learning-Based Workflow for Dendritic Spine Segmentation. Front. Neuroanat. 16:817903. doi: 10.3389/fnana.2022.817903

[9] Minaee, S., Boykov, Y. Y., Porikli, F., Plaza, A. J., Kehtarnavaz, N., and Terzopoulos, D. (2021). Image segmentation using deep learning: a survey. IEEE Trans. Pattern Anal. Mach. Intell. 1. doi: 10.1109/TPAMI.2021.3059968

[10] Benavides-Piccione, R., Fernaud-Espinosa, I., Robles, V., Yuste, R., and DeFelipe, J. (2013). Age-based comparison of human dendritic spine structure using complete three-dimensional reconstructions. Cereb. Cortex 23, 1798–1810. doi: 10.1093/cercor/bhs154

[11] K. He, G. Gkioxari, P. Dollár, and R. Girshick, ''Mask R-CNN,'' in Proc. 616 IEEE Int. Conf. Comput. Vis., Oct. 2017, pp. 2961–2969.

[12] Schneider, C. A., Rasband, W. S., & Eliceiri, K. W. (2012). NIH Image to ImageJ: 25 years of image analysis. Nature Methods, 9(7), 671–675. doi:10.1038/nmeth.2089

Neuromorphic computing

Leveraging PyTorch on BrainScaleS-2: Training a real-world application

Author
Elias Arnold – Kirchhoff-Institute for Physics, Ruprecht-Karls-Universität Heidelberg, Heidelberg, Germany
Philipp Spilger – Kirchhoff-Institute for Physics, Ruprecht-Karls-Universität Heidelberg, Heidelberg, Germany
Eric Müller – Kirchhoff-Institute for Physics, Ruprecht-Karls-Universität Heidelberg, Heidelberg, Germany; European Institute for Neuromorphic Computing, Heidelberg University, Heidelberg, Germany
Georg Böcherer – Munich Research Center, Huawei Technologies Duesseldorf GmbH, Munich, Germany
Maxim Kuschnerov – Munich Research Center, Huawei Technologies Duesseldorf GmbH, Munich, Germany
Johannes Schemmel – Kirchhoff-Institute for Physics, Ruprecht-Karls-Universität Heidelberg, Heidelberg, Germany

Citation
Arnold, E., Spilger, P., Müller, E., Böcherer, G., Kuschnerov, M., Schemmel, J. Leveraging PyTorch on BrainScaleS-2: Training a real-world application.

Introduction

The usability of novel computing paradigms, in high-performance computing (HPC) often realized as domain-specific accelerators [6], and, in particular

neuromorphic hardware, is largely dictated by software allowing non-expert users to describe experiments effortlessly [5]. Especially when approaching gradient-based optimization tasks with spiking neural networks (SNNs) on such hardware, support for model definition and auto-differentiation is indispensable. Here we discuss the abstraction of training on the accelerated mixed-signal neuromorphic hardware system BrainScaleS-2 (BSS-2) in our high-level PyTorch-based framework `hxtorch.snn` and demonstrate it on a real-world application. We describe `hxtorch.snn` in detail and motivate our design decisions affecting the encapsulation of network topology, data flow, and training methodology. As an example, we consider an optical data communication link in data centers. In [1] we train SNNs emulated in analog on BSS-2 for equalizing an intensity modulation / direct detection (IM/DD) optical link and show that SNNs on BSS-2 are capable of compensating nonlinear impairments.

Methods

The BSS-2 system [3] is a mixed-signal neuromorphic system emulating 512 spiking AdEx [7] neurons and 131k 6-bit plastic synapses in parallel in analog circuits and in continuous time. To achieve a desired neural dynamic, neurons are individually parameterized. To realize different topologies, input and on-chip spikes are routed internally to desired synapses. Spikes are recorded and accessed from the host computer. Analog membrane voltages of the neurons are measured via parallel analog-to-digital converters. The neurons on BSS-2 can be configured to behave like leaky-integrate and fire (LIF) neurons [2].

Given their energy-efficient hardware implementation, SNNs are studied for machine learning tasks, using software libraries typically deployed for ANNs. Tools like PyTorch [4] allow computing weight updates seamlessly by applying the backpropagation through time algorithm. For this, a network model is described by composition of PyTorch modules (layers). PyTorch builds a differentiable computational graph, by assigning to each operation a backward function, allowing computing the gradient of the network with respect to its parameters, needed for learning.

SNNs on BSS-2 can be trained in-the-loop within PyTorch's ecosystem by emulating the forward pass on BSS-2 and injecting the recorded observables in the backward pass on the host computer. Since PyTorch executes the computational graph eagerly by computing all nodes successively upon definition, we construct and execute the model on hardware before the PyTorch graph is built to ensure that the data is present for the backward pass. hxtorch.snn builds on top of the existing software ecosystem for BSS-2 [5] and handles the hardware-related aspects automatically.

As an application, we train a SNN equalizer for a simulated IM/DD link [1]. A bit sequence is modulated to a signal , optically transmitted through a fiber, and measured at the receiver by a photodiode. The resulting sequence is impaired linearly by chromatic dispersion, nonlinearly by the photodiode, effectively squaring the electric field, and noise is added. The SNN equalizes and demaps , translated into spikes, to the received bits . The SNN, consisting of a hidden LIF and a leaky-integrate output layer, is emulated on BSS-2 and trained to minimize the bit error rate (BER).

Results

The schematics of the **hxtorch.snn** framework is depicted in Fig 1A. In hxtorch.snn we define models in a PyTorch fashion with the difference that our modules are derived from our hardware-specific PyTorch base-class **HXModule** (yellow), e.g., the **Neuron** module, a neuron population, and the **Synapse** module, a projection on BSS-2. All modules share an instance of **Instance** (blue), in which they register themselves. Each module holds a PyTorch-differentiable function **func(...)**, defining the forward pass (used in mock-mode, where the SNN is simulated in software) and the backward pass. By passing a **Handle**-type input to the forward method of a module, a Handle-typed data handle is returned, which is a reference to data that will be available in the future after hardware execution. These input and output handles are kept in the Instance for extracting the network's topology when calling a function run with the given Instance. After the network's topology is extracted, a corresponding hardware experiment is created and executed on BSS-2. The recorded hardware observables are assigned to their module

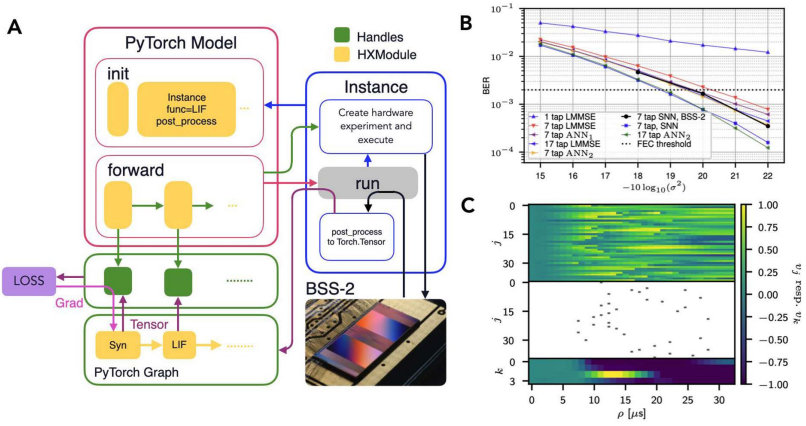

FIGURE 1

A) Schematic of the `hxtorch.snn` *PyTorch-based framework. B) Achieved BER in simulation and on BSS-2 [1]. C) Analog membrane traces on spikes on BSS-2 [1].*

(e.g., spikes to a Neuron module) and post-processed to torch.Tensors. A PyTorch graph is constructed by executing the modules' functions func, each returning the modules data tensors holding the hardware data. The returned tensors are assigned to the data Handles allowing access to the hardware data. The gradient is then computed by utilizing the hardware data in func's backward method. It is possible to easily switch between mock-mode and BSS-2 execution by toggling a flag.

We demonstrate the framework by equalizing the IM/DD link. In Fig. 1B, the BER is depicted over noise in the link. Both, the simulated SNN (blue squares) and the SNN emulated on BSS-2 (black) achieve lower BERs at the same noise levels than the linear equalizer (LMMSE, cf. Fig. 1B)). Fig. 1C shows the LIF neurons' membrane voltages over time (upper), their spikes (middle) and membrane traces of the output layer while equalizing/demapping one sample. The output neuron, producing the maximum voltage, dictates the demapped bits.

Discussion

The presented software framework enables the description of high-level SNN models in a PyTorch-compatible way and their emulation on BSS-2. We provide an abstract modeling API which relies on the BSS-2 software stack to translate user-defined experiments to corresponding hardware configurations. By utilizing PyTorch data types and its auto-differentiation mechanism, the computation of gradients and thus learning on BSS-2 is as effortless as for ANNs. The design of the API enables the definition of arbitrary network topologies, different neuron types (limited to the ones supported by BSS-2) and backward functions, all without expert-level hardware knowledge. Moreover, we envisage feedback connections over several modules, which will be demonstrated in the future. Hence, **`hxtorch.snn`** unfolds plenty of possibilities to explore SNNs on BSS-2 and eases the machine learning community into using BSS-2.

Funding and Acknowledgements

The contributions of the BrainScaleS team have been supported by the EC Horizon 2020 Framework Programme under grant agreements 785907 (HBP SGA2) and 945539 (HBP SGA3), the Deutsche Forschungsgemeinschaft (DFG, German Research Foundation) under Germany's Excellence Strategy EXC 2181/1- 390900948 (the Heidelberg STRUCTURES Excellence Cluster), the Helmholtz Association Initiative and Networking Fund [Advanced Computing Architectures (ACA)] under Project SO-092.

We thank S. Billaudelle, L. Blessing, and C. Pehle for rich discussions, J. Weis for his valuable hardware knowledge, C. Mauch for BSS-2 system support and the whole Electronic Vision(s) research group.

References

[1] Elias Arnold, Georg Böcherer, Eric Müller, Philipp Spilger, Johannes Schemmel, Stefano Calabrò, and Maxim Kuschnerov. Spiking neural network equalization on neuromorphic hardware for IM/DD optical communication.

In *Proc. Eur. Conf. Optical Commun. (ECOC)*, Paper Th1C.5, Basel, Switzerland, Sep. 2022. ArXiv Preprint: arXiv:2206.00401.

[2] W. Gerstner, W. M. Kistler, R. Naud, and L. Paninski, *Neuronal dynamics: From single neurons to networks and models of cognition*. Cambridge University Press, 2014.

[3] C. Pehle, S. Billaudelle, B. Cramer, J. Kaiser, K. Schreiber, Y. Stradmann, J. Weis, A. Leibfried, E. Müller, and J. Schemmel, "The BrainScaleS-2 accelerated neuromorphic system with hybrid plasticity", *Front. Neurosci.*, vol. 16, 2022, ISSN: 1662-453X. doi:10.3389/fnins 2022.795876.

[4] A. Paszke, S. Gross, F. Massa, A. Lerer, J. Bradbury, G. Chanan, T. Killeen, Z. Lin, N. Gimelshein, L. Antiga, A. Desmaison, A. Kopf, E. Yang, Z. DeVito, M. Rai- son, A. Tejani, S. Chilamkurthy, B. Steiner, L. Fang, J. Bai, and S. Chintala, "PyTorch: An imperative style, high-performance deep learning library", in *Advances in Neural Information Processing Systems 32*, H. Wallach, H. Larochelle, A. Beygelzimer, F. d'Alché-Buc, E. Fox, and R. Garnett, Eds., Curran Associates, Inc., 2019, pp. 8024–8035. Available Online.

[5] Müller, E., Arnold, E., Breitwieser, O., Czierlinski, M., Emmel, A., Kaiser, J., Mauch, C., Schmitt, S., Spilger, P., Stock, R., Stradmann, Y., Weis, J., Baumbach, A., Billaudelle, S., Cramer, B., Ebert, F., Göltz, J., Ilmberger, J., Karasenko, V., Kleider, M., Leibfried, A., Pehle, C., and Schemmel, J. (2022). A scalable approach to modeling on accelerated neuromorphic hardware. *Front. Neurosci.*, 16:884128. doi: 10.3389/fnins.2022.884128.

[6] Dally, W. J., Turakhia, Y., and Han, S. (2020). Domain-specific hardware accelerators. *Commun. ACM* 63, pp. 48–57. doi:10.1145/3361682.

[7] Brette, R., and Gerstner, W. (2005). Adaptive exponential integrate-and-fire model as an effective description of neuronal activity. *J. Neurophysiol.* 94, 3637–3642. doi: 10.1152/jn.00686.2005.

Towards Meta-Learning on BrainScaleS-2

Author
Philipp Spilger – Kirchhoff-Institute for Physics, Heidelberg University, Heidelberg, Germany
Henrik D. Mettler – Department of Physiology, University of Bern, Bern, Switzerland
Andreas Baumbach – Kirchhoff-Institute for Physics, Heidelberg University, Heidelberg, Germany
Jakob Jordan – Department of Physiology, University of Bern, Bern, Switzerland
Mihai A. Petrovici – Kirchhoff-Institute for Physics, Heidelberg University, Heidelberg, Germany; Department of Physiology, University of Bern, Bern, Switzerland
Eric Müller – Kirchhoff-Institute for Physics, Heidelberg University, Heidelberg, Germany; European Institute for Neuromorphic Computing, Heidelberg University, Heidelberg, Germany
Johannes Schemmel – Kirchhoff-Institute for Physics, Heidelberg University, Heidelberg, Germany

Citation
Spilger, P., Mettler, H.D., Baumbach, A., Jordan, J., Petrovici, M.A., Müller, E., Schemmel, J. Towards Meta-Learning on BrainScaleS-2.

Introduction/Motivation

Accelerated analog neuromorphic hardware, paired with programmable plasticity, promises to enable the research of learning in neural networks over long emulated time periods. In this work we use BrainScaleS-2, an accelerated mixed-signal neuromorphic hardware system providing analog neuronal circuits. They are accompanied by two embedded general-purpose SIMD processors which allow for the implementation of programmable plasticity algorithms [3]. Their versatility, both in terms of programmability, but also in terms of access to dynamic observables from the neural network, allow the implementation of near-arbitrary learning rules. In particular, we

can reproduce well-known ones, but also develop new rules. Additionally, plasticity rules can be used to mitigate imperfections in the analog emulation and can themselves be subject to substrate-specific optimization.

The experiment notation for BrainScaleS-2 follows a layered, data-flow-centric software abstraction, At the lowest level streams of instructions are processed. At the highest level, experiments are described graph-based in the form of neuron populations, represented as vertices, and projections of synaptic connections, represented as edges, in-between [5]. On top, PyNN [1] and a PyTorch extension, *hxtorch* [6], are supported as thin top-level APIs aimed to provide modeling interfaces for computational neuroscience and machine learning frameworks.

This work integrates plasticity rules into the experiment description of the BrainScaleS-2 software stack and into the front-end language PyNN [1]. The developed interface will be used for testing evolutionary-generated learning rules [8], starting with the Urbanczik-Senn learning rule [9].

Methods

Plasticity is treated as a property of elements —such as neurons and synapses— in the neural network. As such, plasticity rules are treated as part of the abstract experiment description in the user-facing top-level APIs. The user supplying the plasticity rule does not need to specify the placement of the neural network on the neuromorphic hardware. However, during execution, this information is required for acquiring observables and modifying topological, synaptic or neuronal parameters. Therefore, the integration shall in addition automate execution scope restrictions, for example to only alter the synapses of a particular projection equipped with a learning rule. This approach separates resource allocation and algorithmic specification.

The execution of plasticity rules requires provision of timing information specifying when execution is to be performed in relation to the asynchronously evolving, time-continuous network dynamics on BrainScaleS-2.

Results and discussion

We provide an extension to the PyNN API allowing for specifying plasticity kernels in projections. In the end, the user-specified algorithms are applied to individual network elements, reading and modifying observables during the experiment runtime.

Following the graph-based experiment notation, plasticity rules are integrated as graph nodes. Each rule features user-specifiable C++-code —a plasticity rule kernel— for the embedded processors to be executed. During the experiment execution, this code is just-in-time compiled and then executed concurrently with the neural network emulation.

To allow abstract formulation of the rule's code without placement knowledge, each plasticity rule receives this information as arguments to the user-defined plasticity kernel function. Similarly, during execution, storage for observables to be recorded is provided and read-out after execution. This collected data is annotated at the plastic network component in the front end data structure, e.g. a particular projection. By this, arbitrary observables can be recorded and analyzed during the learning process. Such observables include synaptic weights, neuron membrane potentials or intermediate calculation results. This interface therefore mimics the already present way in PyNN of accessing observables of neurons like spike times or membrane recordings. The same interface can be used for defining and interfacing on-chip virtual environments and agents with neural networks.

While this approach allows arbitrary programmatic plasticity descriptions, its use is constrained by several properties: first, the system offers a limited set of observables and controllables; second, the execution time of plasticity rules depends on the number, type and location of observables or controllables accessed and the complexity of the computations. In models requiring a minimal frequency of plasticity rule executions, these limitations can constrain the maximum network size possible, or even prohibit a successful implementation.

Meta-learning of plasticity rules is the ideal test-case to evaluate the versatility and performance of our implementation. We therefore plan to apply the developments onto evolutionary optimization of learning rules for different tasks.

One such task is error correction learning without dependencies, cf. Figure 1, where a neuron's membrane potential shall mimic that of another by modification of the synaptic weight to a common stimulus, see panel A.

A known solution for this task is the Urbanczik-Senn learning rule [9] , for which the rule specification is depicted in panel C. Since all rules to be explored follow a polynomial form, an intermediate step generating the source code for such a weight update formula is inserted there. In panel B, the recorded observables for an experiment are graphed, where, in the middle, the membrane potentials converge by synaptic weight alterations seen on top.

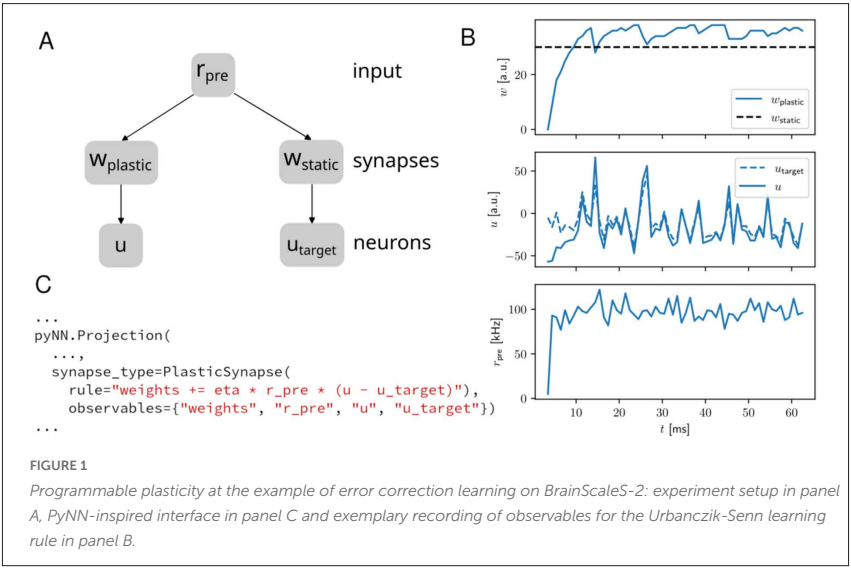

FIGURE 1

Programmable plasticity at the example of error correction learning on BrainScaleS-2: experiment setup in panel A, PyNN-inspired interface in panel C and exemplary recording of observables for the Urbanczik-Senn learning rule in panel B.

In future work, we plan to utilize this established baseline and explore mutated learning rules and automatically evaluate their fitness to the problem. There, the accelerated emulation on neuromorphic hardware promises fast runtime, while the exploration promises to find learning rules optimized to the substrate.

Furthermore, by applying the same methodology to other tasks and network constellations, such as learning with spike rates [4] or learning with spike times [2], the requirements to the plasticity interface are to be refined and extended.

Lastly, compared to specifying snippets of C++ source code representing plasticity rules, the introduction of a domain-specific language, cf. [7], would help users to focus on the model dynamics instead of hiding them in largely system-specific low-level code.

Funding and Acknowledgements

The presented work has received funding from the German Federal Ministry of Education and Research (BMBF)

under grant number 16ES1127, from the European Union (H2020/2014-2020: 720270, 785907, 945539 (HBP)), from the Lautenschläger-Forschungspreis 2018 for Karlheinz Meier and from German Research Foundation (DFG) under Germany's Excellence Strategy EXC 2181/1-390900948 (Heidelberg STRUCTURES Excellence Cluster). The authors wish to thank all present and former members of the Electronic Vision(s) research group contributing to the BrainScaleS-2 neuromorphic platform.

References

[1] Davison, A. P., Brüderle, D., Eppler, J., Kremkow, J., Muller, E., Pecevski, D., et al. (2009). PyNN: a common interface for neuronal network simulators. Front. Neuroinform. 2. doi:10.3389/neuro.11.011. 2008

[2] Göltz, J., Kriener, L., Baumbach, A., Billaudelle, S., Breitwieser, O., Cramer, B., et al. (2021). Fast and energy-efficient neuromorphic deep learning with first-spike times. Nature Machine Intelligence 3, 823–835. doi:10.1038/s42256-021-00388-x

[3] Pehle, C., Billaudelle, S., Cramer, B., Kaiser, J., Schreiber, K., Stradmann, Y., et al. (2022). The BrainScaleS-2 accelerated neuromorphic system with hybrid plasticity. Frontiers in Neuroscience 16. doi:10.3389/fnins.2022.795876

[4] Mettler, H., Schmidt, M., Senn, W., Petrovici, M., Jordan, J. (2021). Evolving Neuronal Plasticity Rules using Cartesian Genetic Programming. ArXiv preprint. doi:10.48550/arXiv.2102.04312

[5] Müller, E., Arnold, E., Breitwieser, O., Czierlinski, M., Emmel, A., Kaiser, J., Mauch, C., Schmitt, S., Spilger, P., Stock, R., Stradmann, Y., Weis, J., Baumbach, A., Billaudelle, S., Cramer, B., Ebert, F., Göltz, J., Ilmberger, J., Karasenko, V., Kleider, M., Leibfried, A., Pehle, C., and Schemmel, J. (2022). A scalable approach to modeling on accelerated neuromorphic hardware. Front. Neurosci. 16:884128. doi: 10.3389/fnins.2022.884128

[6] Spilger, P., Müller, E., Emmel, A., Leibfried, A., Mauch, C., Pehle, C., et al. (2020). hxtorch: PyTorch for BrainScaleS-2 — perceptrons on analog neuromorphic hardware. In IoT Streams for Data-Driven Predictive Maintenance and IoT, Edge, and Mobile for Embedded Machine Learning (Cham: Springer International Publishing), 189–200. doi:10.1007/978-3-030-66770-2_14

[7] Blundell I, Brette R, Cleland TA, Close TG, Coca D, Davison AP, Diaz-Pier S, Fernandez Musoles C, Gleeson P, Goodman DFM, Hines M, Hopkins MW, Kumbhar P, Lester DR, Marin B, Morrison A, Müller E, Nowotny T, Peyser A, Plotnikov D, Richmond P, Rowley A, Rumpe B, Stimberg M, Stokes AB, Tomkins A, Trensch G, Woodman M and Eppler JM (2018) Code Generation in Computational Neuroscience: A Review of Tools and Techniques. Front. Neuroinform. 12:68. doi:10.3389/fninf.2018.00068

[8] Jordan, J., Schmidt, M., Senn, W., Petrovici, M (2021). Evolving interpretable plasticity for spiking networks. eLife 10:e66273. doi:10.7554/eLife.66273

[9] Urbanczik, R., Senn, W. (2014). Learning by the Dendritic Prediction of Somatic Spiking. Neuron, Volume 81, Issue 3, Pages 521-528. doi:10.1016/j.neuron.2013.11.030.

Optimising spike throughput and latency for spike-event accumulation on packet-based interconnection networks

Author
Tobias Thommes, Andreas Grübl, Johannes Schemmel – Kirchhoff-Institute for Physics, University of Heidelberg, Heidelberg, Germany

Citation
Thommes, T., Grübl, A., Schemmel, J. Optimising spike throughput and latency for spike-event accumulation on packet-based interconnection networks.

Introduction/Motivation

When communicating spike-events between neurons of a spiking neural network (SNN), that is simulated or emulated on different chips or parts of a larger system like BrainScaleS-2 [1]–[4] or SpiNNaker [5], one can either transmit and route each spike-event separately across the used interconnection network (IN) or collect them to packets of larger payload size. The former can be efficient, when using a dedicated special purpose IN with minimised packet header size as in [6]. However, when using a more general-purpose IN that is not specifically designed for the spike-communication task, as e.g. EXTOLL [7], event aggregation significantly increases the throughput. This is because the fraction of transmitted metadata per packet (header overhead), is largely decreased compared to single event transmission. This planned approach will aggregate subsequent events featuring the same IN destination.

The proposed architecture features a number of aggregation buffers (buckets) *B* for a number of destinations *D* occurring with a certain probability distribution among the events from one source.

Each bucket is thereby assigned to one or more destinations and accumulates events with identical destination until the first event with a different destination occurs. We call this situation a destination conflict. In this case, the already accumulated events are sent out to the IN and the accumulation starts from scratch with the new destination. A conflict can only occur, in case more than one destination should be assigned to a single bucket.

The goal of this work is to acquire a theoretical estimation of how many events could typically be gathered in a bucket until a conflict occurs (accumulation length) and how much time this takes (accumulation time). We investigate, how these numbers depend on the strategy of assigning the different destinations to the buckets and on the probability distribution of destinations amongst the spike-events.

Finally, we propose optimisation goals for assigning IN destinations to buckets in order to optimise the expected accumulation length and time. Doing so will directly affect the usable IN bandwidth and transmission latency.

Methods

To tackle these questions, we model the accumulation of events at a particular bucket as a discrete-time Markov chain [9]. The state graph of this model is shown in Figure 1. The process starts with no events in the bucket at (0) and models the probabilities of accumulating another event in (k++) or not doing so in (0) or (k). The process ends in () when a destination conflict occurs.

The accumulation length can now be identified as the number of returns to the state (k++) and the accumulation time is identified as the number of steps through the Markov graph until reaching (). These quantities can be calculated using Markov chain probability mathematics.

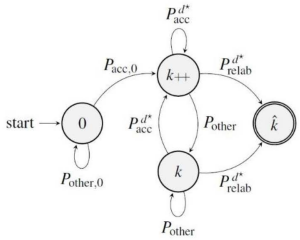

$P_{acc,0}$:	probability of accumulating the first event
P_{acc}^{d*}:	probability of accumulating another event; depends on the destination currently assigned ($d*$)
$P_{other,0}$:	probability of the first event being assigned to another bucket
P_{other}:	probability for the nth event being assigned to another bucket
P_{relab}^{d*}:	probability of a destination conflict;

FIGURE 1
State graph of the bucket accumulation Markov chain.

In contrast to the accumulation length, when determining the accumulation time, one has to consider the mean time between input events by multiplying it to the obtained step number. The mean input rate from a single neuron as well as from an ensemble of neurons can be modelled using a Poisson process [10].

The input conditions like the assignment strategy to buckets and the probability distribution of IN destinations across the events are incorporated in the transition probabilities between the states in Figure 1.

Results and discussion

This analysis was carried out for different numbers of buckets *B* and occurring destinations *D* respectively. The result is that the accumulation length is best approximated by the ratio of the most probable destination's probability to the sum over the probabilities of all other destinations, assigned to the respective bucket. This intuitively approximates the inverse frequency at which the most probable destination's accumulation is interrupted. A plot of the resulting expected accumulation length against the described probability ratio is shown in Figure 2. For low ratios, the accumulation length converges to one, as we must accumulate a first event before a destination conflict is defined.

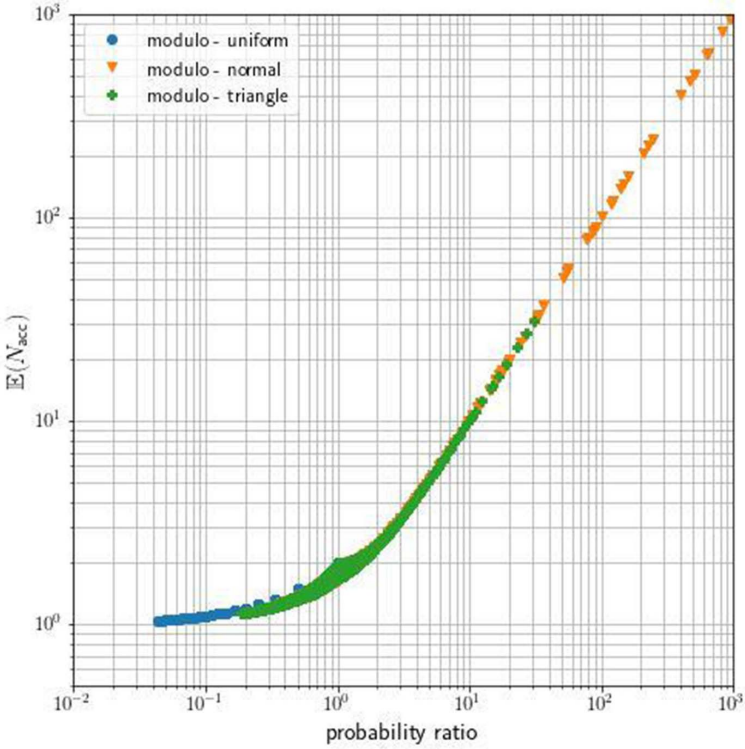

FIGURE 2

Plot of the expected accumulation length against the described probability ratio for different probability distributions of the input destinations. Modulo-Assignment was exemplarily used for assigning each of the destination distributions to the ensemble of buckets.

This leads to the insight, that the accumulation length largely depends on the applied strategy of assigning destinations to the available buckets. The assignment should be optimised in a way to maximise the described probability ratio of destinations for each bucket.

Another possibility of optimising the accumulation length is to provide more buckets, thereby reducing the number of possible conflicts. However, this is limited by the available resources on the target FPGA.

In a real implementation, the possible number of events per packet is limited by the maximum packet size. As stated in [8], this is approximately events, so any probability ratio above this value will produce full i.e., optimal packets.

As a remark, the probability distributions used here for the occurring destinations (uniform, normal and triangle) must not be interpreted as directly biologically motivated. This is because the (biologically inspired) post-synaptic connectome of an emulated neuron population can be freely mapped across several BrainScaleS-2 chips. The distribution of IN destinations from a source-chip does thereby not only depend on the implemented SNN, but also on the applied mapping to the neuromorphic hardware. Instead, they merely serve as example distributions. It can be seen that a normal distribution of the occurring destinations performs best compared to the uniform (worst case) and triangle distributions.

In conclusion we have shown a way to find optimal assignments of IN destinations to available buckets in each node of the IN, to maximise the throughput of spike-events of a multi-chip SNN that is run with this IN. These results will be used to guide the mapping of SNNs to the BSS-2 multi-chip system. Experiments on the physical hardware will be carried out in future work, to verify the correctness of this study.

Funding & Acknowledgements
The presented work has received funding from the European Union (H2020/2014-2020: 720270, 785907, 945539 (HBP)). The authors wish to thank all present and former members of the Electronic Vision(s) research group contributing to the BrainScaleS-2 neuromorphic platform.

References

[1] S. Billaudelle *et al.*, "Versatile Emulation of Spiking Neural Networks on an Accelerated Neuromorphic Substrate," in *2020 IEEE International Symposium on Circuits and Systems (ISCAS)*, 2020, pp. 1–5, doi: 10.1109/ISCAS45731.2020.9180741.

[2] C. Pehle *et al.*, "The BrainScaleS-2 Accelerated Neuromorphic System With Hybrid Plasticity," *Front. Neurosci.*, vol. 16, p. 795876, Feb. 2022, doi: 10.3389/fnins.2022.795876.

[3] E. Müller *et al.*, "A Scalable Approach to Modeling on Accelerated Neuromorphic Hardware," *Front. Neurosci.* | *www.frontiersin.org*, vol. 1, p. 22, May 2022, doi: 10.3389/fnins.2022.884128.

[4] S. Billaudelle, J. Weis, P. Dauer, and J. Schemmel, "An accurate and flexible analog emulation of AdEx neuron dynamics in silicon," *arXiv Prepr. 2209.09280*, Sep. 2022.

[5] S. B. Furber, F. Galluppi, S. Temple, and L. A. Plana, "The SpiNNaker Project," *Proc. IEEE*, vol. 102, no. 5, pp. 652–665, May 2014, doi: 10.1109/JPROC.2014.2304638.

[6] J. Navaridas, M. Luján, J. Miguel-Alonso, L. A. Plana, and S. Furber, "Understanding the interconnection network of SpiNNaker," in *Proceedings of the 23rd international conference on Conference on Supercomputing - ICS '09*, 2009, p. 286, doi: 10.1145/1542275.1542317.

[7] T. Thommes, S. Bordukat, A. Grübl, V. Karasenko, E. Müller, and J. Schemmel, "Demonstrating BrainScaleS-2 Inter-Chip Pulse-Communication using EXTOLL," in *Neuro-Inspired Computational Elements Conference*, 2022, pp. 98–100, doi: 10.1145/3517343.3517376.

[8] T. Thommes, N. Buwen, A. Grübl, E. Müller, U. Brüning, and J. Schemmel, "BrainScaleS Large Scale Spike Communication using Extoll," *arXiv Prepr. 2111.15296*, Nov. 2021, doi: 10.48550/arXiv.2111.15296.

[9] N. Privault, *Understanding Markov Chains*, 2nd ed. 20. Singapore: Springer Singapore, 2018.

[10] D. Heeger, "Poisson Model of Spike Generation," New York NY, Sep. 2000.

Neurorobotics

Electropolymeric electronics compiler approach to fabrication of ferroelectric memristors with applications in auditory neurotechnologies

Author
Davin Browner, Sina Sareh – Robotics Laboratory, Royal College of Art, London, United Kingdom

Citation
Browner, D., Sareh, S. Electropolymeric electronics compiler approach to fabrication of ferroelectric memristors with applications in auditory neurotechnologie.

Introduction/Motivation

Auditory neurotechnology development focuses on hardware and software in the augmentation and enhancement of human hearing and in the development of machine audition methods that can be integrated into sensors for robots or bio-informational interfaces such as prosthetics. Spike-enabled auditory neurotechnologies that make use of spiking neural networks (SNNs) in combination with acoustic processing circuitry could be utilised in a wide range of devices for human-interventional medicine and novel sensory technologies for neurorobotic and neuroprosthetic

applications [1]. Auditory neurotechnologies where learning is based on memristive SNNs (MemSNNs) may offer the promise of low power Artificial Neural Networks (ANNs) via resistive memory and switching phenomena [2]. Existing methods for memristor fabrication are difficult to implement in durable polymer-based substrates and do not have suitable biocompatibility or acoustic impedance matching profiles for integration into auditory neurotechnologies. More generally, many of the resistive switching methods in the literature rely on phenomena with significant cycle-to-cycle and device-to-device stochastic switching characteristics (e.g., phase change, ion migration, conductive filament formation, etc) that complicate hardware implementation and device modelling.

Ferroelectric polymer memristors with good biocompatibility and acoustic impedance matching profiles would be beneficial for development of MemSNNs for auditory neurotechnologies [3]. In general, ferroelectric memristors are excellent candidates for auditory learning applications due to their cycle-to-cycle endurance based on continuous ferroelectric polarisation, i.e., the "ferroelectric plasticity" that can be obtained by regulating the amplitude or duration of the applied voltage pulses. The two-terminal type ferroelectric artificial synapses, which include memristor based devices, comprise of two electrodes that are separated by a ferroelectric film. When a presynaptic signal is applied to one electrode, an update of the conductance is generated accordingly, and the synaptic weight can be readout from the other electrode. In this way, spike signals are transferred from pre- synaptic terminal to the postsynaptic one. Ferroelectric spike-enabled memristors also benefit from potential multi-functionality such as concurrent piezoelectric, pyroelectric, and/or multiferroic phenomena.

In terms of fabrication, inorganic ferroelectric memristors require procedures that are highly sensitive to initial conditions such epitaxial growth and complex crystal growth optimisations such as use of specific substrates for lattice matching. In contrast, ferroelectric polymers can easily be dissolved in an organic solution and directly printed onto flexible substrates. This means that their easy processing, low cost, and versatility offer feasible solutions

for large scale synaptic design and network formation while also having excellent properties for use in bio-informational interfaces such as those required in auditory learning devices due to their biocompatibility and low acoustic impedance.

Despite these general advantages the optimal methods for fabrication of ferroelectric memristors for neuromorphic hardware based on polymers is not established. Electropolymeric deposition could provide several advantages in terms of fabrication based on polymers due to bench-top scale fab, rapid speed of deposition, low cost, and use of flexible and soft substrates. Compared to methods such as spin coating and screen printing the technique could allow for control over thickness and resulting conductivity profiles. Electrical control of these properties would aid in fine tuning of programmable resistance values and intervals between high-resistance and low resistance states, emulation of synaptic functionality evidenced by the cycle-to-cycle hysteresis loops of the resulting polymeric electrode-ferroelectric-electrode (EFE) structure.

Methods

A polymeric memristor "compiler" approach to fabrication of memristors is developed and implemented based on the respective EFE structure via electropolymeric deposition of the ferroelectric resistive switching layer. Here, "compiler" is referred to as a method to assemble analogue ferroelectric memristive elements via potentiostatic control of deposition of alternating EFE layers. The implemented system uses a silver coated working electrode, silver/silver chloride reference electrode, and steel wire counter electrode in the potentiostatic experiment. We used an open source potentiostat (Rodeostat, IO-Rodeo) and a Raspberry Pi 4 single board computer to control the deposition process. The procedure is simple. First, a ferroelectric resistive switching layer material based on an organometallic glycinate complex is deposited onto the conductive substrate via electropolymeric deposition. Then, a PEDOT: PSS top electrode layer is deposited on top of the ferroelectric layer matching the geometry of the conductive substrate and allowing for electrical connection.

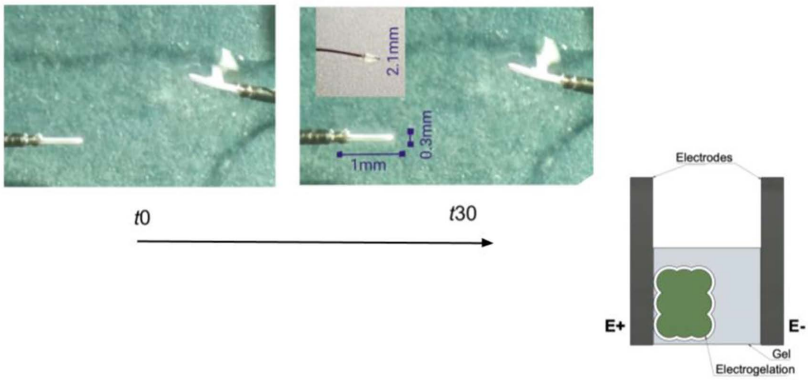

FIGURE 1
Electrogelation of the ferroelectric resistance layer showing 0.3mm thickness and PEDOT: PSS (inset photo) resulting in a 2.1mm concentric device width.

Results and discussion

Here, we have shown a proof of concept for an accessible implementation of an electropolymeric electronics compiler approach to deposition of the ferroelectric layer of an EFE. The compiler is used in the design and fabrication of a ferroelectric memristor.

The output of the potentiostat for (a) the ferroelectric layer and (b) the PEDOT: PSS electrode are outlined (Fig.1.). The device is then tested using IV and GV curve hysteresis fingerprinting techniques (Fig.2.) and post-pulse response indicating initial proof of concept for use in auditory applications of memSNNs (Fig.2.).

Limitations of the device study are established including issues with quality of the deposited structures using the existing setup (deposition thicknesses of under 1mm are inconsistently deposited). Scope for future work is outlined including how to integrate the fabrication methods into design of specific auditory learning technologies based around improvement of the SNN-like post-pulse response ((C), (D), (E) in Fig.2.) and coupling with piezoelectric

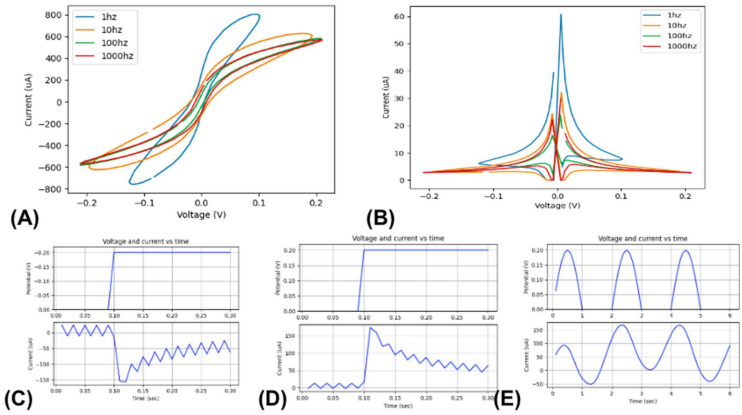

FIGURE 2
(**A**) ferroelectric memristor hysteresis I-V fingerprint at 1hz, 10hz, 100hz, and 1000hz respectively; (**B**) ferroelectric memristor hysteresis G-V fingerprint at the same frequencies; (**C**) post-pulse response with positive voltage; (**D**) post-pulse response with negative voltage; (**E**) resistance programmability.

sensing. While the device and fabrication methods show promise for alternative fabrication schemes for ferroelectric memristors there are issues with the design of the platform including the need for a pre-deposition step in the form of photomasking. There are many unknown parameters in this study including the effect of over potentials on the resulting PEDOT: PSS conductivity.

Despite these issues, the electropolymeric electronics compiler method offers opportunities for design of auditory devices beyond those based on conventional inorganic oxide materials for resistive switching and towards use of polymeric ferroelectric memristive devices. These methods have promise for applications such as neuroprosthetics where custom morphology is paramount to success of the device as well as a range of auditory learning technologies including cochlear devices requiring biocompatible and compliant neuromorphic substrates.

References

[1] Goodman, D. and Brette, R., 2010. Learning to localise sounds with spiking neural networks. Advances in Neural Information Processing Systems, 23.

[2] Wu, X., Dang, B., Wang, H., Wu, X. and Yang, Y., 2022. Spike-Enabled Audio Learning in Multilevel Synaptic Memristor Array-Based Spiking Neural Network. Advanced Intelligent Systems, 4(3), p.2100151

[3] Tian, B., Liu, L., Yan, M., Wang, J., Zhao, Q., Zhong, N., Xiang, P., Sun, L., Peng, H., Shen, H. and Lin, T., 2019. A robust artificial synapse based on organic ferroelectric polymer. Advanced Electronic Materials, 5(1), p.1800600.

[4] Niu, X., Tian, B., Zhu, Q., Dkhil, B. and Duan, C., 2022. Ferroelectric polymers for neuromorphic computing. Applied Physics Reviews, 9(2), p.021309.

Application of working memory adapted navigation for human robot interaction in an industrial context

Author
Alice Nardelli – DIBRIS Department, University of Genoa, Genoa, Italy
Dario Pasquali – Cognitive Architecture for Collaborative Technologies (CONTACT) Unit, Italian Institute of Technology (IIT), Genoa, Italy
Lorenzo Landolfi – Cognitive Architecture for Collaborative Technologies (CONTACT) Unit, Italian Institute of Technology (IIT), Genoa, Italy
Jasmin Bernotat – Cognitive Architecture for Collaborative Technologies (CONTACT) Unit, Italian Institute of Technology (IIT), Genoa, Italy
Francesco Rea – Cognitive Architecture for Collaborative Technologies (CONTACT) Unit, Italian Institute of Technology (IIT), Genoa, Italy

Citation
Nardelli, A., Pasquali, D., Landolfi, L., Bernotat, J., Rea, F. Application of working memory adapted navigation for human robot interaction in an industrial context.

Introduction

Robots are increasingly entering various fields. This raises the importance of creating robots as collaborators that interact with humans instead of creating any technical tool to be used. In human-human interaction, working memory plays a crucial role in responding to each other's behavior because it is involved in complex cognitive tasks [2] that require a common understanding of the real world between collaborators.

In the present research, we thus took a step toward improving human-robot collaboration by implementing a cognitive working memory architecture on an RB-KAIROS robot platform. This allowed robust controlling of the navigation framework to assure human and context awareness [3] and safer interaction [4].

In robotic software architectures working memory is represented by learning a rule about specific perceptions and proper motor actions. This becomes fundamental when some specific task-relevant stimuli are no longer present so that an agent needs to act according to the stimuli's representation stored in memory. We hypothesized that a biologically inspired working memory would improve human-robot interaction by increasing the mutual understanding between two human workers and the robot. To test this hypothesis, we designed an experiment involving human-robot interaction in a shared industrial environment where we compared two algorithms of working memory: a biologically inspired and a performance-driven one.

Methods

We chose WorkMATe [1] as implementation of a biologically inspired memory. WorkMATe is a state-of-the-art neural network model that learns to flexibly control its working memory content in a biologically plausible fashion through reinforcement. Instead, the performance-driven competitor of WorkMATe has been implemented through a deep neural network that contained a Gated Recurrent Unit (GRU) [5]. To implement the architectures on the robot, we designed a modular software architecture in ROS (see Figure 1, top).

The implementations of WorkMATe and GRU were each tested against a no memory condition in a lab experiment. An industrial setting was simulated in which the robot navigated between two rooms (Figure 1): A crowded room where humans placed objects from a table to an opposite one, and a non-crowded room. We let the robot navigate twenty times between the rooms in a pre-defined path per condition.

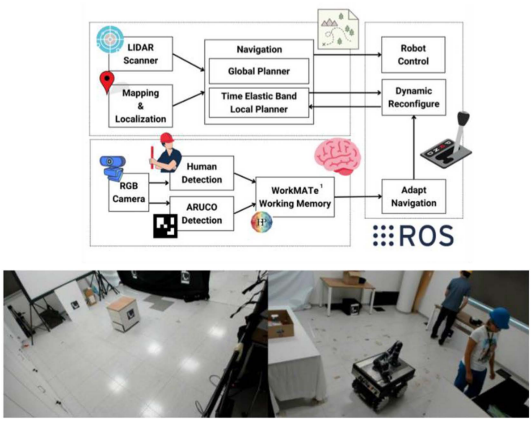

FIGURE 1
Top: Outline of the software architecture, developed in ROS. The architecture is divided into two main components: the perception module including people and aruco detection, and the navigation module. The working memory component adapts navigation parameters according to the perception output.
Bottom: Screenshot of the in-lab experiment. Two different rooms are visible: the left one is the uncrowded room, the one on the right is the crowded room.

In the WorkMATe and the GRU conditions, robot working memory was reflected by the robot's capability to adapt its velocity and local planning depending on the detection of workers and Aruco markers [7] that were used to distinguish between the two areas. In addition, when the robot detected humans, it switched from holonomic to differential navigation because the latter was supposed to be easier predicted by humans [8]. In the no memory condition, the robot did not adapt in terms of velocity and navigation type.

Results

In the training phase, we reached 100% accuracy with the GRU and an accuracy of 95% with the WorkMATe implementation. Accuracy was defined as the matching between the chosen navigation strategy and the desired one. The desired strategy depended on the last reliable perception.

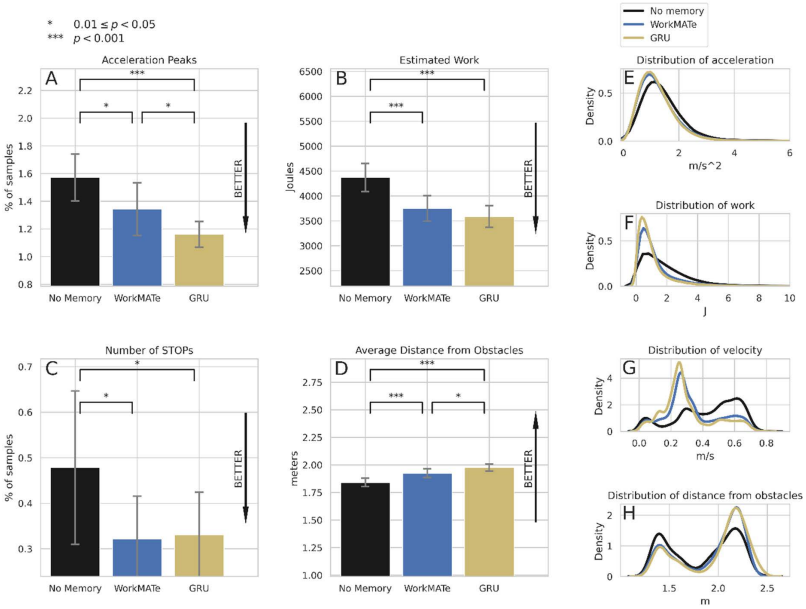

FIGURE 2

This figure reports quantitative evaluation of robot navigation through data recorded by robot sensors. Measurements reported in **A**, **B**, **C**, **E**, **F**, **G** were derived from odometry sensors recording at 50Hz on average. Measurements reported in **D** and **H** were obtained from lidar sensors recording at 7Hz.

A, B, C, D: Each data point was measured for a single path traversal (trial). Trials were paired sequentially for statistical evaluation. Reported p values were Bonferroni corrected.

E, F, G, H: Distribution of recorded acceleration (**E**), work (**F**), velocity (**G**), and average distance from obstacles(**H**).

A: Percentage of acceleration peaks: percentage of recorded acceleration samples exceeding the mean value by three times the standard deviation of the associated distribution (See panel **E**).**B**: Energy consumption: computed as estimated work. Work was computed considering all the mass of the robot to be placed at the most distant point to the center of rotation.

C: Number of STOPS: percentage of recorded velocity samples lower than 0.01 m/s

D: Distance from obstacles: average distance from obstacles recorded from laser data.

In the main experiment, the frequency of acceleration anomalies and the percentage of stops were higher in the non-memory condition (see Figure 2 A).

In both working memory conditions, the robot approached workers with a slower velocity profile and avoided abrupt accelerations and decelerations.

The average distance from obstacles was greater with the adaptive navigation, allowing safer interaction. In addition, non-adaptive navigation consumes a greater amount of energy.

Discussion

Our results confirmed that Working Memory plays a fundamental role in improving the performance of the RB-KAIROS robot in a collaborative navigation task in terms of energy consumption, safety, and smoothness of navigation. We expect that these benefits might positively affect human-robot collaboration. That is, workers might feel more comfortable while collaborating with a robot which might very likely increase their working performance. This, however, needs to be tested in a follow-up study conducted in a real industrial setup. In this follow-up research, we will evaluate the implementation of the working memory architectures from a user perspective. This way, the technological and the user perspective will likewise be considered within the developmental process with the next steps being taken based on empirical findings such as those we here presented. With this approach, we answer previous researchers' call to take a holistic technological, user-centered, empirical-driven view to create a smooth human-robot interaction [6].

Acknowledgments

The research reported in this abstract has been funded by HBP SGA3 Grant agreement 945539.

References

[1] Kruijne, Wouter, et al. "Flexible working memory through selective gating and attentional tagging." *Neural Computation* 33.1 (2021): 1-40.

[2] Baddeley, Alan. "Working memory." *Current biology* 20.4 (2010): R136-R140.

[3] Vega-Magro, Araceli, et al. "Socially acceptable robot navigation over groups of people." *2017 26th IEEE International Symposium on Robot and Human Interactive Communication (RO-MAN)*. IEEE, 2017.

[4] Gualtieri, Luca, et al. "The opportunities and challenges of SME manufacturing automation: safety and ergonomics in human–robot collaboration." *Industry 4.0 for SMEs* (2020): 105-144.

[5] Cho, Kyunghyun, et al. "On the properties of neural machine translation: Encoder-decoder approaches." *arXiv preprint arXiv:1409.1259* (2014).

[6] Bernotat, J., Schiffhauer, B., Eyssel, F., Holthaus, P., Leichsenring, C., Richter, V., ... & Wrede, S. (2016, November). Welcome to the future–How naïve users intuitively address an intelligent robotics apartment. In *International conference on social robotics* (pp. 982-992). Springer, Cham.

[7] S. Garrido-Jurado, R. Muñoz-Salinas, F. J. Madrid-Cuevas, and M. J. Marín-Jiménez. 2014. "Automatic generation and detection of highly reliable fiducial markers under occlusion". Pattern Recogn. 47, 6 (June 2014), 2280-2292. DOI=10.1016/j.patcog.2014.01.005

[8] Kollmitz, Marina, et al. "Time dependent planning on a layered social cost map for human-aware robot navigation." *2015 European Conference on Mobile Robots (ECMR)*. IEEE, 2015.

Biomorphic control for high-speed robotic applications

Author
Yannik Stradmann, Johannes Schemmel – Kirchhoff-Institute for Physics, Heidelberg University, Heidelberg, Germany

Citation
Stradmann, Y., Schemmel, J. Biomorphic control for high-speed robotic applications.

Introduction/Motivation

Embodiment is often perceived as one of the key features of biological cognitive systems and has therefore been subject to increasing interest within the neuroscientific community [1][2]. Following this endeavor, the field of neurorobotics has evolved a multitude of different strategies for linking simulations of biologically inspired neural networks to either real-world robots [3] or virtual agents in simulated environments [4]. The complexity of these approaches is however often limited by the available compute resources for either the network simulation – especially in the case of latency-restricted interactions with real-world actuators – or for environmental simulations with rich physical dynamics.

In this work, we present a hardware framework for connecting the accelerated neuromorphic BrainScaleS-2 platform to real-world sensors and actuators and propose an application that utilizes the system's properties for controlling the coils of brushless electric motors with microsecond-precision. The presented setup will enable research in the field of biologically plausible spiking neural networks in interaction with fast physical processes.

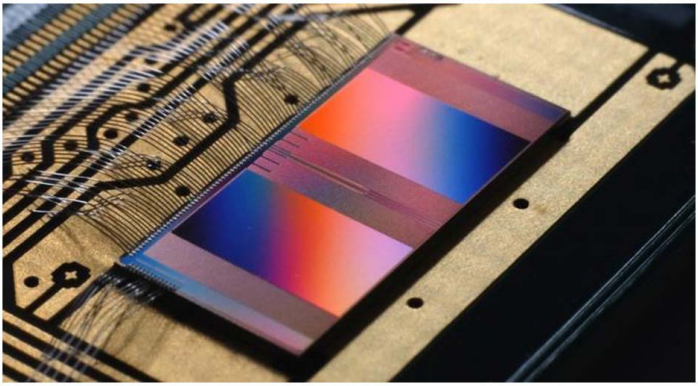

FIGURE 1
Photograph of the 65nm BrainScaleS-2 neuromorphic ASIC. It features 512 AdEx neurons, 612x512 plastic synapses and two embedded SIMD processors for implementing arbitrary on-chip plasticity rules.

Methods

BrainScaleS-2 [5][6] is an established neuromorphic platform based on the likewise named mixed-signal ASIC (**Figure 1**). It features 512 analog neuron circuits that implement the Adaptive-Exponential Leaky-Integrate-and-Fire model [7]. Each neuron receives synaptic input from 256 plastic synapses with a digitally controlled weight of 6bit precision and integrated correlation sensors for STDP-type learning rules. Amongst other observables, the accumulated correlations can be digitized by highly parallel on-chip ADCs and used within two embedded SIMD processors for calculating freely programmable plasticity rules. The analog circuits of BrainScaleS-2 run in continuous time, their time constants are accelerated 1000-fold compared to biology. This speedup factor makes BrainScaleS-2 predestined for ultra-fast robotic tasks that require control loops far beyond biological reaction times.

In addition to the ASIC, each BrainScaleS-2 system contains an FPGA used for stimulating the analog accelerator, recording responses and connecting it to external compute clusters. For the presented robotic hardware framework, we implement a low-latency link for event data from external sensors (sensor

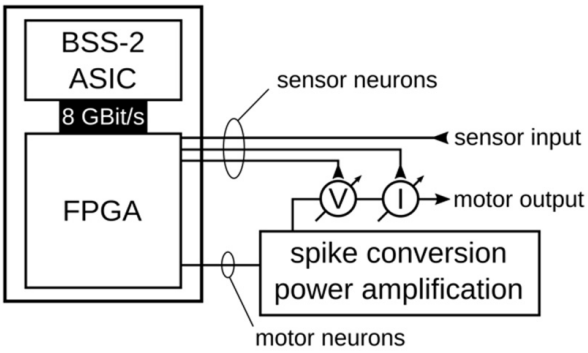

FIGURE 2
Overview on the presented hardware framework for high-speed robotics. Sensory spikes are sent to the ASIC via an FPGA and processed by the analog neural network. Motoric events are processed vice versa.

neurons) and to actuators (motor neurons) in this FPGA (Figure 2). Outgoing and incoming spike traffic is channeled through separate serial links, which – at the cost of serialization latency – allow for runtime-configurable virtual spike channels without excessive hardware requirements for a parallel connection. We separate incoming and outgoing spike traffic in separate physical links to enable the use of different hardware modules for sensory spike sources and motoric spike sinks.

Results and discussion

The presented hardware framework for connecting the BrainScaleS-2 system to external spike-based sensors and actuators has been implemented and tested in an experimental setup. With a serial clock of 16MHz and 256 virtual input- and output channels, we measure a serialization latency of 640ns. Adding the latency between ASIC and FPGA, we measure a total neuron-to-output latency of 1.2us – one order of magnitude faster than typical membrane dynamics on BrainScaleS-2. If less external spike channels are required, the serialization latency is reduced accordingly.

Using this framework, we present an initial biomorphic control circuit for high-speed robotics: Interpreting the coils and magnets of a conventional, fast-rotating brushless electric motor as muscular actors, we have implemented the prototype of a spike-base controller for generating the required rotating electric field. We envision this setup as a versatile platform for the development of biologically plausible learning in spike-based robotic systems. The 1000-fold acceleration factor will allow for greatly reduced training time and thereby facilitate robotic experiments with spiking neural networks of beyond-state-of-the-art size and complexity.

Acknowledgements
The presented work has received funding from the German Federal Ministry of Education and Research (BMBF) under grant number 16ES1127, from the European Union (H2020/2014-2020: 720270, 785907, 945539 (HBP)), from the Lautenschläger-Forschungspreis 2018 for Karlheinz Meier and from the German Research Foundation (DFG) under Germany's Excellence Strategy EXC 2181/1-390900948 (Heidelberg STRUCTURES Excellence Cluster).

The authors wish to thank all present and former members of the Electronic Vision(s) research group contributing to the BrainScaleS-2 neuromorphic platform.

References

[1] F. Kaplan, "Neurorobotics: an experimental science of embodiment", Frontiers in Neuroscience, vol. 2, 2008.

[2] R. Pfeifer and J. Bongard, "How the body shapes the way we think: a new view of intelligence", MIT press, 2006.

[3] H. Hagras, A. Pounds-Cornish, M. Colley, V. Callaghan and G. Clarke, "Evolving spiking neural network controllers for autonomous robots," IEEE International Conference on Robotics and Automation, 2004. Proceedings. ICRA '04. 2004, 2004, pp. 4620-4626 Vol.5.

[4] E. Falotico, L. Vannucci, A. Ambrosano, U. Albanese, S. Ulbrich, J. C. Vasquez Tieck, G. Hinkel, J. Kaiser, I. Peric, O. Denninger, N. Cauli, M. Kirtay, A. Roennau, G. Klinker, A. Von Arnim, L. Guyot, D. Peppicelli, P. Martínez-Cañada, E. Ros, P. Maier, S. Weber, M. Huber, D. Plecher, F. Röhrbein, S. Deser, A. Roitberg, P. van der Smagt, R. Dillman, P. Levi, C. Laschi, A. C. Knoll and M.-O. Gewaltig, "Connecting artificial brains to robots in a comprehensive simulation framework: The neurorobotics platform", Frontiers in Neurorobotics, vol. 11, 2017.

[5] C. Pehle, S. Billaudelle, B. Cramer, J. Kaiser, K. Schreiber, Y. Stradmann, J. Weis, A. Leibfried, E. Müller and J. Schemmel, "The BrainScaleS-2 accelerated neuromorphic system with hybrid plasticity", Frontiers in Neuroscience, vol. 16, 2022.

[6] E. Müller, E. Arnold, O. Breitwieser, M. Czierlinski, A. Emmel, J. Kaiser, C. Mauch, S. Schmitt, P. Spilger, R. Stock, Y. Stradmann, J. Weis, A. Baumbach, S. Billaudelle, B. Cramer, F. Ebert, J. Göltz, J. Ilmberger, V. Karasenko, M. Kleider, A. Leibfried, C. Pehle and J. Schemmel, "A scalable approach to modeling on accelerated neuromorphic hardware", Frontiers in Neuroscience, vol. 16, 2022.

[7] R. Brette and W. Gerstner, "Adaptive Exponential Integrate-and-Fire Model as an Effective Description of Neuronal Activity", J. Neurophysiol. 94: 3637 – 3642, 2005.

Emergent Self-Coordination in simulated swarms steered by spiking neural networks

Author
Alper Yegenoglu – SDL Neuroscience, Institute for Advanced Simulation, Jülich Supercomputing Centre (JSC), Jülich Research Center and JARA; Institute of Geometry and Applied Mathematics, Department of Mathematics,RWTH Aachen University, Aachen, Germany
Cristian Jimenez Romero – SDL Neuroscience, Institute for Advanced Simulation, Jülich Supercomputing Centre (JSC), Jülich Research Center and JARA
Aaron Perez Martin – SDL Neuroscience, Institute for Advanced Simulation, Jülich Supercomputing Centre (JSC), Jülich Research Center and JARA
Sandra Diaz-Pier – SDL Neuroscience, Institute for Advanced Simulation, Jülich Supercomputing Centre (JSC), Jülich Research Center and JARA
Abigail Morrison – SDL Neuroscience, Institute for Advanced Simulation, Jülich Supercomputing Centre (JSC), Jülich Research Center and JARA; Institute of Neuroscience and Medicine (INM-6), Institute for Advanced Simulation (IAS-6), Theoretical Neuroscience, Computational and Systems Neuroscience, Jülich Research Center and JARA; Department of Computer Science - 3, Faculty 1, RWTH Aachen University

Citation
Yegenoglu, A., Romero, C.J., Martin, A.P., Diaz-Pier, S., Morrison, A. Emergent Self-Coordination in simulated swarms steered by spiking neural networks.

Introduction

Stigmergy is a form of communication observed in nature which refers to indirect interactions between individuals and takes place via the environment for the purpose of navigation, coordination or collaboration. Social insects

use stigmergic communication to self-organize their behaviour as a swarm. Evolutionary processes over many generations shaped this behaviour [1]. In this work we evolve a swarm of agents that use stigmergic communication to solve complex tasks which involve self-coordination in order to achieve an efficient solution. In the literature self-coordination in swarms has been implemented using simple, pre-defined action rules, which allows the agents to interact with other cohorts in the environment. Those systems exhibit stigmergic communication via simulated chemical signals [2,3,4]. For example, the model presented in [5] illustrates self-coordination and collaboration in an ant colony. Contrary to the works presented in the literature, where collaborative behaviour is enforced via action rules, our approach does not utilize pre-defined rules, instead we evolve spiking neural networks (SNNs) to steer the agents. The evolutionary algorithm, i.e. a genetic algorithm [7], optimizes the weights and delays of an SNN in order to exploit the embedded physiological properties of the agent and the characteristics of the environment.

Methods

We use an evolutionary algorithm to optimize SNNs which serve as artificial brains to control the behaviour of each agent in the swarm. In this setting, the SNN consists of 36 leaky integrate and fire neurons separated into 3 layers, where 12 input neurons are responsible for sensory information, 20 all-to-all connected neurons form the middle layer and 4 output neurons steer the movement (left, right, forward) and the pheromone depositing. The goal of the evolved swarm is to find optimal ways to complete a given task, e.g. ants forage for food and return it to the nest in the shortest amount of time (Figure 1). Here, the ants have to bring the food to the nest within a simulation time of 2000 steps. The usage of a chemical signal is not manually encoded into the network; instead, this behaviour is established through the optimization procedure. We use the L2L framework [6], which is an implementation of the concept of learning to learn, to optimize the weights and delays of the connections in the network. The concept of learning to learn consists of a two loop structure, the inner and outer loop. While in the inner loop the swarm is being simulated executing a specific task, a

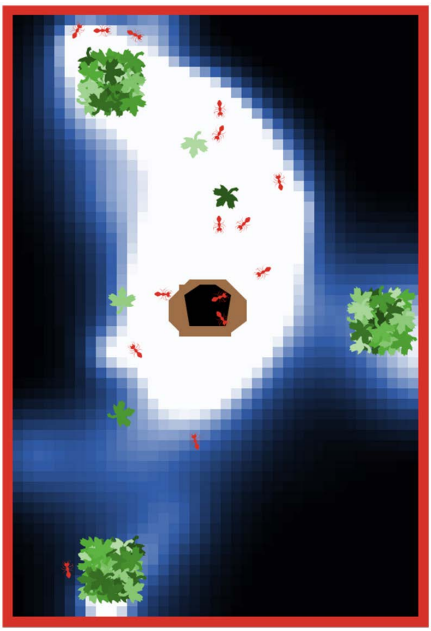

FIGURE 1
Screenshot of an ant swarm foraging for food. Blue patches show the distribution of pheromone. A bright color indicates a high pheromone concentration. The green patches with leaves are food piles. The hexagon in the middle is the nest.

genetic algorithm optimizes the network parameters in the outer loop. The performance of the swarm is evaluated via a fitness function specifically designed for the given task. The fitness increases with the amount of food the ants bring to the nest, and decreases whenever the ants exhibit excessive movements or pheromone depositing. Furthermore, we analyze the network evolution over multiple generations to better understand the behaviour of the agents.

Results and discussion

We observe that stigmergy emerges as a means of communication and self-organized coordination between agents in the absence of pre-defined action rules. Neither the mechanism to activate the release of pheromone nor the mechanism of interpreting these signals was explicitly described as part of the behaviour of the agents. To test the effect of stigmergy regarding the performance of the swarm, we deactivated the sensory pathway related to the chemical signal and executed the task again. From the experiments it can be observed that in this case the swarm was unable to perform the task, they were not able to collect and return the food as efficiently as the SNN model with an active sensory pathway. This suggests that, in this setup, the ability of the swarm to perform the task relies completely on the stigmergic communication. Thus, we can infer that the embedded physiological properties of the agents and the characteristics of the environment are exploited by the optimization algorithm. We assess the task performance of the evolved swarm and compare our SNN based approach to a multi-agent rule based system [5]. In this case, the food brought into the nest within the simulation time determines the performance, i.e. the higher the amount of food the better the score. A maximum of 150 point can be reached, which corresponds to the three food patches (see Figure 1) with 50 points per pile. Our results show, that the swarm controlled by the SNN outperforms the rule based system. In future work, we want to extend our approach to the application on robotic swarm systems and exploit the outer loop in L2L to explore hyper-parameters of the network, such as number of neurons and layers.

References

[1] Smith, C. R., Toth, A. L., Suarez, A. V., and Robinson, G. E. (2008). Genetic and genomic analyses of the division of labour in insect societies. Nature Reviews Genetics 9

[2] Bandeira de Melo, E. B. and Araújo, A. F. R. (2008). Modeling ant colony foraging in dynamic and confined environment. In Proceedings of the 10th annual conference on Genetic and evolutionary computation.

[3] Hecker, J. P. and Moses, M. E. (2015). Beyond pheromones: evolving error-tolerant, flexible, and scalable ant-inspired robot swarms. Swarm Intelligence 9

[4] Duan, H. and Sun, C. (2014). Swarm intelligence inspired shills and the evolution of cooperation. Scientific reports 4

[5] Wilensky, U. (1997). Netlogo ants model. Center for Connected Learning and Computer-Based Modeling, Northwestern University, Evanston, IL

[6] Yegenoglu A, Subramoney A, Hater T, Jimenez-Romero C, Klijn W, Pérez Martín A, van der Vlag M, Herty M, Morrison A and Diaz-Pier S (2022). Exploring Parameter and Hyper-Parameter Spaces of Neuroscience Models on High Performance Computers With Learning to Learn. Front. Comput. Neurosci.

[7] Fortin, F. A., De Rainville, F. M., Gardner, M. A. G., Parizeau, M., & Gagné, C. (2012). DEAP: Evolutionary algorithms made easy. The Journal of Machine Learning Research, 13(1)

Systems and cognitive neuroscience

Longitudinal changes in electrophysiological functional connectivity during inhibitory control task associated with binge drinking predisposition

Author

Antón-Toro, L., – Center for cognitive and computational neuroscience (C3N), University Complutense of Madrid (UCM), 28223 Madrid, Spain; Department of psychology, University Camilo José Cela (UCJC). Villafranca del Castillo, 28692, Madrid, Spain
Shpakivska, D. – Center for cognitive and computational neuroscience (C3N), University Complutense of Madrid (UCM), 28223 Madrid, Spain; Department of experimental psychology, Complutense University of Madrid (UCM), 28223, Madrid, Spain
Del-Cerro-León, A. – Center for cognitive and computational neuroscience (C3N), University Complutense of Madrid (UCM), 28223 Madrid, Spain; Department of experimental psychology, Complutense University of Madrid (UCM), 28223, Madrid, Spain
Uceta, M. – Center for cognitive and computational neuroscience (C3N), University Complutense of Madrid (UCM), 28223 Madrid, Spain
Bruña, R. – Center for cognitive and computational neuroscience (C3N), University Complutense of Madrid (UCM), 28223 Madrid, Spain; Department of radiology, Complutense University of Madrid (UCM), 28040, Madrid, Spain
Maestú, F. – Center for cognitive and computational neuroscience (C3N), University Complutense of Madrid (UCM), 28223 Madrid, Spain; Department of experimental psychology, Complutense University of Madrid (UCM), 28223, Madrid, Spain
García-Moreno, LM. – Department of Psychobiology and Methodology in Behavioral Sciences, Complutense University of Madrid (UCM), 28040, Madrid, Spain

Citation
Antón-Toro, L., Shpakivska, D., Del-Cerro-León, A., Uceta, M., Bruña, R., Maestú, F., García-Moreno, L.M. Longitudinal changes in electrophysiological functional connectivity during inhibitory control task associated with binge drinking predisposition.

Introduction/Motivation

Binge Drinking (BD) is a prevalent alcohol consumption pattern among adolescents, becoming a significant social and health concern. BD episode is characterized by the intake of at least four standard alcohol units (SAUs -10mg ethanol-) for women and five SAUs for men within two hours. Among adolescent population, BD commonly takes place on weekends followed by periods of abstinence during the week. It drives the organism into an ethylic intoxication (Blood alcohol concentration > 0.08g/ml), with harmful neurobiological and neuropsychological consequences (Courtney and Polich, 2009). During adolescents' neurodevelopment, the nervous system is engaged in critical neurobiological changes of the prefrontal, temporal and parietal regions making teenagers especially vulnerable to the outcomes of BD consumption. The optimal maturation of these cortical regions is important to the development of executive control processes along adolescence, such the inhibitory control (IC) (Blakemore and Choudhury, 2006). Inhibitory control refers to the cognitive process oriented to suppress an irrelevant and/or maladaptive responses in a particular context. This ability is crucial for behavioral regulation, and it has been suggested that its dysfunction may predispose some individuals to develop alcohol misuse behaviors (Lopez-Caneda et al., 2014). Previous longitudinal fMRI work has evidenced altered BOLD activation during IC tasks before and after BD initiation (Wetheril et al., 2013). Nevertheless, longitudinal studies which explore this matter from electrophysiological perspective are scarce at this time (Antón-Toro et al., 2021). In the current Magnetoencephalography (MEG) study, we aimed to describe the relationship between electrophysiological Functional Connectivity (FC) during IC task and the development of alcohol binge drinking years later. Moreover, we analysed

the relationship between the longitudinal changes in FC and the intensity of alcohol misuse.

Methods

We recruited a sample formed by 67 adolescents (mean age = 14.6 ± 0.7) from different secondary schools of the community of Madrid. All subjects reported no previous alcohol intake, measured by means of the *Alcohol Use Disorder Identification Test* (AUDIT) and a semi-structured interview. Participants did not report any familiar history of alcohol misuse, and no psychiatric or neurological disorders. In the first stage ('stage pre') brain's electrophysiological activity of each participant was recorded by a MEG during an IC task go/no-go. Two years later, in the second stage, 32 of 67 participants (mean age 16.7 ± 0.7) completed a similar protocol (AUDIT test and a semi-structured interview, plus MEG recording during the go/no-go task). Based on the information of the AUDIT and the interview, for each participant we calculated the number of Standard Alcohol Units (SAU) ingested in a regular consumption episode. Regarding 'stage-pre' analysis, for each participant, we calculated the source-space FC matrix using a *Phase Locking Value* (PLV) approach, in three frequency bands: alpha (8 – 12 Hz), beta (12 – 30 Hz), and gamma (30 – 45 Hz). From these matrices, we calculated the strength of FC for each cortical source, or '*nodal-strength',* defined as the averaged FC of each cortical source with each other's. Next, using a *cluster based permutation test* (CBPT) based on Spearman's correlation, we calculated the correlation between FC of each cortical source and the number of SAUs per subject. This analysis allows us to identify cortical clusters with significant correlations with the intensity of future alcohol intake. In the 'Stage-post' analysis, we followed a similar approach. First, we calculated the FC matrix and the '*nodal strength'* from second stage MEG-signals. Next, to assess the change in FC between 'Stage-pre' and 'Stage-post', we calculated the *Symmetrized percent of change (SPC)*. This approach offers an index of the bidirectional rate of change of FC between two time points considering the time variance within the sample. An SPC value equal to zero means the absence of change in FC between stages, while positive values reflect an increase, and negative values a decrease. The

higher the absolute values, the higher the change in that direction. Finally, we calculated the correlation between SPC values and the number of SAUs using a CBPT approach.

Results and discussion

Regarding stage pre, analysis revealed two clusters with positive correlations in beta band with future alcohol use (Cluster A: p = 0.0014, *rho* = 0.680; Cluster B: p = 0.0160, *rho* = 0.569). See figure 1A. Cluster A was composed of 245 cortical sources mainly localized in the medial and right parts of the prefrontal cortex (Superior, middle, inferior, and orbital frontal gyrus), part of the left medial frontal gyrus, Anterior and posterior cingulate cortex (ACC, PCC), right and medial temporal lobe (including hippocampus and parahippocampus), and parts of the right precuneus. Cluster B was formed by 33 cortical sources located in the medial part of the somatosensorial and motor cortex, and the left middle cingulate cortex. Both clusters indicate that

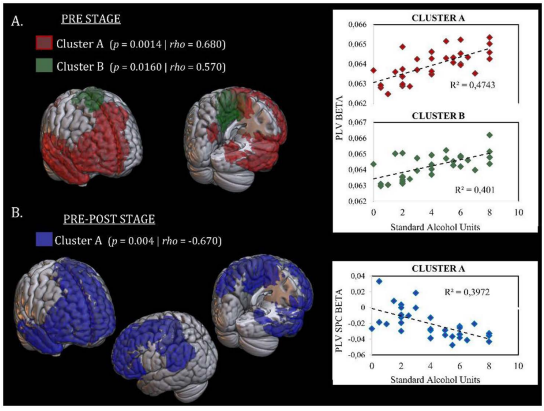

FIGURE 1

Functional connectivity correlations in pre and post stages

Note. Distribution of cortical clusters and scatter plots. Panel A represent FC before BD initiation significantly correlated with number of SAUs years later. Panel B represent changes pre-post BD in FC (SPC) correlated with the number of SAUs.

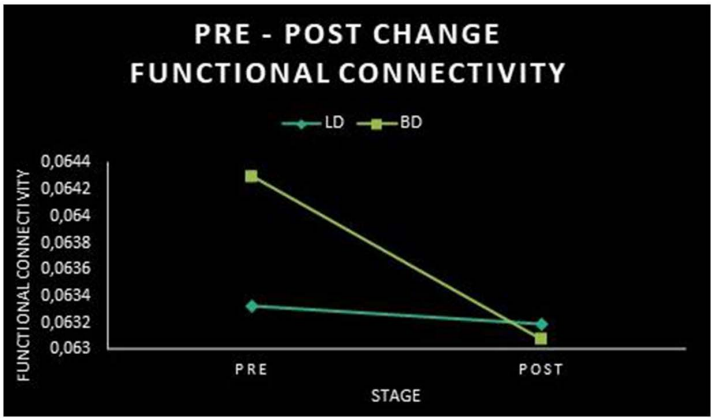

FIGURE 2

Slopes of change between light-drinkers and Binge-drinkers

Note. Slope-based representation of pre – post change. Sample was divided into two groups for this purpose: light-drinkers (SAUs < 4); Binge-drinkers (SAUs > 4).

the higher the FC in those regions, the higher the level of alcohol use two years later. Regarding analysis of change between stages pre and post, results showed one cluster with negative correlation in beta band between the rate of change in FC and the intensity of alcohol intake (p = 0.004; *rho* = -0.670). This cluster was composed of 290 cortical sources with a similar distribution to those found in both clusters of the stage pre. Additionally, this cluster encompassed a more expended part of the left prefrontal cortex (including the superior, middle, and inferior frontal gyrus), the left inferior parietal gyrus, the left angular gyrus, and the left supramarginal gyrus (see Figure 1B). Figure 2 shows a slope-based representation of these change.

Higher SAU levels were associated with negative and lower SPC values, while lower SAU level was related predominantly to higher SPC values around zero, both positive and negative. This point to an exacerbated reduction of FC in previously hyperconnected areas as alcohol consumption becomes more intense. These results show differential FC profiles prior to alcohol

use and a different pattern of evolution depending on the consumption behaviour. Previous MRI studies have shown similar patterns in local Blood Oxygen Level Dependent activation (BOLD) associated with BD consumption (although in opposite directions), characterized by lower pre-consumption brain activation followed by hyperactivation after consumption (Wetherill et al., 2013). Similarly, structural MRI studies have shown how BD consumption is associated with an exacerbated reduction in cortical thickness in regions similar to those found in this work (Pfefferbaum et al., 2018). This evidence underlines the importance of explore the neurofunctional profiles regarding this matter from different neuroimaging perspectives, as they provide complementary information. Nevertheless, despite the different nature of the evidence provided by BOLD local activity and the electrophysiological FC, these results underline the existence of diverse brain's functional abnormalities predating alcohol misuse, as we as the distinctive impact of alcohol consumption in adolescent's neuromaturation.

References

Courtney, K. E., & Polich, J. (2009). Binge drinking in young adults: Data, definitions, and determinants. *Psychological bulletin*, *135*(1), 142.

Blakemore, S. J., & Choudhury, S. (2006). Development of the adolescent brain: implications for executive function and social cognition. *Journal of child psychology and psychiatry*, *47*(3-4), 296-312.

López-Caneda, E., Rodríguez Holguín, S., Cadaveira, F., Corral, M., & Doallo, S. (2014). Impact of alcohol use on inhibitory control (and vice versa) during adolescence and young adulthood: a review. *Alcohol and alcoholism*, *49*(2), 173-181.

Wetherill, R. R., Squeglia, L. M., Yang, T. T., & Tapert, S. F. (2013). A longitudinal examination of adolescent response inhibition: neural differences before and after the initiation of heavy drinking. *Psychopharmacology*, *230*(4), 663-671.

Antón-Toro, L. F., Bruña, R., Suárez-Méndez, I., Correas, Á., García-Moreno, L. M., & Maestú, F. (2021). Abnormal organization of inhibitory control functional networks in future binge drinkers. *Drug and Alcohol Dependence*, *218*, 108401.

Wetherill, R. R., Squeglia, L. M., Yang, T. T., & Tapert, S. F. (2013). A longitudinal examination of adolescent response inhibition: neural differences before and after the initiation of heavy drinking. *Psychopharmacology*, *230*(4), 663-671.

Pfefferbaum, A., Kwon, D., Brumback, T., Thompson, W. K., Cummins, K., Tapert, S. F., ... & Sullivan, E. V. (2018). Altered brain developmental trajectories in adolescents after initiating drinking. *American journal of psychiatry*, *175*(4), 370-380.

Impact of acute stress on mechanical pain sensitivity: An experimental study pilot

Author
Nicole Bailey – ICORD, University of British Columbia, Vancouver, BC, Canada; Department of Medicine, Faculty of Medicine, University of British Columbia, Vancouver, British Columbia, Canada
Lukas Linde – ICORD, University of British Columbia, Vancouver, BC, Canada; Department of Anesthesiology, Pharmacology & Therapeutics, Faculty of Medicine, University of British Columbia, Vancouver, British Columbia, Canada;Djavad Mowafaghian Centre for Brain Health, University of British Columbia, Vancouver, British Columbia, Canada
John Kramer – ICORD, University of British Columbia, Vancouver, BC, Canada; Department of Anesthesiology, Pharmacology & Therapeutics, Faculty of Medicine, University of British Columbia, Vancouver, British Columbia, Canada;Djavad Mowafaghian Centre for Brain Health, University of British Columbia, Vancouver, British Columbia, Canada

Citation
Bailey, N., Linde, L., Kramer, J. Impact of acute stress on mechanical pain sensitivity: An experimental study pilot.

Introduction/Motivation

Chronic pain is a global health crisis affecting 1 in 5 adults in North America[1,2], and between a third to a half of the UK population.[3] Treatment options are currently limited with novel interventions urgently needed. Stress has long been attributed to aggravations in chronic pain symptoms.[4–8]associated disability, impact on quality of life and the costs associated with the extensive use of health care services by individuals living with it.

objective: To summarize the research evidence and elicit health system policymakers', stakeholders' and researchers' tacit knowledge and views about improving chronic pain management in Canada and engaging provincial and territorial health system decision makers in supporting comprehensive chronic pain management in Canada. Methods: For these two topics, the global and local research evidence regarding each of the two problems were synthesized in evidence briefs. Three options were generated for addressing each problem, and implementation considerations were assessed. A stakeholder dialogue regarding each topic was convened (with 29 participants in total However, previous studies on experimental pain and acute stress models have mixed results, with different studies showing stress has an analgesic (reduced pain), hyperalgesic (increased pain), or no effect on pain. Therefore, before a relationship between stress and pain can be established, the variability in stress responses must be considered. Variability in stress can be quantified in various ways. Subjectively, participants can report degree of experienced stress (e.g., rate how stressful from 0-100). Objectively, stress can be quantified by the degree certain cardiac measures are elevated (e.g., max heart rate). Additionally, stress indices, such as Kubios Sympathetic Nervous System (SNS) Index, have been derived from cardiac measures to objectively quantify stress.[9]

Another quantification method involves the biopsychosocial model of stress, which stipulates that individuals may perceive stress as either a challenge or threat.[10]it is not necessarily so. According to the biopsychosocial model of challenge and threat, evaluations of personal resources and situational demands determine to what extent individuals experience a relatively positive (challenge Because on a conscious level it is often difficult to distinguish a challenge/threat response, researchers can rely on the ratio of cardiac output (CO) and total peripheral resistance (TPR) reactivity.[10]it is not necessarily so. According to the biopsychosocial model of challenge and threat, evaluations of personal resources and situational demands determine to what extent individuals experience a relatively positive (challenge CO is the amount of blood pumped by the heart in a minute; in challenge responses CO increases and in threat responses CO may slightly increase, decrease, or stay the same.

TPR is the amount of resistance in peripheral blood vessels; in challenge responses TPR slightly increases, decreases, or stays the same, whereas in threat responses TPR increases.

To our knowledge, no study has investigated if either the degree of stress arousal or a challenge/threat state effect pain rating to experimental pain.

Methods

CO and TPR were captured using a Finometer Pro, an apparatus that noninvasively measures cardiac measures with a finger cuff.[11] Other cardiac measures (e.g., max heart rate) were recorded by an EKG and processed in Kubios to create a SNS Index.[9] In the baseline period, the Finometer and EKG recorded participants as they watch a non-stimulating video of landscapes. Weighted pinprick testing then captured mechanical pain sensitivity. Stress was achieved through the validated Trier Social Stress Test (TSST), involving a social-evaluative threat with actors as a panel of judges.[12] During TSST, cardiac measures were recorded to determine degree of stress arousal and participants' challenge/threat states. Pinprick testing was repeated following TSST.

Challenge/threat indexes were created for each participants' CO and TPR over a 5-minute time interval during baseline and over 16 1-minute time intervals during TSST. A single time interval was chosen for baseline due to the consistency in task engagement (i.e., participants watched the same video for the entire duration) while 16 different 1-minute time intervals accounted for the different TSST tasks. Z-scores were created for each CO and TPR reactivity from baseline to each 1-minute time interval averages**.** CO was assigned a weight of +1 and TPR assigned a weight of -1; then each interval's CO and TPR Z-scores were summed to get an index for every minute during TSST. This index creation strategy was adapted from previous literature.[10]it is not necessarily so. According to the biopsychosocial model of challenge and threat, evaluations of personal resources and situational demands determine to what extent individuals experience a relatively positive (challenge Participants were categorized as "challenge" or "threat" based on which state they spent the majority of time intervals in.

Results and discussion

A LMER comparison of pilot results (n=10) indicates stress was achieved with significantly increased max heart rate from baseline to stress (p-value<0.001). Pilot data also found an analgesic linear correlation between SNS Index during stress and verbal pain rating immediately after stress, with greater physiological stress correlating to lower pain ratings (R^2=0.9, p-value<0.001). This correlation suggests that the degree of stress arousal (larger SNS Index indicates higher stress arousal) may predict perceived pain immediately after the stressor, see Figure 1.

For challenge and threat states, the 16 time intervals demonstrated that participants generally did not have a fixed challenge or threat state, see Figure 2. Rather, fluctuations over time reflect that individual responses to stress are dynamic and cannot be simplified down to a single metric across time. Two participants only had Finometer recordings for the first 6 minutes

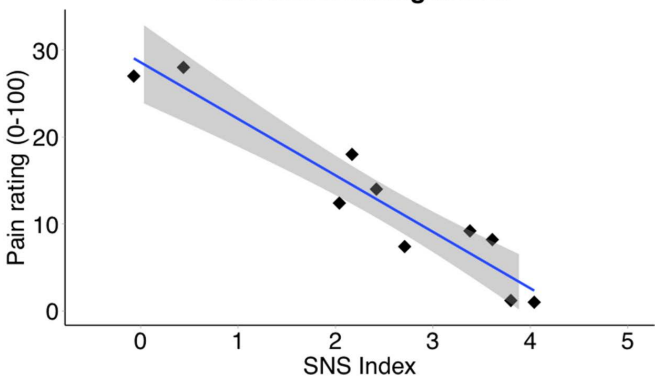

FIGURE 1
Linear correlation between SNS Index during TSST and verbal pinprick pain ratings immediately after TSST.
y = -6.4963x + 28.582
R^2 = 0.9
p-value: 0.00002***

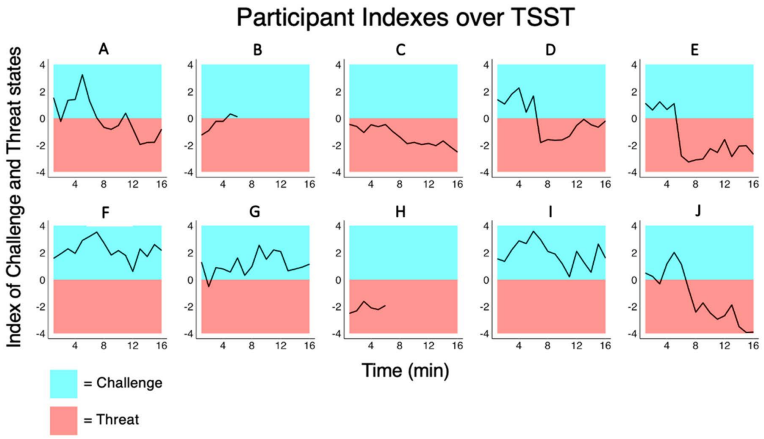

FIGURE 2
Challenge/Threat states plotted over the 16 1-minute time intervals for each participant. Individual plots demonstrate the variability in participants over time, with some participants changing between challenge and threat states throughout the task (going from blue to red regions).

due to machine malfunction. A LMER pilot data comparison of pain ratings across time (baseline and immediately after stress) and group (challenge and threat) did not indicate a difference in group pain rating over time (p=0.2).

Previous literature has not investigated if the variability in individuals' SNS responses to acute stress effects pain perception. This preliminary data indicates that the heterogeneous results in the literature (i.e., hyperalgesia, analgesia, or no change after acute stress)[13–15] could be due to the sample population studied (i.e., different proportion of high vs low stress responders). The pilot results explained here are currently being expanded in a double-blinded randomized control study (n=40) with a control non-stressful condition (n=20) and the current stress paradigm (n=20).

References

1. Canadian Pain Task Force Report: September 2020 - Canada.ca. Accessed June 17, 2022. https://www.canada.ca/en/health-canada/corporate/about-health-canada/public-engagement/external-advisory-bodies/canadian-pain-task-force/report-2020.html

2. Yong RJ, Mullins PM, Bhattacharyya N. Prevalence of chronic pain among adults in the United States. *Pain*. 2022;163(2):E328-E332. doi:10.1097/J.PAIN.0000000000002291

3. Fayaz A, Croft P, Langford RM, Donaldson LJ, Jones GT. Prevalence of chronic pain in the UK: a systematic review and meta-analysis of population studies. *BMJ Open*. 2016;6(6). doi:10.1136/BMJOPEN-2015-010364

4. Wilson MG, Lavis JN, Ellen ME. Supporting chronic pain management across provincial and territorial health systems in Canada: Findings from two stakeholder dialogues. *Pain Res Manag*. Published online 2015. doi:10.1155/2015/918976

5. Dufton LM, Konik B, Colletti R, et al. Effects of stress on pain threshold and tolerance in children with recurrent abdominal pain. *Pain*. Published online 2008. doi:10.1016/j.pain.2007.06.012

6. Fischer S, Doerr JM, Strahler J, Mewes R, Thieme K, Nater UM. Stress exacerbates pain in the everyday lives of women with fibromyalgia syndrome-The role of cortisol and alpha-amylase. *Psychoneuroendocrinology*. Published online 2016. doi:10.1016/j.psyneuen.2015.09.018

7. Gil KM, Carson JW, Porter LS, Scipio C, Bediako SM, Orringer E. Daily Mood and Stress Predict Pain, Health Care Use, and Work Activity in African American Adults with Sickle-Cell Disease. *Heal Psychol*. Published online 2004. doi:10.1037/0278-6133.23.3.267

8. Crettaz B, Marziniak M, Willeke P, et al. Stress-induced allodynia--evidence of increased pain sensitivity in healthy humans and patients with chronic pain after experimentally induced psychosocial stress. *PLoS One*. 2013;8(8). doi:10.1371/JOURNAL.PONE.0069460

9. HRV in evaluating ANS function – Kubios. Accessed November 12, 2022. https://www.kubios.com/hrv-ans-function/

10. Seery MD. Challenge or threat? Cardiovascular indexes of resilience and vulnerability to potential stress in humans. *Neurosci Biobehav Rev*. 2011;35(7):1603-1610. doi:10.1016/J.NEUBIOREV.2011.03.003

11. Schutte AE, Huisman HW, Van Rooyen JM, Malan NT, Schutte R. Validation of the Finometer device for measurement of blood pressure in black women. *J Hum Hypertens*. 2004;18(2):79-84. doi:10.1038/SJ.JHH.1001639

12. Kirschbaum C, Pirke KM, Hellhammer DH. The "Trier social stress test" - A tool for investigating psychobiological stress responses in a laboratory setting. In: *Neuropsychobiology*. ; 1993. doi:10.1159/000119004

13. Hoeger Bement M, Weyer A, Keller M, Harkins AL, Hunter SK. Anxiety and stress can predict pain perception following a cognitive stress. *Physiol Behav*. 2010;101(1):87-92. doi:10.1016/J.PHYSBEH.2010.04.021

14. Butler RK, Finn DP. Stress-induced analgesia. *Prog Neurobiol*. 2009;88(3):184-202. doi:10.1016/J.PNEUROBIO.2009.04.003

15. Jennings EM, Okine BN, Roche M, Finn DP. Stress-induced hyperalgesia. *Prog Neurobiol*. 2014;121:1-18. doi:10.1016/J.PNEUROBIO.2014.06.003

Resting-state EEG functional connectivity in schizophrenia

Author
Melinda Becske – Department of Psychiatry and Psychotherapy, Semmelweis University, Budapest, Hungary
Csilla Marosi – Department of Psychiatry and Psychotherapy, Semmelweis University, Budapest, Hungary
Hajnalka Molnár – Department of Psychiatry and Psychotherapy, Semmelweis University, Budapest, Hungary
Zsuzsanna Fodor – Department of Psychiatry and Psychotherapy, Semmelweis University, Budapest, Hungary
Kinga Farkas – Department of Psychiatry and Psychotherapy, Semmelweis University, Budapest, Hungary
Frigyes Sámuel Rácz – Department of Physiology, Semmelweis University, Budapest, Hungary
Gábor Csukly – Department of Psychiatry and Psychotherapy, Semmelweis University, Budapest, Hungary

Citation
Becske, M., Marosi, C., Molnár, H., Fodor, Z., Farkas, K., Rácz, F.S., Csukly, G. Resting-state EEG functional connectivity in schizophrenia.

Introduction

Schizophrenia is a serious and particularly complex mental disorder, known to be associated with various subtle structural and functional deviations in the brain [1]. The topics of brain connectivity and global brain network parameters in schizophrenia are increasingly becoming the focus of attention, however methods and results are quite heterogeneous [2,3,4,5].

Methods

37 patients with schizophrenia and 33 matched healthy control subjects were enrolled in our study. Two 2 minutes long 64 channel EEG recordings were registered during resting (in eyes open and eyes closed conditions respectively). Average connectivity strength was estimated with Weighted Phase Lag Index (wPLI) [6] for delta (0.5-4 Hz) and theta (4-7 Hz) frequency bands. In order to analyse functional network topology, Minimum Spanning Tree (MST) algorithms [7] were also applied.

Results and discussion

Our results show that patients have weaker average functional connectivity in both delta (eyes closed condition) and theta (eyes open condition) frequency bands compared to healthy controls. Concerning network differences, the results – lower diameter, higher leaf number, higher maximum degree and higher maximum betweenness centrality in patients compared to controls – indicate a more star-like network topology in patients with schizophrenia. Our findings of disturbed global functional connectivity in patients are in accordance with some previous findings based on resting state EEG [3] (and fMRI [5]) data, suggesting that network structure in schizophrenia is biased towards a less optimal, more centralized organization.

Acknowledgements

Our work was supported by the following grants: Hungarian Research Found - OTKA PD 115837; Bolyai Research Fellowship Program of the Hungarian Academy of Sciences; ÚNKP - New National Excellence Program of the Ministry of Human Capacities. Higher Education Institutional Excellence Programme of the Ministry of Human Capacities in Hungary, within the framework of the Neurology thematic programme of Semmelweis University.

References

[1] Karlsgodt, K. H., Sun, D., & Cannon, T. D. (2010). Structural and Functional Brain Abnormalities in Schizophrenia. Current Directions in Psychological Science, 19(4), 226–231

[2] Mackintosh, A. J., de Bock, R., Lim, Z., Trulley, V.-N., Schmidt, A., Borgwardt, S., & Andreou, C. (2021). Psychotic disorders, dopaminergic agents and EEG/MEG resting-state functional connectivity: A systematic review. Neuroscience & Biobehavioral Reviews, 120, 354–371.

[3] Krukow, P., Jonak, K., Karpiński, R., & Karakuła-Juchnowicz, H. (2019). Abnormalities in hubs location and nodes centrality predict cognitive slowing and increased performance variability in first-episode schizophrenia patients. Scientific Reports, 9(1), 9594.

[4] van Dellen, E., Börner, C., Schutte, M., van Montfort, S., Abramovic, L., Boks, M. P., Cahn, W., van Haren, N., Mandl, R., Stam, C. J., & Sommer, I. (2020). Functional brain networks in the schizophrenia spectrum and bipolar disorder with psychosis. Npj Schizophrenia, 6(1), 22.

[5] Liu, X., Yang, H., Becker, B., Huang, X., Luo, C., Meng, C., & Biswal, B. (2021). Disentangling age- and disease-related alterations in schizophrenia brain network using structural equation modeling: A graph theoretical study based on minimum spanning tree. Human Brain Mapping, 42(10), 3023–3041.

[6] Vinck, M., Oostenveld, R., van Wingerden, M., Battaglia, F., & Pennartz, C. M. A. (2011). An improved index of phase-synchronization for electrophysiological data in the presence of volume-conduction, noise and sample-size bias. NeuroImage, 55(4), 1548–1565.

[7] Stam, C. J., Tewarie, P., Van Dellen, E., van Straaten, E. C. W., Hillebrand, A., & Van Mieghem, P. (2014). The trees and the forest: Characterization of complex brain networks with minimum spanning trees. International Journal of Psychophysiology, 92(3), 129–138.

Structural insights into the functional amyloid hCPEB3 from single-molecule studies

Author
Ada Bernaus, María Eugenia Vaquero, Nora Serrano, Paula López-García, Mariano Carrión-Vázquez – Molecular, Cellular and Development Neurobiology, Cajal Institute, Madrid, Spain

Citation
Bernaus, A., Vaquero, M.E., Serrano, N., López-García, P., Carrión-Vázquez, M. Structural insights into the functional amyloid hCPEB3 from single-molecule studies.

Introduction

The cytoplasmic polyadenylation element-binding protein (CPEB) family is involved in multiple vital cell functions. Is key in the regulation of messenger RNA transcription and polyadenylation, cell cycle control and senescence, synaptic plasticity, learning, and memory consolidation [1]. The mammalian CPEB3 isoform is highly expressed in the brain and localized at the postsynaptic densities where it regulates the translation of several key mRNAs for long-term synaptic plasticity in the hippocampus [2]. It works as a functional prion that fluctuates between two forms. In the basal state, highly SUMOylated CPEB3 is in a monomeric form, which localizes in P-bodies repressing translation [3]. After neuronal stimulation, there is a decrease of SUMOylation and becomes ubiquitinylated. Then, CPEB3 interacts with the actin cytoskeleton forming amyloid aggregates and switching to an active state that promotes the translation of target mRNAs. Hereby, triggering

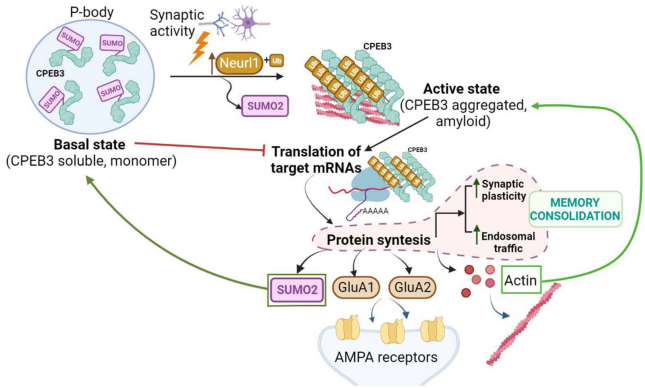

FIGURE 1
CPEB3 structural switch and its regulation. On its basal state, CPEB3 is a soluble monomer localized in P-bodies were it binds target mRNAs repressing their translation. In this form, CPEB3 is repressing synaptic activity. Upon synaptic stimulation, CPEB3 is deSUMOlayted and ubiquitinated. This triggers a conformational change in the protein, which aggregates forming a functional amyloid. CPEB3 goes over to activate the translation of the previous repressed target mRNAs and allowing memory consolidation. By SUMO2 production, active CPEB3 is creating a negative loop, while simultaneously establishing a positive one by actin synthesis.

simultaneously positive and negative loops ensuring a tightly regulated fine tuning while promoting basal state synaptic modifications that favour long-term memory consolidation [2,4,5] (Figure 1).

The human form of CPEB3 (hCPEB3) contains two RRM-type RNA-binding domains and a zinc finger domain at the C-terminus. The N-terminal region is an intrinsically disordered region (IDR) which contains both the amyloid forming domain, required for prion seeding and foci heritability in the murine ortholog (mCPEB3) [5], and the liquid demixing domain [6].

Considering that the key conformational change that endows aggregation occurs in the monomer and that the first 200 residues of the IDR of mCPEB3 are essential for prion seeding and were also reported to be the amyloid-forming domain, we selected this region of hCPEB3 to analyse

its conformational polymorphism by AFM-based Single Molecule Force Spectroscopy (AFM-SMFS).

Methods

AFM-SMFS pulls single protein molecules and used in its length-clamp modality, piconewton-scale forces and nanometre distances can be measured directly monitoring intramolecular interactions (mechanical stability) and their location. Extension of a molecule by retraction of the piezoelectric positioner results in deflection of the AFM cantilever. The force required to unfold a domain changes the angle of reflection of the laser beam striking the cantilever, measured from a photodetector (Figure 2, A). Experimental results are plotted as force–extension recordings, which in modular proteins show a characteristic sawtooth pattern. Mechanical stability is then measured by fitting them to the worm-like chain (WLC) model of polymer elasticity (Figure 2, B). For the unequivocal nanomechanical analysis

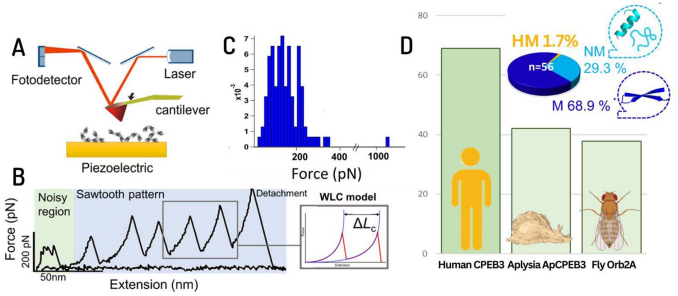

FIGURE 2

AFM-SMFS schematics and hCPEB3 nanomechanics. A) The laser beam is positioned on the tip of the cantilever. The laser light reflected by the tip arrives to a photodetector. When the tip enters in contact with the protein, it is stretched vertically during the piezoelectric retraction. The force applied to stretch a domain modifies the angle of reflection of the laser beam. B) This is expressed as force-extension wave-like plots that reflect the force required to break each domain as well as the amino acid residues length that comprises this domain. C) hCPEB3 nanomechanical analysis: histograms of mechanical stability and increase in contour length. D) Results of AFM-SMFS analysis of hCPEB3 and their orthologs. The human ortholog shows a higher frequency of mechanostable structures (68.9%) than *Ap*CPEB3 (42.1%) and Orb2A (37.7%).

of IDRs like prion-like proteins or amyloids by AFM-SMFS the "carrier-guest" strategy was developed [7]. Here, the non-structured protein is mechanically protected, inside a carrier module, assuring its stretching after a reported carrier. Based on this methodology, the first 200-residue region of the prion-like domain of hCPEB3 was analysed to study its conformational polymorphism, a hallmark of amyloidogenic proteins.

We validated the carrier-guest strategy for $hCPEB3_{1\text{-}200}$ using an array of techniques that corroborate its amyloidogenic properties, which remain unaffected by its fusing to the ubiquitin carrier used in this strategy.

Results and discussion

Based on the force needed for protein stretching, we can distinguish two types of structures: non-mechanically resistant, all those transient states of the IDR which do not generate any force peak during the pulling, and mechanostable ones. Among the later we also distinguish those especially stable structure which take more than 400 pN to break, as hyper-mechanostables, as could potentially pose a challenge for the proteosome.

Focusing in hCPEb3 IDR, mechanostable structures could be in principle associated with its active form as a functional amyloid.

AFM-SMFS results indicated that hCPEB31-200 displayed a rich conformational polymorphism at the monomer level with 29.3% non-mechanically resistant events and 70.7% mechanostable conformers, including 1.8% of hyper-mechanostable ones. hCPEB31-200 has showed the highest frequency of mechanostable events out of the fifteen amyloidogenic IDRs analysed so far in our laboratory by AFM-SMFS [7-9], including its CPEB orthologues from Aplysia (ApCPEB3) (42.1%) and Drosophila (Orb2A) (37.7%) (Figure 2, D). Considering that an elevated mechanostability is related with an increased acquisition of secondary structure within the IDR, we suggest that the higher structuring of hCPEB3 may be related to a critical evolutionary step to fulfil its biological function, endowing humans with a more complex regulatory mechanism for memory consolidation [10].

Recent research carried out by our team suggests that the hCPEB3 amyloid domain is rather restricted to the 50 amino acid residues of the 100-150 region. We've also patented a small peptide as a potential amyloid inhibitory drug. In the light of these results, we are currently working on analysing the effect of this peptide on the conformational polymorphism of hCPEB3100-200. We expect these new results could be ready to be presented at the time of the congress.

References

[1] Richter, J. D. CPEB: a life in translation. Trends Biochem. Sci. 32, 279–285 (2007).

[2] Pavlopoulos, E. et al. Neuralized1 activates CPEB3: a novel function of ubiquitination in synaptic plasticity and memory storage. Cell 147, 1369–1383 (2012).

[3] Ford, L. et al. CPEB3 inhibits translation of mRNA targets by localizing them to P bodies. Proc. Natl. Acad. Sci. U. S. A. 116, 18078–18087 (2019).

[4] Drisaldi, B. et al. SUMOylation is an inhibitory constraint that regulates the prion-like aggregation and activity of CPEB3. Cell Rep. 11, 1694–1702 (2015).

[5] Stephan, J. S. et al. The CPEB3 Protein is a functional prion that interacts with the actin cytoskeleton. Cell Rep. 11, 1772–1785 (2015).

[6] Ramírez de Mingo, D. et al. Molecular determinants of Liquid demixing and amyloidogenesis in human CPEB3. BioRxiv 2020.06.02.129783.

[7] Hervás, R. et al. Common features at the start of the neurodegeneration cascade. PLoS Biol. 10, (2012).

[8] Hervás, R. et al. Molecular basis of Orb2 amyloidogenesis and blockade of memory consolidation. PLoS Biol. 14, 1–32 (2016).

[9] Hervás, R. et al. Divergent CPEB prion-like domains reveal different assembly mechanisms for a generic amyloid-like fold. BMC Biol. 19, 1–14 (2021).

[10] Ramírez de Mingo, D. et al. Conformational dynamics in the disordered region of human CPEB3 linked to memory consolidation. BMC Biol. 20, 1-18 (2022).

Brain signal analysis for inner speech detection

Author
Valeria Buenrostro-Leiter, Fellipe Torquato Rollin, Foteini Simistira Liwicki, Vibha Gupta, Rajkumar Saini, Kanjar De – Department of Computer Science, Electrical and Space Engineering, Luleå University of Technology, Luleå, Sweden

Citation
Buenrostro-Leiter, V., Rollin, F.T., Liwicki, F.S., Gupta, V., Saini, R., De, K. Brain signal analysis for inner speech detection.

Introduction/Motivation

The Brain Computer Interface (BCI) research started in the 1960s [1] and has accelerated in recent years [2]. The primary purpose of BCI is to acquire brain signals to analyse and translate them into commands that are then transferred to an external device that can carry out desired actions by the user. Research technologies like BCI have outstanding medical uses, like replacing or restoring useful functions for individuals with severe disabilities who cannot perform actions without using peripheral nerves and muscles through a BCI. They can also improve rehabilitation for people with strokes, head trauma, and other disorders.

In this work, taking advantage of the BCI technology, we investigated the feasibility of using brain signal analysis to classify the recorded electroencephalography (EEG) data from participants engaged in tasks involving inner speech and made publicly available by Nieto et al. [3]. The inner speech, or self-talk, is a process by which we talk to ourselves to think through problems or plan actions. People suffering from locked-in syndrome [4] could use their inner speech to communicate with their environment.

We demonstrate a method to classify the recorded EEG data using four machine learning models, display the results, and compare using different protocols. We achieved state-of-the-art results when using a Linear Support Vector Classifier, reporting an overall accuracy of 35.56%, well above the reported accuracy of 29.67% obtained by Berg et.al. [5] with a deep learning architecture.

Methods

This work uses the inner speech dataset that Nieto et al. [6] created as part of their research. We apply four classical machine learning classifiers: Random Forest, Artificial Neural Network (basic multilayer perceptron with one hidden layer), Support Vector Classifiers, and Linear Support Vector Classifiers, for EEG signal classification, following a subject-independent (Figure 1) and subject-dependent approach (Figure 2). The Support Vector Classifiers and Linear Support Vector Classifiers were chosen because Support Vector Machines have successfully been used previously in the classification of EEG data, since they show a good generalization performance for high dimensional data [7]. In order to ensure that the results have an accuracy above pure randomness, we calculate a baseline with which to compare all the accuracy results from the four algorithms of 27%, obtained with the *DummyClassifier* algorithm from Sci-kit Learn, a very basic model that makes predictions ignoring the input features and using only the labels. The following independent approach uses the leave-one-out protocol [8], where the data of the n-1 subjects are used as a training set and the data of the n-subject as test set. On the contrary, the subject-dependent approach uses part of each subject's data as training and the remaining as test set [8]. We also use the Nested Cross Validation technique to fine-tune and find the best parameters for each classifier to adapt the algorithm for the best performance automatically, where an inner Cross Validation is used to implement the hyperparameter optimization scheme, and an outer Cross Validation is used to implement the model selection scheme. The accuracies were calculated using the test set with the help of Sci-Kit Learn *accuracy_score*, using the following formula:

$$accuracy(y, \hat{y}) = \frac{1}{n_{samples}} \sum_{i=0}^{n_{samples}-1} (\hat{y}_i = y_i) \quad (1)$$

where is the predictive label of the i-th sample, is the corresponding true label, and is the number of samples.

Results and discussion

When using the subject-independent approach, where we trained on nine subjects and tested on the subject that was left out, the Random Forest classifier performed poorly in all the tests, obtaining accuracies below the baseline level accuracy as well as the chance level accuracy. In contrast, the Support Vector Classifier and Linear Support Vector Classifier obtained higher results, with 29.9% and 30.35%, overall test accuracy respectively (see Fig. 1). When following a subject-dependent approach, we got the highest test accuracy, with an average of 35.56% (see Fig. 2), well above the average

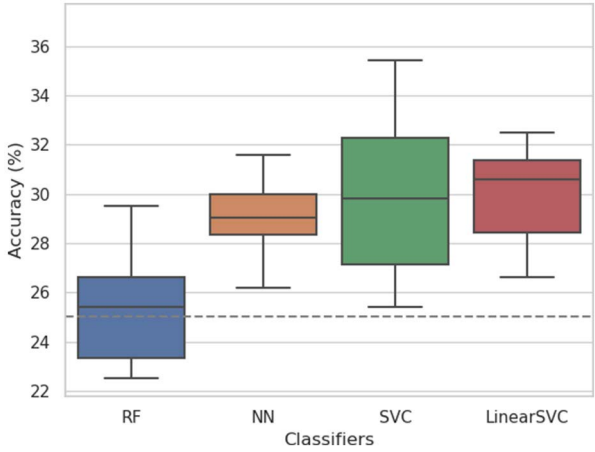

FIGURE 1

(A) Live cell imaging combining bright-field and green fluorescence. On the left, we found HF infected with RV-MyoD-GFP 21DPT. On the right, it is shown the primary culture of MNs 13 days in culture (DIC). Projections of these MNs crossing microgrooves can be seen. (B) Phenotypic differences between iMTs obtained by the conversion of HF from control donors and ALS patients.

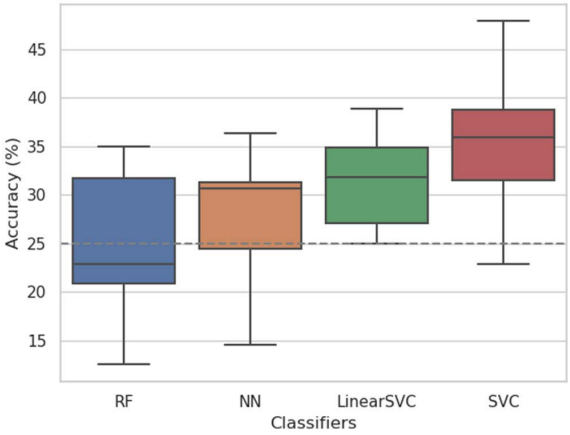

FIGURE 2
Average test accuracy obtained by each classifier when training and testing on each individual subject, following a subject dependent approach. The grey dotted line shows the chance accuracy of 25%.

accuracy of 29.67% obtained by Berg et al. [5] when using EEGNet [9]. After comparing the accuracy rates of the different classifiers, the best results are achieved by the SVC and Linear SVC classifiers, even competing against deep learning classifiers such as EEGNet by Berg et al. The code of this work can be found at [10].

Acknowledgements
This research was funded by the Grants for excellent research project proposals of SRT.ai 2022.

References

[1] Shih JJ, Krusienski DJ, Wolpaw JR. *Brain-computer interfaces in medicine*. Mayo Clin Proc. 2012 Mar; 87(3):268-79. doi: 10.1016/j.mayocp.2011.12.008. Epub 2012 Feb 10. PMID: 22325364; PMCID: PMC3497935.

[2] Mridha MF, Das SC, Kabir MM, Lima AA, Islam MR, Watanobe Y. *Brain-Computer Interface: Advancement and Challenges*. Sensors (Basel). 2021 Aug 26;21(17):5746. doi: 10.3390/s21175746. PMID: 34502636; PMCID: PMC8433803.

[3] Nieto, N., Peterson, V., Rufiner, H.L., Kamienkowski, J. E. & Spies, R., 2021. *Inner Speech*. OpenNeuro. [Dataset] doi: 10.18112/openneuro.ds003626.v2.0.0

[4] Smith, Eimear, and Mark Delargy. *Locked-in syndrome*. Bmj 330.7488, 2005: 406-409.

[5] Berg, B. v. d., Donkelaar, S. v., and Alimardani, M., *Inner Speech Classification using EEG Signals: A Deep Learning Approach*, 2021 IEEE 2nd International Conference on Human-Machine Systems (ICHMS), 2021, pp. 1-4, doi: 10.1109/ICHMS53169.2021.9582457.

[6] Nieto, N., Peterson, V., Rufiner, H.L., Kamienkowski, J. E. & Spies, R., *Thinking out loud, an open-access EEG-based BCI dataset for inner speech recognition*. Sci Data 9, 52, 2022. doi: 10.1038/s41597-022-01147-2.

[7] B. Richhariya, M. Tanveer, *EEG signal classification using universum support vector machine*, Expert Systems with Applications, Volume 106, 2018, pp. 169-182, doi: /10.1016/j.eswa.2018.03.053.

[8] Simistira Liwicki, Foteini, et al. Rethinking the Methods and Algorithms for Inner Speech Decoding and Making Them Reproducible. NeuroSci 3.2 (2022): 226-244.

[9] Lawhern, V. J., Solon, A. J.. Waytowich, N. R., Gordon, S. M., Hung, & Lance, B. J. *EEGNet: a compact convolutional neural network for EEG-based brain–computer interfaces*, Journal of Neural Engineering, vol. 15, no. 5, pp. 056013, 2018.

[10] https://github.com/LTU-Machine-Learning/InnerSpeech_Nieto_DSMasterThesis_2022

Rest in Binge: An exploration of the effects of alcohol consumption during adolescent neurodevelopment

Author
Alberto del Cerro-León – Center for Cognitive and Computational Neuroscience (C3N), Universidad Complutense de Madrid (UCM), Madrid, Spain
Luis Fernando Antón-Toro – Center for Cognitive and Computational Neuroscience (C3N), Universidad Complutense de Madrid (UCM), Madrid, Spain; Department of Psychology, Faculty of health, University Camilo José Cela (UCJC), Madrid, Spain
Danylyna Shpakivska – Center for Cognitive and Computational Neuroscience (C3N), Universidad Complutense de Madrid (UCM), Madrid, Spain
Marcos Uceta – Center for Cognitive and Computational Neuroscience (C3N), Universidad Complutense de Madrid (UCM), Madrid, Spain
Ricardo Bruña – Center for Cognitive and Computational Neuroscience (C3N), Universidad Complutense de Madrid (UCM), Madrid, Spain; Departamento Radiología, Rehabilitación y Fisioterapia. Universidad Complutense de Madrid (UCM), Madrid, Spain
Fernando Maestú – Center for Cognitive and Computational Neuroscience (C3N), Universidad Complutense de Madrid (UCM), Madrid, Spain; Departamento de Psicología experimental, Universidad Complutense de Madrid (UCM), Madrid, Spain
Luis Miguel García-Moreno – Departamento de Psicobiología y Metodología en Ciencias del Comportamiento, Universidad Complutense de Madrid (UCM), Spain

Citation
del Cerro-León, A., Antón-Toro, L.F., Shpakivska, D., Uceta, M., Bruña, R., Maestú, F., García-Moreno, L.M. *Rest in Binge:* An exploration of the effects of alcohol consumption during adolescent neurodevelopment.

Introduction/Motivation

Alcohol is a psychoactive drug capable of depressing the central nervous system (CNS), with its effects varying according to the dose ingested, genetic factors and the drinker's previous experience. Generally, it involves a slowing down of brain functions and the capacity for self-control. In addition, alcohol is one of the most widely consumed drugs and the one that causes the highest social and health costs. Since 2000, the percentage of alcohol drinkers has decreased by 5%, while total alcohol per capita among drinkers has increased from 11.5 liters in 2005 to 15.1 liters in 2016 showing an overall increase. These facts show that despite the decline in total drinkers, drinking patterns are becoming increasingly dangerous [1]. In this context, heavy alcohol consumption or binge drinking (BD) has become a widespread habit among adolescents [1,2] despite its detrimental effects on the anatomical-functional integrity of the brain, especially in executive control networks [3]. This pattern of consumption is of particular concern during adolescence, as the neurotoxic effects of alcohol can alter the normal neuromaturational course, causing deficits in the neuroanatomical [4,5] and neurofunctional integrity of young people [6]. However, recent findings of brain abnormalities in pre-consumption stages have made it difficult to separate the predisposing features from the effects of alcohol consumption. Thus, we proposed a longitudinal magnetoencephalography study to assess potential differences in brain activation associated with inhibitory control processes during the neurodevelopment of BD in adolescents.

Methods

In the first stage, we recorded the electrophysiological activity of 67 non-consuming adolescents (mean age = 14.6 $\pm$ 0.7) during a go no-go task. Subsequently, a total of 33 participants (mean age 16.7 $\pm$ 0.7) completed the second phase of the study, where we again recorded brain activity under the same conditions and divided the sample according to their drinking habits (measured by the *Alcohol use disorders identification test* (AUDIT) [7]). From the recorded electrophysiological signal, a preprocessing was performed to eliminate artifacts and noisy components in the signal. Then the clean data was reconstructed at the cortical source level using the linear Constrained

Minimum Variance (LCMV) beamformer method [8]. Subsequently, the power spectra was calculated using the *discrete prolate spheroidal (Slepian) sequences* (dpss) for each source and frequency band (theta, alpha, beta and gamma). To measure the change in power between phases of the study, the ratio of change in power was used as Power_post/Power_pre. These values were then compared between groups using a cluster-based permutations test (CBPT) [9] The power values of each source were compared between subjects using a Spearman Correlation test with level of alcohol consumption using the age and sex as factors. The resulting p-values were selected based on an alpha value of 0.05 and contiguous sources were grouped as members of the same cluster. The overall statistic of each cluster is calculated as the sum of all F-values of its members. Subsequently, the null distribution of clusters was re-approximated over 50000 random partitions of the original data. Once completed, the p-value of each cluster was calculated according to this null distribution.

Results and discussion

Our results, in line with the findings present in the literature, suggest that subjects who develop BD in later stages present neurofunctional abnormalities in stages prior to consumption, which may reflect possible predisposing traits. In this scenario, we found that in the first phase of the study, power between 33-43 Hz was positively correlated with future consumption levels within a cluster located in the precuneus and middle cingulate cortex (Figure 1). With respect to these results, other studies have found that despite no change in task performance there is an increased activation of regions responsible for inhibitory control in conjunction with the activation of unrelated regions. In response to these findings, different hypotheses have been proposed, such as compensatory mechanisms [10]. However, it should be noted that the changes that occur within brain networks during adolescent neurodevelopment lead to a reduction in power [11], which could indicate that the neurophysiological differences obtained as a function of consumption are reflecting asynchronies in brain maturational processes.

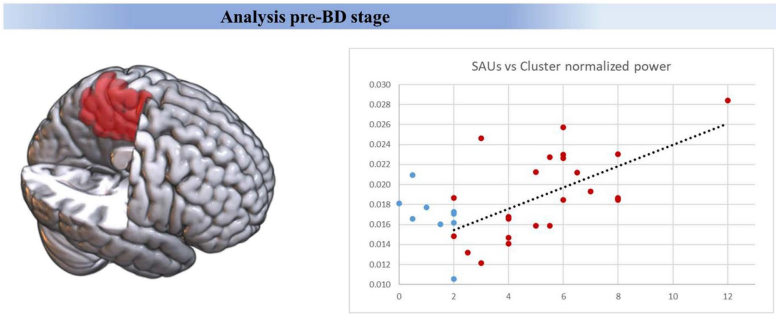

FIGURE 1
Prior to alcohol consumption, the CBPT test showed in the BD group a significant bilateral cluster in the middle cingulate and superior parietal gyrus. This cluster showed a positive correlation between the power of 33 to 43 Hz and future consumption levels ($p<0.05$, rho=0.65).

In order to observe the differences produced throughout the study, the differences in the rate of change were evaluated according to consumption levels. In this analysis we obtained that the gamma power (30-43 Hz) of a cluster formed by regions such as the precuneus, anterior and medial cingulate cortex showed a rate of change with an inverse correlation to consumption levels (Figure 2). These results indicate that during the two years of follow-up there was a decrease in power in this cluster, which presents great similarities with the differences found in the first phase of the study. Taken together, these correlations could indicate that there is a neuromaturational delay in these regions that causes subjects with higher consumption to decrease their potency at later ages than non-consuming subjects. In addition, these maturational changes could be affected by the consumption itself, promoting differences in future brain activation profiles as reflected in studies at later stages of development [12]. Thus, we conclude that there are asynchronies in the brain development of adolescents before initiation of drug use. Subsequently, the consumption of this substance could be generating neurodevelopmental consequences in addition to the alterations prior to consumption, causing sustained neurofunctional alterations throughout adolescence.

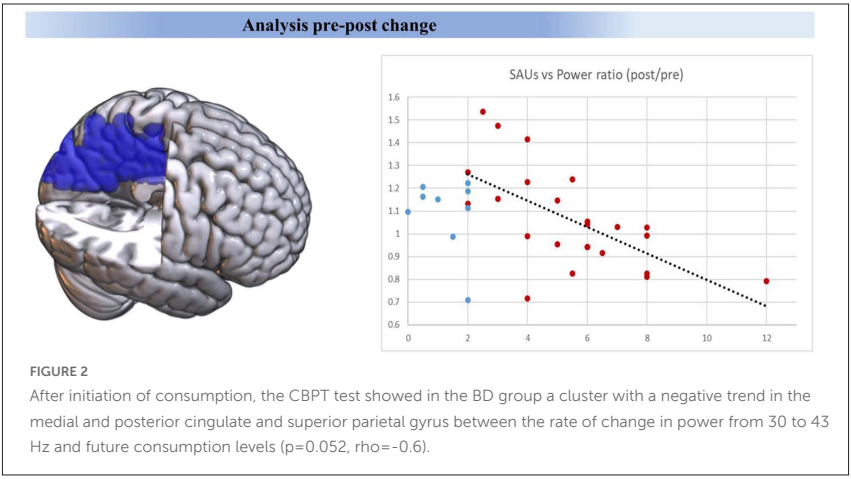

FIGURE 2
After initiation of consumption, the CBPT test showed in the BD group a cluster with a negative trend in the medial and posterior cingulate and superior parietal gyrus between the rate of change in power from 30 to 43 Hz and future consumption levels (p=0.052, rho=-0.6).

References

[1] Hammer, J. H., Parent, M. C., Spiker, D. A., & World Health Organization. (2018). Global status report on alcohol and health 2018. In *Global status report on alcohol* (Vol. 65, Issue 1). https://doi.org/10.1037/cou0000248

[2] Leal-López, E., Sánchez-Queija, I., Rivera, F., & Moreno, C. (2019). Tendencias en el consumo de alcohol en adolescentes escolarizados en España (2010-2018). *Gaceta Sanitaria*. https://doi.org/10.1016/j.gaceta.2019.07.011

[3] Herman, A. M., & Duka, T. (2019). Facets of impulsivity and alcohol use: What role do emotions play? *Neuroscience and Biobehavioral Reviews*, *106*(January), 202–216. https://doi.org/10.1016/j.neubiorev.2018.08.011

[4] Heikkinen, N., Niskanen, E., Könönen, M., Tolmunen, T., Kekkonen, V., Kivimäki, P., Tanila, H., Laukkanen, E., & Vanninen, R. (2017). Alcohol consumption during adolescence is associated with reduced grey matter volumes. *Addiction*, *112*(4), 604–613. https://doi.org/10.1111/add.13697

[5] Sousa, S. S., Sampaio, A., Marques, P., Gonçalves, Ó. F., & Crego, A. (2017). Gray matter abnormalities in the inhibitory circuitry of Young Binge drinkers: A voxel-based morphometry study. *Frontiers in Psychology*, *8*(SEP), 1–8. https://doi.org/10.3389/fpsyg.2017.01567

[6] Correas, A., Cuesta, P., López-Caneda, E., Rodríguez Holguín, S., García-Moreno, L. M., Pineda-Pardo, J. A., Cadaveira, F., & Maestú, F. (2016). Functional and structural brain connectivity of young binge drinkers: A follow-up study. *Scientific Reports*, *6*(September). https://doi.org/10.1038/srep31293

[7] Guillamón C, Solé G, Farran C. Test para la identificación de transtornos por uso de alcohol (AUDIT): Traducción y validación del AUDIT al catalán y castellano. Adicciones. 1999;11(1):347.

[8] Nolte G. The magnetic lead field theorem in the quasi-static approximation and its use for magnetoenchephalography forward calculation in realistic volume conductors. Phys Med Biol. 2003;48(22):3637–52.

[9] Oostenveld R, Fries P, Maris E, Schoffelen J-M. FieldTrip: Open Source Software for Advanced Analysis of MEG, EEG, and Invasive Electrophysiological Data. Comput Intell Neurosci. 2011;2011:1–9.

[10] Squeglia LM, Schweinsburg AD, Pulido C, Tapert SF. Adolescent Binge Drinking Linked to Abnormal Spatial Working Memory Brain Activation: Differential Gender Effects. Alcohol Clin Exp Res. 2011 Oct;35(10):1831–41.

[11] Stevens MC, Pearlson GD, Calhoun VD. Changes in the interaction of resting-state neural networks from adolescence to adulthood. Hum Brain Mapp. 2009;30(8):2356–66

[12] Correas A, Cuesta P, López-Caneda E, Rodríguez Holguín S, García-Moreno LM, Pineda-Pardo JA, et al. Functional and structural brain connectivity of young binge drinkers: A follow-up study. Sci Rep. 2016 Sep;6.

Prevention of α-synuclein misfolding using the anti-amyloidogenic peptide QBP1 as a promising therapy for Parkinson's disease

Author
María M Tejero-Ojeda – Department of Molecular, Cell, and Developmental Neurobiology, Cajal Institute (CSIC), Madrid, Spain
Rubén Hervás – School of Biomedical Sciences at The University of Hong Kong
Javier Oroz – Department of Biological Physical Chemistry, Institute of Physical Chemistry "Rocasolano" (IQFR), Madrid, Spain
Mariano Carrión-Vázquez. – Department of Molecular, Cell, and Developmental Neurobiology, Cajal Institute (CSIC), Madrid, Spain

Citation
Tejero-Ojeda, M.M., Hervás, R., Oroz, J., Carrión-Vázquez, M. Prevention of α-synuclein misfolding using the anti-amyloidogenic peptide QBP1 as a promising therapy for Parkinson's disease.

Introduction/Motivation

Protein misfolding and aggregation in the brain have been recognized to be critical in the pathogenesis of Alzheimer's (AD) or Parkinson's disease (PD), but the specific molecular events underlying this process remain unclear[1]. A neuropathological hallmark of PD is the presence of aggregates called Lewy bodies, in which presynaptic α-synuclein (αSyn) is a major component. αSyn is an intrinsically disordered protein that, under certain conditions,

transitions from a soluble monomer to toxic oligomeric and fibrillar species[2]. Furthermore, mutations such as E46K, A30P and A53T in the α-syn gene are identified to cause autosomal-dominantly inherited forms of PD, in which the αSyn aggregation propensity is increased. Significant efforts have been made to develop different amyloid inhibitors since they are ideal tools towards the modulation and treatment of these currently incurable diseases, but they are so far ineffective. Here, we test the effect of the anti-amyloidogenic peptide QBP1[3] as a therapeutic approach for PD by characterizing the aggregation behaviour of both, wildtype form and αSyn mutants, in the presence of QBP1.

Methods

The lack of a well-defined structure as well as the high tendency of these proteins to aggregate make them difficult to study using conventional techniques. In this work, we used atomic force spectroscopy (AFM-SMFS) to analyse the conformational polymorphism of αSyn at the single-molecule level. This technique allows us to identify the proportion of mechanostable conformers (M) adopted by this protein, which are associated with toxicity and disease[4]. Furthermore, we complemented this methodology with an array of *in vitro* techniques to characterize its amyloidogenic pathway: Thioflavin-T (ThT) fluorescence assay, conformational immunoassay methods, electron microscopy visualization and analysis of the human αSyn preformed fibrils (hPFF) effect on neuronal-like SH-SY5Y cells. We performed immunoblotting and immunofluorescence analyses to study whether SH-SY5Y human neuroblastoma-derived cells were able to internalize hPFF. Finally, we analysed whether these protofibrils initiated the conversion of monomeric αSyn towards the pathogenic conformation by seeding the formation of inclusions through templating, as well as if they induced intracellular accumulation of the pS129-αSyn pathogenic form.

Results and discussion

Our preliminary results showed the ability of QBP1 to inhibit in vitro the αSyn amyloid formation. Specifically, we found that QBP1 can block the formation of mechanostable conformers associated to pathology (M), including hyper-mechanostable forms (hM) (Fig1.A). It also abolished in

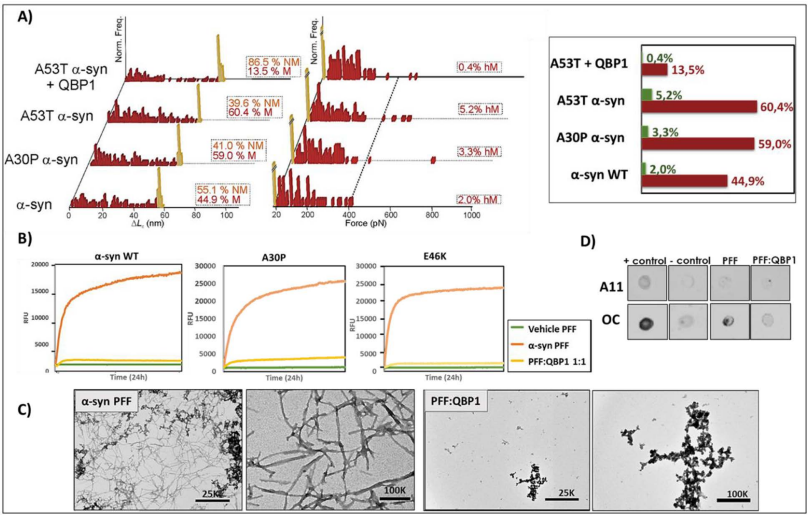

FIGURE 1

Aggregation behaviour of αSyn WT and autosomal dominant PD variants (E46K, A30P and A53T) by AFM-SMFS and techniques to characterize the amyloid pathway, in the presence of the anti-amyloidogenic peptide QBP1. A) Nanomechanical analysis of α-synuclein. The wildtype protein shows a wide-range polymorphism ranging from NM conformers to M conformers (red bars), including some hyper-mechanostable conformers (green bars). Familial-disease mutations A30P and A53T increase the frequency of M and hM conformers of α-synuclein when compared to the wt form. Treatment with QBP1 peptide lowers the formation of M (including the hM) conformers in A53T α-synuclein. B) 24 hours' time-course of αSyn aggregate formation monitored by ThT binding assay. C) Monitoring preformed α-Syn fibrils after 7 days of incubation (at 37 °C and 1000 rpm) by transmission electron microscopy and by using conformational antibodies A-11 and OC (D). The amyloidogenic αSyn aggregation was lowered using just equimolar amounts of QBP1 (A-D).

vitro the formation of preformed fibrils (PFFs)5, lowering cellular toxicity (Fig1.B-D). Immunoblotting and immunofluorescence analysis showed that SH-SY5Y human cells internalise less hPFF and show a lesser amount of the pS129-αSyn pathogenic form in the presence of QBP1. These results suggesting a promising aggregation inhibitor leading to a disease-modifying therapy that will tackle in the future both the onset and progression of the disease. To further progress in these preclinical studies, our objective is

to design a suitable QBP1 delivery system (nanoencapsulated) capable of bypassing the blood brain barrier (BBB), which could be administered and tested in a rodent's PD model6. As an PD's animal model we propose a single intracerebral injection of PFFs in non-transgenic rodents, as it results in time-dependent αSyn aggregation[6] and accumulation in anatomically-interconnected brain areas[7]. Finally, by modelling multi-level QBP1-protein interaction (using a proteomic approach to integrate in vitro and in vivo results) we will develop a deep-learning framework[8] for prediction of future scenarios in order to avoid side effects and more precise treatments so that we can make a step forward to modern clinical translation. We expect that our project will demonstrate QBP1 as a promising PD-modifying therapy for halting the onset and progression of PD.

References

[1] Knowles T, Vendruscolo M, & Dobson C. (2014). The amyloid state and its association with protein misfolding diseases. *Nat Rev Mol Cell Biol.* 15.

[2] Pajares M, *et al*. (2020). Inflammation in Parkinson's Disease: Mechanisms and Therapeutic Implications. *Cells*. 9 (7).

[3] Popiel HA, Takeuchi T, Burke JR, Strittmatter WJ, Toda T, Wada K, Nagai Y. (2013). Inhibition of protein misfolding/aggregation using polyglutamine binding peptide QBP1 as a therapy for the polyglutamine diseases. *Neurotherapeutics*. 10 (3).

[4] Hervas R, Oroz J, Galera-Prat A, Goñi O, Valbuena A, Vera AM, Gómez-Sicilia A, Losada-Urzáiz F, Uversky V, Menéndez M, Laurents DV, Bruix M, Carrión-Vázquez M. (2012). Common features at the start of the neurodegeneration cascade. *PLOS Biol.* 10 (1-32)

[5] Patterson JR, *et al.* (2019). Generation of Alpha-Synuclein Preformed Fibrils from Monomers and Use *in Vivo*. *J. Vis. Exp*., 148.

[6] Luk KC, Kehm V, Carroll J, Zhang B, O'Brien P, Trojanowski JQ, & Lee VM. (2012). Pathological α-synuclein transmission initiates Parkinson-like neurodegeneration in nontransgenic mice. *Science (New York, N.Y.),* 338 (6109).

[7] Paumier KL, Luk KC, Manfredsson FP, Kanaan NM, Lipton JW, Collier TJ, Steece-Collier K, Kemp CJ, Celano S, Schulz E, Sandoval IM, Fleming S, Dirr E, Polinski NK, Trojanowski JQ, Lee VM, & Sortwell CE. (2015). Intrastriatal injection of pre-formed mouse α-synuclein fibrils into rat's triggers α-synuclein pathology and bilateral nigrostriatal degeneration. *Neurobiology of disease*, 82 (185–199).

[8] Lei Y, Li S, Liu Z, Wan F, Tian T, Li S, Zhao D, Zeng J. (2021). A deep-learning framework for multi-level peptide-protein interaction prediction. *Nature Communication,* 12.

Usually, I don't ruminate, only from time to time: The predictive value of trait and state measures of rumination for the intensity of affective states

Author
Flóra Hann – Department of Cognitive Science, University of Technology and Economics, Budapest, Hungary
Levente Rónai – Department of Cognitive Science, University of Technology and Economics, Budapest, Hungary; Institute of Psychology, University of Szeged, Szeged, Hungary
Szabolcs Kéri – Department of Cognitive Science, University of Technology and Economics, Budapest, Hungary; National Institute of Mental Health, Neurology and Neurosurgery – Nyírő Gyula Hospital, Budapest, Hungary
Bertalan Polner – Institute of Psychology, ELTE, Eötvös Loránd University, Budapest, Hungar

Citation
Hann, F., Rónai, L., Kéri, S., Polner, B. Usually, I don't ruminate, only from time to time: The predictive value of trait and state measures of rumination for the intensity of affective states.

Introduction/Motivation

Emotions and their flexible regulation are essential in adapting to our environment [1]. People differ significantly in their ability to regulate their emotions, and research has traditionally focused on these differences between individuals [2,3]. However, evidence emerges that traditional

laboratory measures capturing trait emotion regulation may not correspond to emotion regulation ability in real life [4]. These processes appear to show different variability between and within individuals, implying that characteristics regarded as traits in psychology – e.g., emotion regulation strategy use – may not reflect everyday functioning [5,6]. Correspondingly, recent research reported weak correlations between trait and state emotion regulation [7,8].

One of the most extensively researched emotion regulation strategies is rumination, a cognitive process that involves repeatedly and passively dwelling on negative feelings and their consequences [9]. Rumination is a putatively maladaptive strategy [10,11], and recent work argues that it intensifies stress responses and symptoms of psychopathology by extending and amplifying negative affect and interfering with proactive cognition and behavior [12].

A suitable indicator to measure the effectiveness of emotion regulation, as done in previous research [2], is emotional reactivity, the emotional reactions experienced in response to a negative occurrence [13]. Besides being a robust correlate for poor mental health [14,15], evidence supports that increased state (but not trait) rumination is associated with higher emotional reactivity [7]. However, based on the evidence about variabilities of certain constructs differing within and between individuals, as described above, the within-person examination of rumination may predict emotional reactivity even more accurately.

Based on the above, we assumed that trait indicators of rumination will not display a strong correlation with momentary rumination aggregates (Hypothesis 1).

The main aim of this study was to confirm that momentary rumination use has a substantial predictive value for emotional reactivity within the same time window (Hypothesis 2a). We also expected that the aggregated mean of these momentary rumination measures will also be associated with

emotional reactivity, although not as strongly (Hypothesis 2b). We expected trait rumination to have the lowest predictive value for emotional reactivity in daily life (Hypothesis 2c).

Additionally, since rumination is generally regarded as a putatively maladaptive emotion regulation strategy we expected rumination measures to have independent predictive values for momentary negative affect, regardless of perceived stress. Based on the reasoning above, we anticipate that these measures will show the same pattern (momentary > average state-level > trait questionnaire) in the prediction of negative affect as in the prediction of emotional reactivity (Hypotheses 3a,3b,3c).

Methods

Our sample comprised 247 individuals (N[female] = 198, Mean[age] = 38.38 years, SD[age] = 12.86 years, Range[age] = 19-73 years) recruited from the general population through the press and social media. First, they completed a baseline assessment including trait-like measures such the Cognitive Emotion Regulation Questionnaire [16]. Then, they spent up to 28 days in the Experience Sampling Method [17–19] phase of the study where they received 8 short surveys every day assessing their momentary affective states, emotion regulation, and perceived stress. 14,265 observations were obtained (per capita: Median = 45, Obs. Range = 1-197, Theor. Range = 1-224).

We ran a Spearman correlation analysis to examine the association between trait and aggregated state measures of rumination (Hypothesis 1). To test our second and third sets of hypotheses, we fitted a linear mixed-effects model (using *lme4* in R) with random intercepts and slopes for the interaction of perceived stress and negative affect per participant. A momentary negative affect composite score obtained with multilevel confirmatory factor analysis was the dependent variable. Perceived stress, the three different measures of rumination, and their interactions were entered in order to test the prediction of negative affect (main effects of rumination variables) and moderation on emotional reactivity (rumination x perceived stress interactions).

Results and discussion

First, we found only a moderate positive correlation ($r_s(245) = 0.46$, $p < 0.001$, 95% CI [0.36, 0.55]) between trait and state rumination indicators (Hypothesis 1). One may expect a higher correlation between indicators of the same construct. Certain psychometric and contextual differences could account for this result, as well as the different self-report techniques tapping different sources of self-related information.

Turning to the prediction of emotional reactivity, we found that state, aggregated mean state, and trait measures all had significant independent effects on emotional reactivity (Hypotheses 2a,b,c). However, the magnitude of these effects overlapped, and therefore, the importance of the measures could not be ranked (see Figure 1).

On the other hand, when we looked at the main effects on negative affect (Hypotheses 3a,b,c), the mean of state measures of rumination emerged

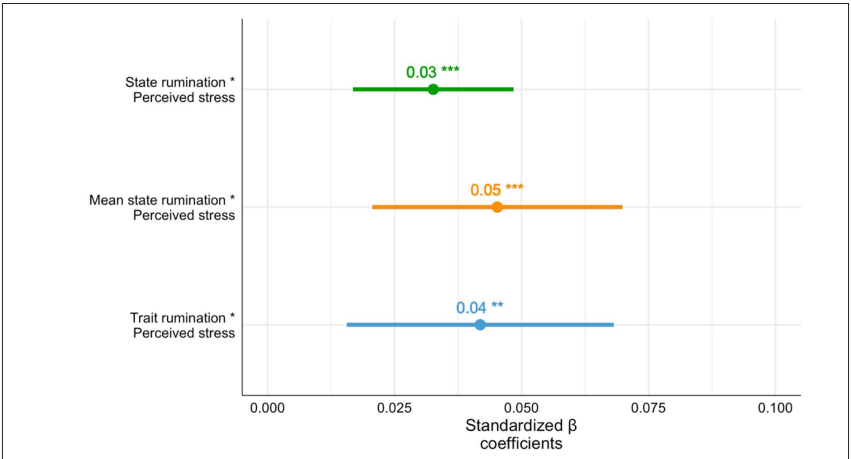

FIGURE 1
Standardized β coefficients indicating the moderation of emotional reactivity by different measures of rumination. Error bars show 95% confidence intervals.

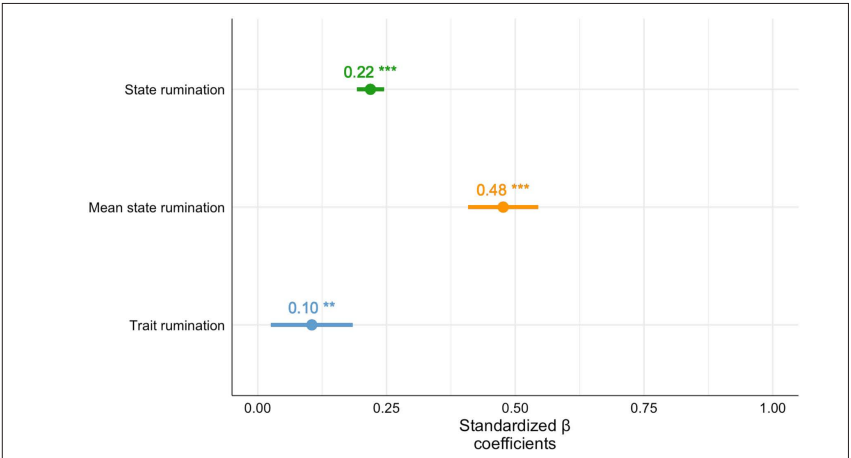

FIGURE 2
Standardized β coefficients indicating the prediction of negative affect by different measures of rumination. Error bars show 95% confidence intervals.

as the strongest predictor (see Figure 2). This composite indicator can essentially be considered a trait measure to some degree (as it captures the typical level of rumination in a given period), however, it incorporates the everyday variability of rumination within an individual; thus, it differs from traditional, self-report trait measures that can be subject to recall bias and lower ecological validity. Therefore, it could be regarded as a measurement 'halfway between' trait and state indicators that could possibly combine the advantages of both, thereby having the best incremental validity in predicting emotional reactivity.

In conclusion, our findings provide valuable insight for understanding the within-individual dynamics of emotion regulation and their relationship to stress and affectivity, nuancing the common trait approach and overcoming some of its limitations. Thereby, our results corroborate the need to re-evaluate the traditional measurement of psychological constructs based on single-shot retrospective self-assessments [5,6]. Trait conceptualization

and assessment is also relevant for the cognitive neuroscientific study of individual differences, which are often based on analyzing correlations between behavioral traits and neuroscientific measures.

Additionally, our findings have clinically relevant, practical implications for the personalized prediction of emotional responses to stress through simple self-report tools applicable in everyday contexts [see 20].

References

[1] Gross JJ. Emotion Regulation: Current Status and Future Prospects. Psychological Inquiry. 2015;26(1):1–26. doi:10.1080/1047840X.2014.940781

[2] Blanke ES, Brose A, Kalokerinos EK, Erbas Y, Riediger M, Kuppens P. Mix it to fix it: Emotion regulation variability in daily life. Emotion. 2020;20(3):473–485. doi:10.1037/emo0000566

[3] Wang X, Blain SD, Meng J, Liu Y, Qiu J. Variability in emotion regulation strategy use is negatively associated with depressive symptoms. Cognition and Emotion. 2021;35(2):324–340. doi:10.1080/02699931.2020.1840337

[4] Aldao A, Sheppes G, Gross JJ. Emotion Regulation Flexibility. Cognitive Therapy and Research. 2015;39(3):263–278. doi:10.1007/s10608-014-9662-4

[5] Fisher AJ, Medaglia JD, Jeronimus BF. Lack of group-to-individual generalizability is a threat to human subjects research. Proceedings of the National Academy of Sciences. 2018;115(27):E6106–E6115. doi:10.1073/pnas.1711978115

[6] Enkavi AZ, Eisenberg IW, Bissett PG, Mazza GL, MacKinnon DP, Marsch LA, Poldrack RA. Large-scale analysis of test–retest reliabilities of self-regulation measures. Proceedings of the National Academy of Sciences. 2019;116(12):5472–5477. doi:10.1073/pnas.1818430116

[7] Hilt LM, Aldao A, Fischer K. Rumination and multi-modal emotional reactivity. Cognition and Emotion. 2015;29(8):1486–1495. doi:10.1080/02699931.2014.989816

[8] Brockman R, Ciarrochi J, Parker P, Kashdan T. Emotion regulation strategies in daily life: mindfulness, cognitive reappraisal and emotion suppression. Cognitive Behaviour Therapy. 2017;46(2):91–113. doi:10.1080/16506073.2016.1218926

[9] Nolen-Hoeksema S, Wisco BE, Lyubomirsky S. Rethinking Rumination. Perspectives on Psychological Science. 2008;3(5):400–424. doi:10.1111/j.1745-6924.2008.00088.x

[10] Aldao A, Nolen-Hoeksema S. Specificity of cognitive emotion regulation strategies: A transdiagnostic examination. Behaviour Research and Therapy. 2010;48(10):974–983. doi:10.1016/j.brat.2010.06.002

[11] Aldao A, Nolen-Hoeksema S. When are adaptive strategies most predictive of psychopathology? Journal of Abnormal Psychology. 2012;121(1):276.

[12] Watkins ER, Roberts H. Reflecting on rumination: Consequences, causes, mechanisms and treatment of rumination. Behaviour Research and Therapy. 2020;127:103573. doi:10.1016/j.brat.2020.103573

[13] Thompson RJ, Mata J, Jaeggi SM, Buschkuehl M, Jonides J, Gotlib IH. The everyday emotional experience of adults with major depressive disorder: Examining emotional instability, inertia, and reactivity. Journal of Abnormal Psychology. 2012;121(4):819–829. doi:10.1037/a0027978

[14] Myin-Germeys I, van Os J, Schwartz JE, Stone AA, Delespaul PA. Emotional Reactivity to Daily Life Stress in Psychosis. Archives of General Psychiatry. 2001;58(12):1137. doi:10.1001/archpsyc.58.12.1137

[15] Myin-Germeys I, Peeters F, Havermans R, Nicolson NA, DeVries MW, Delespaul P, Van Os J. Emotional reactivity to daily life stress in psychosis and affective disorder: an experience sampling study: Emotional reactivity. Acta Psychiatrica Scandinavica. 2003;107(2):124–131. doi:10.1034/j.1600-0447.2003.02025.x

[16] Garnefski N, Kraaij V, Spinhoven P. Negative life events, cognitive emotion regulation and emotional problems. Personality and Individual Differences. 2001;30(8):1311–1327. doi:10.1016/S0191-8869(00)00113-6

[17] Csikszentmihalyi M, Larson R. Validity and reliability of the experience-sampling method. In: Csikszentmihalyi M, editor. Flow and the Foundations of Positive Psychology: The Collected Works of Mihaly Csikszentmihalyi. Springer; 2014. p. 35–54.

[18] Myin-Germeys I, Oorschot M, Collip D, Lataster J, Delespaul P, van Os J. Experience sampling research in psychopathology: opening the black box of daily life. Psychological Medicine. 2009;39(9):1533–1547. doi:10.1017/S0033291708004947

[19] Myin-Germeys I, Kasanova Z, Vaessen T, Vachon H, Kirtley O, Viechtbauer W, Reininghaus U. Experience sampling methodology in mental health research: new insights and technical developments. World Psychiatry. 2018;17(2):123–132. doi:10.1002/wps.20513

[20] Hitchcock PF, Fried EI, Frank MJ. Computational Psychiatry Needs Time and Context. Annual Review of Psychology. 2022;73:243–270.

Positive schizotypy predicts increased susceptibility to the Müller-Lyer visual illusion

Author
Orsolya Lányi – Department of Cognitive Science, Budapest University of Technology and Economics, Budapest, Hungary; Department of Psychiatry and Psychotherapy, Semmelweis University, Budapest, Hungary
Szabolcs Kéri – Department of Cognitive Science, Budapest University of Technology and Economics, Budapest, Hungary; National Institute of Mental Health, Neurology and Neurosurgery - Nyírő Gyula Hospital, Budapest, Hungary
Zsófia Pálffy – Department of Cognitive Science, Budapest University of Technology and Economics, Budapest, Hungary
Bertalan Polner – Department of Cognitive Science, Budapest University of Technology and Economics, Budapest, Hungary

Citation
Lányi, O., Kéri, S., Pálffy, Z., Polner, B. Positive schizotypy predicts increased susceptibility to the Müller-Lyer visual illusion.

Introduction and Hypothesis

Visual illusions provide a unique opportunity to understand cognitive and perceptual alterations in schizophrenia-spectrum conditions[1]. A tendency of decreased susceptibility to visual illusions has been widely reported among patients living with schizophrenia[2], which results are in line with visual perceptual deficits present in the schizophrenia-spectrum conditions[3]memory, and executive functioning. To date, less work has focused on perceptual processing. However, perceptual functions are frequently disrupted in schizophrenia, and thus this domain has been included in the CNTRICS (Cognitive Neuroscience Treatment Research

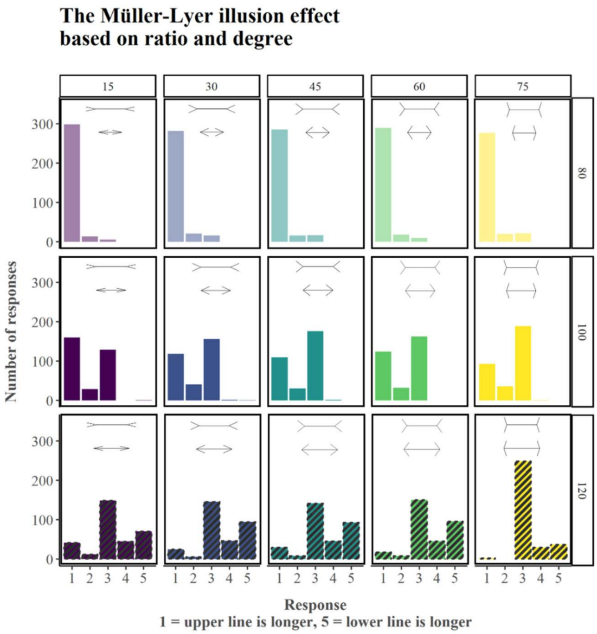

FIGURE 1

The 15 Müller-Lyer conditions (3 ratio x 5 degree) designed for the research and the distribution of the responses representing susceptibility. Susceptibility in the ratio-100% was calculated as response <3, and in the ratio-120% condition response <= 3.

to Improve Cognition in Schizophrenia. Research results concerning one specific visual illusion, the Müller-Lyer illusion contradicts this tendency. It is a well-established visual illusion where two lines identical in length are perceived to be different when arrow-heads and -tails are shown at the end of each line (for examples please see Figure 1.). Critically, it is unclear why most studies reported an increased Müller-Lyer effect in schizophrenia[4–7]using methods such as contrast sensitivity. Higher, integrative stages of functioning, such as susceptibility to visual illusions, have been evaluated less extensively. For example, patients show increased susceptibility to (ie, are more easily affected by.

The aim of this research is to resolve this contradiction. Here, we broadened our perspective to the psychosis-spectrum and studied the illusion magnitude in relation to positive schizotypal traits and anomalous perceptions in a population-based sample. Schizotypy is a useful construct for testing neurocognitive models of schizophrenia symptoms in a dimensional framework, since positive schizotypy and anomalous perceptions are closely associated with psychosis-proneness[8–10]child and adult social adversity, psychoactive drug use, and also male sex and migrant status. The small difference between prevalence and incidence rates, together with data from follow-up studies, indicates that approximately 75-90% of developmental psychotic experiences are transitory and disappear over time. There is evidence, however, that transitory developmental expression of psychosis (psychosis proneness. We hypothesized that anomalous perceptions and positive schizotypal traits predict a greater Müller-Lyer effect.

Methods

Data of 390 participants were collected through an online survey platform (formr) and participants were recruited through Facebook advertisement. Participants completed the Müller-Lyer illusion, the Cardiff Anomalous Perceptions Scale (CAPS)[11]a new validated measure of perceptual anomalies. The 32-item CAPS measure is a reliable, self-report scale, which uses neutral language, demonstrates high content validity, and includes subscales that measure distress, intrusiveness, and frequency of anomalous experience. The CAPS was completed by a general population sample of 336 participants and 20 psychotic inpatients. Approximately 11% of the general population sample scored above the mean of the psychotic patient sample, although, as a group, psychotic inpatients scored significantly more than the general population on all CAPS subscales. A principal components analysis of the general population data revealed 3 components: "clinical psychosis" (largely Schneiderian first-rank symptoms and the Multidimensional Schizotypy Scale – Brief (MSS-B)[12]. In order to control for bias and increase the predictive value of the Müller-Lyer illusion, the parameters of the illusions (angle of the arrows: 15°/30°/45°/60°/75°; ratio of shaft length: 80%/100%/120%) were

varied, yielding 15 illusion conditions (see Figure 1.) Participants reported their perception on a 5-point Likert-scale (1 = top line is longer; 5 = bottom line is longer).

To ensure data quality, we excluded participants 1.) who reported using any kind of help (e.g. a ruler) when responding to the illusions (N = 42), 2.) who gave a wrong response in the *ratio-80%* condition (Figure 1, top row), which served as a control condition as the correct response (top line is longer) is obvious here (N = 29) 3.) above the age of 60, in order to avoid confounding by aging-related schizotypy-like alterations (N = 6). 312 participants were included in the analysis (females N = 219, mean age [SD] = 46.5 [9.57], mean [SD] of MSS-B positive schizotypy = 2.53 [2.5]).

Data was analyzed in R. We fitted multilevel logistic regression models using the lme4 package. The dependent variable was a binary variable of susceptibility indicating the presence of the illusion effect on a given trial. To account for the nested property of our data, a random intercept for participants was used to measure between-subject variance in susceptibility, while a random slope for ratio conditions was used to capture variability across subjects in the influence of ratio manipulation on the illusion effect. The set of predictor variables included the CAPS score, MSS-B subscores, and also age, gender, smoking and device (laptop/smartphone/desktop) as control variables. We constructed 15 models with various, theoretically plausible combinations of these predictors. We pooled information from these models using an information theoretical model averaging over coefficients[13]. Models were weighed by their goodness-of-fit (corrected Akaike Information Criterion). A coefficient was set to zero with zero variance if the predictor was not included in a given model (full average approach, which effectively shrinks coefficients).

Results

The distribution of responses in different illusion conditions (Figure 1.) confirmed the role of multiple illusion variations in data quality control. Coefficient estimates obtained from model averaging (Figure 2.) shows that

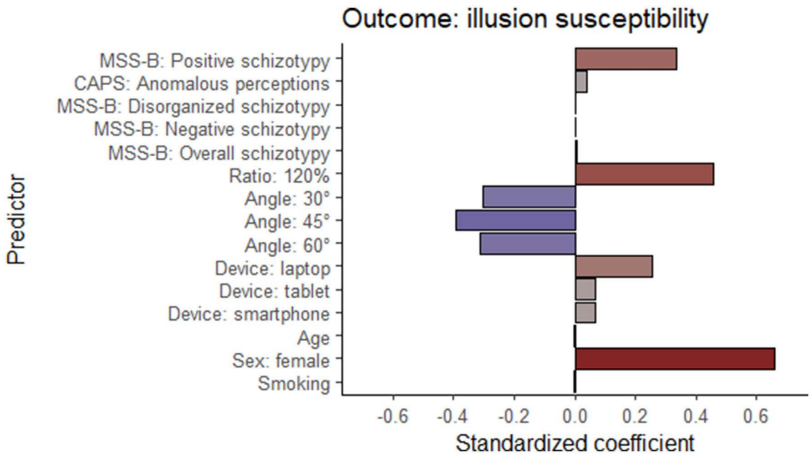

FIGURE 2
Predictors of susceptibility to the Müller-Lyer illusion according to logistic mixed effects modeling. Estimates are based on model averaging, using the full average approach. CAPS: total score on the Cardiff Anomalous Perceptions Scale ; MSS-B: Multidimensional Schizotypy Scale - Brief total score and score of subscales (positive, negative and disorganized schizotypy).

participants were more susceptible to the illusion in the ratio-120% condition (vs ratio-100%), while increasing angle had a nonlinear effect (increased illusion effect in each angle larger than the 15° baseline). Importantly, the results support our hypothesis of increased illusion susceptibility among individuals with high positive schizotypy. The effect was comparable in magnitude to that of angle and ratio. However, anomalous perceptions, negative and disorganized schizotypy (as well as schizotypy total scores) did not predict an enhanced illusion effect.

Discussion

Our results can be interpreted in the predictive coding framework of the psychosis-spectrum14there has been increasing interest in the underlying neurocomputational mechanisms of psychosis. One successful approach

involves predictive coding and Bayesian inference. Here, inferences regarding the current state of the world are made by combining prior beliefs with incoming sensory signals. Mismatches between prior beliefs and incoming signals constitute prediction errors that drive new learning. Psychosis has been suggested to result from a decreased precision in the encoding of prior beliefs relative to the sensory data, thereby garnering maladaptive inferences. Here, we review the current evidence for aberrant predictive coding and discuss challenges for this canonical predictive coding account of psychosis. For example, hallucinations and delusions may relate to distinct alterations in predictive coding, despite their common co-occurrence. More broadly, some studies implicate weakened prior beliefs in psychosis, and others find stronger priors. These challenges might be answered with a more nuanced view of predictive coding. Different priors may be specified for different sensory modalities and their integration, and deficits in each modality need not be uniform. Furthermore, hierarchical organization may be critical. Altered processes at lower levels of a hierarchy need not be linearly related to processes at higher levels (and vice versa. We argue that the enhanced Müller-Lyer effect in high positive schizotypy could be explained by increased reliance on prior expectations during higher-level perceptual processing. As anomalous perceptions did not predict illusion susceptibility, the association might be specific to delusion-like beliefs and magical ideation. Even though empirical evidence supports the assumption of stronger priors in positive symptoms of schizophrenia and schizotypy[14–16] there has been increasing interest in the underlying neurocomputational mechanisms of psychosis. One successful approach involves predictive coding and Bayesian inference. Here, inferences regarding the current state of the world are made by combining prior beliefs with incoming sensory signals. Mismatches between prior beliefs and incoming signals constitute prediction errors that drive new learning. Psychosis has been suggested to result from a decreased precision in the encoding of prior beliefs relative to the sensory data, thereby garnering maladaptive inferences. Here, we review the current evidence for aberrant predictive coding and discuss challenges for this canonical predictive coding account of psychosis. For example, hallucinations and delusions may relate to distinct alterations in predictive coding, despite their

common co-occurrence. More broadly, some studies implicate weakened prior beliefs in psychosis, and others find stronger priors. These challenges might be answered with a more nuanced view of predictive coding. Different priors may be specified for different sensory modalities and their integration, and deficits in each modality need not be uniform. Furthermore, hierarchical organization may be critical. Altered processes at lower levels of a hierarchy need not be linearly related to processes at higher levels (and vice versa, further research is needed to clarify the Müller-Lyer effect from a Bayesian point of view.

References

1. Notredame CE, Pins D, Deneve S, Jardri R. What visual illusions teach us about schizophrenia. Front Integr Neurosci. 2014;8:63. doi:10.3389/fnint.2014.00063

2. King DJ, Hodgekins J, Chouinard PA, Chouinard VA, Sperandio I. A review of abnormalities in the perception of visual illusions in schizophrenia. Psychon Bull Rev. 2017;24(3):734-751. doi:10.3758/s13423-016-1168-5

3. Butler PD, Silverstein SM, Dakin SC. Visual Perception and Its Impairment in Schizophrenia. Biol Psychiatry. 2008;64(1):40-47. doi:10.1016/j.biopsych.2008.03.023

4. Kantrowitz JT, Butler PD, Schecter I, Silipo G, Javitt DC. Seeing the world dimly: the impact of early visual deficits on visual experience in schizophrenia. Schizophr Bull. 2009;35(6):1085-1094. doi:10.1093/schbul/sbp100

5. Letourneau JE. The Oppel-Kundt and the Müller-Lyer Illusions among Schizophrenics. Percept Mot Skills. 1974;39(2):775-778. doi:10.2466/pms.1974.39.2.775

6. Parnas J, Vianin P, Saebye D, Jansson L, Volmer-Larsen A, Bovet P. Visual binding abilities in the initial and advanced stages of schizophrenia. Acta Psychiatr Scand. 2001;103(3):171-180. doi:10.1034/j.1600-0447.2001.00160.x

7. Weckowicz TE, Witney G. The Muller-Lyer illusion in schizophrenic patients. J Ment Sci. 1960;106:1002-1007. doi:10.1192/bjp.106.444.1002

8. van Os J, Linscott RJ, Myin-Germeys I, Delespaul P, Krabbendam L. A systematic review and meta-analysis of the psychosis continuum: evidence for a psychosis proneness-persistence-impairment model of psychotic disorder. Psychol Med. 2009;39(2):179-195. doi:10.1017/S0033291708003814

9. Markon KE, Chmielewski M, Miller CJ. The reliability and validity of discrete and continuous measures of psychopathology: A quantitative review. Psychol Bull. 2011;137:856-879. doi:10.1037/a0023678

10. Michelini G, Palumbo IM, DeYoung CG, Latzman RD, Kotov R. Linking RDoC and HiTOP: A new interface for advancing psychiatric nosology and neuroscience. Clin Psychol Rev. 2021;86:102025. doi:10.1016/j.cpr.2021.102025

11. Bell V, Halligan PW, Ellis HD. The Cardiff Anomalous Perceptions Scale (CAPS): A New Validated Measure of Anomalous Perceptual Experience. Schizophr Bull. 2006;32(2):366-377. doi:10.1093/schbul/sbj014

12. Gross GM, Kwapil TR, Raulin ML, Silvia PJ, Barrantes-Vidal N. The multidimensional schizotypy scale-brief: Scale development and psychometric properties. Psychiatry Res. 2018;261:7-13. doi:10.1016/j.psychres.2017.12.033

13. Harrison XA, Donaldson L, Correa-Cano ME, et al. A brief introduction to mixed effects modelling and multi-model inference in ecology. PeerJ. 2018;6:e4794. doi:10.7717/peerj.4794

14. Sterzer P, Adams RA, Fletcher P, et al. The Predictive Coding Account of Psychosis. Biol Psychiatry. 2018;84(9):634-643. doi:10.1016/j.biopsych.2018.05.015

15. Powers AR, Mathys C, Corlett PR. Pavlovian conditioning-induced hallucinations result from overweighting of perceptual priors. Science. 2017;357(6351):596-600. doi:10.1126/science.aan3458

16. Teufel C, Subramaniam N, Dobler V, et al. Shift toward prior knowledge confers a perceptual advantage in early psychosis and psychosis-prone healthy individuals. Proc Natl Acad Sci U S A. 2015;112(43):13401-13406. doi:10.1073/pnas.1503916112

QBP1 peptide as a lead compound to treat post-traumatic stress disorder

Author
Paula López-García – Department of Molecular, Cellular and Developmental Neurobiology. Instituto Cajal (IC-CSIC), Madrid, Spain
María Eugenia Vaquero Morales – Department of Molecular, Cellular and Developmental Neurobiology. Instituto Cajal (IC-CSIC), Madrid, Spain
Daniel Ramírez de Mingo – Department of Molecular, Cellular and Developmental Neurobiology. Instituto Cajal (IC-CSIC), Madrid, Spain
Kerry R. McGreevy– Department of Translational Neuroscience. Instituto Cajal (IC-CSIC), Madrid, Spain
Helena Akiko Popiel – Department of Degenerative Neurological Diseases. National Center of Neurology and Psychiatry, Japan
Andrea Santi – Department of Psychological & Brain Sciences. Johns Hopkins University, Maryland, USA
Yoshitaka Nagai – Department of Neurotherapeutics. Osaka University. Osaka, Japan
José Luis Trejo – Department of Translational Neuroscience. Instituto Cajal (IC-CSIC), Madrid, Spain
Mariano Carrión-Vázquez – Department of Molecular, Cellular and Developmental Neurobiology. Instituto Cajal (IC-CSIC), Madrid, Spain

Citation
López-García, P., Morales, M.E.V., de Mingo, D.R., McGreevy, K.R., Popiel, H.A., Santi, A., Nagai, Y., Trejo, J.L., Carrión-Vázquez, M. QBP1 peptide as a lead compound to treat post-traumatic stress disorder.

Introduction

The cytoplasmic polyadenylation element binding protein-3 (CPEB3) is a functional amyloid whose importance for long-term memory consolidation in mammals has been widely demonstrated[1] (Fig. 1A). Recently, it has

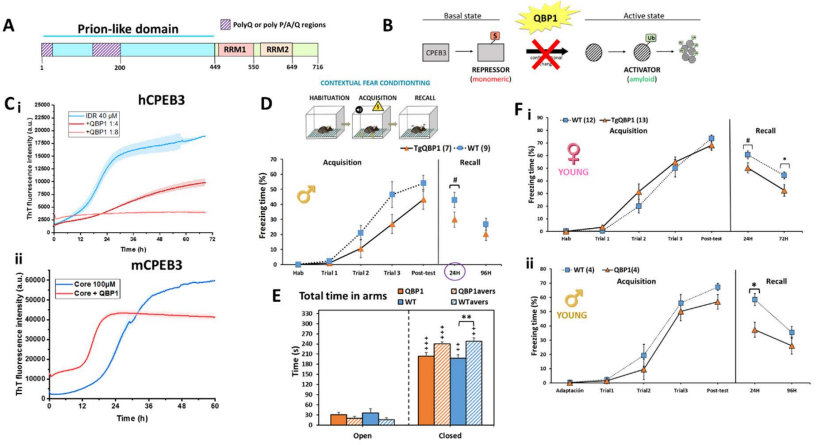

FIGURE 1

QBP1 peptide impairs consolidation of aversive memories in mice.

A) Simplified schematic of the mouse CPEB3 protein, showing its functional domains: RNA-binding domains (RRM, red), prion-like domain (blue) that coincides with the intrinsically disordered region (IDR); as well as the two glutamine-rich regions (purple striped), in which its amyloid propensity resides.

B) A schematic representation of CPEB3 conformational change. CPEB3 is mostly found on its repressive monomeric state in basal conditions, with a SUMOylation as a constraint that, after synaptic stimulation, give raise to the prionic/amyloidogenic state that is ubiquitinated (positive posttranslational modification) and acts as an activator of synaptic plasticity by mRNAs translation activation.

C) hCPEB3 and mCPEB3 are inhibited by QBP1 in vitro. Time-course of amyloid fibrillation followed by Thioflavine-T fluorescence emission in the presence of QBP1 peptide for human CPEB3 IDR (**i**) and core of murine CPEB3 (**ii**).

D) Aversive memories are impaired in the QBP1 transgenic mice. Freezing time percentage of adult male mice showed no differences at acquisition phase, but then QBP1 reduces its recall after 24h (p=0.097) and 96h.

E) Elevated plus maze comparison of basal *versus* aversive conditions. Total time spent in arms showed that QBP1 mice did not significantly increase its anxiety after fear conditioning while WT mice did (p=0.005).

F) Fear memories are more affected in younger mice at contextual fear conditioning. i) Freezing time percentage of young female mice reflected an impaired fear recall trend at 24h (p=0,060) and a significant reduce at 72h (p=0,042). We made an exception by measuring at 72h in females to better visualize memory inhibition over time. **ii)** Freezing time percentage of young male mice just showed a strong reduction in fear recall at 24h (p=0,019).

also been pointed out as a potential risk gene for Post-traumatic Stress Disorder (PTSD)[2]. This mental health disorder is triggered by the exposure to a traumatic event that manifests with anguish, intrusive memories, and negative mood changes[3]. Currently, there is no efficient treatment for PTSD other than symptomatic palliative care. Here, we propose the active amyloid state of CPEB3[4] as a promising therapeutic target to block the consolidation of traumatic memories through by the anti-amyloidogenic polyglutamine binding peptide 1 (QBP1)[5] (Fig. 1B).

Methods

We have used a wide spectrum of techniques from cloning and protein engineering to amyloid characterization in case of CPEB3. We have cloned the protein to be expressed recombinantly in E. coli, then used amyloid staining (Thioflavine-T and Congo Red), conformational antibodies6 (A11 and OC) and SDD-AGE/Western blot to characterize its amyloidogenic properties. On the other hand, classic behavioral tests were performed to assess neurological and basal conditions of the new QBP1 transgenic mouse and then specific memory tests were applied to study memory consolidation (Morris water maze, novel object recognition and contextual fear conditioning). Finally, mice brain samples were obtained to assess the level of murine CPEB3 oligomerization and confirm the presence of QBP1.

Results and discussion

Here we report the preclinical development of a pharmacological treatment for PTSD based on the action of QBP1 peptide. We first characterized both human and murine CPEB3 proteins in vitro **(Fig. 1C)**, showing how its amyloid is inhibited by QBP1 peptide without affecting any other functional process (i.e., phase separation). As the next step, we have demonstrated the effectiveness of QBP1 at reducing the cytotoxicity of CPEB3 oligomeric species in cell cultures. Secondly, we have produced and characterized a novel transgenic mouse that constitutively expresses QBP1. We first showed the innocuity of this peptide and the normal locomotor activity and anxiety levels of QBP1 mice. Thus, QBP1 mice have showed that the consolidation of simple learning is impaired after 24h for both hippocampal dependent

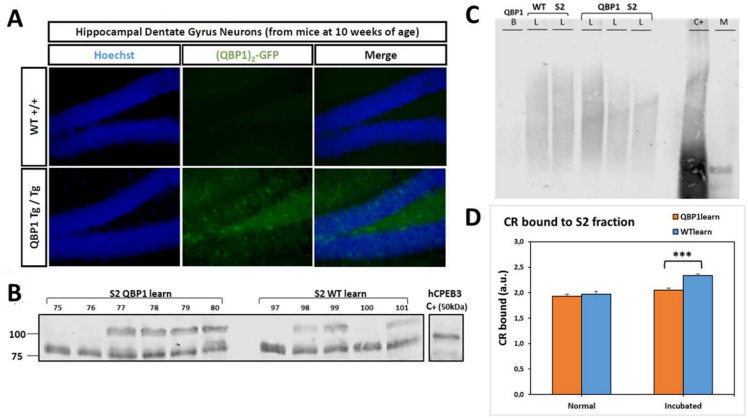

FIGURE 2

QBP1 impairs memory consolidation by blocking CPEB3 oligomerization.

A) Confocal images of hippocampal sections obtained from WT and QBP1 transgenic mice, in which green-fluorescent protein (GFP) revealed the presence of QBP1 and Hoechst was used as a cell viability control.

B) Western blot for soluble cytosolic fraction (S2) in learning conditions for murine CPEB3. QBP1 mice samples showed a more intense posttranslational modification band (~100kDa, related to its SUMOylated and soluble state) than WT mice samples.

C) SDD-AGE for soluble fractions (S2) in learning and basal conditions for murine CPEB3. S2 fractions showed reduced oligomerization in those QBP1-derived samples, thus suggesting that CPEB3 from transgenic QBP1 mice did not undergoes oligomerization as much as WT samples.

D) The amyloid stain Congo red (CR) showed that QBP1 samples do not aggregate. WT soluble samples (S2) are significantly increased when incubated at 37°C ($p<0.001$), which suggests that the amyloid proteins involved are able to aggregate over time; while those treated with QBP1 do not.

and aversive memories **(Fig. 1D)** and that it is limited to new learned memories. Furthermore, fear-induced anxiety of TgQBP1 mice was reduced in comparison to WT mice **(Fig. 1E)**, revealing that PTSD-like symptoms are also being ameliorated. Intriguingly, we found that aversive memories seem to be more affected in younger mice **(Fig. 1F)**, which will need further investigation on the underlying mechanisms. Finally, we analyzed the amyloid

presence in hippocampal extracted samples **(Fig. 2A-B)** showing a correlative decrease in murine CPEB3 oligomerization in the transgenic QBP1 mouse brains **(Fig.2 C-D)**, which confirms CPEB3 protein as the therapeutic target of QBP1 action. In conclusion, our results extend the inhibitory effect of QBP1 over memory consolidation to mammals, reinforcing previous research[9]**t** Our results point out to QBP1 peptide is a promising lead compound for prevention and therapy of PTSD and acute stress disorder.

Acknowledgements
This project is being carried out within the framework of an Industrial Doctorate 2020 grant (CAM) within the company Disrupep S.L. at the Cajal Institute-CSIC. This work has been published as two preprint manuscripts [10,11] is an RNA-binding protein which in its soluble state is localized in membraneless neuronal RNA granules keeping target mRNAs in a repressed state. The stimulus-dependent aggregation of CPEB3 activates target mRNAs translation, a central event for the maintenance of long-term memory-related synaptic plasticity in mammals. To date, the molecular determinants that govern both connected events remain unclear. Here, to gain insight into these processes, the biophysical properties of the human CPEB3 (hCPEB3.

References

[1] Qu, W. R. et al. Role of CPEB3 protein in learning and memory: new insights from synaptic plasticity. Aging (Albany. NY). 12, 15169–15182 (2020).

[2] Lu, W. H. et al. CPEB3-dowregulated Nr3c1 mRNA translation confers resilience to developing posttraumatic stress disorder-like behavior in fear-conditioned mice. Neuropsychopharmacology 1–11 (2021). doi:10.1038/s41386-021-01017-2

[3] Abdallah, C. G. et al. The Neurobiology and Pharmacotherapy of Posttraumatic Stress Disorder. Annu. Rev. Pharmacol. Toxicol. 59, 171–189 (2019).

[4] Si, K. & Kandel, E. R. The role of functional prion-like proteins in the persistence of memory. Cold Spring Harb. Perspect. Biol. 8, (2016).

[5] Popiel, H. A. et al. Inhibition of Protein Misfolding/Aggregation Using Polyglutamine Binding Peptide QBP1 as a Therapy for the Polyglutamine Diseases. Neurotherapeutics 10, 440–446 (2013).

[6] Kayed, R. & Glabe, C. G. Conformation-Dependent Anti-Amyloid Oligomer Antibodies. Methods Enzymol. 413, 326–344 (2006).

[7] Lu, W. H., Yeh, N. H. & Huang, Y. S. CPEB2 Activates GRASP1 mRNA Translation and Promotes AMPA Receptor Surface Expression, Long-Term Potentiation, and Memory. Cell Rep. 21, 1783–1794 (2017).

[8] Rayman, J. B. & Kandel, E. R. TIA-1 Is a Functional Prion-Like Protein. Cold Spring Harb Perspect Biol 1–14 (2017). doi:10.1101/cshperspect.a030718

[9] Hervás, R. et al. Molecular Basis of Orb2 Amyloidogenesis and Blockade of Memory Consolidation. PLoS Biol. 14, 1–32 (2016).

[10] de Mingo, D. R., López-García, P., Hervás, R., Laurents, D. V & Carrión-Vázquez, M. Molecular Determinants of Liquid Demixing and Amyloidogenesis in Human CPEB3. bioRxiv 2020.06.02.129783 (2020). doi:10.1101/2020.06.02.129783

[11] López-García, P. et al. An anti-amyloidogenic treatment to specifically block the consolidation of traumatic events in mouse. bioRxiv preprint. bioRxiv 1–34 (2020). doi:10.1101/2020.01.21.913053

Hippocampal activity associated with the visual processing of moving objects

Author
Paloma Manubens – Department of Biodiversity, Ecology and Evolution, Complutense University of Madrid, Madrid, Spain
Tereza Dvorakova – Institute of Physiology, Czech Academy of Sciences, Prague, Czech Republic
Abel Sánchez-Jiménez – Department of Biodiversity, Ecology and Evolution, Complutense University of Madrid, Madrid, Spain
Sergio Díez-Hermano – Department of Biodiversity, Ecology and Evolution, Complutense University of Madrid, Madrid, Spain
José A. Villacorta-Atienza – Department of Biodiversity, Ecology and Evolution, Complutense University of Madrid, Madrid, Spain
Ales Stuchlik – Institute of Physiology, Czech Academy of Sciences, Prague, Czech Republic
David Levcik – Institute of Physiology, Czech Academy of Sciences, Prague, Czech Republic

Citation
Manubens, P., Dvorakova, T., Sánchez-Jiménez, A., Díez-Hermano, S., Villacorta-Atienza, J.A., Stuchlik, A., Levcik, D. Hippocampal activity associated with the visual processing of moving objects.

Introduction/Motivation

The ability to navigate in our environment involves using internal representations of space in which hippocampal neurons play a fundamental role. Most of the findings regarding the underlying brain mechanisms are related to purely static environments, while the neural coding of dynamic stimuli remains to be understood. These stimuli are an essential source of information, especially in interactions (e.g., fight or flee) where a rapid

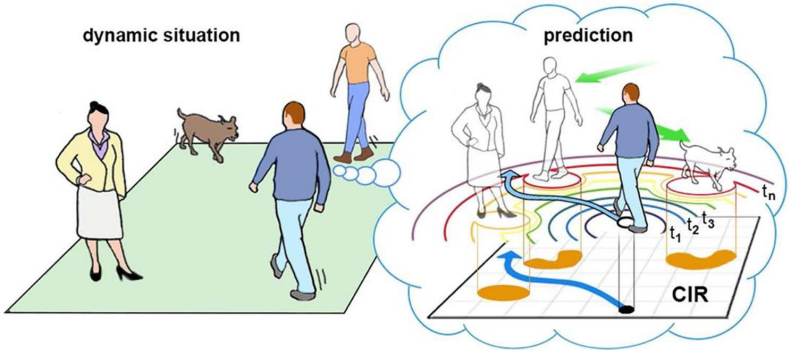

FIGURE 1
Theory of time compaction. In order to move in this situation, this theory propose that the main subject (the man in the blue sweatshirt) predicts the movement of the other components of the scene (green arrows), as well as his own movement. Based on this, it also predicts the areas where future collisions would happen (orange and t_n areas, respectively) with the rest of the subjects in order to establish a trajectory avoiding these virtual obstacles. The spatial arrangement of these interaction zones together with the proper trajectories is a static map called compact internal representation, or CIR. In other words, we would reduce a dynamic situation into a static mental representation containing the most relevant information of the time-changing situation.

response to the situation at hand is critical. In this regard, the existence of a novel cognitive process in humans has recently been demonstrated, anticipated by the theory of time compaction. According to it, what our brain does when, e.g., we move through a crowd (Fig. 1) is to predict the future positions of the moving elements and represent their future interactions in a static mental map. This mental image is called compact internal representation (CIR), and guides our actions to avoid collisions or reach desired elements [1]. Furthermore, the relevance of interactions is supported by recent findings in bats, where hippocampal CA1 principal cell activity has been reported to respond to their future positions in relation to intersections between trajectories [2]. Beyond the potential impact of this novel cognitive process, which could generalize to dynamic situations the well-known concept of cognitive map, different questions arise: Is time compaction

exclusive to humans or does it constitute an evolutionary invariant in mammalian cognition? Which brain region encapsulates these mechanisms?

To explore these questions, we must also bear in mind that for survival in nature the subject must be able to abstract the information in the environment without the need for direct interaction with it, as a purely empirical trial-and-error process would lead to the almost certain death. In this regard, it has been shown that there are cells in hippocampal CA1 that encode motion features of a simple visual stimulus independent of self-motion or even the presence of reward [3]. Furthermore, rats have also been shown to discriminate positions of objects displayed on an inaccessible screen [4] and use the hippocampus for such ability [5].

According to the theory, time compaction should be a salient mechanism when the animal is also a spectator of the dynamic situation. Thus, our main goal was to characterise the hippocampal processing of inaccessible visual stimuli in order to find evidence for the existence of time compaction in rodents.

Methods

We performed in vivo electrophysiological recordings in hippocampal CA1 of 4 rats placed in an operant conditioning chamber. We recorded 341 cells from which we selected 132 for further analysis.

The stimuli that the rats had to learn to discriminate were displayed on a screen inaccessible to the rats. The visual stimuli (Fig. 2) consisted of one or two white circles on a black background, making up four different scenes, two of which were static and two dynamic. The trajectories of the circles in the dynamic situation converged on one point, which they approached throughout the projection, but disappeared before they reached it. Nevertheless, this point of convergence was indeed shown in the paired static situation. Thus, each static scene was related to a dynamic situation through the CIR since the static scene corresponds to the theoretical CIR of the dynamic situation.

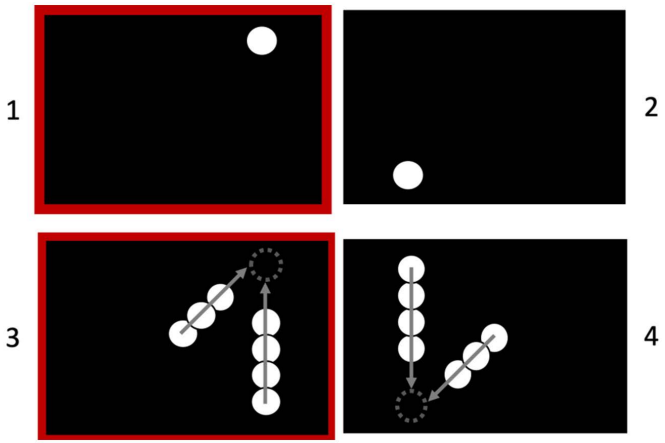

FIGURE 2
Visual stimuli. Stimuli 1 and 2 correspond to static stimuli, and stimuli 3 and 4 to dynamic stimuli. In addition, the pair of stimuli 1 and 3 and stimuli 2 and 4 present a relationship according to the CIR: the point where the circles trajectories in the dynamic stimulus cross (dashed circumference, not shown to the animal) is where the circle is presented in the static stimulus (the circles disappear before reaching this point). Pair of stimuli 1 and 3 was rewarded (red frame).

Based on the data obtained, we modelled the activity of the cells during presentations of individual stimuli using a generalised linear mixed model (GLMM), which was used to classify the cells according to which stimuli they respond.

Results and discussion

More than 60% of recorded hippocampal CA1 principal cells modulated their activity related to the stimuli displayed. Since the stimuli could only be perceived by sight, these results indicate that the hippocampus is not only able to respond to stimuli perceived by direct exploration. We also found a greater number of cells modulated by dynamic stimuli than static stimuli (7 and 1 cell, respectively; p-value 0.017), which is consistent with the biological relevance these stimuli may have for the animal.

We also found neurons differently modulated by the two pairs of stimuli related by CIR (i.e. reward vs. non-reward stimuli). However, their activity could be modulated due to the presence of a reward, as CA1 hippocampal neuronal subpopulations specific to reward signalling have been described [6] although it is not yet known whether visual signals can trigger the same behaviour by these neurons. On the other hand, we also found some neurons that discriminate two equally rewarded stimuli, which indicate the possible existence of a more complex reason behind this neural response. Therefore, the results obtained could be an indication of the existence of time compactation in rats. Nervertheless, in order to be able to state this with certainty, the presented study should be extended by introducing unrewarded, non-CIR-related control stimuli to further refine the pattern of cell responses.

Acknowledgements
This study was supported by the Ministry of Education, Youth and Sports of the Czech Republic (MSMT) programme OP VVV project FGÚ MSCA Mobilita IV. CZ.02.2.69/0.0/0.0/20_079/0017164

References

[1] Villacorta-Atienza, J. A., Calvo Tapia, C., Díez-Hermano, S., Sánchez-Jiménez, A., Lobov, S., Krilova, N., Murciano, A., López-Tolsa, G. E., Pellón, R., & Makarov, V. A. (2021). Static internal representation of dynamic situations reveals time compaction in human cognition. Journal of Advanced Research, 28, 111–125. https://doi.org/10.1016/j.jare.2020.08.008

[2] Dotson, N. M., & Yartsev, M. M. (2021). Nonlocal spatiotemporal representation in the hippocampus of freely flying bats. Science, 373(6551), 242–247. https://doi.org/10.1126/science.abg1278

[3] Purandare, C. S., Dhingra, S., Rios, R., Vuong, C., To, T., Hachisuka, A., Choudhary, K., & Mehta, M. R. (2022). Moving bar of light evokes vectorial spatial selectivity in the immobile rat hippocampus. Nature, 602(7897), 461–467. https://doi.org/10.1038/s41586-022-04404-x

[4] Klement, D., Levcik, D., Duskova, L., & Nekovarova, T. (2010). Spatial task for rats testing position recognition of an object displayed on a computer screen. Behavioural Brain Research, 207(2), 480–489. https://doi.org/10.1016/j.bbr.2009.10.041

[5] Levcik, D., Nekovarova, T., Antosova, E., Stuchlik, A., & Klement, D. (2018). The role of the hippocampus in object discrimination based on visual features. Neurobiology of Learning and Memory, 155, 127–135. https://doi.org/10.1016/j.nlm.2018.06.003

[6] Gauthier, J. L., & Tank, D. W. (2018). A Dedicated Population for Reward Coding in the Hippocampus. Neuron, 99(1), 179-193.e7. https://doi.org/10.1016/j.neuron.2018.06.008

The role of the ipsilateral cerebral cortex for functional recovery after stroke

Author
Alexander Noll, Carsten M. Klingner, Stefan Brodoehl, Franziska Wagner, Alexander Schmidt, Christiane Dahms – Department of Neurology, Jena University Hospital, Jena, Germany; Biomagnetic Center, Jena University Hospital, Germany

Citation
Noll, A., Klingner, C.M., Brodoehl, S., Wagner, F., Schmidt, A., Dahms, C. The role of the ipsilateral cerebral cortex for functional recovery after stroke

Introduction/Motivation

Stroke is the most common cause of long-term disability in western industrialized countries. Until today, there is no prognostic marker to predict functional recovery during rehabilitation (Grefkes und Fink 2020).

Current rehabilitation programs are deficit-based and primarily focus on training the affected areas (Langhorne et al. 2009). However, it is described that stroke does not only affect the damaged region but also influences the brain as functional network (Guggisberg et al. 2019). Several functional brain imaging studies show increased activation of ipsilateral (contralesional) primary motor cortex while performing an active motor task (Rehme et al. 2012). It is discussed whether the increased activation of contralesional motor areas has positive or negative effects on motor recovery in stroke patients (Dodd et al. 2017).

The core hypothesis of our work is that the potential to engage the contralesional sensorimotor cortex in motor learning tasks is an important factor in recovery of sensorimotor functions after stroke. These functions are essential to personal and professional life and rely on the ability to learn motor sequences, such as writing or using a keyboard (Dahms et al. 2020).

Methods

Twenty-seven chronic ischemic stroke patients aged between 46-88 (66.7 ± 11.37 years, mean ± SD) were included in our prospective clinical cross-sectional study. The participants were examined using functional imaging methods (resting-state fMRI as well as task-related fMRI), a sensorimotor and a neuropsychological test battery. Measuring was done during the chronic phase at 90 days up to a maximum of 331 days after stroke (171.22 ± 80.26 days mean ± SD). Inclusion criterion was a motor impairment of upper extremity in the acute phase of stroke (baseline NIHSS=4.26 ± 3.504 mean ± SD). Exclusion criteria were major depression (BDI ≥19), visual limitation that affects the performance of the manual sequence task, contraindications to MRI, and cognitive limitations that interfere with the understanding of instructions and performance of motor task. Due to MRI restrictions, two participants were excluded from the fMRI examination.

The assessment included a standardized questionnaire (BDI-II, EQ-5D, SF36) and an anamnesis questionnaire. We examined each participant using National Institute of Health Stroke Scale (NIHSS), modified Rankin Scale (mRs), Fugl-Meyer (motor function of upper limp), Nine-Hole-Peg-Test, and Montreal Cognitive Assessment (MoCA). NIHSS and mRs were also documented at the time of admission and discharge and compared with current chronic data to evaluate recovery.

We quantify short-term cerebral adaptability by measuring cerebral connectivity changes in the ipsilateral sensorimotor cortex during a short motor learning paradigm performed in fMRI. The participants were asked to tap a consistent sequence of 5 numbers with the corresponding finger as quickly and as accurately as possible. (Karni et al. 1995). This manual

sequence task (MST) was performed with the non-impaired hand and lasted 12 minutes, alternating 30 seconds task blocks and 30 seconds pause blocks.

These connectivity data will be compared to the short-term motor learning ability and long-term functional recovery after stroke. We calculated a learning curve based on correctly typed sequences per block over time to define short-term motor learning ability. In this way, both accuracy and speed were taken into account.

Results and discussion

Data collection is finished, and first data evaluation is currently ongoing. FMRI data analysis, addressing the main question regarding the role of the ipsilateral (contralesional) cortex in motor learning, is currently ongoing and we hope to present some early results at the conference. During first evaluation of behavioral data, we found a significant positive correlation between relative improvement from time of admission to discharge using individual NIHSS to the motor learning task performance of chronic phase (r=0.539, p=0.005). Although this study focuses on long-term recovery, the short-term recovery in the acute phase after stroke seems to play an important role in motor learning capability in the later chronic phase. Also, we investigated if the baseline NIHSS correlates with the short-term learning performance in the MST and found a significant negative correlation (r=-0,588, p=0,002).

With this project, we want to answer the question if the ipsilateral cortex influences adaptive learning and functional recovery after stroke. Moreover, we want to investigate whether the individual long-term rehabilitation outcome correlates with the potential for short-term learning. This may contribute to understanding recovery processes and help individualize rehabilitation concepts after stroke.

Acknowledgements

The author received research grants from the "Interdisciplinary Centre for Clinical Research (IZKF Jena)".

References

Dahms C, Brodoehl S, Witte OW, Klingner CM. 2020. The importance of different learning stages for motor sequence learning after stroke. Hum Brain Mapp, 41 (1):270-286.

Dodd KC, Nair VA, Prabhakaran V. 2017. Role of the Contralesional vs. Ipsilesional Hemisphere in Stroke Recovery. Front Hum Neurosci, 11:469.

Grefkes C, Fink GR. 2020. Recovery from stroke: current concepts and future perspectives. Neurol Res Pract, 2:17.

Guggisberg AG, Koch PJ, Hummel FC, Buetefisch CM. 2019. Brain networks and their relevance for stroke rehabilitation. Clin Neurophysiol, 130 (7):1098-1124.

Karni A, Meyer G, Jezzard P, Adams MM, Turner R, Ungerleider LG. 1995. Functional MRI evidence for adult motor cortex plasticity during motor skill learning. Nature, 377 (6545):155-158.

Langhorne P, Coupar F, Pollock A. 2009. Motor recovery after stroke: a systematic review. Lancet Neurol, 8 (8):741-754.

Rehme AK, Eickhoff SB, Rottschy C, Fink GR, Grefkes C. 2012. Activation likelihood estimation meta-analysis of motor-related neural activity after stroke. Neuroimage, 59 (3):2771-2782.

Sensitivity of the reward system in Post-Covid-fatigue

Author
Insa Petersen – Department of Neurology, Jena University Hospital, Jena, Germany; Biomagnetic Centre, Jena University Hospital, Jena, Germany; Graduate Program Experimental Medicine "IZKF", Jena University Hospital, Jena, Germany
Laura Schmidt – Department of Neurology, Jena University Hospital, Jena, Germany; Biomagnetic Centre, Jena University Hospital, Jena, Germany
Laura Opitz – Department of Neurology, Jena University Hospital, Jena, Germany; Biomagnetic Centre, Jena University Hospital, Jena, Germany
Jenny Rogenz – Department of Neurology, Jena University Hospital, Jena, Germany; Biomagnetic Centre, Jena University Hospital, Jena, Germany
Stefan Brodoehl – Department of Neurology, Jena University Hospital, Jena, Germany; Biomagnetic Centre, Jena University Hospital, Jena, Germany
Carsten M. Klingner – Department of Neurology, Jena University Hospital, Jena, Germany; Biomagnetic Centre, Jena University Hospital, Jena, Germany
Franziska Wagner – Department of Neurology, Jena University Hospital, Jena, Germany; Biomagnetic Centre, Jena University Hospital, Jena, Germany; Clinician Scientist Program OrganAge, Jena University Hospital, Jena, Germany

Citation
Petersen, I., Schmidt, L., Opitz, L., Rogenz, J., Brodoehl, S., Klingner, C.M., Wagner, F. Sensitivity of the reward system in Post- Covid-Fatigue.

Introduction/Motivation

The health consequences of the SARS-CoV-2 pandemic are dominating the international healthcare systems. More than 15% of patients with supposedly mild SARS-CoV-II disease develop persisting symptoms (Sudre et al. 2021). In addition to known internal limitations, such as respiratory distress or tachycardia, severe neurological deficits are prominent. For example,

fatigue persisting for months, cognitive impairment, and a marked increase in daytime fatigue, sometimes accompanied by an inability to work, are described (Taquet et al. 2021). These clinical symptoms are grouped under the term chronic fatigue syndrome (CFS), a condition that is now becoming the focus of interdisciplinary research in the context of the global pandemic. Previous research indicates, that hospitalized patients suffering COVID-19 often develop fatigue or muscle weakness (63%), difficulties in sleep (26%), but psychiatric disorders as well, such as anxiety and depression (23%) (Taquet et al. 2021). This severe constellation of symptoms can lead to drastic limitations in the everyday life of the people concerned.

The pathophysiology of this multifaceted neurological and also dysautonomic symptom complex is not yet understood. There is evidence that the specific cerebral reward system is also altered in CFS, which is an important modulator of learning processes and involved in various homeostatic regulatory processes (Wylie und Flashman 2017).

Based on the similarity of symptoms in CFS and Post-COVID fatigue, the aim of this study is to investigate whether there is a reduced sensitivity of the reward system in the context of postviral fatigue syndrome. This could explain, among other things, the sometimes severe cognitive impairment of post-COVID fatigue patients.

Looking into the future, a better characterization of network changes in the context of fatigue symptoms also opens up therapeutic options for drug or psychotherapeutic interventions.

Methods

To find out about the impact of this condition on this particular neuronal network, our study compares healthy individuals to patients with Post-Covid-Syndrome in association with a fatigue.

Included are subjects between the age of 18 to 55 without relevant neurological or psychiatric disorders in the medical record.

The monetary incentive delay task (MID, Figure 1: (Frank et al. 2004)) in

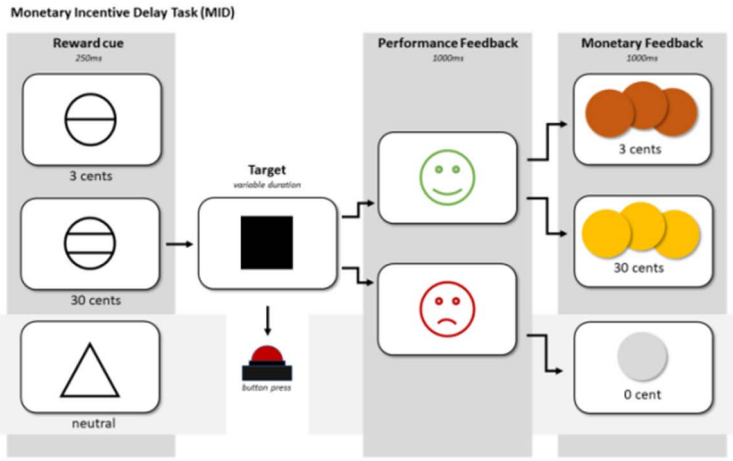

FIGURE 1
The monetary incentive delay task (MID).

conjunction with a simultaneous magnetoencephalography (MEG) and an electroencephalography (EEG) will behaviorally characterize the reward system as utilized in similar publications (Opitz et al. 2022). The paradigm is structured in three blocks with breaks in between. The different reward incentives were 0 cents, 3 cents and 30 cents and were randomized in the game. In addition, standardized questionnaires were used to obtain further information about the living conditions and the severity of symptoms of included individuals. For these purposes, the Beck's Depression Inventory II (BDI-II) (Kuhner et al. 2007, Hautzinger et al. 2006, Osman et al. 2008), the EQ-VAS, a visual analogue scale of the EQ-5D (Rabin und de Charro 2001), the Short Form 36 (SF-36) (Bullinger 1995, Bullinger et al. 1995), the Snaith-Hamilton Pleasure Scale (SHAPS) (Nakonezny et al. 2015), the Hospital Anxiety and Depression Scale (HADS) (Snaith 2003), the Positive and Negative Affect Schedule (PANAS) (Cunha et al. 2019), the Epworth Sleepiness Scale (ESS) (Lok und Zeitzer 2021, Alami et al. 2018), the Fatigue Assessment Scale (FAS) (Michielsen et al. 2003, El Sayed et al. 2021) and a

self-developed questionnaire for socio-demographic information (Biomag Questionnaire Standard 1) were utilized. With its help, conclusions can be drawn about possible influence of certain factors on the reward system, including the consumption of alcohol, nicotine or drugs, the use of video games, subjective addiction tendency, physical exercise, relationship status, professional qualification, religiousness and the tendency to worry.

Results and discussion

The hypothesis we test is, that the sensitivity of the reward system in patients with Post-Covid-Syndrome is reduced in comparison to healthy adults. Therefore 24 subjects with a diagnosed Post-Covid-Syndrome and 20

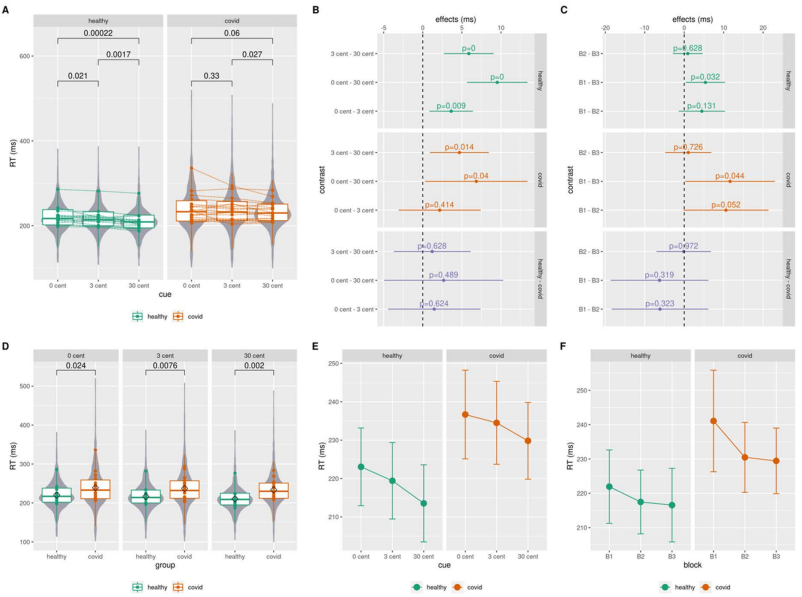

FIGURE 2
Reaction times in the MID.

healthy individuals were examined with the MID during an EEG and MEG to measure the neuronal correlates.

According to the study design, all participants were between 18 and 55 years of age.

At the moment we are still working on the analysis of the collected data.

First results of the analysis of the MID reaction times (Figure 2) suggest, that there are significant differences in specific aspects of learning and the rapidity of reaction depending on potential monetary reward. Further analysis of cerebral connectivity and the final results will be presented at the conference.

Acknowledgements
This work is funded by the Interdisziplinäres Zentrum für Klinische Forschung Jena (IZKF Jena, interdisciplinary centre for clinical research Jena).

References

Alami YZ, Ghanim BT, Zyoud SH. 2018. Epworth sleepiness scale in medical residents: quality of sleep and its relationship to quality of life. J Occup Med Toxicol, 13:21.

Bullinger M. 1995. German translation and psychometric testing of the SF-36 Health Survey: preliminary results from the IQOLA Project. International Quality of Life Assessment. Soc Sci Med, 41 (10):1359-1366.

Bullinger M, Kirchberger I, Ware J. 1995. Der deutsche SF-36 Health Survey Übersetzung und psychometrische Testung eines krankheitsübergreifenden Instruments zur Erfassung der gesundheitsbezogenen Lebensqualität. Zeitschrift für Gesundheitswissenschaften = Journal of public health, 3 (1):21-36.

Cunha LF, Pellanda LC, Reppold CT. 2019. Positive Psychology and Gratitude Interventions: A Randomized Clinical Trial. Front Psychol, 10:584.

El Sayed S, Shokry D, Gomaa SM. 2021. Post-COVID-19 fatigue and anhedonia: A cross-sectional study and their correlation to post-recovery period. Neuropsychopharmacol Rep, 41 (1):50-55.

Frank MJ, Seeberger LC, O'Reilly R C. 2004. By carrot or by stick: cognitive reinforcement learning in parkinsonism. Science, 306 (5703):1940-1943.

Hautzinger M, Keller F, Kühner C. 2006. BDI II Beck Depressions-Inventar Revision Manual. Frankfurt am Main: Harcourt Test Servises GmbH.

Kuhner C, Burger C, Keller F, Hautzinger M. 2007. [Reliability and validity of the Revised Beck Depression Inventory (BDI-II). Results from German samples]. Nervenarzt, 78 (6):651-656.

Lok R, Zeitzer JM. 2021. Physiological correlates of the Epworth Sleepiness Scale reveal different dimensions of daytime sleepiness. Sleep Adv, 2 (1):zpab008.

Michielsen HJ, De Vries J, Van Heck GL. 2003. Psychometric qualities of a brief self-rated fatigue measure: The Fatigue Assessment Scale. J Psychosom Res, 54 (4):345-352.

Nakonezny PA, Morris DW, Greer TL, Byerly MJ, Carmody TJ, Grannemann BD, Bernstein IH, Trivedi MH. 2015. Evaluation of anhedonia with the Snaith-Hamilton Pleasure Scale (SHAPS) in adult outpatients with major depressive disorder. J Psychiatr Res, 65:124-130.

Opitz L, Wagner F, Rogenz J, Maas J, Schmidt A, Brodoehl S, Klingner CM. 2022. Still Wanting to Win: Reward System Stability in Healthy Aging. Front Aging Neurosci, 14:863580.

Osman A, Barrios FX, Gutierrez PM, Williams JE, Bailey J. 2008. Psychometric properties of the Beck Depression Inventory-II in nonclinical adolescent samples. J Clin Psychol, 64 (1):83-102.

Rabin R, de Charro F. 2001. EQ-5D: a measure of health status from the EuroQol Group. Ann Med, 33 (5):337-343.

Snaith RP. 2003. The Hospital Anxiety And Depression Scale. Health Qual Life Outcomes, 1:29.

Sudre CH, Murray B, Varsavsky T, Graham MS, Penfold RS, Bowyer RC, Pujol JC, Klaser K, Antonelli M, Canas LS, Molteni E, Modat M, Jorge Cardoso M, May A, Ganesh S, Davies R, Nguyen LH, Drew DA, Astley CM, Joshi AD, Merino J, Tsereteli N, Fall T, Gomez MF, Duncan EL, Menni C, Williams FMK, Franks PW, Chan AT, Wolf J, Ourselin S, Spector T, Steves CJ. 2021. Attributes and predictors of long COVID. Nat Med, 27 (4):626-631.

Taquet M, Dercon Q, Luciano S, Geddes JR, Husain M, Harrison PJ. 2021. Incidence, co-occurrence, and evolution of long-COVID features: A 6-month retrospective cohort study of 273,618 survivors of COVID-19. PLoS Med, 18 (9):e1003773.

Wylie GR, Flashman LA. 2017. Understanding the interplay between mild traumatic brain injury and cognitive fatigue: models and treatments. Concussion, 2 (4):CNC50.

Network dynamics of the human cerebral cortex in vitro

Author
Rita M. Robles – Systems Neuroscience, IDIBAPS, Barcelona, Spain
Joana Covelo – Systems Neuroscience, IDIBAPS, Barcelona, Spain
José Manuel Sanchez – Systems Neuroscience, IDIBAPS, Barcelona, Spain
Alessandra Camassa – Systems Neuroscience, IDIBAPS, Barcelona, Spain
Arnau Manasanch – Systems Neuroscience, IDIBAPS, Barcelona, Spain
Silvia Tapia-Gonzalez – Centro de Tecnología Biomédica, Universidad Politécnica de Madrid, Madrid, Spain; Instituto Cajal, Consejo Superior de Investigaciones Científicas, Madrid, Spain
Almudena Barbero-Castillo – Systems Neuroscience, IDIBAPS, Barcelona, Spain
Mar Carreño – Epilepsy Unit, Hospital Clinic, Barcelona, Spain
Estefanía Conde – Epilepsy Unit, Hospital Clinic, Barcelona, Spain
Pedro Roldán – Epilepsy Unit, Hospital Clinic, Barcelona, Spain
Jordi Rumià Arboix – Epilepsy Unit, Hospital Clinic, Barcelona, Spain
Javier DeFelipe – Centro de Tecnología Biomédica, Universidad Politécnica de Madrid, Madrid, Spain; Instituto Cajal, Consejo Superior de Investigaciones Científicas, Madrid, Spain
Maria V. Sanchez-Vives – Systems Neuroscience, IDIBAPS, Barcelona, Spain; ICREA, Barcelona, Spain

Citation
Robles, R.M., Covelo, J., Sanchez, J.M., Camassa, A., Manasanch, A., Tapia-Gonzalez, S., Barbero-Castillo, A., Carreño, M., Conde, E., Roldán, P., Arboix, J.R., DeFelipe, J., Sanchez-Vives, M.V. Network dynamics of the human cerebral cortex in vitro

Introduction / motivation

Cortical slices from animal models have been widely used for both physiological and pathological in vitro research. Even when the investigation of cortical mechanisms and dynamics in animal models is highly valuable,

from a translational perspective it is critical to learn also directly from human tissue. Indeed, such pre-clinical and clinical interaction has gained interest in recent decades. It has been possible taking advantage of human neocortical tissue from neurosurgeries to perform electrophysiological studies in vitro [3]–[6]was associated with a mean 67-nS increase in membrane conductance, was reduced by the GABA(A, allowing investigation of the function of local networks, circuits, and individual neurons. So far, the results obtained from electrophysiology and histochemical experiments using cortical slices have revealed some principles of network and cellular physiology of human cells [13], however, many questions remain open. Resorting to in vitro electrophysiological recordings, we studed the spontaneous and evoked dynamics of the human cerebral cortex network during spontaneous slow-wave activity and the modulation of the excitatory/inhibitory balance, aiming at bridging the gap between animal studies and potential clinical implications.

Methods

Human cortical tissue samples were obtained during surgery of epileptic or tumoral patients at the Neurology Department of Hospital Clinic of Barcelona. The sample was transported in oxygenated cold (4-10 °C) bathing medium and then we obtained 400 µm-thick coronal slices and the tissue surplus was preserved in paraformaldehyde for anatomical reconstruction. To increase the tissue viability during slice preparation, we used the sucrose-substitution technique from Aghajanian and Rasmussen (1989)[7]. To further increase human tissue viability, 3 mM Sodium Pyruvate and 0.5 mM Ascorbic Acid were added to the solution. Slices were placed in an interface style recording and bathed for 30 minutes in an equal mixture of the sucrose-substituted solution and ACSF (Artificial Cerebral Spinal Fluid). Slices were then maintained for 1 hour in ACSF [9] for recovery and in an in vivo-like modified ACSF [8]how do dynamic interactions between excitatory and inhibitory neurons produce these firing patterns, and how do networks switch from one firing pattern to the other? We investigated these questions theoretically by examining the intrinsic dynamics of large networks of neurons. Using both a semianalytic model based on mean firing

rate dynamics and simulations with large neuronal networks, we found that the dynamics, and thus the firing patterns; are controlled largely by one parameter, the fraction of endogenously active cells. When no endogenously active cells are present, networks are either silent or fire at a high rate; as the number of endogenously active cells increases, there is a transition to bursting; and, with a further increase, there is a second transition to steady firing at a low rate. A secondary role is played by network connectivity, which determines whether activity occurs at a constant mean firing rate or oscillates around that mean. These conclusions require only conventional assumptions: excitatory input to a neuron increases its firing rate, inhibitory input decreases it, and neurons exhibit spike-frequency adaptation.
These conclusions also lead to two experimentally testable predictions: 1 throughout the rest of the experiment. Solutions were aerated with 95% O2 and 5% CO2 to a final pH of 7.4. Temperature was kept at 34.5-36ºC. Electrophysiological recordings started following a recovery period of 2 h. Voltage was recorded as extracellular Local Field Potentials (LFP) that represent the activity of local neuronal populations, reflecting their cellular-synaptic architectural organization of the network and synchrony of the current sources [1, 2]. Extracellular LFPs were recorded from the cortical slices in vitro (40 slices from 12 samples) expressing slow-wave activity, and were band-pass filtered to obtain the Multiunit activity (MUA, blue trace) used to perform the analysis (FIGURE 2). Superficial and deep layers of the cortex were simultaneously recorded with 16- and 32-multielectrode arrays (MEA) or tungsten electrodes. MEAs spanning over several cortical columns and cortical layers provided a two-dimensional characterization of the cortical activity of human brain slices (FIGURE 1). To modulate excitability levels, bicuculline methiodide (BMI), a GABAA receptor antagonist which blocks fast inhibition [11], was added to the bath medium in increasing concentrations ranging from 0.5 to 8 µM. Following electrophysiological recordings, human slices were processed for Nissl staining and cut in 50µm sections. Layer reconstruction allowed alignment of electrode position within cortical cytoarchitectonic areas. Images of the slices during electrophysiological recording were superimposed on the Nissl staining images as displayed in (FIGURE 1).

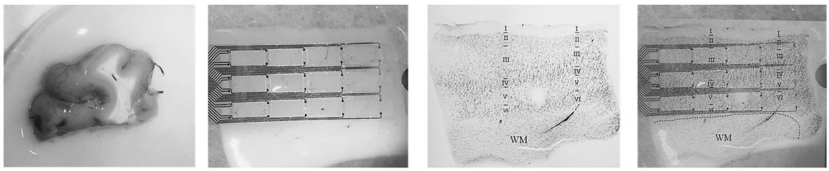

FIGURE 1
A. Human brain tissue. B. Fresh human brain slice with recording multielectrode array (32 channels). C. Nissl staining image of the same slice with different layers identified. D. Composition of Nissl staining and multielectrode array image from human brain tissue.

Results and discussion

We recorded spontaneous emergent rhythmic activity from human slices (FIGURE 2). Slow oscillatory activity is characterized by periods of activity (Up states) interspersed by periods of silence (Down states), at a frequency <1Hz [12]. Interestingly, we found differences in the activity between slices corresponding to peritumoral and those from epileptic tissue. Epileptic tissue was characterized shorter Up-states (<0.2s) with higher firing rate and longer Down-states. These findings are reminiscent of those observed while blocking GABAA receptors [9,11] where gradual GABAA receptor blockage resulted in shorter Up states, higher firing rates and more synchronized discharges. Indeed, by applying GABAA-Rs blocker, neurons in the peritumoral tissue had similar firing rates to those in the epileptic one. Hence, GABAergic blockade increased network excitability and induced a strong synchronization in the network as described for other species. Finally, we found a layer-specific dynamics consistent with the one described for other species, with Up states initiating preferentially in deep cortical layers.

The validation of findings provided by animal models in human-based systems is relevant since the complexity of the cellular makeup and function of the human brain is higher than nonhuman species [10], for example, the synapses received by a cortical pyramidal neuron is ca. 40K in humans

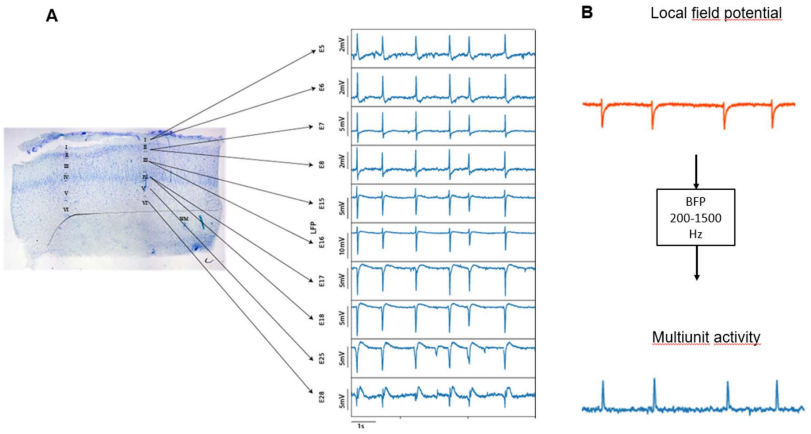

FIGURE 2
A. Spontaneous slow-wave activity of a human cortical slice across layers with different peak amplitudes and polarities. B. LFPs (orange trace) expressed slow-wave activity and they were band pass filtered to obtain the Multiunit activity (MUA, blue trace) used to perform the analysis.

and 10K in the mouse. In the spontaneous dynamics of the isolated cortical network, characterized by the recurrent connections, we find a large similarity with that from other species, given that the activity is self-organized into slow waves consisting in Up and Down states. The structural investigation of the human tissue that we report here found that the cortical structure was preserved, not corresponding to dysplasia or tumoral tissue. However, the differences observed between the cortex from epileptic and tumoral cases may reflect intrinsic functional changes derived from the intense seizure activity experienced by the epileptic patients [13]. The dynamical characterization through the use of different levels on excitability broadens our understanding of the mechanistic organization of the human cortical network at the mesoscale.

Acknowledgements
Funded by: European Union's Horizon 2020 No. 945539 (Human Brain Project SGA3) and CORTICOMOD PID2020-112947RB-I00 by MCIN/ AEI

/10.13039/501100011033. J.C. is a doctorate student supported by EUSNN MSCA-ITN-ETN H2020-860563 and JMS is supported by FPI Spanish Ministry of Science PRE2018-086203.

References

[1] Buzsáki, G.,Draguhn,A. "Neuronal oscillations in cortical networks," Science 304, 1926–1929, 2004,

[2] Buzsáki, G., Anastassiou, C. & Koch, C. "The origin of extracellular fields and currents — EEG, ECoG, LFP and spikes,"Nat Rev Neurosci 13, 407–420, 2012.

[3] D. A. McCormick, "GABA as an inhibitory neurotransmitter in human cerebral cortex," J. Neurophysiol., vol. 62, no. 5, pp. 1018–1027, 1989.

[4] M. Avoli and A. Williamson, "Functional and pharmacological properties of human neocortical neurons maintained in vitro," Prog. Neurobiol., vol. 48, no. 6, pp. 519–554, 1996.

[5] R. Köhling et al., "Spontaneous sharp waves in human neocortical slices excised from epileptic patients,"Brain, vol. 121, no. 6, pp. 1073–1087, 1998.

[6] D. A. McCormick and A. Williamson, "Convergence and divergence of neurotransmitter action in human cerebral cortex," Proc. Natl. Acad. Sci. U. S. A., vol. 86, no. 20, pp. 8098–8102, 1989.

[7] Aghajanian, G. K., & Rasmussen, K. (1989). Intracellular studies in the facial nucleus illustrating a simple new method for obtaining viable motoneurons in adult rat brain slices. Synapse, 3(4), 331-338.

[8] M. V. Sanchez-Vives and D. A. McCormick, "Cellular and network mechanisms of rhythmic recurrent activity in neocortex," Nat. Neurosci. 2000 310, vol. 3, no. 10, pp. 1027–1034.

[9] Barbero-Castillo, P. Mateos-Aparicio, L. D. Porta, A. Camassa, L. Perez-Mendez, and M. V. Sanchez-Vives, "Impact of GABA A and GABA B Inhibition on Cortical Dynamics and Perturbational Complexity during Synchronous and Desynchronized States," J. Neurosci. vol. 41, no. 23, pp. 5029–5044.

[10] K. Lee et al., "Human in vitro systems for examining synaptic function and plasticity in the brain," J. Neurophysiol., vol. 123, no. 3, pp. 945–965..

[11] Sanchez-Vives, M. V., Mattia, M., Compte, A., Perez-Zabalza, M., Winograd, M., Descalzo, V. F., & Reig, R. (2010). Inhibitory modulation of cortical up states. Journal of neurophysiology, 104(3), 1314-1324.

[12] Sanchez-Vives, M. V. (2012). Spontaneous rhythmic activity in the adult cerebral cortex in vitro. Neuromethods, 73, 263–284. Ed. by K. Ballanyi pringer Protocols. Humana Press, Totowa, NJ,

[13] Tóth, K., Hofer, K. T., Kandrács, Á., Entz, L., Bagó, A., Erőss, L., Jordán, Z., Nagy, G., Sólyom, A., Fabó, D., Ulbert, I., & Wittner, L. (2018). Hyperexcitability of the network contributes to synchronization processes in the human epileptic neocortex. Journal of Physiology, 596(2), 317–342.

A spiking neural network model of excitation and inhibition of primary visual cortex during fear conditioning

Author
Alejandro Santos-Mayo – Center for Cognitive and Computational Neuroscience, Complutense University of Madrid, Spain; Department of Experimental Psychology, Psychology Faculty, Complutense University of Madrid, Spain
Gianluca Susi – Center for Cognitive and Computational Neuroscience, Complutense University of Madrid, Spain; Department of Structure of Matter, Thermal Physics and Electronics, School of Physics, Complutense University of Madrid, Spain
Inés Abalo-Rodriguez – Center for Cognitive and Computational Neuroscience, Complutense University of Madrid, Spain; Department of Experimental Psychology, Psychology Faculty, Complutense University of Madrid, Spain
Stephan Moratti – Center for Cognitive and Computational Neuroscience, Complutense University of Madrid, Spain; Department of Experimental Psychology, Psychology Faculty, Complutense University of Madrid, Spain

Citation
Santos-Mayo, A., Susi, G., Abalo-Rodriguez, I., Moratti, S. A spiking neural network model of excitation and inhibition of primary visual cortex during fear conditioning

Introduction/Motivation

Fear conditioning represents the study of threat associative learning whereby a conditioned stimulus (CS+), for example, a Gabor patch, is paired with an aversive unconditioned stimulus (US) such as a loud noise. In sensory cortices like the primary visual cortex (V1), this learning shows an increase of early gamma band responses (30 Hz to 60 Hz) after CS+ presentation [1],

while a safety cue never paired with the US (i.e. a CS-) express an inhibition of this response [2]. Recently, this modulation has been observed in occipital areas ranging from primary to secondary visual cortex (V1-V2) in humans [1].

During the last few years, computational models enhanced our understanding of the amygdala role in fear conditioning [3]. However, the neural mechanisms underlying sensory cortex modulations by fear conditioning are less understood. Recent findings propose a cholinergic modulation of the sensory cortex in fear conditioning. In particular, Letzkus and cols. [4] described a disinhibitory circuit whereby basal forebrain (BF) projections into layer I inhibitory interneurons can inhibit layer II/III inhibitory neurons and in turn disinhibit layer II/III pyramidal cells. This circuit results in excitability of the sensory cortex at CS+ presentation due to US-mediated activation of the BF. In contrast, the inhibitory counterpart associated with CS- processing has not been considered yet. However, recent findings claim the existence of cholinergic inhibition [6] such as the lateral inhibition mechanisms mediated by BF projections towards inhibitory Martinotti cells (MT) located between pyramidal neurons [5] that may explain the inhibition of sensory cortex by CS-. Taken together, here we present a spiking neural model that integrates these assumptions and successfully simulates the effects of opposite gamma band modulations in areas V1-V2 by fear conditioning as observed in humans [1].

Methods

The model is composed by a spiking neural network simulating the behaviour of two cortical columns of sensitive neurons related to orthogonal orientations (discriminating orientation 45º and 135º) in areas V1-V2 and a BF population. Layer II/III of the V2 area mainly receives the feed-forward activity from the V1 where the orientation of the presented Gabor patch is discriminated. In addition, cholinergic inhibitory interneurons (layers I and MT cells) in V1-V2 receive input from the BF. Paralleling a standard fear conditioning paradigm, CS+ and CS- patches (45º and 135º respectively) were presenting during habituation, acquisition and extinction blocks. In

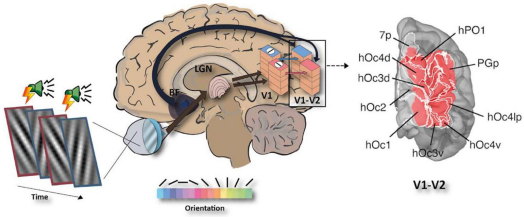

FIGURE 1
Left: Explanation of the model. Oriented Gabor patches are presented to the visual system and discriminated at V1. Visual feedforward and BF projections reach the V1-V2 area where cholinergic modulation takes place. Right: Area V1-V2 (right hemisphere back view) where gamma band responses were found to be modulated in fear conditioning [1].

total, 15 CS+ and 15 CS- trials were alternatively presented. Figure 1 shows a scheme of the proposed model.

During the acquisition phase, arousal and the US increase BF activity facilitating the firing of V1-V2 layer I inhibitory neurons and MT cells. Plastic connections between V1 and the V1-V2 area learn to increase its firing rate to layer I inhibitory neurons (excitation pathway, CS+) or to MT cells (inhibitory pathway, CS-). The weight change of these connections followed the widely used rules of spike time dependent plasticity (STDP) [6]. In extinction, arousal is removed and the US no longer presented.

Multiple simulations (20 runs) were computed to obtain a more realistic variability in the model activity. An integrate and fire (IAF) neuron model was selected because of its efficiency and used to reproduce all the neurons of the network (3,018 in total). All simulations were carried out using the NEST Simulator [8]. Discriminative activity evoked by oriented Gabor patches was

computed using an V1 model previously developed by our group [9] and can be downloaded at: https://github.com/LCCN/MDPI2021. Finally, the 20 model outcomes are used to generate a simulated signal and a time-frequency analysis was conducted to compare them against the empirical data previously found in humans (n = 30) using MEG [1].

Results and discussion

After the acquisition phase where the US is paired with the CS+ and high arousal is present during all trials, the model learns to discriminate between the CS+ and the CS-. In the case of the CS+, the mere presence of the stimulus activates layer I inhibitory neurons thus triggering an excitation of pyramidal cells of layers II/III, V and VI in the CS+ associated column. In contrast, the CS- stimulus provokes the firing of MT cells causing an inhibition within the CS- column. In absence of arousal during the extinction phase, these inhibitory interneurons reduce their activity undoing the learning effects and return to activity levels like during habituation.

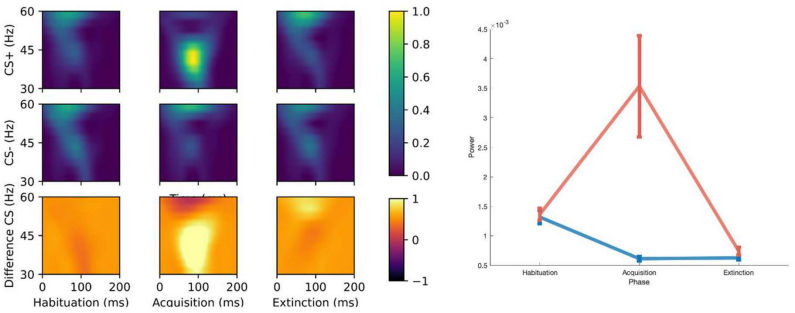

FIGURE 2

Left: Time-frequency analysis of gamma-band power in V1-V2 area during habituation, acquisition and extinction for the CS+ (first row) and the CS- (second row). The third row shows the difference between CS presentations. Right: Averaged time-frequency power across the significant cluster for each condition and phase (CS+ in red line, CS- in blue line).

To provide a more realistic perspective on the results of the model, its outcomes were compared with those recorded in humans. Time frequency analysis of the simulated signal revealed a significant cluster ($F(1,49) = 7667.5$, $p = 0.0013$) for the interaction experimental phase by condition (CS+ increase and CS- decrease only during acquisition) ranging from 40 ms to 160 ms and encompassing 30 Hz to 60 Hz (see Figure 2).

The performance of the model accords with the empirical data [1], showing similar time-frequency modulations. Whilst our model cannot fully confirm any neurobiological hypothesis underlying fear conditioned modulation of visual cortex, it provides a plausible mechanism with respect to cholinergic processes that explain the excitation but also the inhibition of cortical areas that code CS+ and CS- representations, respectively. Interestingly, our model provides an explanation of the visual cortex modulation without the involvement of the amygdala.

Acknowledgements
The current work was funded by the Spanish Ministry of Science (project PGC2018-097940-B-100 and grant Formación de Doctores PRE2019-088305).

References

[1] A. Santos-Mayo, J. de Echegaray & S. Moratti, «Conditioned up and down modulations of short latency gamma band oscillations in visual cortex during fear learning in humans», Sci. Rep., vol. 12, n.o 1, p. 2652, dic. 2022, doi: 10.1038/s41598-022-06596-8.

[2] M. Yuan, T. Giménez-Fernández, C. Méndez-Bértolo & S. Moratti, «Ultrafast Cortical Gain Adaptation in the Human Brain by Trial-To-Trial Changes of Associative Strength in Fear Learning», J. Neurosci., vol. 38, n.o 38, pp. 8262-8276, sep. 2018, doi: 10.1523/JNEUROSCI.0977-18.2018.

[3] A. Mattera, M. Pagani & G. Baldassarre, «A Computational Model Integrating Multiple Phenomena on Cued Fear Conditioning, Extinction, and Reinstatement», Front. Syst. Neurosci., vol. 14, p. 569108, sep. 2020, doi: 10.3389/fnsys.2020.569108.

[4] J. J. Letzkus et al., «A disinhibitory microcircuit for associative fear learning in the auditory cortex», Nature, vol. 480, n.o 7377, pp. 331-338, dic. 2011, doi: 10.1038/nature10674.

[5] J. Obermayer et al., «Lateral inhibition by Martinotti interneurons is facilitated by cholinergic inputs in human and mouse neocortex», Nat. Commun., vol. 9, n.o 1, Art. n.o 1, oct. 2018, doi: 10.1038/s41467-018-06628-w.

[6] R. B. Poorthuis, L. Enke & J. J. Letzkus, «Cholinergic circuit modulation through differential recruitment of neocortical interneuron types during behaviour», J. Physiol., vol. 592, n.o 19, pp. 4155-4164, 2014, doi: 10.1113/jphysiol.2014.273862.

[6] G. Bi & M. Poo, «Synaptic Modifications in Cultured Hippocampal Neurons: Dependence on Spike Timing, Synaptic Strength, and Postsynaptic Cell Type», J. Neurosci., vol. 18, n.o 24, pp. 10464-10472, dic. 1998, doi: 10.1523/JNEUROSCI.18-24-10464.1998.

[8] Spreizer, Sebastian et al., «NEST 3.3». Zenodo, March 22, 2022. doi: 10.5281/ZENODO.6368024.

[9] A. Santos-Mayo, S. Moratti, J. de Echegaray & G. Susi, «A Model of the Early Visual System Based on Parallel Spike-Sequence Detection, Showing Orientation Selectivity», Biology, vol. 10, n.o 8, p. 801, ago. 2021, doi: 10.3390/biology10080801.

Machine learning for predicting individual disease progression in early stage of cognitive deficits

Author
Anna Schweinar – Department of Neurology, Jena University Hospital, Germany; Biomagnetic Center, Jena University Hospital, Germany; Else Kröner Graduate School for Medical Students „JSAM", Jena University Hospital, Germany
Franziska Wagner – Department of Neurology, Jena University Hospital, Germany; Biomagnetic Center, Jena University Hospital, Germany; Clinician Scientist Program OrganAge, Jena University Hospital, Germany
Stefan Brodoehl – Department of Neurology, Jena University Hospital, Germany; Biomagnetic Center, Jena University Hospital, Germany

Citation
Schweinar, A., Wagner, F., Brodoehl, S. Machine learning for predicting individual disease progression in early stage of cognitive deficits.

Introduction

Dementia is one of the most common neurodegenerative diseases in old age. It currently affects 55 million people worldwide. The number of elderly people is continuously increasing and represents one of the main risk factors for dementia. If there is no breakthrough in early diagnosis and treatment, the number of dementia patients will rise to 130 million in 2050 [1]. Dementia often develops from mild cognitive impairment (MCI). MCI is a condition characterized by minimal cognitive impairment in everyday life. MCI manifests itself individually in each patient; it may remain stable, progress to dementia, or the neurological state may normalize. People with MCI have a higher risk of developing dementia than comparable people of the same age. MCI provides a good opportunity for early targeted intervention to delay

or prevent the development of dementia [2]. Meanwhile, artificial intelligence is gaining importance in neurodegenerative diseases. Imaging and machine learning have been used mainly to predict the transformation of MCI into definite dementia (e.g., AD) [3]. Progression in relation to milestones of cognitive decline important to the patient has not been considered here. In particular, the combination of clinical parameters and imaging techniques has not yet been investigated. A typical generative adversarial network is one of the most rapidly expanding methods of ML and is already finding extensive use in image processing and prediction of complex patterns [4]. The core principle here is to compete for a generator and a discriminator against each other. The discriminator tries to distinguish between real data (training data) and fake data (from the generator), while the generator tries to "trick" the discriminator and make its products look as real as possible. Multi-Label Time-Series GAN (MTGAN) can be used to generate time series of visit data. MTGAN can create improved prediction models [5].

In this research work, a generative adversarial network is trained by combining different parameters: medical history, laboratory parameters, neuropsychological test and imaging by machine learning methods:

1. to predict the individual course of the disease

2. to create an artificial patient based on real data (synthetic patient) and test the effects of different factors on the course of a synthetic patient.

Methods

In order to predict the disease course of a patient with MCI and to generate an artificial patient, we created a database of 60-100 patients with MCI (Figure 2) [6]. Patients with an initial diagnosis of MCI, aged 55-85 years, who had been examined for at least two consecutive years at the memory center in Jena, Germany, were included. This individual longitudinal patient data include over 50 parameters such as imaging, laboratory values, cerebrospinal fluid, neuropsychological tests, and background information about the patient. This data set, with the known outcome, trains a generative adversarial

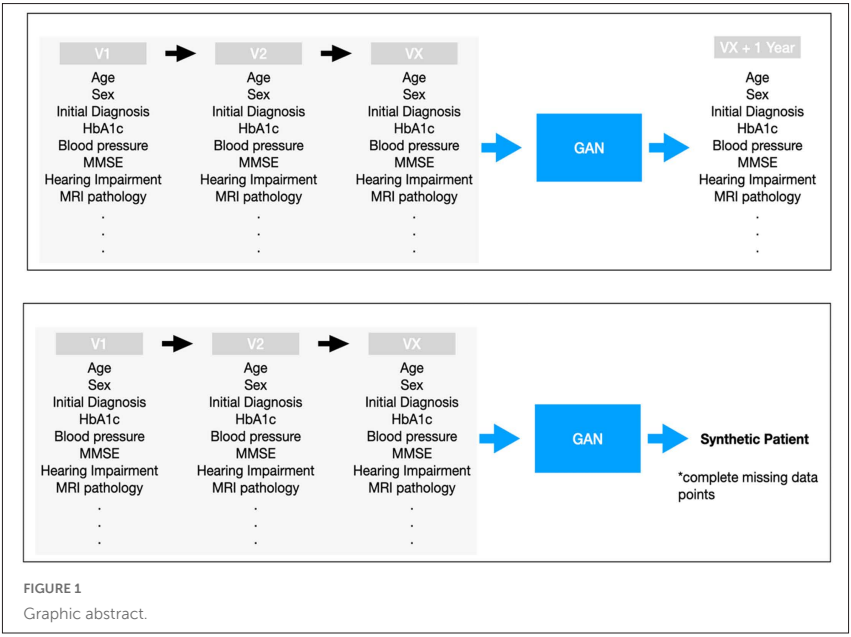

FIGURE 1
Graphic abstract.

network (GAN) in a machine learning approach. We are currently working on the exact architecture of the GAN, which should generate an artificial patient and predict the course of a patient's disease (Figure 1).

Results and discussion

The hypothesis we are testing is that the individual disease course of an MCI patient can be predicted by machine learning. For this purpose, we have prepared a database for training a neural network (Figure 2). At the moment we still work on the exact architecture of the GAN. The final results will be presented at the conference.

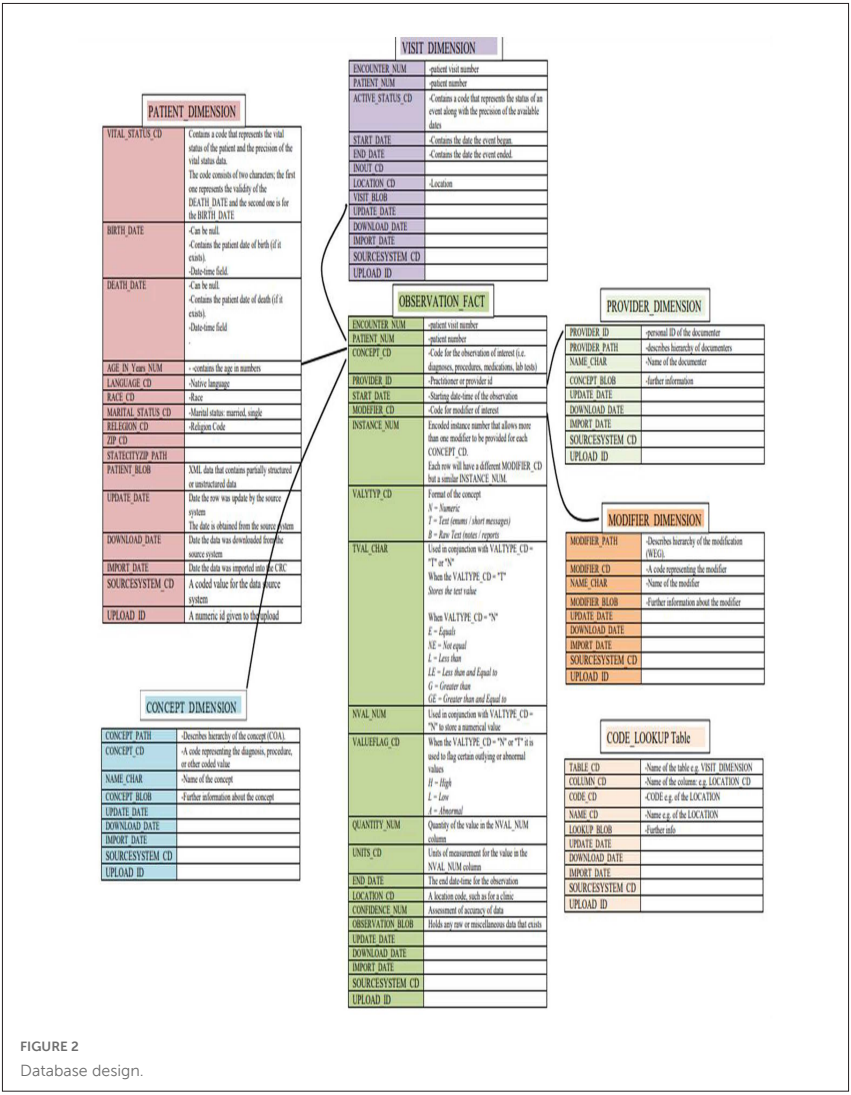

FIGURE 2
Database design.

Acknowledgements
This work is supported by funding from the Foundation „Else Kröner-Fresenius-Stiftung" within the Else Kröner Graduate School for Medical Students „Jena School for Ageing Medicine (JSAM).

References

[1] WHO. Global Status Report on the Public Health Response to Dementia; WHO: Geneva, Switzerland, 2021.

[2] R. C. Petersen, O. Lopez, M. J. Armstrong, T. S. D. Getchius, M. Ganguli, D. Gloss, 2018. ´Practice guideline update summary: Mild cognitive impairment: Report of the Guideline Development, Dissemination, and Implementation Subcommittee of the American Academy of Neurology´. Neurology Vol. 90 Issue 3 Pages 126-135. DOI: 10.1212/WNL.0000000000004826

[3] Grueso, Sergio, and Raquel Viejo-Sobera. 2021. 'Machine Learning Methods for Predicting Progression from Mild Cognitive Impairment to Alzheimer's Disease Dementia: A Systematic Review'. Alzheimer's Research & Therapy 13(1):162. doi: 10.1186/s13195-021-00900-w

[4] Goodfellow, Ian J., Jean Pouget-Abadie, Mehdi Mirza, Bing Xu, David Warde-Farley, Sherjil Ozair, Aaron Courville, and Yoshua Bengio. 2014. 'Generative Adversarial Nets'. Pp. 2672–80 in Proceedings of the 27th International Conference on Neural Information Processing Systems - Volume 2, NIPS'14. Cambridge, MA, USA: MIT Press.

[5] Chang Lu, Chandan K. Reddy, , Ping Wang, Dong Nie, and Yue Ning. 2022. `Multi-Label Clinical Time-Series Generation via Conditional GAN`. ArXiv 2022 Vol. abs/2204.04797

[6] Data model. Star schema. Available at https://community.i2b2.org/wiki/display/BUN/2.+Quick+Start+Guide. 30.10.22 (2022)

Effects of acute stress and epinephrine administration on memory impairment and anxiety behavior

Author
Zehra Sezgin – Department of Medical School, Zonguldak Bulent Ecevit University, Zonguldak, Turkey
Hale Sayan Ozacmak – Department of Physiology, Zonguldak Bulent Ecevit University, Zonguldak, Turkey

Citation
Sezgin, Z., Ozacmak, H.S. Effects of acute stress and epinephrine administration on memory impairment and anxiety behavior.

Introduction/Motivation

Stress is a life experience that affects the daily behavior and well-being of organisms and, in extreme cases, contributes to numerous psychopathologies in humans, including anxiety, post-traumatic stress disorder, depression, schizophrenia, and relapse of drug use [1]. Acute stress includes stress that occurs over a relatively short period of time, whereas chronic stress is measured over a lifetime and includes exposure to many repeated stressors [2]. In contrast to chronic stress, which impairs learning and memory processes, acute stress has been reported to have positive or negative effects on memory formation and memory recovery [3].

The new experience causes changes in neuronal protein content and synaptic strength, eventually leading to memory encoding through long-term changes in neural connectivity pattern [4]. Sympathetic nervous system responses include the release of the catecholamines epinephrine and

norepinephrine from the adrenal medulla [5]. Neurogranin is a small neuronal protein that undergoes local translation in an activity-dependent manner expressed in the somato-dendritic compartment. Neurogranin is reported to critically affect Ca2+ or Ca2+/CaM-dependent neuronal processes such as synaptic plasticity and ultimately learning and memory [6]. The aim of the study is to examine the effects of acute stress and high-dose epinephrine administration on learning, memory and anxiety behavior, as well as neurogranin and brain metabolism changes.

Methods

In the study, 3 groups were formed with 8 rats in each group: Control, acute stress and acute stress + epinephrine administered groups. As the acute stress model, restraint stress for 2.5 hours was applied. Epinephrine was administered as a single dose of 1 mg/kg (subcutaneously) after acute stress.

The anxiety behavior was determined by the open field test, the hippocampal learning was determined by the Morris water maze (MWM).

Neurogranin and glycogen levels were measured in the hippocampus and prefrontal cortex. Neurogranin levels in hippocampus and prefrontal cortex tissues were measured using a commercial kit. For this purpose, protein levels were determined in accordance with the study procedure as suggested by the commercial kit. These parameters were measured by preparing hippocampal synaptosomes.

Hippocampus and prefrontal cortex glycogen levels were measured with the technique of Lo and colleagues [7]. Tissue samples taken for this purpose were kept in a boiling water bath with KOH for 30 minutes, then 95% ethanol was added and centrifuged at 2400 rpm. After discarding the supernatant and diluting the pellets with distilled water, 1 ml was taken. 5% phenol and H2SO4 were added to it. It was read in a spectrophotometer at 490 nm after 20 minutes in a water bath.

Results and discussion

In the open field test; Anxiety-like behavior determined by the number of defecations and the number of entrances to the central squares was found to be significantly higher in the stress+epinephrine group compared to the other groups ($p < 0,05$). The probe test evaluated in MWM was found to be lower in the acute stress group compared to the control group ($p<0,05$). A decrease in hippocampus and prefrontal cortex neurogranin levels was found in rats treated with stress+epinephrine compared to controls ($p<0,05$). In addition, hippocampus and prefrontal cortex glycogen levels decreased with acute stress ($p<0,05$).

It has been shown that administration of epinephrine in addition to acute stress causes a negative effect on learning and anxiety behavior with a decrease in hippocampus neurogranin (Figure 1-2) and glycogen levels. Probe trail (removed platform test) was performed to evaluate the memory performance of rats in acute stress and the time spent in the target quadrant was determined in the probe test.

The time spent in the target quadrant decreased after acute stress group compared to that of the control group. Epinephrine treatment did not change memory performance in stressed rats.

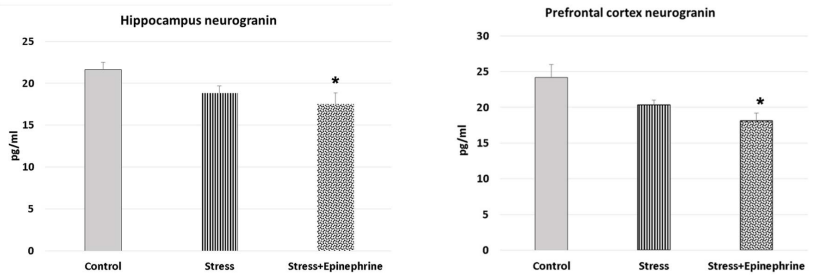

FIGURE 1-2

Effects of acute stress and epinephrine administration on neurogranin level in hippocampus and prefrontal cortex. Data are presented as mean ±standard error. *p<0,05 compared to control group.

In this study, the decrease in neurogranin level in animals treated with stress epinephrine affected the decrease in probe test performance. It is important to understand acute stress in daily life, both theoretically and practically, in terms of its effects on memory and stress-related diseases. Experiments investigating the neural mechanisms and networks underlying the effects of stress in humans will enrich our understanding of the interactions between acute stress and memory and guide potential interventions that can enable individuals to overcome life challenges [8]. Previous studies have shown that Ng levels change in response to behavioral, environmental, and hormonal stimulation in rodent models, and schizophrenic and aging brains in humans [9]. In future studies, the levels of neurogranin under chronic stress can be investigated.

Acknowledgements
The study was supported by TUBITAK (The Scientific and Technological Research Council of Turkey, 2209/A Undergraduate Research Project Support program).

References

[1] Shields, G. S., Sazma, M. A., McCullough, A. M., & Yonelinas, A. P. (2017). The effects of acute stress on episodic memory: A meta-analysis and integrative review. Psychological bulletin, 143(6), 636.

[2] Sazma, M. A., Shields, G. S., & Yonelinas, A. P. (2019). The effects of post-encoding stress and glucocorticoids on episodic memory in humans and rodents. *Brain and cognition*, 133, 12-23.

[3] Shields, G. S., Sazma, M. A., McCullough, A. M., & Yonelinas, A. P. (2017). The effects of acute stress on episodic memory: A meta-analysis and integrative review. *Psychological bulletin*, 143(6), 636.

[4] Kennedy, M. B. (2016). Synaptic signaling in learning and memory. Cold Spring Harbor perspectives in biology, 8(2), a016824.

[5] Schwabe, Lars, et al. "Stress effects on memory: an update and integration." Neuroscience & Biobehavioral Reviews 36.7 (2012): 1740-1749.

[6] Jones KJ, Templet S, Zemoura K, Kuzniewska B, Pena FX, Hwang H, Lei DJ, Haensgen H, Nguyen S, Saenz C, Lewis M, Dziembowska M, Xu W. Rapid, experience-dependent translation of neurogranin enables memory encoding. Proc Natl Acad Sci U S A. 2018 Jun 19;115(25):E5805-E5814. doi: 10.1073/pnas.1716750115. Epub 2018 Jun 7. PMID: 29880715; PMCID: PMC6016824.

[7] Lo S, Russell JC, Taylor AW: Determination of glycogen in small tissue samples. J Appl Physiol 28(2): 234–236, 1970

[8] Gagnon, S. A., & Wagner, A. D. (2016). Acute stress and episodic memory retrieval: neurobiological mechanisms and behavioral consequences. Annals of the New York Academy of Sciences, 1369(1), 55-75.

[9] Jones, K. J., Templet, S., Zemoura, K., Kuzniewska, B., Pena, F. X., Hwang, H., ... & Xu, W. (2018). Rapid, experience-dependent translation of neurogranin enables memory encoding. Proceedings of the National Academy of Sciences, 115(25), E5805-E5814.

Brain bases of attitude and preference change motivated by cognitive dissonance: A scoping review

Author
Estrella Veiga-Zarza, Luis Carretié – Biological and Health Psychology Department, Faculty of Psychology, Autonomous University of Madrid, Madrid, Spain

Citation
Veiga-Zarza, E., Carretié, L. Brain bases of attitude and preference change motivated by cognitive dissonance: A scoping review.

Introduction/Motivation

Cognitive dissonance (CD) theory[1] proposes that when we evaluate our attitudes and behaviours as inconsistent with each other, a negative affective state emerges, prompting cognitive and behavioural adaptations to reduce perceived "dissonance" or incoherence. This mechanism by which adaptations are made to adjust contradictory psychological elements is what has been explored in studies on attitude and preference change motivated by CD. These studies address three functional processes[2]: 1) the detection of initial inconsistency, 2) that would generate the unpleasant psychological state or the aversive and discomfort emotions and 3) that, finally, would predispose to generate cognitive or behavioural efforts to reduce the dissonance. The recent neuroscientific approach to this psychological process has opened relevant possibilities for future research.[3] There is growing evidence of the involvement of the anterior cingulate cortex (ACC) in attitude and preference change motivated by CD.[4,5] Different studies also

suggest that the activity of the dorsolateral prefrontal cortex (dlPFC) is linked to preference change.[6,7] Likewise, as these paradigms include subjective assessment tasks, the participation of regions that encode stimulus values has been pointed out,[8,9] such as the ventromedial prefrontal cortex (vmPFC), posterior cingulate cortex (PCC), and ventral striatum (VS). However, the participation of some of these and other structures has not been confirmed unanimously in the literature. This fact leaves room to hypothesize whether these regions participate depending on the experimental paradigm used in the studies, the stimuli presented, the characteristics of the sample, or the temporal moment of the paradigm in which the brain activity was recorded or stimulated. That highlights the need to synthesize the knowledge produced to date on the brain bases of attitude and preference change induced by CD. Furthermore, systematizing those studies can help to identify issues that have not yet been explored, suggest possible ways of approaching future research, and propose models of brain function to explain this change in attitudes and preferences. This work aims to review the existing literature on the neural bases of the attitude and preference change induced by CD through experimental paradigms of Cognitive Neuroscience and draw conclusions from the available information to date.

Methods

The review follows PRISMA (Preferred Reporting Items for Systematic Reviews and Meta-Analysis) guidelines for scoping reviews[10]. Three electronic databases (Medline, PsycInfo, and PsycArticles) were searched combining search terms such as "cognitive dissonance", "attitude change" or "preference change" with others related to the recording or stimulation of brain activity (e.g., "electroencephalography"). Afterwards, the sample of primary articles was expanded following the snowball sampling, based on the references of the studies reviewed. The search was limited to the following seven inclusion criteria: (i) They were empirical studies, (ii) the difference in attitudes/preferences were quantitatively analysed *a posteriori* -as a consequence of the manipulation of CD-, (iii) conditions of high and low CD were compared, (iv) electrophysiological measures of brain activity were taken, or functional brain imaging records, or brain stimulation techniques were used to study

this change in attitudes/preferences, (v) studies were peer-reviewed, (vi) written in English or Spanish, and (vii) performed on a healthy human sample. No temporal inclusion criteria were established due to the relatively recent appearance of neuroscientific studies on this research problem. For those relevant articles that met the criteria, the following information was extracted: (i) the experimental design, the attitude/preference change paradigm used and the stimuli presented, (ii) the brain activity recording or stimulation technique, and the specific moment of application of the technique, (iii) the sample size and characteristics of the sample, (iv) the sampling method by which they were included in this review (through database search or snowball sampling), (v) the year of publication and (vi) the main behavioural and cerebral results.

Results and discussion

After duplicate removal, screening, and full-text assessment, 15 studies were included in the review. Based on the results of this review (Figure 1), attitude and preference change motivated by CD occurs after a process of inconsistency detection between previous attitudes or preferences and subsequent behaviours. Here, the participation of the ACC is especially relevant.[5,9,11,12] Afterwards, a process of updating the representation of the value of the stimuli (preference or attitude change) would take place. It seems to be linked to the activity of the dlPFC,[6,7] which promotes changes in regions that encode the preferences of the stimuli, such as the VS.[6,12,13] Although to a lesser extent than the regions mentioned above, some studies[6,8,9] suggest the involvement of other regions in preference or attitude change motivated by CD (e.g., middle frontal gyrus, PCC, or hippocampus). In addition, we also identified and highlighted some relevant issues still unexplored, which should be further examined and detailed in future research. For instance, whether the activity of the ACC decreases after adjusting attitudes/preferences, whether and how conscious and automatic processes of preference change coexist, and what is more precisely the role of the precuneus or the anterior insula in this process. This review constitutes the first systematic approach to the existing literature on the neural bases of the preference and attitude change motivated by CD.

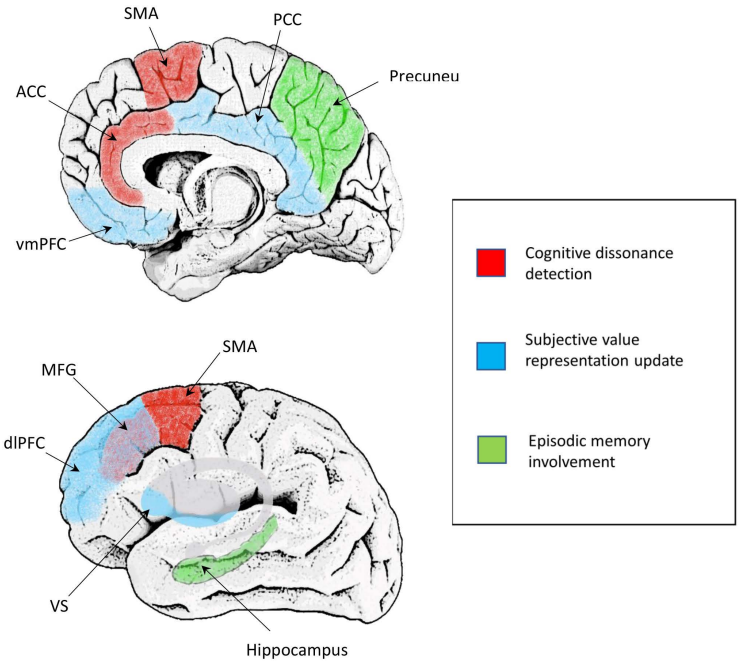

FIGURE 1

Main brain structures involved in attitude and preference change motivated by cognitive dissonance

Note. Medial and lateral views of the brain representing illustratively the main brain structures involved in the different subprocesses of attitude and preference change motivated by cognitive dissonance: the detection of dissonance and the updating of subjective value, in addition to the participation of episodic memory. The hippocampus and VS, located internally, have been semi-transparently represented in the lateral view. dlPFC and MFG are partially overlapped. Abbreviations: SMA, Supplementary motor area; ACC, Anterior cingulate cortex; PCC, Posterior cingulate cortex; dlPFC, Dorsolateral prefrontal cortex; vmPFC, Ventromedial prefrontal cortex; VS, Ventral striatum; MFG, Middle frontal gyrus. Adapted from Carretié[14].

Acknowledgements

Spanish Ministry of Science and Innovation (MICINN; PGC2018-093570-B-I00) and the Spanish Ministry of Universities (FPU20/04952) supported the preparation of this work.

References

[1] Festinger L. A theory of cognitive dissonance. Stanford: Stanford University Press; 1957.

[2] De Vries J, Byrne M, Kehoe E. Cognitive dissonance induction in everyday life: An fMRI study. Social Neuroscience. 2014;10(3):268–81.

[3] Harmon-Jones E, Mills, J. (2019). An introduction to cognitive dissonance theory and an overview of current perspectives on the theory. In: Harmon-Jones E. Cognitive dissonance: Reexamining a pivotal theory in psychology. American Psychological Association; 2019. p. 3–24.

[4] Colosio M, Rybina EP, Shestakova AN, Klucharev VA. Neural mechanisms of post-decisional spreading of alternatives. Psychology. Journal of the Higher School of Economics. 2018;15(3):606–614.

[5] Van Veen V, Krug MK, Schooler JW, Carter CS. Neural activity predicts attitude change in cognitive dissonance. Nature Neuroscience. 2009;12(11):1469–1474.

[6] Izuma K, Matsumoto M, Murayama K, Samejima K, Sadato N, Matsumoto K. Neural correlates of cognitive dissonance and choice-induced preference change. Proceedings of the National Academy of Sciences. 2010;107(51):22014–22019.

[7] Mengarelli F, Spoglianti S, Avenanti A, di Pellegrino G. Cathodal tDCS over the left prefrontal cortex diminishes choice-induced preference change. Cerebral Cortex. 2013;25(5):1219–27.

[8] Chammat M, Karoui IE, Allali S, Hagège J, Lehongre K, Hasboun D, et al. Cognitive dissonance resolution depends on episodic memory. Scientific Reports. 2017;7(1): 1-10.

[9] Voigt K, Murawski C, Speer S, Bode S. Hard decisions shape the neural coding of preferences. The Journal of Neuroscience. 2018;39(4):718–726.

[10] Page MJ, McKenzie JE, Bossuyt PM, Boutron I, Hoffmann TC, Mulrow CD, et al. The Prisma 2020 statement: An updated guideline for reporting systematic reviews. British Medical Journal. 2021; 372.

[11] Ito A, Kawachi Y, Kawasaki I, Fujii T. Effect of aging on choice-induced cognitive conflict. Behavioural Brain Research. 2019; 363:94–102.

[12] Kitayama S, Chua HF, Tompson S, Han S. Neural mechanisms of dissonance: An fMRI investigation of choice justification. NeuroImage. 2013; 69:206–212.

[13] Sharot T, De Martino B, Dolan RJ. How choice reveals and shapes expected hedonic outcome. Journal of Neuroscience. 2009;29(12):3760–3765.

[14] Carretié L. Anatomía de la mente. 3rd ed. Madrid: Ediciones Pirámide; 2021. p.262

Theoretical neuroscience

Allosteric modulation of nicotinic acetylcholine receptor α7 studied by molecular dynamics

Author
Mariia Avstrikova – Channel-Receptors Unit, CNRS UMR 3571, Institut Pasteur, Paris, France; Institut de Chimie de Strasbourg, CNRS UMR 7177, Université de Strasbourg, Strasbourg, France
Jean-Pierre Changeux – Channel-Receptors Unit, CNRS UMR 3571, Institut Pasteur, Paris, France; Kavli Institute for Brain and Mind, University of California, San Diego, La Jolla, CA, USA; Collège de France, Paris, France
Marco Cecchini – Institut de Chimie de Strasbourg, CNRS UMR 7177, Université de Strasbourg, Strasbourg, France

Citation
Avstrikova, M., Changeux, J.-P., Cecchini, M. Allosteric modulation of nicotinic acetylcholine receptor α7 studied by molecular dynamics

Introduction

Nicotinic acetylcholine receptors (nAChRs) are neurotransmitter receptors that mediate communication between nerve cells [1]. nAChRs are known to be involved in various neurological disorders including Alzheimer's, depression, schizophrenia, etc. [2]. Recently nAChRs have been also associated with COVID-19 pathophysiology [3, 4]. This makes nAChRs an interesting target for both: neuropharmacology and, potentially, COVID-19 treatment.

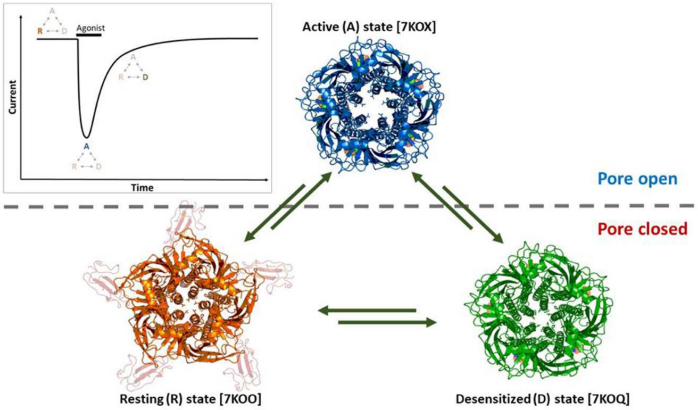

FIGURE 1
Physiological states of α7 nAChR (PDB code of each structure is in square brackets). The plot describes the effect of agonist (neurotransmitter) binding on the equilibrium between the states.

The concept of allosteric regulation of nAChRs assumes that ligands modulate the protein activity by binding to the site that is distinct from the neurotransmitter putative site. Such molecules regulate the response to agonist, which is the transition between resting (R), active (A) and desensitized (D) states of receptor (Fig.1) [5]. Positive allosteric modulators (PAMs) of α7 nAChR are classified into two types: type I PAMs are just increasing the agonist-evoked peak current, while type II PAMs are both increasing the peak current and delaying the desensitization [6]. A structural understanding of the mechanism of action of different PAMs is a crucial step in the pharmacology of nAChRs.

Methods

Molecular dynamics (MD) simulations are commonly used to study the physical motion of molecules with atomistic resolution. In this project we performed all-atom MD simulations of recently published structures of α7 nAChR in A (PDB:7KOX), R (PDB:7KOO) and D (PDB:7KOQ) states [7].

The simulation systems were prepared with CHARMM-GUI [8] web server. The protein structures are embedded into a lipid bilayer composed of POPC molecules and solvated in a rectangular box using TIP3P [9] water model and 0.15M NaCl ions. The unbiased MD simulations of 300 ns were performed using Gromacs2022 [10] with CHARMM36m force field [11] at 300 K. The simulations were performed in three independent replicas to ensure the statistical relevance of the results.

Results and discussion

The simulations of α7 nAChR revealed an unexpected plasticity of the D state structure at the level of the ion transmembrane pore. Exploration of the pore profile within three replicas of 300 ns simulation suggests that unlike A and R states that keep stable conformation of the channel, the D state is capable of spontaneous transitions between open-like and closed-like conformations of the channel. This observation is supported by analysis of the pore hydration in different replicas of D state simulation, which shows that in two out of three replicas the ion channel is hydrated and accessible to ions. In sharp contrast, in the third replica, we observe disruption of pore hydration and formation of the hydrophobic gate at the level of L247. This observation allows for characterizing the channel as closed in this simulation.

Such behaviour of the D state suggests that our simulations sample spontaneous transitions between a desensitized conformation and an intermediate conformation of the receptor, which is structurally similar to the D state but possesses an open channel. Based on this observation, we hypothesize that the characteristic effect of type II PAM on desensitization could be related to the stabilization of such an intermediate conformation.

To validate this hypothesis, we performed MD simulations of several α7 nAChR structures bound to PAMs, including Ivermectin (IVM) that represents type I PAM, PNU-120596 (PNU) and (-)-TQS (TQS) that represent type II PAM. These structures were obtained in collaboration with the group of Dr Ryan Hibbs (University of Texas Southwestern Medical Center).

Analysis of these simulations at the level of the ion channel shows that the structures bound to type II PAM, especially PNU, keep the ion pore open, whereas structures bound to type I PAM remain closed, which is coherent with our hypothesis.

Further analysis of these simulations will be performed to investigate the mechanism underlying such effect of different PAMs.

Acknowledgements
We thank Dr. Ryan Hibbs and his team at the University of Texas Southwestern Medical Center for providing us with cryo-EM structures of α7 nAChR bound to PAMs.

This project is supported by UE H2020-SGA-FETFLAG-HBP-2019 SGA3.

This work was performed using HPC resources from GENCI–IDRIS (Grant 2021- A0110706644).

References

[1] D. Purves, G. J. Augustine, D. Fitzpatrick, W. Hall, A.-S. LaMantia, and L. White, Neurosciences. Oxford University Press, 2018.

[2] A. Taly, P. J. Corringer, D. Guedin, P. Lestage, and J. P. Changeux, "Nicotinic receptors: Allosteric transitions and therapeutic targets in the nervous system," Nature Reviews Drug Discovery, vol. 8, pp. 733–750, 2009.

[3] J. P. Changeux, Z. Amoura, F. A. Rey, and M. Miyara, "A nicotinic hypothesis for covid-19 with preventive and therapeutic implications," Comptes Rendus - Biologies, vol. 343, pp. 33–39, 2020.

[4] A. S. F. Oliveira, A. A. Ibarra, I. Bermudez, L. Casalino, Z. Gaieb, D. K. Shoemark, T. Gallagher, R. B. Sessions, R. E. Amaro, and A. J. Mulholland, "A potential interaction between the sars-cov-2 spike protein and nicotinic acetylcholine receptors," Biophysical Journal, vol. 120, pp. 983–993, 3 2021.

[5] M. Cecchini and J.-P. P. Changeux, "The nicotinic acetylcholine receptor and its prokaryotic homologues: Structure, conformational transitions & allosteric modulation," Neuropharmacology, vol. 96, pp. 137–149, 6 2015.

[6] R. L. Papke and J. M. Lindstrom, "Nicotinic acetylcholine receptors: Conventional and unconventional ligands and signaling," Neuropharmacology, vol. 168, p. 108021, 5 2020.

[7] C. M. Noviello, A. Gharpure, N. Mukhtasimova, R. Cabuco, L. Baxter, D. Borek, S. M. Sine, and R. E. Hibbs, "Structure and gating mechanism of the α7 nicotinic acetylcholine receptor," Cell, pp. 1–14, 3 2021.

[8] S. Jo, T. Kim, V. G. Iyer, and W. Im, "Charmm-gui: A web-based graphical user interface for charmm," Journal of Computational Chemistry, vol. 29, pp. 1859–1865, 8 2008.

[9] W. L. Jorgensen, J. Chandrasekhar, J. D. Madura, R. W. Impey, and M. L. Klein, "Comparison of simple potential functions for simulating liquid water," The Journal of Chemical Physics, vol. 79, p. 926, 8 1998.

[10] D. Van Der Spoel, E. Lindahl, B. Hess, G. Groenhof, A. E. Mark, and H. J. C. Berendsen, "Gromacs: Fast, flexible, and free," Journal of Computational Chemistry, vol. 26, no. 16, pp. 1701–1718, 2005.

[11] J. B. Klauda, R. M. Venable, J. A. Freites, J. W. O'Connor, D. J. Tobias, C. Mondragon-Ramirez, I. Vorobyov, A. D. MacKerell, and R. W. Pastor, "Update of the charmm all-atom additive force field for lipids: Validation on six lipid types," The Journal of Physical Chemistry B, vol. 114, no. 23, pp. 7830–7843, 2010. PMID: 20496934.

A novel computational platform to simulate the oxygen-dependent firing behaviour of biological neural networks

Author
Rachele Fabbri, Arti Ahluwalia, Chiara Magliaro – Research center Enrico Piaggio, University of Pisa, Pisa, Italy; Department of Information Engineering (DII), University of Pisa, Pisa, Italy

Citation
Fabbri, R., Ahluwalia, A., Magliaro, C. A novel computational platform to simulate the oxygen-dependent firing behaviour of biological neural networks

Introduction/Motivation

Current computational models of biological neural networks do not consider local oxygen concentration as a variable. However, oxygen is crucial for cells' viability and so its influence on both cell electrophysiological and metabolic behaviour should be considered in in vitro vessel-free neural constructs, even in monolayers or arranged in 3D (i.e., neurospheres and brain organoids). Thus, the aim of this work is implementing a novel computational platform modelling neural networks in monolayer firing over time, also considering the local oxygen concentration as an input variable influencing the electrical signal generated.

Methods

Experimental monolayers comprise cells distributed on the surface of a Petri dish with a substrate that promotes adhesion. The growth of cells is

supported by the presence of a culture medium above them that allows the oxygen to reach cells from the outer. Also in in vitro cultures, neurons form synaptic connections, creating neural networks similar to the ones observed in in vivo neural tissue. For modelling this setting, a bottom-up approach is adopted: first modelling the building blocks, i.e. the neurons, then connecting them to create the monolayer network. A column of medium stands above each neuron, containing the initial concentration of oxygen that then diffuses through the cell membrane.

In this system, oxygen diffuses and is consumed in part for fuelling neuron's metabolic functions and in part for firing, i.e. for sustaining the activity of the sodium-potassium-ATP pumps generating the action potentials. While oxygen diffusion is modelled through the Fick's second law of diffusion, metabolic consumption is described through Michaelis-Menten kinetics and firing through the modified Hodgkin-Huxley model proposed by Wei et al. [1]. The platform is implemented in MATLAB and Simulink environments. A customized Simulink library has been developed for modelling oxygen dynamics. A single block of this library reproduces the oxygen-dependent firing activity of the single neuron. The block can be then arranged and connected to create the layout of the neural network, by choosing the number of neurons in the network, the network layout, the number and the strength of synaptic connections of each neuron and the initial oxygen concentration.

Three different network layouts were defined and simulated. In the first two topologies, neurons' placement reproduces the matrix of electrodes in microelectrode array (MEA), the technology used to measure electrophysiological activity of neurons' monolayers in experimental settings. These two layouts differ in the neurons' number: one has 60 neurons, the other has 256 neurons. MEA-like networks have been chosen to easily compare their output with the one of an experimental MEA. In the 256 MEA network the outputs of four blocks close to each other have been mediated to simulate the acquisition of signals by MEA electrodes. Connections among the blocks of the two MEA-like arrangements were randomly generated. The third configuration is the so-called *Small World* (SW) network [2]. It has been

FIGURE 1
Scheme of the workflow of the project.

shown that SW networks are able to represent the functional graphs of neural networks of both the brain and *in vitro* monolayers [3–5]. The size of the SW network was set to 60 neurons, with a total of 120 connections. The Watts-Strogatz MATLAB function was used to create the SW graph for placing and wiring neurons within the Simulink model. For each layout, four different experiments were conducted varying the initial oxygen concentration (i.e., 6,4 mg/l to 5 mg/l, 3,6 mg/l and 2 mg/l).

The outputs of the platform are processed for detecting spikes, then exploited for evaluating the Firing Rate (i.e. number of spikes per seconds) of each neuron and the Spike Time Tiling Coefficient (STTC) [6] the correlation index, and 33 other measures of correlation of spike times are blindly tested for the required properties on synthetic and experimental data. Based on this, we propose a measure (the spike time tiling coefficient. STTC is a measure of the degree of correlation between a spike in a train and all the other ones in different spike trains, identified within a time window of 100 ms centred in the reference spike. The described workflow is summarised in Figure 1.

Results and discussion

Figure 2 shows the membrane potential of a single neuron model for different initial oxygen concentration (blue line) and the oxygen concentration at the neuron level (orange line). When the neuron fires bursts, we observe a decay in the oxygen concentration profile and a subsequent increase when the burst ends. This trend is representative of the adopted oxygen-dependent model of the firing activity of neurons, described in the previous section. It is also possible to see how local oxygen availability

influence the firing: the firing rate decreases when oxygen supply is lower. We observed this behaviour in all the three network layouts: mean firing rate decrease with statistically significant difference when oxygen drops from 6,4 mg/l to 3 mg/l and 2 mg/l. No significant difference is highlighted from 6,4 mg/l to 5 mg/l.

For validating the platforms in terms of physiological relevance, we compared outputs with neuronal signals from experimental MEA. Same metrics were calculated and the statistical analysis identified the absence of significant difference between the experimental MEA data and the simulated model with 256 neurons (Figure 2).

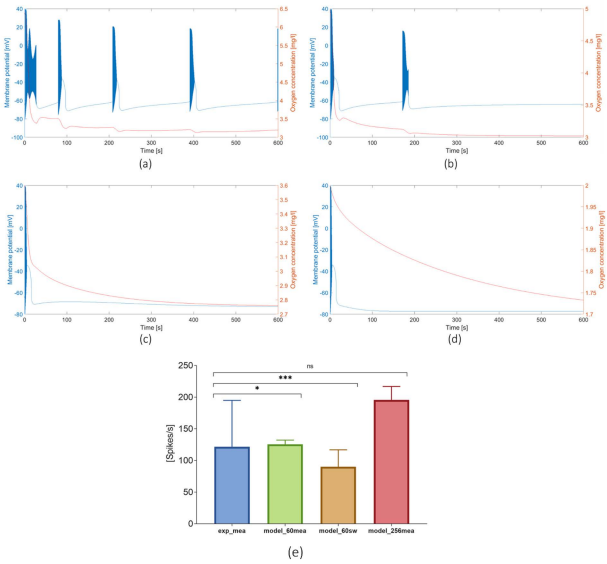

FIGURE 2

Output of the single neuron block, with four different initial oxygen concentrations: (a) 6,4 mg/l, (b) 5 mg/l, (c) 3.6 mg/l, (d) 2 mg/l. (e) comparison of the mean firing rate between the models and experimental MEA data.

The developed platform is able to mimic the oxygen-dependent firing activity of bidimensional neural networks. Scripts generate a different graph according to the desired arrangement of neurons in a bidimensional network. Such graph is automatically translated into a Simulink model where each node corresponds to a neuron block and edges to neuronal connections.

Although the platform is still under development, its features of full scalability, automatization and customization are core characteristics that will make it a very powerful tool for simulating different types of neurons, neural networks' layouts and studying the effects of oxygen local concentration and neurons' density on the output signals. Furthermore, once the platform is completely developed, we will make it open source and accessible to the scientific community.

References

[1] Y. Wei, G. Ullah, J. Ingram, and S. J. Schiff, "Oxygen and seizure dynamics: II. Computational modeling," J. Neurophysiol., vol. 112, no. 2, pp. 213–223, Jul. 2014, doi: 10.1152/jn.00541.2013.

[2] D. J. Watts and S. H. Strogatz, "Collective dynamics of 'small-world' networks," Nature, vol. 393, no. June, pp. 440–442, 1998.

[3] L. M. A. Bettencourt, G. J. Stephens, M. I. Ham, and G. W. Gross, "Functional structure of cortical neuronal networks grown in vitro," Phys. Rev. E - Stat. Nonlinear, Soft Matter Phys., vol. 75, no. 2, pp. 1–10, 2007, doi: 10.1103/PhysRevE.75.021915.

[4] D. S. Bassett and E. Bullmore, "Small-world brain networks," Neuroscientist, vol. 12, no. 6, pp. 512–523, 2006, doi: 10.1177/1073858406293182.

[5] E. Bullmore and O. Sporns, "Complex brain networks: Graph theoretical analysis of structural and functional systems," Nat. Rev. Neurosci., vol. 10, no. 3, pp. 186–198, 2009, doi: 10.1038/nrn2575.

[6] C. S. Cutts and X. S. J. Eglen, "Detecting Pairwise Correlations in Spike Trains: An Objective Comparison of Methods and Application to the Study of Retinal Waves," J. Neurosci., vol. 34, no. 43, pp. 14288–14303, Oct. 2014, doi: 10.1523/JNEUROSCI.2767-14.2014.

Burst-dependent plasticity and dendritic amplification support target-based learning and hierarchical imitation learning

Author
Cosimo Lupo – INFN, Sezione di Roma, Rome, Italy
Cristiano Capone – INFN, Sezione di Roma, Rome, Italy
Paolo Muratore – SISSA, Trieste, Italy
Pier Stanislao Paolucci – INFN, Sezione di Roma, Rome, Italy

Citation
Lupo, C., Capone, C., Muratore, P., Paolucci, P.S. Burst-dependent plasticity and dendritic amplification support target-based learning and hierarchical imitation learning.

Motivation

The brain can efficiently learn a wide range of tasks, motivating the search for biologically inspired learning rules for improving the efficiency of AI. Most biological models are composed of point neurons and cannot achieve the state-of-the-art performances of AI (e.g., they struggle to solve the credit assignment problem [1]).

Recent works have proposed that segregation of dendritic input (neurons receive sensory information and higher-order feedback in segregated compartments) [2] and generation of high-frequency bursts of spikes [1,4] would support backpropagation in biological neurons. However, these error-based approaches require propagating errors with a fine spatio-temporal

structure to all the neurons, and it is not clear whether this is possible in biological networks.

We suggest that dendritic input segregation and bursts generated by a basal-apical coincidence mechanism give the possibility to implement a target-based learning [3] in a biologically plausible fashion, with no need for error propagation, and to solve complex tasks, orchestrating hierarchical imitation learning [5,6].

Methods

Based on L5 pyramidal neurons (Fig. 1A), our neuron model consists of three separated compartments (Fig. 1B): the basal (receiving sensorial inputs), the apical proximal (receiving recurrent connections from the network), and the apical distal (receiving teaching/contextual signals from other brain areas, with a higher level of abstraction). It is known from the literature [4 and refs therein] that apical dendrites can initiate broad calcium action potentials, which cause a sustained depolarization spreading to the axon and lowering its firing threshold. This brings to an associative mechanism between feed-forward (sensorial) inputs and feed-back (abstract/contextual) apical inputs, generating high-frequency bursts of spikes in case of coincidence between the two stimuli ("back-propagation activated coupling").

In our model, this coincidence mechanism is implemented between the somatic compartment and each of the apical compartments, such that an apical spike occurring in coincidence with a somatic spike lowers the firing threshold and allows for high-frequency bursts of spikes (Fig. 1C).
As these bursts are an effect of a positive feedback given by the coincidence of sensorial inputs and higher-level predictions, they represent a powerful cortical coding mechanism and hence it becomes natural to postulate a burst-dependent plasticity rule in a target-based learning framework: the spatio-temporal pattern of bursts generated in presence of the teaching signal (through soma – apical distal coincidence) becomes the internal target, and recurrent connections between neurons are adapted so to autonomously reproduce it (through soma – apical proximal coincidence) when the teaching signal is no longer present.

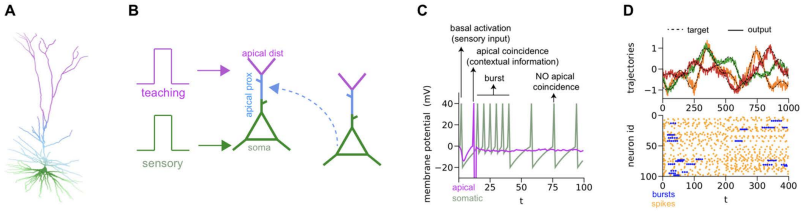

FIGURE 1

A) A typical L5 pyramidal neuron. Color coding refers to compartment modelization in panel B. ***B)*** Our three-compartment pyramidal neuron model. ***C)*** The coincidence mechanism between basal and apical compartments allows for the generation of high-frequency bursts of spikes. ***D)*** The store-and-recall task of a 3D trajectory. The target output (top panel, dashed line) is automatically encoded into a spatio-temporal pattern of bursts (bottom panel, blue points), and correctly reproduced by the network after the training of recurrent connections (top panel, solid lines).

Results

As a first application of this target-based approach through bursts, we consider the store-and-recall of a 3D trajectory (Fig. 1D, top, black dashed lines). Recurrent somatic to apical proximal connections are trained online to reproduce the target sequence of bursts induced by the teaching signal (Fig. 1D, bottom, blue points). Though being way less than isolated somatic spikes (Fig. 1D, bottom, orange points), bursts properly encode the 3D trajectory, that is correctly reproduced at the end of the training with a mse of 0.01 (Fig. 1D, top, colored solid lines).

More complex tasks can then be approached with this architecture. It is the case of those tasks that can be hierarchically decomposed into a series of simpler subtasks, to be addressed by different portions of the network. A typical example is given by the button-and-food task (Fig. 2A), a navigation task where the final reward (the "food") can be actually reached only after having fulfilled an intermediate goal (unlocking the "button"). To this aim, we realized a hierarchical network by organizing the overall network in two levels (Fig. 2B): the higher level acts as a manager, deciding the current goal ("button" or "food") (Fig. 2C, top) and providing such information as a

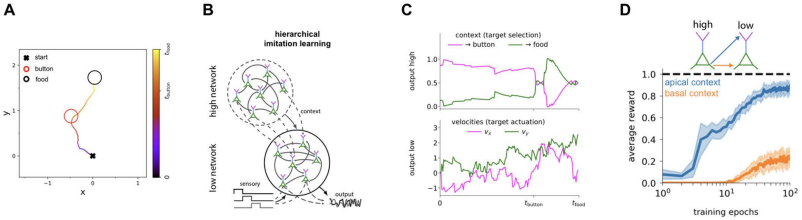

FIGURE 2

A) The button-and-food navigation task, where the final reward is available only upon the fulfilling of an intermediate goal. ***B)*** The two-level hierarchical architecture introduced to solve the button-and-food task, with the higher level acting as a "manager" and the low level representing the "worker". ***C)*** The outputs of the two levels composing the network. ***D)*** Task average performances (blue line), in comparison with a different architecture where manager prediction is provided as a sensorial input to the manager, instead of representing a contextual information (orange line).

contextual signal to the lower level, representing the motor actuator and yielding the sequence of actions (Fig. 2C, bottom) in order to achieve the assigned goal.

The importance of assigning the current subtask through a contextual signal to the apical compartment of lower level neurons, rather than projecting it onto their somatic compartment (as it is done in standard networks with point neurons), is then proved through a performance test (Fig. 2D): regardless of the number of training iterations, the first solution is systematically better than the second one, with an average final score of nearly 0.9 (where 1 means unlocking and reaching the food, 0 otherwise) and a button success rate of nearly 100%.

These promising results in the context of hierarchical imitation learning pave the way to the possibility of solving even more complex tasks, by designing similar biologically plausible hierarchical networks with the three-compartment neurons here introduced.

Acknowledgements

This work has been supported by the European Union Horizon 2020 Research and Innovation program under the FET Flagship Human Brain

Project (grant agreement SGA3 n. 945539) and by the INFN APE Parallel/ Distributed Computing laboratory.

References

[1] Payeur A, Guerguiev J, Zenke F et al. Burst-dependent synaptic plasticity can coordinate learning in hierarchical circuits. Nature Neuroscience 24, 1010–1019 (2021).

[2] Guerguiev J, Lillicrap TP, Richards BA. Towards deep learning with segregated dendrites. eLife 6, e22901 (2017).

[3] Capone C, Muratore P, Paolucci PS. Error-based or target-based? A unified framework for learning in recurrent spiking networks. PLoS Computional Biology 18(6), e1010221 (2022).

[4] Larkum ME. A cellular mechanism for cortical associations: an organizing principle for the cerebral cortex. Trends in Neurosciences 36, 141–151 (2013).

[5] Le H, Jiang N, Agarwal A, Dudik M, Yue Y, and Daumé III H. Hierarchical imitation and reinforcement learning. Proceedings of the 35th International Conference on Machine Learning. Proceedings of Machine Learning Research 80, 2917-2926 (2018).

[6] Capone C, Lupo C, Muratore P, Paolucci PS. Burst-Dependent Plasticity and Dendritic Amplification Support Target-Based Learning and Hierarchical Imitation Learning. Proceedings of the 39th International Conference on Machine Learning. Proceedings of Machine Learning Research 162, 2625-2637 (2022).

Exploring fractal dimensions in electrophysiological recordings of intracranial field potentials during normal and abnormal states: A preliminary study

Author
Ricardo Muñoz – Cajal Institute – CSIC, Av. Doctor Arce 37, Madrid 28002, Spain
Julia Makarova – Cajal Institute – CSIC, Av. Doctor Arce 37, Madrid 28002, Spain
Valeri Makarov – Department of Applied Mathematics, Univ. Complutense of Madrid, Av. Paraninfo s/n, Madrid 28040, Spain
Oscar Herreras – Cajal Institute – CSIC, Av. Doctor Arce 37, Madrid 28002, Spain

Citation
Muñoz, R., Makarova, J., Makarov, V., Herreras, O. Exploring fractal dimensions in electrophysiological recordings of intracranial field potentials during normal and abnormal states: A preliminary study

Introduction/Motivation

Field potentials (FPs) in the brain exhibit an extraordinarily varied and changing assortment of temporal patterns, from dominant irregular activity to complex stereotyped waveforms and network oscillations of different frequency bands. FPs arise from the spatiotemporal mixing of activity from multiple sources, making direct readings of voltage fluctuations unreliable [1]. In former studies we managed to optimize the application of blind source separation techniques to separate the mixed sources, which turned out pathway-specific on account of the spatial coherence provided by stable synaptic territories [2]. This anatomical support enabled a simple interpretation of irregular activity,

which despite constituting the bulk of brain signals is typically excluded from analysis by the lack of appropriate tools. Amongst different approaches, the fractal dimension analysis (FDA) [3] has been proved useful in signal analysis to detect tendencies and patterns, and has been applied to several brain-diseases, such as epilepsy [4]. However, it is not yet clear what features in EEG signals make the FD to rise or decrease as both have been reported for apparently similar patterns. Our objective is to explore the sensitivity of FDA to different levels of spatio-temporal complexity of the signals. First, we explored FDA on single-site vs multisite recordings. Second, since FPs are multisource spatiotemporal signals, we checked the ability of FDA to discriminate raw multisite FPs from virtual FPs reconstructed from the ICA-separated FP generators that are coherent across all recording sites. We are also interested in FDA applicability for characterizing the varying patterns in raw FPs during healthy and abnormal activity in multichannel FP recordings contributed by one or multiple FP generators. To this end we chose episodes of spreading depolarization waves that display several totally different activity patterns. Synthetic signals are also used to benchmark the FDA.

Methods

FP recordings were obtained in former studies [4]. These were made in anaesthetized rats with high-density recording devices (silicon linear arrays, 100 um spacing) spanning the cortex and hippocampus. Signals were acquired with an AC-filter (>0.1 Hz) and sampled at 20 kHz. FP generators were obtained through independent component analysis (ICA), and virtual FP profiles were regenerated from one or multiple ICA components (the FP generators). As a pathological event we chose a cortical spreading depression wave (Herreras and Makarova 2020), which evolves from normal to epileptoid activity, followed by silence and gradual recovery. Synthetic signals were generated numerically ad hoc to test different factors (e.g., frequency, amplitude). The algorithm for the FDA was the correlation dimension variation written by V. Makarov.

Results

The following observations pertain to ongoing research and may see variations in relative global weight as the research progresses. FDA was found

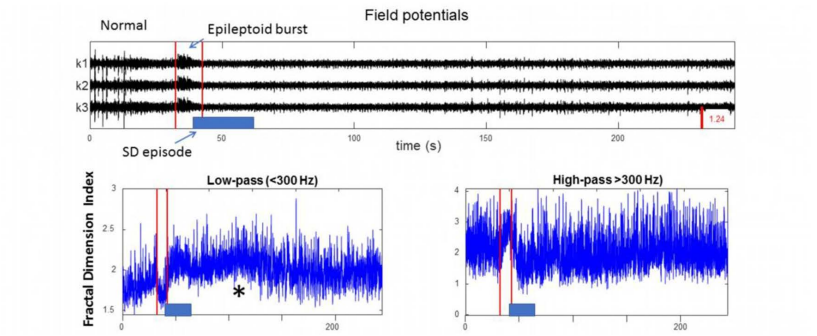

FIGURE 1

Fractal dimension analysis on multisite FP signals in the cortex of anesthetized rats. The upper box shows three simultaneous recordings at different depths during an episode of spreading depolarization (blue box: the DC potential has been filtered out). The plots below show the FDA applied on two copies of the group of signals filtered above or below 300 Hz. Note different FDI baseline levels, noise and relation to specific epochs of the signal.

to detect a time-varying number of dimensions (fractional dimension index FDI) in electrophysiological recordings, but we could not find an obvious correlation of increasing or decreasing FDI with the gross characteristics of the FPs. Thus, the FDI detected epileptoid activity heralding SD (period between red lines) and also the silent period during SD (blue box). These two visually perceptible periods have marked spectral differences. The FDA also detected a transient period during the initial recovery (asterisk) that is characterized by displaying only remote (volume-conducted activity), which is nearly identical in all sites. Despite the variety of patterns contained in the signal that were detected by the FDA, we found that these are dissimilarly detected in filtered replicas of the signals (compare left and right panels, Fig.1). Some epochs even displayed opposite changes (the red lines in Figure 1) relative to each other. We also found differences in FDI between raw FPs and virtual FPs reconstructed from their FP generators.

We also used synthetic signals to explore distinct factors such as frequency and amplitude amongst others. The results were again ambiguous. Both factors appear to be relevant, but in a nonlinear fashion.

Discussion

We report that fractal dimension analysis can be used to reliably detect varying patterns of FP activity in multisite recordings. However, we have not yet determined the signal characteristics that determine the direction of FDI changes. In multisite recordings of FPs the differences between analyzing raw signals and each of the composing FP generators may indicate a possible role in the fine texture arising from the confluence of several dynamics at each recording point. A role for noisy generators omitted during reconstruction of virtual FPS prior to FDA analysis may. In addition, it is possible that the number of channels in which the FP generators show activity plays a role. Understanding the factors that determine the increase or decrease in FDI will pave the way toward automating the analysis and classification of normal and abnormal FP patterns in different brain structures recorded with multiple electrodes. From the use on synthetic signals it was clear that both amplitude and frequency play a role, but the relationship appears to be complex and nonlinear. Obtaining simple cues for interpretation is hampered by the multiple contained in FP signals that appear to have an impact on the FDI. We are screening several parameters alone or in combination over sufficiently wide ranges to better determine the signal features to which FDA is sensitive.

Funding

This work was supported by the Spanish Ministerio de Ciencia e Innovación (MICIN) grant PID2019-111587RB-I00, and the Agencia Estatal de Evaluación, Next Generation EU grant PDC2021-121103-I00 to O.H.

References

[1] Herreras O, Torres D, Martín-Vázquez G, Hernández-Recio S, López-Madrona VJ, Benito N, Makarov VA, Makarova J. (2022) Site-dependent shaping of field potential waveforms. Cerebral Cortex, Aug 16, DOI: 10.1093/cercor/bhac297

[2] Herreras O, Makarova J. (2020). Mechanisms of the negative potential associated with Leao's spreading depolarization: A history of brain electrogenesis. JCBFM, 40: 1934-1952.

[3] Jaquette J, Schweinhart B. (2019). Fractal dimension estimation with persistent homology. Commun Nonlinear Sci Numer Simul 84:105163.

[4] Li Z, Li J, Xia Y, Feng P, Feng F. (2021). Variation trends of fractal dimension in epileptic EEG signals. Algorithms, 14, 316.

[5] Torres D, Makarova J, Ortuño T, Benito N, Makarov VA, Herreras O. (2019) Local and volume-conducted contributions to cortical field potentials. Cerebral Cortex 29: 5234-5254.

Analysis of hippocampal participation in social interactions in a genetic model of autism spectrum disorder

Author
Pilar Rodríguez-Martín – Instituto Cajal, (C.S.I.C), Madrid, Spain
Almudena Sanz – Instituto Cajal, (C.S.I.C), Madrid, Spain
Elisa Cintado – Instituto Cajal, (C.S.I.C), Madrid, Spain
Eva Monserrat – Instituto Cajal, (C.S.I.C), Madrid, Spain
Inés Colmena – Instituto Cajal, (C.S.I.C), Madrid, Spain
Cristina Medina-Menéndez – Instituto Cajal, (C.S.I.C), Madrid, Spain
Véronique Lefebvre – Children's Hospital of Philadelphia, Philadelphia, PA 19104, Pennsylvania, USA
José Luis Trejo – Instituto Cajal, (C.S.I.C), Madrid, Spain
Aixa V. Morales – Instituto Cajal, (C.S.I.C), Madrid, Spain

Citation

Rodríguez-Martín, P., Sanz, A., Cintado, E., Monserrat, E., Colmena, I., Medina-Menéndez, C., Lefebvre, V., Trejo, J.L., Morales, A.V. Analysis of hippocampal participation in social interactions in a genetic model of autism spectrum disorder.

Introduction/Motivation

Many neurodevelopmental disorders associated with deficiencies in social interaction, language difficulties and repetitive behaviours are grouped under the name of autism spectrum disorders (ASD). Although the genetic causes

of ASD are complex, one of the genes that have been associated with ASD is SOX5, which encodes a transcription factor with important functions in the control of neurogenesis (1) and in the specification of projection neurons of the cerebral cortex (2). In humans, heterozygous genetic alterations comprising SOX5 are the cause of Lamb-Shaffer syndrome (L-S; OMIM #616803), which encompasses disorders of the central nervous system such as significant speech delay, cognitive deficits, anxiety and behaviors typical of autism spectrum disorders (ASD), including deficits in social interaction (3). Moreover, it has been described that the CA2 region of the hippocampus is fundamental in social behaviour in mice, a region where we have previously shown that Sox5 is expressed (4,5). In this ongoing project, we propose the use of a conditional Sox5 mutant mouse line specific for the CA2 region to further explore the role of this protein in the specification of CA2 neurons as well as its relevance in social behaviour. Our working hypothesis is that Sox5Amigo2 mice could stand a new, more specific murine model of the alterations in social behavior found in L-S syndrome, with special interest for ASD.

Methods

Using conditional Sox5 mutant mice specific for the CA2 region (Amigo2-cre/Sox5fl/fl;Sox5Amigo2), an extensive battery of behavioural assays were performed to evaluate social memory, anxiety, navigation and spatial memory. As heterozygous mutant mice (Amigo2-cre/Sox5fl/+;Sox5Amigo2/+) do not show loss of Sox5 expression in CA2 neurons, they were considered controls. Sox5Amigo2 mice performance in these tests was assessed in comparison to two control groups: Sox5Amigo2/+ mice, and an assorted control group including WT, Amigo-cre and Sox5fl/+ mice (Fig.1). Effective loss of Sox5 in CA2 and other relevant molecular changes were assessed by immunohistochemistry and RT-qPCR.

Results and discussion

We have determined that robust lack of Sox5 expression causes Purkinje Cell Protein 4 (PCP4) level decrease in more than half of the pyramidal neurons in CA2. Furthermore, $Sox5^{Amigo2}$ mutant mice: i) exhibit normal basic reflexes, weight, locomotion abilities, and anxiety levels; ii) exhibit a good

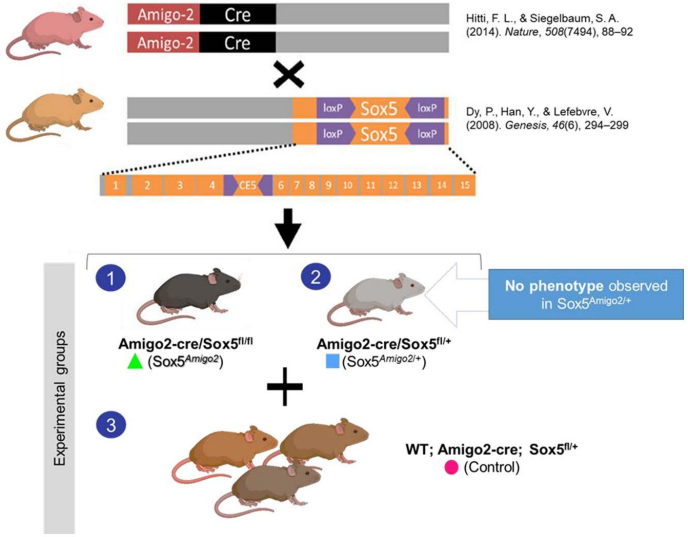

FIGURE 2

Schematic representation of the Sox5^{Amigo2} transgenic line generation. For the experimental setup three groups of mice with C57BL/6J genetic background were established: i) homozygous mice carrying two copies of the floxed Sox5 allele; ii) heterozygous mice carrying one copy of the floxed Sox5 allele; and iii) an assorted control group including WT mice, mice carrying the Amigo-cre allele only, and mice carrying one copy of the floxed Sox5 allele only. Conditional Sox$^{fl/fl}$ mutants were kindly granted by V. Lefebvre's lab, while Amigo2-cre transgenic line was obtained from J.L. Trejo's lab (Instituto Cajal, Madrid, Spain.)

performance in Morris water maze test; iii) present normal social preference and iv) both males and female lose social recognition memory. Thus, we propose that Sox5^{Amigo2} mice could provide a new model of ASD, based on cellular and functional alterations of the CA2 region of the hippocampus, that serves to understand the hippocampal component in the pathophysiology of ASD and for the testing of new therapeutic strategies.

References

[1] Li L, Medina-Menéndez C, García-Corzo L, Córdoba-Beldad CM, Quiroga AC, Calleja Barca E, et al. SoxD genes are required for adult neural stem cell activation. Cell Rep. 2022 Feb;38(5):110313.

[2] Lai T, Jabaudon D, Molyneaux BJ, Azim E, Arlotta P, Menezes JRL, et al. SOX5 controls the sequential generation of distinct corticofugal neuron subtypes. Neuron. 2008 Jan;57(2):232–47.

[3] Lamb AN, Rosenfeld JA, Neill NJ, Talkowski ME, Blumenthal I, Girirajan S, et al. Haploinsufficiency of SOX5 at 12p12.1 is associated with developmental delays with prominent language delay, behavior problems, and mild dysmorphic features. Hum Mutat. 2012 Apr 1;33(4):728–40.

[4] Hitti FL, Siegelbaum SA. The hippocampal CA2 region is essential for social memory. Nature. 2014 Apr 23;508(7494):88–92.

[5] Fernandez-Lamo I, Gomez-Dominguez D, Sanchez-Aguilera A, Oliva A, Morales AV, Valero M, et al. Proximodistal Organization of the CA2 Hippocampal Area. Cell Rep. 2019;26(7):1734-1746.e6.

Differential patterns of transient high power oscillatory events in resting MEG in Alzheimer's disease converters

Author
Danylyna Shpakivska-Bilan – Department of Experimental Psychology, School of Psychology, Complutense University of Madrid, Spain;Center for Cognitive and Computational Neuroscience, Complutense University of Madrid, Spain
Gianluca Susi – Department of Structure of Matter, Thermal Physics and Electronics, School of Physics, Complutense University of Madrid, Spain; Center for Cognitive and Computational Neuroscience, Complutense University of Madrid, Spain
Jesus Cabrera – Department of Experimental Psychology, School of Psychology, Complutense University of Madrid, Spain; Center for Cognitive and Computational Neuroscience, Complutense University of Madrid, Spain
David W Zhou – Department Neuroscience, Carney Institute for Brain Sciences, Brown University, Providence, USA
Ernesto Pereda – Department of Industrial Engineering and Institute of Biomedical Technology, Universidad de La Laguna, La Laguna, Tenerife
Maria Eugenia Lopez – Department of Experimental Psychology, School of Psychology, Complutense University of Madrid, Spain; Center for Cognitive and Computational Neuroscience, Complutense University of Madrid, Spain
Stephanie R Jones – Department Neuroscience, Carney Institute for Brain Sciences, Brown University, Providence, USA
Fernando Maestu – Department of Experimental Psychology, School of Psychology, Complutense University of Madrid, Spain; Center for Cognitive and Computational Neuroscience, Complutense University of Madrid, Spain

Citation

Shpakivska-Bilan, D., Susi, G., Cabrera, J., Zhou, D.W., Pereda, E., Lopez, M.E., Jones, S.R., Maestu, F. Differential patterns of transient high power oscillatory events in resting MEG in Alzheimer's Disease converters.

Introduction/Motivation

Over the last decade, it has been suggested one of the main factors that precipitates Alzheimer's Disease (AD) progression is the loss of the excitatory/inhibitory (E/I) balance. Burden of amyloid oligomers and plaques on inhibitory terminals would lead to the alteration of electrophysiological activity in various aspects, including the hyperexcitability of cortex [1], but the underlying mechanisms are still unknown.

Prior studies [2] show that MCI patients later converting to AD (CONV) exhibit differential patterns on resting power and synchronization between anterior cingulate cortex (ACC) and precuneus (PC), leading to the description of the "X model," a model of the individual trajectories from MCI to dementia.

In order to understand E/I imbalance in AD, it is important to fill the gap between neurophysiology and M/EEG findings in humans. In this context, magnetoencephalography (MEG) is a functional neuroimaging technique that offers an excellent combination of temporal and spatial resolution for mapping brain activity by recording magnetic fields produced by electrical currents occurring naturally in the brain. One of the most prominent signatures of brain activity measured with M/EEG are low-frequency rhythms (<100Hz), particularly in resting brain oscillations that are coordinated across networks, dominated by alpha and beta frequencies. These rhythms are not continuous oscillations but rather can emerge as transient increases in high power in unaveraged data [4]. A first step to link neuropathophysiology of AD to electrophysiological activity can be to explore how these transient events differ on AD converters.

In this study, it is explored how averaged power in CONV compared to NOCONV, in ACC and PC, is related to quantifiable changes in a set of parameters that characterize transient events frequency and shape.

Methods

We have studied MEG resting state oscillations in patients with mild cognitive impairment who later convert (CONV, N=23, Age= 74.1 + 0.50) or do not convert (NOCONV, N=22, Age=71.7 + 0.49) to AD. MEG signals were acquired using a whole-head ElektaNeuromag MEG system with 306 channels (Elekta AB) at the Center for Biomedical Technology (Madrid, Spain). MEG protocol consisted of 5 min at resting state with eyes closed. Raw recording data were processed automatically to remove noise and detect artifacts. Last ones were then visually confirmed by an MEG expert. MEEG activity sources were reconstructed with Brainstorm software obtaining averaged brain activity of the regions of interest (ACC, PC). Then we characterized novel features of transient high-power events in the spectral and temporal domains [3] in the resting state signal that distinguish future AD CONV from NOCONV.

Results and discussion

We find a consistent pattern of a *higher number (rate)* of transient 12-30Hz beta events (see Fig 1) and higher *beta event power* (see Fig 2) in bilateral precuneus for NOCONV compared to CONV. In addition, the CONV group shows a beta frequency slowing both in time series and time-frequency representations. We hypothesize that a higher neuronal excitability, moderated by age, may distort high power beta events in the CONV group [2].

In conclusion, frequency and chape of transient MEEG events differ on AD converters compared to no AD converters. These results may provide new biomarkers for healthy and pathological aging. Therefore, it is necessary to continue the research on the underlying mechanisms responsible for these differences.

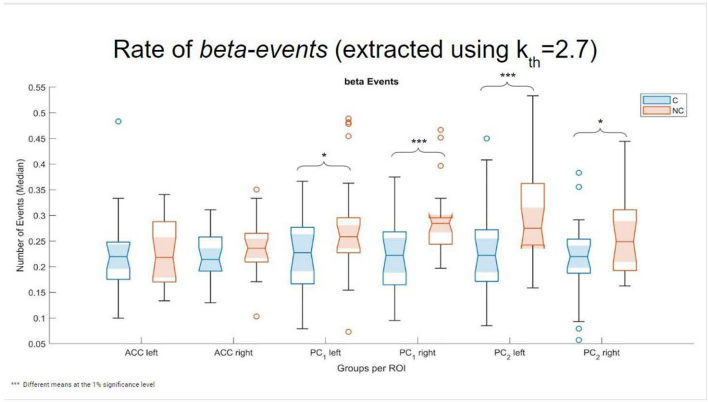

FIGURE 1

Differences between Converters and non Converters in rate of beta-events detected on temporal domain.* *p<0.05.*

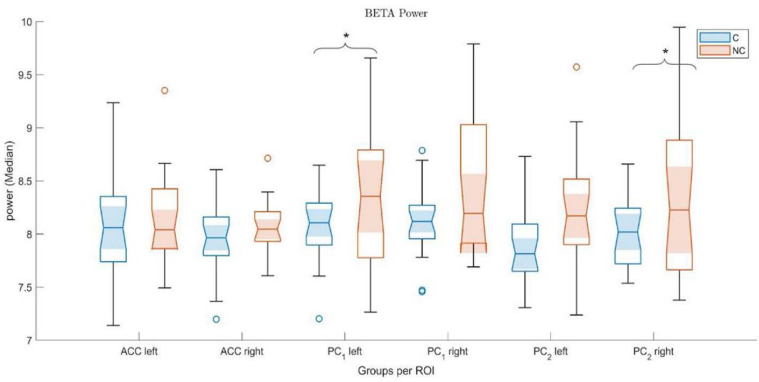

FIGURE 2

Differences between Converters and non Converters in power of beta-events detected on spectral domain. .* *p<0.05.*

References

[1] Insel, P. S., Mormino, E. C., Aisen, P. S., Thompson, W. K., & Donohue, M. C. (2020). Neuroanatomical spread of amyloid β and tau in Alzheimer's disease: implications for primary prevention. Brain communications, 2(1), fcaa007.

[2] Pusil, S., López, M. E., Cuesta, P., Bruna, R., Pereda, E., & Maestu, F. (2019). Hypersynchronization in mild cognitive impairment: the 'X'model. Brain, 142(12), 3936-3950.

[3] Shin H, Law R, Tsutsui S, Moore CI, Jones SR The rate of transient beta frequency events predicts behavior across tasks and species. (2017) eLife 6:e29086.

[4] S. R. Jones, —When brain rhythms aren't _rhythmic': implication for their mechanisms and meaning,|| Current Opinion in Neurobiology, 2016, doi: 10.1016/j.conb.2016.06.010. PMID 27400290.

Where scientists empower society

Creating solutions for healthy lives on a healthy planet

frontiersin.org

Why publish with us?

All Frontiers journals are fully open access, meaning every research article we publish is immediately and permanently free to read.

Our collaborative peer review is handled by experts in the field who objectively certify the quality, validity, and rigor of research.

With the latest custom-built technology and artificial intelligence, we're revolutionizing the way research is published, evaluated, and communicated.

We are the third most-cited publisher with 1.4 billion article views and downloads – reflecting the power of research that is open for all.

Frontiers

Avenue du Tribunal-Fédéral 34
1005 Lausanne, Swizerland
frontiersin.org

Contact us

+41 (0)21 510 17 00
frontiersin.org/about/contact